

REPORT OF
RESEARCH
ON
AIR QUALITY

Library Copy

A REGIONAL-SCALE (1000 KM) MODEL OF PHOTOCHEMICAL AIR POLLUTION
Part 2. Input Processor Network Design

ENVIRONMENTAL SCIENCES RESEARCH LABORATORY
OFFICE OF RESEARCH AND DEVELOPMENT
U.S. ENVIRONMENTAL PROTECTION AGENCY
RESEARCH TRIANGLE PARK, NC 27711

A REGIONAL-SCALE (1000 KM) MODEL OF PHOTOCHEMICAL AIR POLLUTION
Part 2. Input Processor Network Design

Robert G. Lamb
Meteorology and Assessment Division
Environmental Sciences Research Laboratory
Research Triangle Park, North Carolina 27711

ENVIRONMENTAL SCIENCES RESEARCH LABORATORY
OFFICE OF RESEARCH AND DEVELOPMENT
U.S. ENVIRONMENTAL PROTECTION AGENCY
RESEARCH TRIANGLE PARK, NC 27711

NOTICE

This document has been reviewed in accordance with U.S. Environmental Protection Agency policy and approved for publication. Mention of trade names or commercial products does not constitute endorsement or recommendation for use.

PREFACE

After the model described in Part 1 of this report was formulated, a draft of an instruction manual was rather hastily prepared to guide computer programmers in the task of transforming the theory into an operational model. The present report, Part 2, evolved from that manual. The purpose of this document goes beyond that of an instruction manual, however. The broader objective is to provide in conjunction with Part 1 of detailed description of what we regard as EPA's first-generation regional oxidant model.

In attempting to use science as a tool for treating the types of applied problems that are of concern to the EPA, one is not allowed the luxury of simplifying assumptions that reduce problems to forms that possess concise elegant solutions. Instead, one must face the harsh realities of the physical world and search for approximate descriptions of phenomena that strike an acceptable compromise between scientific rigor and practicability. Just what constitutes an "acceptable" compromise in this case is a subjective judgement that each person must make for himself. In my view, several of the techniques presented in this report represent compromises that are not wholly acceptable, but they must suffice for now because time constraints dictate that we move on to the task of model testing. Hopefully, the flexibility that we have built into the basic framework of the model will foster efforts by others to expand and improve upon the work we have done; and a second generation model will emerge significantly better than the model presented here.

R.G. Lamb

November 1983

ABSTRACT

Detailed specifications are given for a network of data processors and submodels that can generate the parameter fields required by the regional oxidant model formulated in Part 1 of this report. Operations performed by the processor network include simulation of the motion and depth of the nighttime radiation inversion layer; simulation of the depth of the convective mixed and cloud layers; estimation of the synoptic-scale vertical motion fields; generation of ensembles of layer-averaged horizontal winds; calculation of vertical turbulence fluxes, pollutant deposition velocities, parameters for a subgrid-scale concentration fluctuation parameterization scheme; and many other functions. This network of processors and submodels, in combination with the core model developed in Part 1, represent the EPA's first-generation regional oxidant model.

CONTENTS

Preface	iii
Abstract	iv
Figures	viii
Tables	xi
Acknowledgements	xiii
 1. Introduction	 1
General Discussion	1
Summary of Processor Functions	5
Processor P1	5
Processor P2	5
Processor P3	7
Processor P4	7
Processor P7	7
Processor P8	7
Processor P9	7
Processor P10	8
Processor P11	8
Processor P12	8
Processor P15	8
BMC	8
Summary of Model Equations	9
Layer 1	9
Layer 2	12
Layer 3	14
Layer 0	15
 2. Processor P1	 18
General Discussion	18
Step 1	18
Step 2	19
Step 3	20
Step 4	20
Step 5	21
Step 6	21
Step 7	22
Step 8	23
Step 9	23
Step 10	24
Stage INT	24
 3. Processor P2	 30
General Discussion	30
Stage LBC: Estimating lateral boundary conditions from monitoring data	 34

CONTENTS (continued)

Stage IC: Estimating initial conditions from monitoring data	34
Stage UBC: Upper boundary conditions	36
4. Processor P3	39
General Discussion	39
Step 1	39
Step 2	40
Step 3	41
Step 4	42
Stage INT	42
5. Processor P4	46
General Discussion	46
Step 1	47
Step 2	48
Step 3	50
Step 4	51
6. Processor P7	56
Motion of a viscous, hydrostatic fluid of constant density over irregular terrain	56
The pressure force	58
The friction force	61
The Coriolis force	65
The momentum equations	65
The fluid depth equation	67
Simplified model equations	76
Solution of the u , v , and z_{vs} equation	79
Stage ZT	82
Stage DELRO	83
Stage ETA	86
Stage PCD	89
Stage IBC	91
Stage H1HO	94
Stage SIG	95
Stage FLOMOD	96
Appendix A to Section 7	101
Appendix B to Section 7	110
Calculation of the BAR variables	120
Calculation of the PRIME variables	122
Calculation of the dependent variables u^i , v^i , and h^i	124
7. Processor 8	131
Introduction	131
Derivation of basic equations	131
Stage ZQ	147
Stage PATH	161
Stage WEWC	165
Stage W2	172

CONTENTS (continued)

Stage WV	182
Mode 0: $\Delta p_1=0$	182
Mode 1: $\Delta p_1=1$	185
8. Processor P9	197
Development	197
Stage DEN	197
Stage ZEN	203
Appendix to Section 8	195
9. Processor P10	207
Stage DELH	208
Stage S	211
Stage ZTA	214
10. Processor P11	219
Summary	219
Introduction	220
Average horizontal winds in a layer bounded by two arbitrary pressure surfaces	222
Stage UV11	247
11. Processor P12	254
Development	254
Stage K	254
Stage WW0	261
Stage WW1	264
12. Processor P15	271
Development	271
Step 1	271
Step 2	275
13. The B-Matrix Compiler	279
Introduction	279
The B-Matrix elements	280
Preparation of terms in the Γ -equation	285
Step 1	287
Step 2	288
Step 3	289
Step 4	290
Step 5	290
References	296

FIGURES

<u>Number</u>		<u>Page</u>
1-1	Schematic illustration of the regional model and the network of processors that supply it information	2
1-2	Modeling region in the NEROS study. Each dot represents a grid cell	6
1-3	Illustration of Processor P1 and its input and output interfaces with the processor network	29
2-1	Illustration of Processor P2 and its input and output interfaces with the processor network	38
3-1	Schematic illustration of Processor P3 and its input and output interfaces with the processor network	45
4-1	Schematic illustration of Processor P4 and its input and output interfaces with the processor network	55
7-1	Illustration of the variables used in the flow model	57
7-2	Air parcel considered in the force balance analysis	58
7-3	Friction forces on a fluid parcel of horizontal dimensions $(\Delta x, \Delta y)$ bounded by z_{vs} and z_t	62
7-4	Projection of the horizontal rectangle $(\Delta x, \Delta y)$ onto the surface H_{vs} centered at point Q	69
7-2	Illustration of the 54 5 min x 5 min cells that are used in the calculation of $z_t(I, J)$	83
7A-1	Illustration of the points used in the numerical solution of Eq. 7A-1. Circled grid points are those from which values Γ and S are taken to derive a biquintic expansion of $F(\bar{x}', t_n)$ about the point (IST, JST) (see Eq. 7-49)	104
7B-1	Flow chart of FIOMOD operations,	119
7B-2	Grid network on which $\bar{\beta}_u, \bar{\beta}_v, \bar{\beta}_h, \bar{S}_u, \bar{S}_v$, and \bar{S}_h are computed. Different spatial derivative operators $\nabla_{\Delta x}$ and $\nabla_{\Delta y}$ are required in these calculations as indicated	122
7B-3	Illustration of the southwest corner zone and the west and south boundary zones of the model domain	129

FIGURES (Continued)

<u>Number</u>		<u>Page</u>
7-6	Schematic illustration of Processor P7 and its input and output interfaces with the processor network	130
8-1	Illustration of surfaces H_2 and H_3 during situations in which convective clouds cover only a portion of the modeling region	132
8-2	Illustration of the air parcel trajectory that arrives at point x_m at hour t_1 . Point x_m' denotes the parcel's location at time $t_0 < t_1$	141
8-3	(a) Idealized profiles of mixing ratio q and potential temperature θ in dry, convective conditions. (b) Second derivatives of the profiles illustrated in panel a	150
8-4	Illustration of the points (dots) at which measurements of ζ are available; and the point z'' at which a measure of $d^2\zeta/dz^2$ is desired. Values of ζ measured at the points $z_i, i=1, \dots, 4$ centered at z'' are used to approximate $\zeta(z)$ in a polynomial about z''	151
8-6	Schematic illustration of Processor P8 and its input and output interfaces with the processor network	196
9-1	Schematic illustration of Processor P9 and its interfaces with the processor network	206
10-1	Illustration of the influence of terrain on model layers 0, 1 and 2 for given values of the penetration fractions σ_{T1} and σ_{T0}	211
10-2	Schematic illustration of Processor P10 and its interfaces with the processor network	218
11-1	Surfaces bounding layer β in which M soundings of the horizontal wind are available on the bottom surface p_α of Layer β	224
11-2	Illustration of Processor P11 and its input and output interfaces with the processor network	253
12-1	Illustration of the superposition of five hypothetical realization of an ensemble of point source plumes. The width Σ of the ensemble of plumes is controlled by the character of the flow field ensemble. The width σ of the plumes in the ensemble is controlled by the turbulent, eddy diffusivity K	256

FIGURES (continued)

<u>Number</u>		<u>Page</u>
12-2	Illustration of Processor P12 and its input and output interfaces with the processor network	270
15-1	Illustration of Processor P15 and its input and output interfaces with the processor network	278
BMC-1	Schematic illustration of the B-Matrix Compiler (BMC). The input interface is the Model Input File (MIF). The output of the BMC is the "b-matrix tape" which is read by the model code CORE (see Figure 1-1)	293

TABLES

<u>Number</u>		<u>Page</u>
1-1	Summary of input and output variables of each step of Processor P1	26
2-1	Pollutant species concentration (ppm) thaken to be representative of "clean" atmospheric conditions	31
2-2	Summary of input and output variables of each stage of Processor P2	37
3-1	Summary of input and output parameters of each step of Processor P3	44
4-1	Summary of input and output parameters in each step of Processor P4	53
7-1	Summary of the input and output requirements of each stage of Processor P7	97
8-1	Summary of the input and output requirements of each stage of Processor P8	188
9-1	Summary of the input and output variables of each stage of Processor P9 and their sources	205
10-1	Summary of input and output parameters for Processor P10 and their sources	215
11-1	Input requirements of stage UV11 and their sources	251
12-1	Summary of the expressions used to estimate the horizontal eddy diffusivity K_n in each of the model's three layers	259
12-2	Input and output variables of each stage of Processor P12	267
15-1	Deposition resistances (sec/m) for SO ₂ as a function of land use type n and stability L	272
15-2	Deposition resistances (sec/m) for ozone as a function of land use type n and stability L	273
15-3	Deposition resistances of several pollutants relative to that of ozone over agricultural land. (Deduced from data of Hill and Chamberlain, 1971)	274

TABLES (Continued)

<u>Number</u>		<u>Page</u>
15-1	Summary of the input and output parameters of each step of Processor P15	277
BMC-1	Definitions of parameters in the Model Input File (MIF)	294

ACKNOWLEDGEMENTS

I am indebted to Dr. Don Pelles of Computer Data Systems, Inc. (CDSI) for his invaluable assistance in developing the ideas on the flow field ensemble presented in Section 10, and to Ms. Achamma Philip, also of CDSI, for her steadfast assistance in developing the numerical boundary condition scheme presented in Section 6. I also want to acknowledge the excellent work of Gayle Webster and Sherry McCoy of Systems Research and Development Corporation (SRD), in preparing the manuscript.

SECTION 1

INTRODUCTION

GENERAL DISCUSSION

In Part 1 of this report, (Lamb 1983d) we developed a theoretical basis for a regional-scale model of photochemical air pollutants. Realizing that the operational model would be very complicated and would require considerable time and effort to develop, we proposed that, rather than integrate all of the various components of the model into a single unit, we construct it by partitioning the mathematical descriptions of small groups of individual physical and chemical processes into discrete modules interconnected by fixed communication channels. Such modular design would facilitate troubleshooting operations, provide a natural division of labor for the tasks required to implement the model, and permit continual incorporation of state-of-the-art techniques without the need to overhaul the model code each time a new technique was introduced.

The overall structure of the proposed model system is illustrated in Figure 1-1. The box labeled CORE represents the computer language analogue of the differential equations that describe all the governing processes considered in the model development in Part 1. (These equations are listed at the end of this section.) The CORE module is expressed in a very primitive mathematical form in the sense that its inputs are matrices and vectors whose

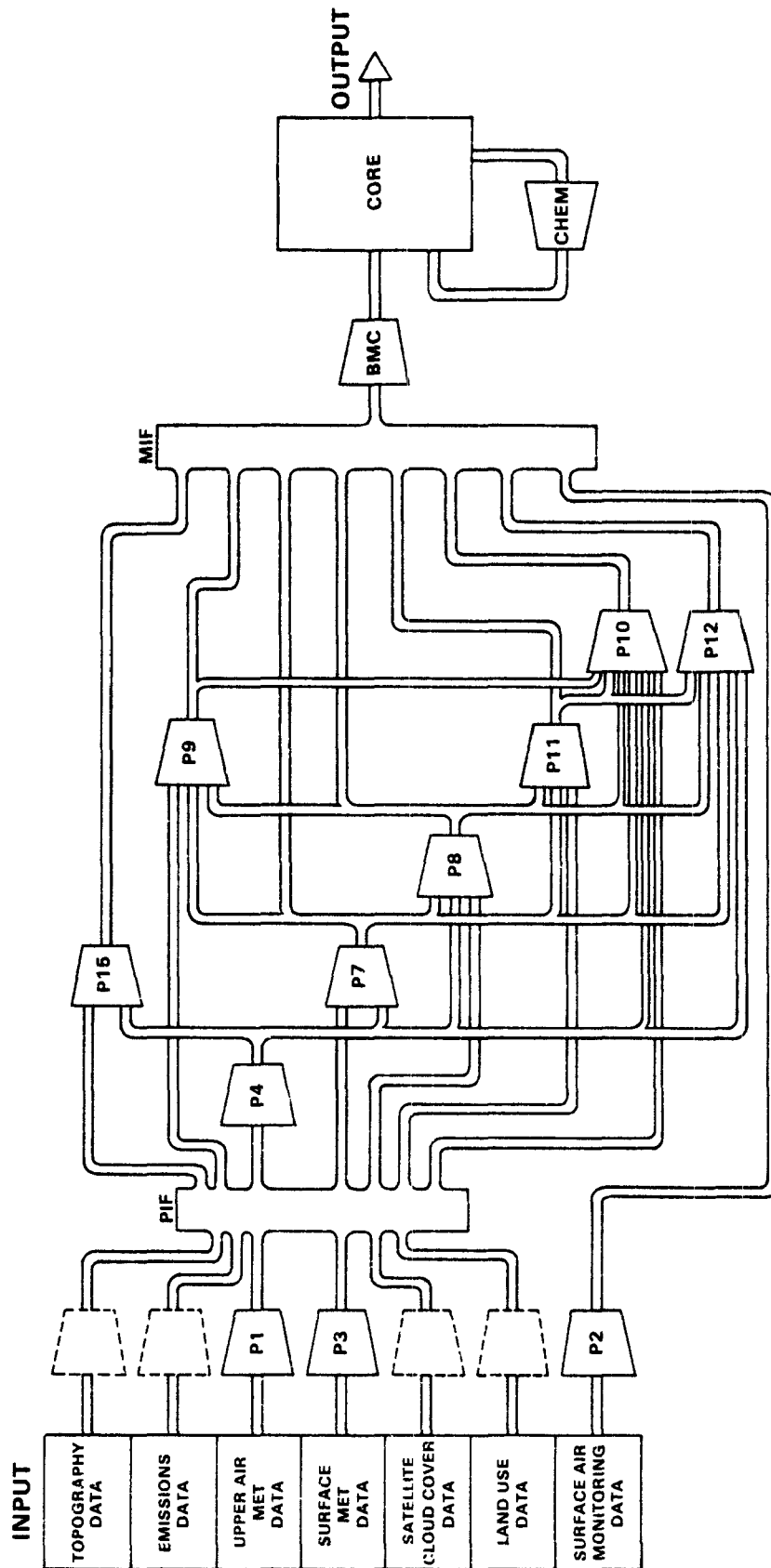


Figure 1-1. Schematic illustration of the regional model and the network of processors that supply it information.

elements are composites of meteorological parameters, chemical rate constants, etc. For example, the link between CORE and the output of the module labeled CHEM, which contains the analogue of the chemical kinetics scheme, consists of two vectors \underline{P} and \underline{Q} , each of length N , where N is the total number of chemical species simulated. The n -th element of \underline{P} is the net rate of production of species n due to source emissions and chemical reactions among all other species, and the n -th element of \underline{Q} is the net rate of destruction of species n due to its chemical interaction with all other species. Thus, any chemical kinetics mechanism can be incorporated into the model as long as it is expressed in a form that is compatible with the vector interfaces that link CORE with the chemistry module CHEM.

The remainder of the inputs required by CORE are prepared by the module designated BMC (b-matrix compiler) in Figure 1-1. The BMC performs essentially the same task that language compilers perform in computers. It translates the parameter fields in the model input file (MIF) into the matrix and vector elements that are required to operate the algorithms in CORE. These parameters include layer thicknesses, horizontal winds in each layer, interfacial volume fluxes, and deposition velocities.

The variables in the model input file (MIF) are supplied in turn by a series of interconnected processors, labeled P7, P8, etc. in Figure 1-1, several of which are rather complex models in themselves. These processors generate the wind fields, the interfacial surfaces that separate the layers, turbulence parameters, source emissions, and many other variables. Their inputs consist of information generated by other processors in the network

and partially processed raw data that are transferred through the processor input file (PIF).

The purpose of this report is to provide detailed specifications of the processor network illustrated in Figure 1-1. This network will consist of both permanent and interchangeable components. The permanent components are the CORE, the BMC, the MIF and PIF, the communication channels that link the processors and the PIF and MIF, and the interfaces between the processors and the communication channels. All processors, i.e., P1, P2, etc. and CHEM are interchangeable components of the network. Any or all of the interchangeable elements can be replaced by other modules as long as the replacements are compatible with the communication channel interfaces. By "interface" we mean the set of input and output variables assigned to each processor. We can think of each processor as being analogous to an electronic device that plugs into a multireceptacle socket (the interface). Each receptacle that provides an input to the processor is connected to a fixed signal source, and each receptacle that receives an output from the processor acts as a signal source on the network of communication lines. Considering the interchangeability of the processors and chemistry module CHEM, one should view the processor designs that we develop in this report as "first generation" versions that may be replaced in the course of future tests and refinements of the model.

Neither the chemistry module nor the results of any test simulations are discussed in this report. These topics will be discussed in later parts of this series of reports. In the following sections we present designs of each processor in the network including the BMC. Theoretical descriptions of the

mathematics contained within the module 'CORE were given in Section 9 of Part 1. We will not elaborate further on this part of the model system in this report other than to describe in more detail the numerical scheme that we apply to the transport and diffusion portion of the model equations. These details are given in Appendix A of Section 6 which describes Processor P7.

Figure 1-2 shows the region in the Northeastern United States to which the regional model will be applied. Each point in the figure represents the center of a grid cell in which values of all pollutant species concentrations are computed by the model.

SUMMARY OF PROCESSOR FUNCTIONS

The functions performed by each processor in the model network, illustrated earlier in Figure 1-1 are summarized below.

Processor P1

Prepares upper air data for use by other processors in the network.

Processor P2

Uses surface air monitoring data to estimate initial, lateral and upper boundary conditions on pollutant species concentrations.

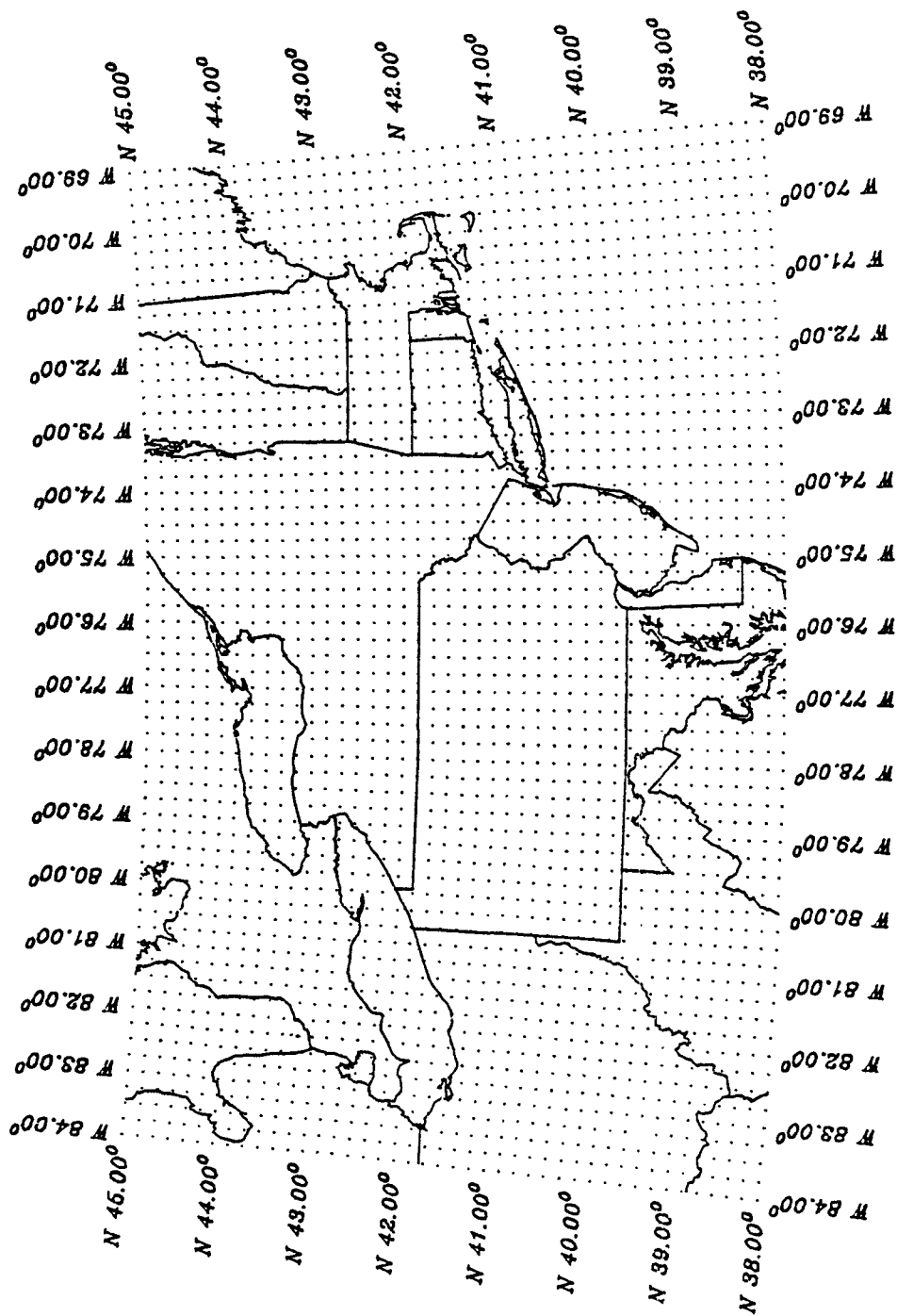


Figure 1-2. Modeling region in the NEROS study. Each dot represents a grid cell.

Processor P3

Prepares surface meteorological data for use in other processors.

Processor P4

Estimates surface roughness, Obukhov length, surface heat flux, and friction velocity.

Processor P7

Simulates the depth and motion of the nighttime surface inversion layer and the depth of the daytime shear layer and provides smoothed terrain elevations.

Processor P8

Computes depths of the convective mixed layer and cloud layer, cloud and turbulent entrainment velocities at the mixed layer top, synoptic-scale mean vertical motion on the top surfaces of model Layers 2 and 3, and layer averaged horizontal wind divergences.

Processor P9

Calculates factors for correcting the chemical rate constants for temperature, density, and sunlight variations.

Processor P10

Transforms the source emissions inventory into source strength functions, and estimates the plume volume fraction parameter required in the subgrid scale chemistry parameterization.

Processor P11

Computes ensembles of volume averaged horizontal winds for each model layer (except the nighttime surface inversion layer which is treated in P7).

Processor P12

Calculates layer interface turbulent volume fluxes; horizontal eddy diffusivities; and cumulus cloud flux partition parameter.

Processor 15

Computes pollutant species deposition velocities.

BMC

Compiles processor network outputs for input into the model core algorithms.

SUMMARY OF MODEL EQUATIONS

The equations upon which the regional-scale mode is based were derived in Part 1 of this study. The basic forms of the governing equations in each of the model's four layers are summarized below.

Layer 1

$$\begin{aligned}
 & \frac{\partial \langle c \rangle_1}{\partial t} + \langle c \rangle_1 \frac{\partial \ln V_1}{\partial t} + \mu_\lambda \langle u \rangle_1 \frac{\partial \langle c \rangle_1}{\partial \lambda} + \mu_\phi \langle v \rangle_1 \frac{\partial \langle c \rangle_1}{\partial \phi} \\
 & + \mu_\lambda \langle u' c' \rangle_1 \frac{\partial \ln V_1}{\partial \lambda} + \mu_\phi \langle v' c' \rangle_1 \frac{\partial \ln V_1}{\partial \phi} \\
 & + \mu_\lambda \frac{\partial \langle u' c' \rangle_1}{\partial \lambda} + \mu_\phi \frac{\partial \langle v' c' \rangle_1}{\partial \phi} \\
 & + \frac{A}{V_1} [+ F_{0,1} - F_{1,1}] = \langle R \rangle_1 + \langle S \rangle_1
 \end{aligned}$$

where

$$\mu_\lambda = \frac{1}{a \cos \phi}$$

$$\mu_\phi = \frac{1}{a}$$

a = earth radius at MSL (in meters)

λ = longitude

ϕ = latitude

$$A = a^2 (\Delta \phi \Delta \lambda) \cos \phi$$

$\Delta \phi, \Delta \lambda$ = latitude, longitude grid cell dimensions

= constants ($\Delta \phi = \frac{1^\circ}{6}$ $\Delta \lambda = \frac{1^\circ}{4}$)

$$V_1(\lambda, \phi, t) = a^2 \cos \phi \int_{\lambda - \Delta\lambda/2}^{\lambda + \Delta\lambda/2} \int_{\phi - \Delta\phi/2}^{\phi + \Delta\phi/2} \text{MAX} \{0, [z_1(\lambda', \phi', t) - \text{MAX} [\hat{z}_T(\lambda', \phi'), z_0(\lambda', \phi', t)]]\} d\phi' d\lambda'$$

$$\left. \begin{array}{l} \langle u'c' \rangle_1 \\ \langle v'c' \rangle_1 \end{array} \right\} \text{ subgrid scale fluxes of } c \text{ (see Part 1, Section 7)}$$

$$\langle R \rangle_1 = \text{all chemical, rainout and washout processes.}$$

$$\langle S \rangle_1 = \text{all emissions of } c \text{ in Layer 1 (includes stacks and surface sources above nighttime radiation inversion.}$$

$$\langle u \rangle_1, \langle v \rangle_1 = \text{layer averaged horizontal wind components} \\ \text{(u = east-west component, positive eastward),} \\ \text{(v = north-south component, positive northward).}$$

$$F_{1,1} = (1 - \sigma_{T1}) [(\langle c \rangle_1 - \langle c \rangle_2) w_{1m} + \langle c \rangle_1 w_1]$$

$$\beta = \text{deposition velocity of species } c$$

$$\sigma_{T1}(\lambda, \phi, t) = \text{fraction of surface } H_1 \text{ penetrated by terrain}$$

$$w_1 = \frac{\psi \sigma_c \bar{w}_c}{1 - \sigma_{T1}} + \frac{\dot{z}_1}{2} [1 + \text{erf} \left(\frac{w_m - \bar{w}_{D1}}{\sqrt{2} \sigma_{w1}} \right)]$$

$$w_{1m} = - \frac{\sigma_{w1}}{\sqrt{2}\pi} \exp \left(- \frac{\bar{w}_{R1}^2}{2\sigma_{w1}^2} \right) + \frac{\bar{w}_{R1}}{2} [1 - \text{erf} \left(\frac{\bar{w}_{R1}}{\sqrt{2}\sigma_{w1}} \right)]$$

$$\bar{w}_{R1} = \begin{cases} \bar{w}_{D1} - \dot{z}_1, & \text{neutral and unstable conditions;} \\ - \bar{\eta}_1, & (= \text{given inversion layer depth growth rate}), \text{ stable} \end{cases}$$

\bar{w}_{D1} = mean vertical velocity on H_1 (terrain induced component excluded)

σ_{w1} = rms vertical turbulence on H_1 (= 0 in stable cases)

w_m = threshold of cumulus "root" updraft velocity on H_1

$\dot{z}_1 = \partial z_1 / \partial t$

$\psi, \sigma_c, \bar{w}_c$ (see Layer 2 equations)

$$\text{erf}(x) = \frac{2}{\sqrt{\pi}} \int_0^x e^{-t^2} dt$$

$$F_{0,1} = (\sigma_{T0} - \sigma_{T1}) \beta_{<c>1} + (1 - \sigma_{T0}) F_0$$

σ_{T0} = fraction of surface H_0 in given grid cell penetrated by terrain

$$F_0 =$$

Ozone:

$$F_0(O_3) = \langle O_3 \rangle_1 w_- \lambda_- - O_3 w_+ \lambda_+ (1 - \xi)(1 - \alpha)$$

$$- (1 - \alpha) \cdot \begin{cases} 0, & \text{if } \tilde{\zeta}_{NO} > v \xi O_3 \\ \frac{O_3 v^2 \xi - \tilde{\zeta}_{NO} v}{\beta_{O_3} + v}, & \text{otherwise} \end{cases}$$

Nitric Oxide:

$$F_0(NO) = \langle NO \rangle_1 w_- \lambda_- - NO w_+ \lambda_+ (1 - \xi)(1 - \alpha)$$

$$- (1 - \alpha) \cdot \begin{cases} \frac{\tilde{\zeta}_{NO} + v \xi (NO - O_3)}{1 + \beta_{NO}/v}, & \text{if } \tilde{\zeta}_{NO} > v \xi O_3 \\ \frac{v \xi NO}{1 + \beta_{NO}/v}, & \text{otherwise} \end{cases}$$

Nitrogen Dioxide:

$$F_0(\text{NO}_2) = \langle \text{NO}_2 \rangle_1 w_- \lambda_- - \text{NO}_2 w_+ \lambda_+ (1 - \xi)(1 - \alpha) - (1 - \alpha) \cdot \begin{cases} \frac{v\xi(\text{NO}_2 + \text{O}_3) + \tilde{\xi}_{\text{NO}_2}}{1 + \beta_{\text{NO}_2}/v} , & \text{if } \tilde{\xi}_{\text{NO}} > v\xi\text{O}_3 \\ \frac{v\xi\text{NO}_2 + \tilde{\xi}_{\text{NO}} + \tilde{\xi}_{\text{NO}_2}}{1 + \beta_{\text{NO}_2}/v} , & \text{otherwise} \end{cases}$$

all other species, χ .

$$F_0(\chi) = \langle \chi \rangle_1 w_- \lambda_- - \chi w_+ \lambda_+ (1 - \xi)(1 - \alpha) - (1 - \alpha)(v\xi\chi + \tilde{\xi}_\chi)(1 + \beta_\chi/v)^{-1}$$

$$\alpha = \frac{\psi\sigma_c}{w_+\lambda_+(1-\sigma_{T_0})} \left[-\frac{\bar{w}_2 - \bar{w}_c}{1 - \sigma_c} - f\theta/\Delta\theta \right]$$

See Layer 0 equations for specification of O_3 , NO , NO_2 , χ , w_+ , λ_+ , etc.

Layer 2

$$\begin{aligned} \frac{\partial}{\partial t} \langle c \rangle_2 + \langle c \rangle_2 \frac{\partial \ln V_2}{\partial t} + \mu_\lambda \langle u \rangle_2 \frac{\partial \langle c \rangle_2}{\partial \lambda} + \mu_\phi \langle v \rangle_2 \frac{\partial \langle c \rangle_2}{\partial \phi} \\ + \mu_\lambda \langle u' c' \rangle_2 \frac{\partial \ln V_2}{\partial \lambda} + \mu_\phi \langle v' c' \rangle_2 \frac{\partial \ln V_2}{\partial \phi} + \mu_\lambda \frac{\partial}{\partial \lambda} \langle u' c' \rangle_2 \\ + \mu_\phi \frac{\partial}{\partial \phi} \langle v' c' \rangle_2 + \frac{A}{V_2} [+ F_{1,2} - F_{2,2}] \\ = \langle R \rangle_2 + \langle S \rangle_2 \end{aligned}$$

$$V_2(\lambda, \phi, t) = a^2 \cos \phi \int_{\lambda - \Delta\lambda/2}^{\lambda + \Delta\lambda/2} \int_{\phi - \Delta\phi/2}^{\phi + \Delta\phi/2} \{ z_2(\lambda', \phi', t) - \text{MAX} [\hat{z}_T(\lambda', \phi'), z_1(\lambda', \phi', t)] \} d\phi' d\lambda'$$

$$\left. \begin{array}{l} \langle u'c' \rangle_2 \\ \langle v'c' \rangle_2 \end{array} \right\} \text{ subgrid scale fluxes of } c \text{ (see Part 1, Section 7)}$$

$\langle R \rangle_2$ = all chemical, rainout and washout processes in Layer 2

$\langle S \rangle_2$ = source emissions in Layer 2 (if any)

$\langle u \rangle_2, \langle v \rangle_2$ = Layer 2 averaged winds.

$$F_{2,2} = \frac{\sigma_c(\bar{w}_2 - \bar{w}_c)}{1 - \sigma_c} (\bar{c}_c - \langle c \rangle_2) + \langle c \rangle_2 \frac{\partial \bar{z}_2}{\partial t} - \frac{f_\theta}{\Delta\theta} [- (1 - \sigma_c) \langle c \rangle_3 - \sigma_c \bar{c}_c + \langle c \rangle_2]$$

$$F_{1,2} = \sigma_{T1} \beta \langle c \rangle_2 + (1 - \sigma_{T1}) [\langle c \rangle_1 w_1 + (\langle c \rangle_1 - \langle c \rangle_2) w_{1m} + (\langle c \rangle_2 - \langle c \rangle_1) \bar{w}_{D1}]$$

w_1, w_{1m} , see Layer 1; \bar{w}_{D1} , see Part 1, Eq. 4-44c)

σ_c = fractional area coverage of cumulus clouds

\bar{w}_c = mean upward velocity in cumulus clouds

$\frac{f_\theta}{\Delta\theta}$ = turbulent entrainment rate of inversion air into mixed layer

\bar{w}_2 = mean vertical velocity (mean of both terrain induced component w_{T2} and divergent component w_{D2})

$\frac{\partial \bar{z}_2}{\partial t} = \dot{z}_2$ = local time rate of change of mixed layer top

$$\bar{c}_c = (1 - \psi) \langle c \rangle_2$$

ψ = fraction of cloud air from surface layer

$$0 \leq \psi \leq 1 \text{ and } \psi \leq w_+ \lambda_+ (1 - \sigma_{T0}) / (V_c \sigma_c)$$

$$V_c = - \frac{\bar{w}_2 - \bar{w}_c}{1 - \sigma_c} - f\theta/\Delta\theta$$

$c, c', \xi, w_+, \lambda_+ =$ See Layer 0 equations

Layer 3

$$\begin{aligned} & \frac{\partial \langle c \rangle_3}{\partial t} + \langle c \rangle_3 \frac{\partial \ln V_3}{\partial t} + \mu_\lambda \langle u \rangle_3 \frac{\partial \langle c \rangle_3}{\partial \lambda} + \mu_\phi \langle v \rangle_3 \frac{\partial \langle c \rangle_3}{\partial \phi} \\ & + \mu_\lambda \langle u' c' \rangle_3 \frac{\partial \ln V_3}{\partial \lambda} + \mu_\phi \langle v' c' \rangle_3 \frac{\partial \ln V_3}{\partial \phi} \\ & + \mu_\lambda \frac{\partial \langle u' c' \rangle_3}{\partial \lambda} + \mu_\phi \frac{\partial \langle v' c' \rangle_3}{\partial \phi} + \frac{A}{V_3} [F_{2,3} - F_{3,3}] = \langle R \rangle_3 \end{aligned}$$

$$V_3(\lambda, \phi, t) = a^2 \cos \phi \int_{\lambda - \Delta\lambda/2}^{\lambda + \Delta\lambda/2} \int_{\phi - \Delta\phi/2}^{\phi + \Delta\phi/2} [z_3(\lambda', \phi', t) - z_2(\lambda', \phi', t)] d\phi' d\lambda'$$

$z_2(\lambda, \phi, t) =$ mixed layer top

$z_3(\lambda, \phi, t) =$ model top

$\left. \begin{array}{l} \langle u' c' \rangle_3 \\ \langle v' c' \rangle_3 \end{array} \right\}$ subgrid scale flux of c (see Part 1, Section 8)

$\langle R \rangle_3 =$ all chemical (wet and dry) rainout and washout processes

$\langle u \rangle_3, \langle v \rangle_3 =$ layer averaged winds

$$F_{2,3} = \sigma_c \left[\frac{\bar{w}_2 - \bar{w}_c}{1 - \sigma_c} + f\theta/\Delta\theta \right] (\bar{c}_c - \langle c \rangle_3) + \langle c \rangle_3 \frac{\partial \bar{z}_2}{\partial t}$$

$$F_{3,3} = \begin{cases} \langle c \rangle_3 \frac{\partial z_3}{\partial t} , & \text{if } \overline{dH_3}/dt \leq 0 ; \\ (c_\infty - \langle c \rangle_3) \overline{dH_3}/dt + \langle c \rangle_3 \frac{\partial z_3}{\partial t} , & \text{otherwise} \end{cases}$$

c_∞ = concentration of species c above z_3

$\overline{dH_3}/dt$ = given volume flux through model top surface

$$\bar{c} = (1 - \psi)\langle c \rangle_2 + \psi[\xi c' + (1 - \xi)c]$$

where c' and c are defined with the Layer 0 variables.

Layer 0

$$\langle O_3 \rangle_0 = (1 - \xi) O_3 + \xi O_3'$$

$$O_3 = \frac{w_{\lambda_-} \langle O_3 \rangle_1}{w_{\lambda_+} + (1 - \xi) \beta_{O_3}}$$

$$O_3' = \begin{cases} 0, & \text{if } \tilde{\xi}_{NO} > \nu \xi O_3 \\ \frac{O_3 \nu - \tilde{\xi}_{NO} / \xi}{\beta_{O_3} + \nu} , & \text{otherwise} \end{cases}$$

$$\langle NO \rangle_0 = (1 - \xi) NO + \xi NO'$$

$$NO = \frac{w_{\lambda_-} \langle NO \rangle_1}{w_{\lambda_+} + (1 - \xi) \beta_{NO}}$$

$$NO' = \begin{cases} \frac{\tilde{S}_{NO}/\xi + v(NO - O_3)}{\beta_{NO} + v} & , \text{ if } \tilde{S}_{NO} > v\xi O_3 \\ \frac{vNO}{\beta_{NO} + v} & , \text{ otherwise} \end{cases}$$

$$\langle NO_2 \rangle_0 = (1 - \xi) NO_2 + \xi NO'_2$$

$$NO_2 = \frac{w_- \lambda_- \langle NO_2 \rangle_1}{w_+ \lambda_+ + (1 - \xi) \beta_{NO_2}}$$

$$NO'_2 = \begin{cases} \frac{NO_2 v + O_3 v + \tilde{S}_{NO_2}/\xi}{\beta_{NO_2} + v} & , \text{ if } \tilde{S}_{NO} > v\xi O_3 \\ \frac{NO_2 v + (\tilde{S}_{NO} + \tilde{S}_{NO_2})/\xi}{\beta_{NO_2} + v} & , \text{ otherwise} \end{cases}$$

Species χ other than O_3 , NO , and NO_2 :

$$\langle \chi \rangle_0 = (1 - \xi) \chi + \xi \chi'$$

$$\chi = \frac{w_- \lambda_- \langle \chi \rangle_1}{w_+ \lambda_+ + (1 - \xi) \beta_\chi}$$

$$\chi' = \frac{\chi v + \tilde{S}_\chi/\xi}{\beta_\chi + v}$$

Parameters:

$$\lambda_+ = \frac{1}{2} \left[1 - \operatorname{erf} \left(\frac{\dot{z}_0}{\sqrt{2} \sigma_{w_0}} \right) \right]$$

$$\lambda_- = 1 - \lambda_+$$

$$-w_- = -\dot{z}_0 - \frac{\sigma_{w_0}}{\sqrt{2\pi}} \exp\left(-\frac{\dot{z}_0^2}{2\sigma_{w_0}^2}\right) + \frac{\dot{z}_0}{2} \left[1 - \operatorname{erf}\left(\frac{\dot{z}_0}{\sqrt{2}\sigma_{w_0}}\right)\right]$$

$$w_+ = w_- - \dot{z}_0$$

$$v = u^* \text{ (plume entrainment velocity)}$$

$$\xi = \frac{v\xi}{w_+\lambda_+}$$

$$\xi = \text{plume volume fraction}$$

$$\sigma_{w_0} = \text{rms vertical turbulent velocity on } H_0$$

SECTION 2

PROCESSOR P1

GENERAL DISCUSSION

This Processor performs a number of standard operations on the raw rawin data to put them into the forms required by the higher level processors in the network. It operates on the rawin data only. We assume that the "raw" rawin record at the m-th station consists of a sequence of I_m "vectors"

$$[SPD, DIR, T, TD, p]_{im}, i=1, \dots, I_m \quad (1-1)$$

where the i-th vector represents the wind speed (m/sec), direction (degrees), temperature ($^{\circ}C$), and dew point depression ($^{\circ}C$) at pressure level p (millibars) at a given station m. The number of observation levels I_m in each record can vary from station to station and from hour to hour. The steps necessary to convert the raw data into the desired forms follow.

Step 1

Convert the speed and direction $(SPD, DIR)_{im}$ into cartesian components (u, v) at each level i and at each station m by

$$u_{im} = - (SPD_{im}) \cdot \sin \theta_{im} \quad (1-2a)$$

$$v_{im} = - (SPD_{im}) \cdot \cos \theta_{im} \quad (1-2b)$$

where

$$\theta_{im} = (DIR_{im}) \cdot (2\pi/360). \quad (1-3)$$

These values must be processed further (in step 10) before recording in the PIF.

Step 2

Convert the temperature and dew point depression TD into the water vapor mixing ratio q (mass of water per total mass of air) at each level i and station m by

$$q_{im} = \frac{0.622e_{im}}{p_{im} - e_{im}} \quad (1-4)$$

where

$$e_{im} = e_o \exp\left[\frac{L}{R} \left(\frac{1}{T_o} - \frac{1}{T_{Dim}}\right)\right] \quad (1-5)$$

$$R = 0.461 \text{ joule g}^{-1} \text{ } ^\circ\text{K}^{-1}$$

$$L = 2500 \text{ joule g}^{-1} \text{ (latent heat of vaporization)}$$

$$e_o = 40 \text{ mb (saturation vapor pressure at } T_o)$$

$$T_o = 29 + 273 = 302^\circ\text{K (reference temperature)}$$

$$T_{Dim} = T_{im} - TD_{im} + 273 \text{ (dew point temperature at level } i, \text{ station } m)$$

$$p_{im} = \text{pressure (mb) at level } i, \text{ station } m.$$

The mixing ratio q_{im} and dew point T_{Dim} are outputs of this stage and require further processing in Step 6.

Step 3

Compute the relative humidity RH_{im} for each level i and station m by

$$RH_{im} = q_{im} \cdot \frac{p_{im} - e_{sm}}{0.622e_{sm}} \quad (1-6)$$

where e_{sm} is found from (1-5) by replacing the dew point T_{Dim} with the temperature T_{im} .

Step 4

Convert the pressure p_{im} at the levels $i=1,2,\dots,I_m$ of the upper air observation at station m to altitudes z_{im} (AGL) by first converting the temperature measurements T_{im} to virtual temperatures

$$T_{vim} = (T_{im} + 273) \cdot (1 + 0.61q_{im}). \quad (1-7a)$$

Then

$$z_{im} = \frac{R_d}{g} \sum_{j=1}^i [\frac{1}{2}(T_{vjm} + T_{v(j-1)m})] \ln \frac{p_{(j-1)m}}{p_{jm}} \quad (1-7b)$$

where

- p_{jm} = pressure at level j ($j=0$ represents ground level) at station m ;
- z_{jm} = elevation (AGL) of observation level j at station m ;
- g = 9.8 m sec^{-2} (gravity);
- R_d = $287 \text{ m}^2 \text{ sec}^{-2} \text{ } ^\circ\text{K}^{-1}$ (gas constant for dry air)
- T_{vjm} = virtual temperature ($^\circ\text{K}$) at level j , station m .

Step 5

Let \hat{z}_m be the known elevation (MSL in meters) of the m -th rawin station, and let p_{om} and T_{vom} be the station pressure and virtual temperature. Using (1-7) we now calculate the sea-level pressure at station m :

$$\begin{aligned} p_{-1m} &= \text{sea-level pressure at station } m \text{ (in millibars)} \\ &= p_{om} \exp \left[\frac{\hat{z}_m g}{R_d T_{vom}} \right]; \end{aligned} \quad (1-8)$$

and we calculate the geopotential height ϕ_{om} (m^2/sec^2) of the 1000 mb surface:

$$\phi_{om} = g\hat{z}_m + R_d T_{vom} \ln \frac{p_{om}}{1000}. \quad (1-9)$$

Using the ϕ_{om} value from the previous observation time, say, $t-\Delta t$, compute

$$\dot{\phi}_{om} = [\phi_{om}(t) - \phi_{om}(t-\Delta t)]/\Delta t \quad (1-9a)$$

Record ϕ_{om} and $\dot{\phi}_{om}$ in the PIF.

Step 6

At this stage the virtual temperature, relative humidity, dew point and mixing ratio are known at each elevation z_i in the sounding (from step 3). These data should now be interpolated to give semi-continuous soundings, e.g., $T_m(z)$ and $q_m(z)$ of virtual temperature and mixing ratio at each rawin station m . That is, we convert

$$(T_{Dim}, z_{im}) \Rightarrow T_{Dm}(z) \quad (1-10a)$$

$$(T_{vim}, z_{im}) \Rightarrow T_{vm}(z), \quad (1-10a')$$

$$(q_{im}, z_{im}) \Rightarrow q_m(z) \quad (1-10b)$$

$$(RH_{im}, z_{im}) \Rightarrow RH_m(z) \quad (1-10c)$$

where

$$z = \hat{z}_m + n\Delta z, \quad n=0, \dots, m; \quad (1-10d)$$

$\Delta z=50$ meters, and

$$m = \frac{5000 - \hat{z}_m}{50}. \quad (1-10e)$$

The third-order interpolation scheme described in Processor P8 (see Eqs. 8-56, 8-60, ...69, and 8-70) should be used in performing the transformations indicated by Eqs. (1-10). Record the T_m , q_m , T_{Dm} , and RH_m values for each of the z given by (1-10d) in the PIF.

Step 7

The pressure-height pairs (p_{im}, z_{im}) should be transformed into a semi-continuous sounding as in Step 6 above. In this task the sequence begins with the sea-level pressure, followed by the station pressure, and the observation levels aloft, i.e.,

$$(p_{-1m}, 0), (p_{0m}, \hat{z}_m), (p_{1m}, z_{1m}) \dots (p_{Im}, z_{Im}) \Rightarrow p_m(z), \quad (1-11a)$$

where

$$z=n\Delta z, \quad n=0, 1, \dots, 100; \quad (1-11b)$$

and $\Delta z=50$ meters. In performing the interpolation (1-11a), an exponential formula should be employed based on the hydrostatic condition

$$\frac{\Delta p}{\Delta z} = - \frac{pg}{R_d T_v}. \quad (1-12)$$

Record the p_m values at each z given by (1-11b) in the PIF.

Step 8

Using the $p_m(z)$ profile obtained in Step 7, determine the geopotential ($m^2 \text{sec}^{-2}$) of the 850, 700, and 500 millibar surfaces at each station m . For example,

$$\phi_{(850)m} = g z_{850} \quad (1-13)$$

where g is gravity and z_{850} is the elevation (MSL) that satisfies

$$p_m(z_{850}) = 850 \text{ mb.} \quad (1-14)$$

By the same process compute $\phi_{(700)m}$ and $\phi_{(500)m}$.

Step 9

Using the virtual temperature profile $T_{vm}(z)$ from step 6, Eq. 1-10a above, and the pressure profile $p_m(z)$ from Step 7, Eq. 1-11, compute the potential temperature profile $\theta_m(z)$ for each level z defined by (1-10d):

$$\theta_m(z) = T_m(z) \left(\frac{1000}{p_m(z)} \right)^{0.286} \quad (1-15)$$

where p_m is in millibars, as above, and T_m is in degrees Kelvin. Now compute the air density at each of the same levels z using

$$\rho_m(z) = \frac{p_m(z)}{R_d T_{vm}(z)} \cdot 10^2 \quad (1-16)$$

where p_m is in millibars and $R_d=287 \text{ m}^2\text{sec}^{-2} \text{ }^\circ\text{K}^{-1}$, T_{vm} is in $^\circ\text{K}$, and $\rho=\text{kg m}^{-3}$. From θ and ρ compute the profile $\sigma_{sm}(z)$ of static stability from

$$\sigma_{sm}(z) = \frac{-[\theta_m(z+\Delta z)-\theta_m(z-\Delta z)] \cdot 10^{-2}}{\rho_m(z)\theta_m(z)[p_m(z+\Delta z)-p_m(z-\Delta z)]}. \quad (1-17)$$

With p in millibars and ρ in kg m^{-3} , σ_s has units of $\text{m}^4\text{sec}^2\text{kg}^{-2}$. Record the profiles $\theta_m(z)$, $\rho_m(z)$ and $\sigma_{sm}(z)$ in the PIF for each rawin station m .

Step 10

Interpolate the wind components u_{im} and v_{im} of Eq. (1-2) above to obtain the profile

$$u_{im} \rightarrow \hat{u}(x_m, z) \quad (1-18a)$$

$$v_{im} \rightarrow \hat{v}(x_m, z) \quad (1-18b)$$

where z takes the values given by (10d).

Stage INT

The raw rawin data are generally available only at 12-hour intervals, but the output variables produced by this processor, P1, are required each hour by processors further along in the network. Therefore, an interpolation of all output variables must be performed to provide values at hourly intervals. The specific interpolation formula that is used for this purpose is left to the discretion of the user.

Table 1-1 summarizes the inputs and outputs of each step of Processor P1 and Figure 1-3 illustrates the processor and its data interfaces.

Table 1-1 Summary of input and output variables
of each step of Processor P1.

Input Variable	Description	Source	Step	Output Variable	Description
SPD_{im}	wind speed (ms^{-1}) at level i at rawin station m.	RAW	1	$u_{im}(t_k)$	east-west wind component at level i, station m, hour t_k .
DIR_{im}	Wind direction (compass degrees) at level i at rawin station m	RAW		$v_{im}(t_k)$	north-south wind component at level i, station m, hour t_k .
P_{im}	pressure (mb) at level i, station m.	RAW	2	$q_{im}(t_k)$	mixing ratio (dimensionless) at level i, station m, hour t_k .
TD_{im}	dew point depression ($^{\circ}C$) at level i, station m.	RAW		$T_{Dim}(t_k)$	dew point temperature at level i, station m, hour t_k .
T_{im}	temperature ($^{\circ}C$) at level i, station m.	RAW			
P_{im}	see above	RAW	3	$RH_{im}(t_k)$	relative humidity at level i, station m, hour t_k .
T_{im}	see above	RAW			
q_{im}	see above	Step 2			
T_{im}	see above	RAW	4	$T_{vim}(t_k)$	virtual temperature ($^{\circ}C$) at level i, station m, hour t_k .
q_{im}	see above	Step 2			
P_{im}	see above	RAW		$z_{im}(t_k)$	elevation (AGL) of level i at station m, hour t_k .

Table 1-1 Summary of input and output variable
of each step of Processor P1. (Continued)

Input Variable	Description	Source	Step	Output Variable	Description
\hat{z}_m	elevation (meters, msl) of rawin station m	RAW	5	$\phi_{om}(t_k)$	geopotential (m^2s^{-2}) of 1000 mb surface at station m, hour t_k .
p_{om}	station pressure (mb) at station m.	RAW		$\dot{\phi}_{om}(t_k)$	time rate of change (m^2s^{-3}) of geopotential of 1000 mb surface at station m.
T_{vom}	virtual temperature ($^{\circ}C$) at station m.	Step 4			
T_{vim}	see above	Step 4	6	$T_{vm}(z, t_k)$	Temperature, mixing ratio, relative humidity, and dew point profiles at station m resolved to $\Delta z=50m$ as prescribed by Eqs. (1-10d,e) at hour t_k .
q_{im}	see above	Step 2		$q_m(z, t_k)$	
RH_{im}	see above	Step 3		$RH_m(z, t_k)$	
z_{im}	see above	Step 4		$T_{Dm}(z, t_k)$	
T_{Dim}	see above	Step 2			
p_{im}	see above	RAW	7	$p_m(z, t_k)$	pressure (mb) at elevation z (msl) above station m, resolved to $\Delta z=50m$ as prescribed by Eqs. (1-10d,e) at hour t_k .
z_{im}	see above	Step 4			
$p_m(z)$	pressure at elevation z (MSL) over station m.	Step 7	8	$\phi_{(850)m}$ $\phi_{(700)m}$ $\phi_{(500)m}$	geopotential (m^2sec^{-2}) of the 850, 700, and 500mb surfaces at station m.
$p_m(z)$	see above	Step 7	9	$\theta_m(z)$	potential temperature ($^{\circ}K$) at elevation z over station m, resolved to $\Delta z=50m$ as prescribed by Eqs. (1-10d,e).
$T_{vm}(z)$	see above	Step 6		$\rho_m(z, t_k)$	air density (kgm^{-3}) at elevation z (resolved as above) over station m, hour t_k .
				$\sigma_{sm}(z, t_k)$	static stability ($m^4s^2kg^{-2}$) at elevation z at station m, hour t_k .

Table 1-1. Summary of input and output variables
of each step of Processor P1. (Concluded).

Input Variable	Description	Source	Step	Output Variable	Description
u_{im}	see above	Step 1	10	$\hat{u}(\tilde{x}_m, z, t_k)$	east-west and north- south wind
v_{im}	see above	Step 1		$\hat{v}(\tilde{x}_m, z, t_k)$ [also \hat{u}_m, \hat{v}_m]	at elevation z (as given by Eqs. 1-10d,e at location \tilde{x}_m of station m , at hour t_k .

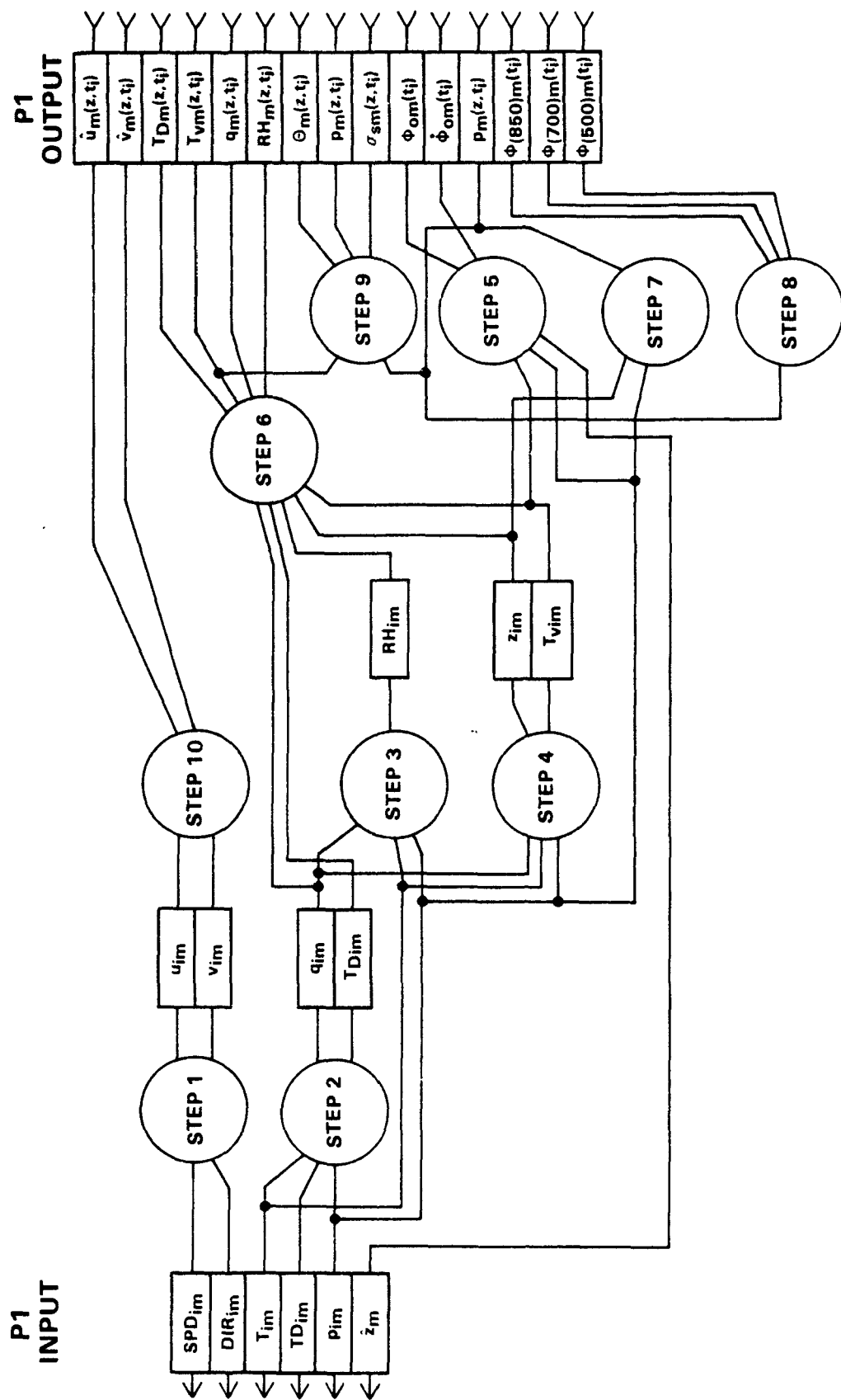


Figure 1-3. Illustration of Processor P1 and its input and output interfaces with the processor network.

SECTION 3

PROCESSOR P2

GENERAL DISCUSSION

This processor determines initial, upper and lateral boundary conditions on all of the pollutant species simulated by the regional model. Presently, it is impossible to estimate these conditions with an accuracy anywhere near that of available emissions estimates, because: (1) the pollutant monitoring data from which the initial and boundary conditions must be derived are few and nonuniformly distributed, (2) no measurements are routinely available aloft, and (3) most of the intermediate pollutant species that must be treated to simulate the chemistry properly are not measured at all. In addition, the model requires conditions on the cell averaged concentrations but only point measurements are made at the monitoring sites.

The problems caused by the paucity of data can be mitigated by initializing the model on a "clean" day, such as a day immediately following the passage of a cold front, and by choosing a model domain that is large enough that the quantities of pollutants emitted by sources just outside the model boundaries are small compared to those generated within the simulation area itself. In such a case, we can use "clean atmosphere" conditions for the initial, upper and lateral boundary values of each species. Table 2-1 lists these values for each of the 23 pollutants modeled by the Demerjian-Schere (1979) kinetics scheme that we have been using during the development phase of the regional model.

Table 2-1. Pollutant species concentrations (ppm) taken to be representative of "clean" atmospheric conditions*.
(Notation: $1.000-01 = 10^{-1}$.)

NO	4.499-04	NO2	1.404-03	CO	1.010-01	HC1	1.084-03
HC2	3.390-03	HC3	7.679-03	HC4	6.911-04	O3	3.522-02
HN02	3.473-05	HN03	7.215-04	PAN	3.808-04	RN03	1.004-06
H2O2	8.784-05	O	1.284-10	NO3	5.434-07	HO	3.734-07
HO2	2.078-05	HO4N	7.583-06	RO	5.848-08	RO2	5.578-05
R2O	2.452-09	R102	1.550-05	R202	5.319-06		

*Values reported here were obtained by initializing the Demerjian-Schere (1979) 23-species kinetics mechanism with the following species concentrations and allowing reactions for 90 minutes in full sun conditions:

NO = .001ppm, NO₂ = .002ppm, total non-methane hydrocarbon = .05ppm, CO = .1ppm, O₃ = .02ppm, all other species = 0ppm.

Hydrocarbon classes are as follows:

HC1 = olefin, HC2 = paraffin, HC3 = aldehydes, HC4 = aromatics. Initial values of each of these lumped species were obtained from the total nonmethane hydrocarbon concentration using the speciation method suggested by Demerjian (1983).

The problems caused by the unavailability of volume-averaged concentration data cannot be eliminated because there is no unique relationship between the concentration values measured at one or several discrete points within a given volume of space and the concentration averaged over that volume. This is the so-called subgrid-scale closure problem encountered in all modeling studies in which it is impossible to choose a grid size small enough to resolve the smallest spatial variations in the simulated variables. In Part 1, Section 5, we developed a crude subgrid-scale closure scheme for use in treating the pollution chemistry. Proceeding along lines similar to those described there we could formulate an approximate way of extracting volume-averaged concentration estimates from point measurements. However, we will not attempt this here because the improvement in accuracy gained in the initial concentration fields would probably not be significant enough to warrant the development and implementation efforts. Perhaps future modeling studies can investigate this problem in detail if the need is great.

In the remainder of this section we outline a procedure for obtaining rough estimates of initial and boundary conditions on pollutant concentrations in situations where the "clean atmosphere" assumption does not apply. An important point to note in the preparation of initial and boundary conditions is that, due to inaccuracies and uncertainties in the methods used, the set of concentrations obtained for any given grid cell or boundary point will generally not be consistent with chemical equilibrium conditions. For example, if one deduces concentration values for O_3 , NO , NO_2 and olefin from the monitoring data and assigns "nominal" or zero values to all the other species included in the chemical kinetics scheme, one would find upon initializing the model with these values that a period of rapid chemical

transformations immediately ensues. These rapid changes indicate that the concentration conditions selected for the initial state do not represent a state near equilibrium. These spurious reactions are an artifact of the chosen set of concentrations and are not representative of the chemical activity that occurs just after the initial moment. This is analogous to the initialization problem in meteorological models where failure to prescribe an initial state that is in geostrophic balance results in the generation of spurious gravity waves.

The transient concentration variations excited by errors in the initial state diminish the accuracy of the model's predictions within some finite period following the initial instant t_0 . They also exact a significant penalty in computer time. Because when the chemical state is far from equilibrium, the mathematical algorithm in the model that handles the chemical rate equation must utilize many small time steps to track the approach of the state of the system to equilibrium. Since this operation must be performed initially at every grid point in the model and at all boundary points at all times where the boundary condition specification is inexact, a considerable portion of the computation time required by the model can be wasted on this fictitious phenomenon. The remedy is to use the initial concentrations deduced from the monitoring data as the initial state in a batch reactor model; to run that model for a time long enough for the chemical state to settle down to a point where changes are occurring relatively slowly (say, time scales ~ 10 min); and then to use the concentrations of each species given by the batch reactor model at that point as the initial conditions in the regional model. The same procedure should be used to obtain the upper and lateral boundary conditions.

Stage LBC: Estimating lateral boundary conditions from monitoring data

- (1) Collect hourly surface monitoring data for each species $x_i(\text{ppm})$ $i = 1, \dots, \text{IMAX}$ from all stations within 20 km either side of each of the regional model's four lateral boundaries. Each station within this 40 km wide boundary zone is treated as though it lies on the model boundary at the point closest to the station location.
- (2) Use a cubic spline or other acceptable interpolation formula to estimate concentrations $\hat{x}_i(\lambda_B, \phi_B, t)(\text{ppm})$ at each grid point (λ_B, ϕ_B) on the boundary. Here (λ, ϕ) denotes the longitude and latitude of a cell center on the boundary of the regional model domain.
- (3) Using the functions \hat{x}_i obtained in step 2, estimate layer averaged concentrations along the boundaries as follows:

$$\langle x_i(\lambda_B, \phi_B, t) \rangle_n = B_n \hat{x}_i(\lambda_B, \phi_B, t), \quad \begin{matrix} n=1,2,3 \\ i=1, \dots, \text{IMAX} \end{matrix} \quad (2-1)$$

where the B_n are empirical constants to be estimated from the NEROS field experiment data.

- (4) For each hour t_m , each boundary point (λ_B, ϕ_B) , and each layer n perform the batch reactor equilibration process, described in the introduction to this section, to the set of concentrations $\langle x_i(\lambda_B, \phi_B, t) \rangle_n$, $i=1, \dots, \text{IMAX}$ given by (2-1). Record the results in the ICBC portion of the model input file MIF (units = ppm for each species).

STAGE IC: Estimating initial conditions from monitoring data

- (1) Collect surface monitoring data for all pollutant species at all stations within the regional model domain at the initial hour t_0 (=1200 EST) of

the period to be simulated. Noon is chosen as the initialization hour because, at this time, pollutants are usually distributed nearly uniformly in the mixed layer and initial values for Layers 1 and 2 can be equated with minimum error.

- (2) In places where more than one monitoring station lies within a grid cell, compute a weighted average of the reported values taking into account the proximity of each station to sources and the distribution of land use types within that cell. For example, if one monitoring site is in a rural area and 70% of that cell is in rural land use, the rural station would be given a weight of 0.7 in computing the cell average concentration.
- (3) Fit a two-dimensional function to the finite set of cell averaged concentrations obtained in step 2 and from this function derive values of the concentration of each measured pollutant species at all grid cells in the model region.
- (4) Subject each set of concentrations $i=1, \dots, \text{IMAX}$ obtained in step 3 to the batch reactor equilibration process. Call the results of this operation $x_i(\lambda, \phi, t_0)$ where (λ, ϕ) ranges over all grid points in the model region. Now record the following initial layer averaged concentrations (ppm) in the ICBC portion of MIF:

$$\langle x_i(\lambda, \phi, t_0) \rangle_1 = x_i(\lambda, \phi, t_0) \quad (2-2)$$

$$\langle x_i(\lambda, \phi, t_0) \rangle_2 = x_i(\lambda, \phi, t_0) \quad (2-3)$$

$$\langle x_i(\lambda, \phi, t_0) \rangle_3 = \xi_i x_i(\lambda, \phi, t_0) \quad (2-4)$$

where ξ_i is an empirical constant to be derived from the NEROS field experiment data.

Stage UBC: Upper boundary conditions

- (1) In the first generation model we will use the "clean" atmosphere species concentrations listed in Table 2-1 for the upper boundary conditions x_{∞} for all cells and all hours. Record these in the ICBC portion of MIF(units = ppm for all species), i.e.

$$x_{\infty,i}(\lambda, \phi, t) = x_{\text{CLEAN}, i} \quad \begin{array}{l} i=1, \dots, \text{IMAX}; \\ \text{all } (\lambda, \phi, t) \end{array} \quad (2-5)$$

Table 2-2 summarizes the inputs and outputs of Processor P2, and Figure 2-1 illustrates the processor and its interfaces with the processor network.

Table 2-2 Summary of input and output variables of each stage of Processor P2.

Input Variable	Description	Source	Stage	Output Variable	Description
$x_{ik}(t_m)$	concentration (ppm) of i-th pollutant at hour t_m measured at surface monitoring station $k=1, \dots, K$.	RAW	LBC	$\langle x_i(\lambda_B, \phi_B, t_m) \rangle_n$	average concentration (ppm) of i-th pollutant in layer $n=1,2,3$ at boundary cell (λ_B, ϕ_B) at hour t_m .
$x_{ik}(t_m)$	see Stage LBC input.	RAW	IC	$\langle x_i(\lambda, \phi, t_0) \rangle_n$	average concentration (ppm) of i-th pollutant in layer $n=1,2,3$ in grid cell (λ, ϕ) at the initial instant t_0 .
$x_i(t_m)$	see Stage LBC input.	RAW	UBC	$x_{\infty,i}(\lambda, \phi, t_m)$	concentration (ppm) of i-th pollutant at top surface of model over grid cell (λ, ϕ) at hour t_m .

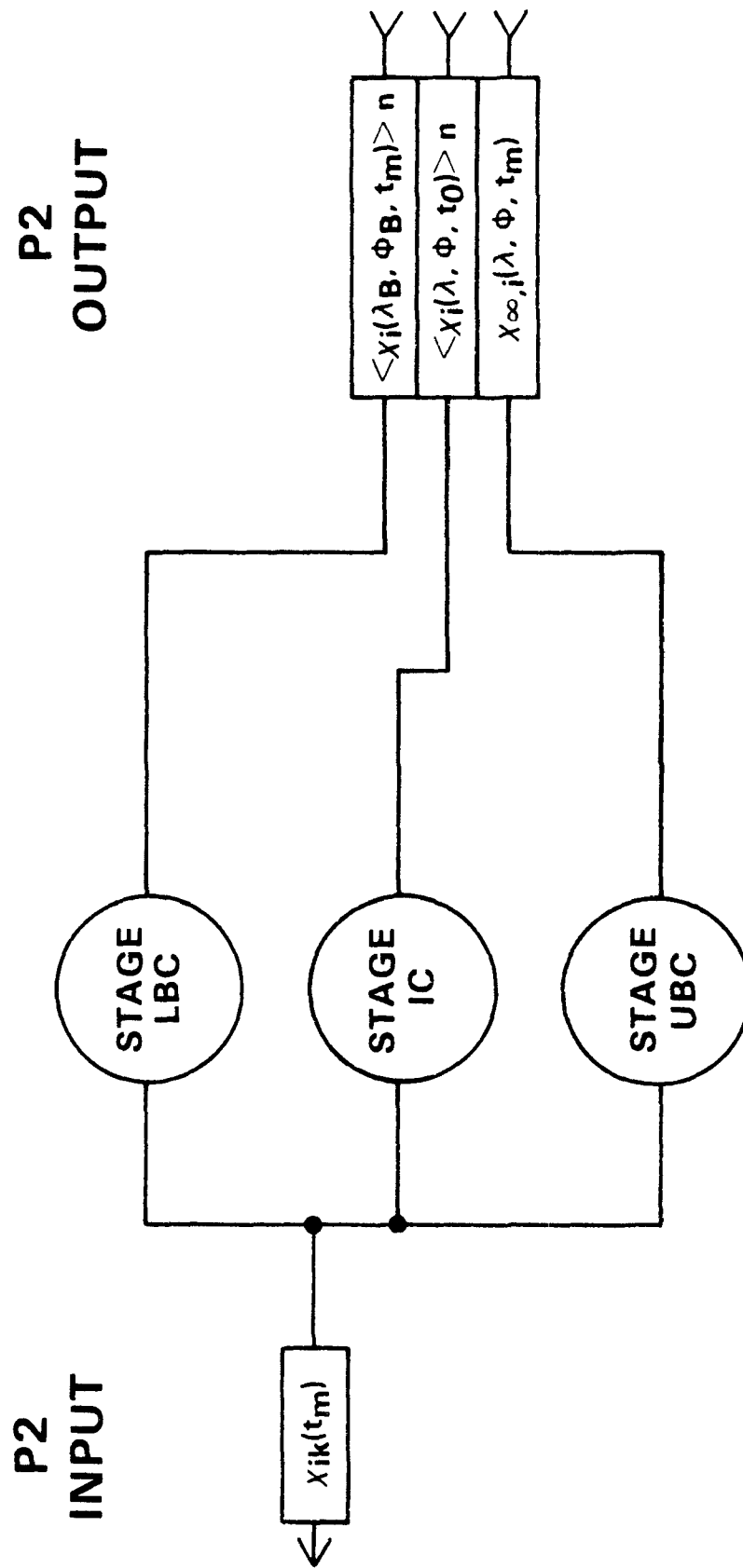


Figure 2-1. Illustration of Processor P2 and its input and output interfaces with the processor network.

SECTION 4
PROCESSOR P3

GENERAL DISCUSSION

This processor performs standard operations on the surface meteorological data to put them into forms required by the higher level processors in the network. The surface and rawin data are treated in separate processors to facilitate future alterations in the data analyses and to permit easier incorporation of additional data.

We assume that at given time intervals (not necessarily hourly intervals) the surface observations consist of the set

$$[SPD, DIR, T, TD, p]_n$$

where n denotes the surface station, whose location is x_n ; and the other variables represent wind speed (ms^{-1}), direction (compass degrees), temperature ($^{\circ}C$), dew point depression ($^{\circ}C$) and station (not sea-level) pressure (mb).

Step 1

Convert the wind speed and direction into north-south and east-west components as follows:

$$\hat{u}_n = \hat{u}(x_n) = - SPD_n \cdot \sin \theta_n \quad (3-1a)$$

$$\hat{v}_n = \hat{v}(x_n) = - SPD_n \cdot \cos \theta_n \quad (3-1b)$$

where

$$\theta_n = \text{DIR}_n \cdot (2\pi/360).$$

The components (\hat{u}_n, \hat{v}_n) are outputs of this processor for each time interval.

Step 2

Convert the temperature and dew point depression to mixing ratio, dew point temperature, relative humidity and virtual temperature as follows:

$$q_n = \frac{0.622e_n}{p_n - e_n} \quad (= \text{mixing ratio}) \quad (3-2a)$$

where

$$e_n = e_o \exp\left[\frac{L}{R} \left(\frac{1}{T_o} - \frac{1}{T_{Dn}}\right)\right] \quad (3-2a')$$

$$R = 0.461 \text{ joule g}^{-1} \text{ } ^\circ\text{K}^{-1}$$

$$L = 2500 \text{ joule g}^{-1}$$

$$e_o = 40\text{mb (saturation vapor pressure at temperature } T_o)$$

$$T_o = 302 \text{ } ^\circ\text{K}$$

$$p_n = \text{station pressure (mb)}$$

and

$$T_{Dn} = T_n - TD_n + 273 \quad (= \text{dew point temperature}) \quad (3-2b)$$

$$\text{RH}_n = q_n \frac{p_n - e_{sn}}{0.622e_{sn}} \quad (= \text{relative humidity}) \quad (3-2c)$$

where e_{sn} is obtained from (3-2a') by replacing the dew point temperature T_{Dn} in the formula with the dry bulb temperature T_n (expressed in $^\circ\text{K}$);

$$T_{vn} = T_n (1 + 0.61q_n) \quad (= \text{virtual temperature}) \quad (3-2d)$$

where T_n (and hence T_{vn}) is in $^{\circ}\text{K}$.

The mixing ratio q_n (dimensionless) and the relative humidity RH_n (dimensionless) can be recorded in PIF (they are outputs of this processor). Before recording the dew point and virtual temperature in PIF, they should be converted to degrees Celsius as follows:

$$T_{Dn} (^{\circ}\text{C}) = T_{Dn} (^{\circ}\text{K}) - 273$$

$$T_{vn} (^{\circ}\text{C}) = T_{vn} (^{\circ}\text{K}) - 273$$

where $T_{Dn} (^{\circ}\text{K})$ is from Eq. 3-2b and $T_{vn} (^{\circ}\text{K})$ is from (3-2d).

Step 3

Let \hat{z}_n be the elevation (meters, MSL) of surface station n . Compute the geopotential of the 1000 mb surface

$$\phi_{on} = g\hat{z}_n + R_d T_{vn} \ln \frac{p_n}{1000} \quad (3-3)$$

where T_{vn} is from (3-2d) above (in $^{\circ}\text{K}$) and $R_d = 287 \text{ m}^2 \text{s}^{-2} \text{ } ^{\circ}\text{K}^{-1}$. Using the value of ϕ_{on} from the previous time interval, estimate the time rate of change of ϕ_{on} by

$$\dot{\phi}_{on} = [\phi_{on}(t) - \phi_{on}(t-\Delta t)]\Delta t^{-1} \quad (3-4)$$

Compute the sea-level pressure p_{s1} at each station site $x_n, n=1,2,\dots,N$ as follows.

$$p_{s1,n} = p_n \exp \left[\frac{g\hat{z}_n}{R_d T_{vn}} \right] \quad (3-5)$$

where p_n is the station pressure (mb) and all other variables have the same definitions as above. If the surface temperature T_{vn} undergoes large variations between day and night, a 12-hour moving averaged temperature must be used in (3-5) to avoid fictitious variations in the estimated sealevel pressure.

Step 4

Compute the surface potential temperature and air density at each station

$$\theta_n = T_n \left(\frac{1000}{p_n} \right)^{0.286} \quad (= \text{potential temperature}) \quad (3-6)$$

$$\rho_n = \frac{p_n}{R_d T_{vn}} \cdot 10^{-2} \quad (= \text{density, kg m}^{-3}) \quad (3-7)$$

where T_{vn} is from Eq. 3-2d and is in degrees Kelvin ($^{\circ}\text{K}$), p_n is the station pressure in millibars and

$$R_d = 287 \text{ m}^2 \text{sec}^{-2} \text{ } ^{\circ}\text{K}^{-1}.$$

Record $\theta_n(^{\circ}\text{K})$ and $\rho_n(\text{kg m}^{-3})$ in PIF.

Stage INT

Values of each of the parameters produced by this processor are required at hourly intervals by higher level processors in the network. However, most of the inputs to this processor, P3, may only be available at 3-hour intervals. Thus, it is necessary to interpolate each of the parameter values produced in this processor by some means adequate to produce reasonable

estimates of parameter values each hour. Stage INT is intended to perform this task. We leave the detailed specification of the interpolation algorithm to the discretion of the user.

The inputs and outputs of each step of Processor P3 are summarized in Table 3-1 and illustrated schematically in Figure 3-1.

Table 3-1 Summary of input and output parameters
of each step of Processor P3.

Input Variable	Description	Source	Step	Output Variable	Description
SPD_n	surface wind speed (m/s) at station n	RAW	1	$\hat{u}_n(t_m)$	east-west surface wind component at station n, hour t_m .
DIR_n	surface wind direction (compass degrees) at station n.	RAW		$\hat{v}_n(t_m)$	north-south surface wind component at station n, hour t_m .
T_n	surface temperature ($^{\circ}\text{C}$) at station n	RAW	2	$q_n(t_m)$	surface mixing ratio (dimensionless) at station n, hour t_m .
TD_n	surface dew point depression ($^{\circ}\text{C}$) at station n.	RAW		$RH_n(t_m)$	surface relative humidity (dimensionless) at station n, hour t_m .
p_n	station pressure (mb) at station n.	RAW		$T_{Dn}(t_m)$	surface dew point ($^{\circ}\text{C}$) at station n, hour t_m .
				$T_{vn}(t_m)$	surface virtual temperature ($^{\circ}\text{C}$) at station n, hour t_m .
\hat{z}_n	elevation (meters MSL) of surface station n.	RAW	3	$\phi_{on}(t_m)$	geopotential (m^2s^{-2}) of 1000mb surface at location \hat{x}_n of station n, hour t_m .
T_{vn}	virtual temperature ($^{\circ}\text{K}$).	Step 2			
p_n	station pressure (mb)	RAW		$\dot{\phi}_{on}(t_m)$	time rate of change (m^2s^{-3}) of geopotential of 1000mb surface at station n location, \hat{x}_n , at hour t_m .
				$p_{sl,n}(t_m)$	sea-level pressure (mb) at station n, hour t_m .
p_n	see above	RAW	4	$\theta_n(t_m)$	surface potential temperature ($^{\circ}\text{K}$) at station n, hour t_m .
T_{vn}	see above	Step 2		$\rho_n(t_m)$	surface air density (kg m^{-3}) at station n, hour t_m .

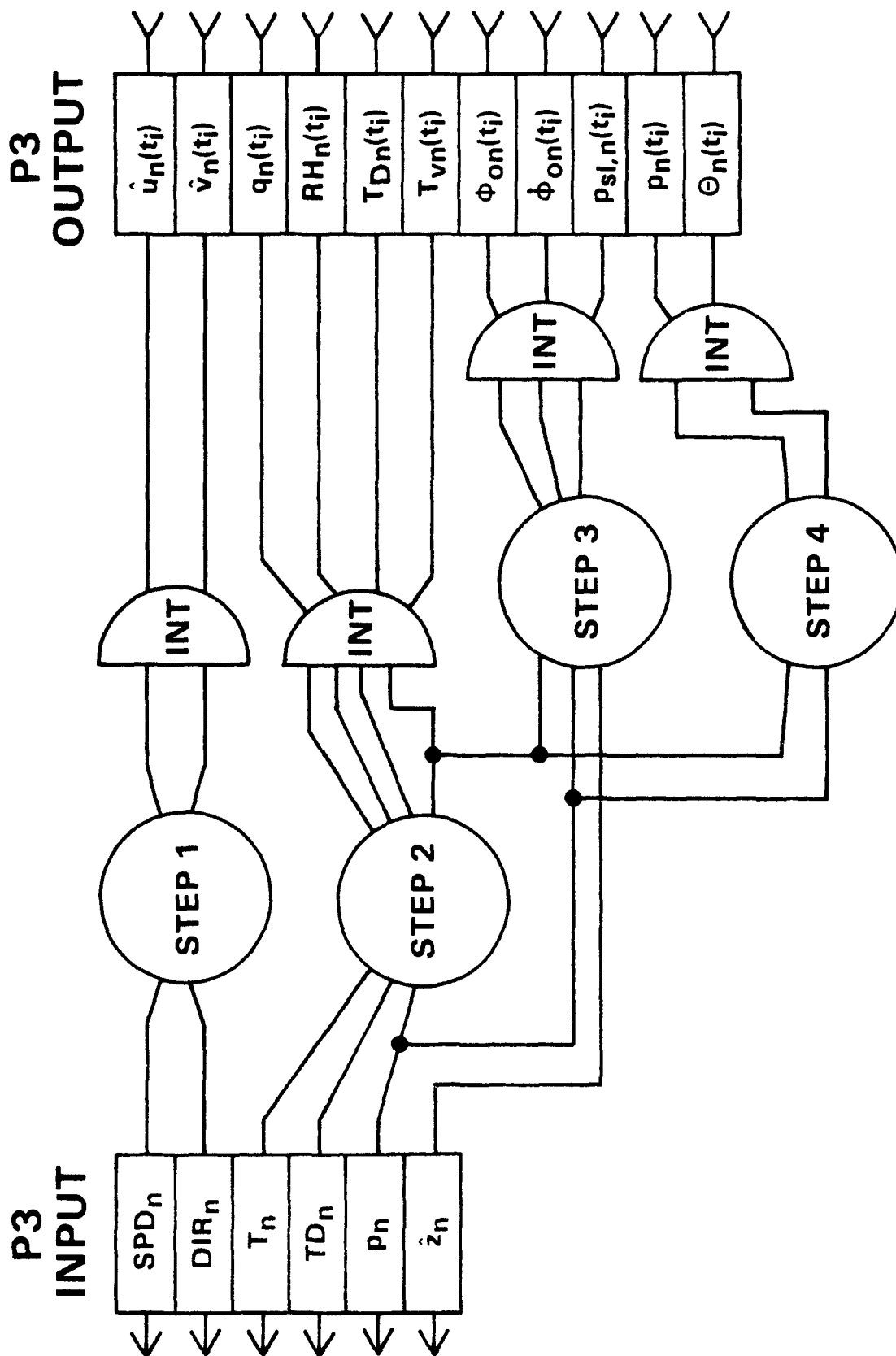


Figure 3-1. Schematic illustration of Processor P3 and its input and output interfaces with the processor network.

SECTION 5

PROCESSOR P4

GENERAL DISCUSSION

This processor estimates the surface roughness z_0 , the Obukhov length L , the surface heat flux Q , and the friction velocity u_* in each cell of the NEROS grid. The last three parameters are treated in a single processor, rather than distributed among several, because they are interrelated variables and the value estimated for one can be altered by a change in the method used to estimate another. The method we use in this first generation processor network to estimate Q is based on the scheme proposed by Golder (1972). More refined methods have recently been reported, e.g., Holtslag and van Ulden (1983), and these should be considered in the development of the second generation model.

We should also point out that the estimates of the friction velocity u_* that we outline here are derived from the raw surface wind observations, i.e., (\hat{u}, \hat{v}) , rather than from the flow fields that are finally used in the model, i.e., the output $(\langle u \rangle_1, \langle v \rangle_1)$ of P11. To utilize data from the latter source would result in complex interconnections of P11 with other processors that require L , Q and u_* values. The difficulty of operating such a system cannot be justified considering that the method of estimating u_* is itself quite crude, and that the flow fields that P11 generates are constrained locally in space-time by the observed winds. That is, the observed surface winds that we will use here to estimate u_* are explicitly incorporated into the flow fields generated by P11.

Each of the steps below must be performed for each cell in the NEROS grid.

Step 1

Determine the wind speed and exposure classes C_w and C_e for use in estimating the Obukhov length L . First, using the locations \underline{x}_n of the N surface meteorological stations ($n=1,2,\dots,N$) and the observed winds (\hat{u}_n, \hat{v}_n) at each station and at each hour t_m , estimate the wind speed \underline{u} in the given grid cell at hour t_m by performing a weighted average of the observations (\hat{u}_n, \hat{v}_n) at the nearest sites \underline{x}_n . The r^{-2} weighting formula (given by Eq. 11-88) may be used. The wind speed class for this grid cell is now defined to be

$$C_w = \begin{cases} \frac{|\underline{u}|}{2}, & \text{if } 0 \leq |\underline{u}| \leq 8 \text{ m s}^{-1}; \\ 4, & \text{otherwise} \end{cases} \quad (4-1)$$

Next, using the fraction $\sigma_{CT}(\underline{x}, t_m)$ of local sky coverage by all cloud types and the local land use distribution $\Upsilon(\underline{x}, j)$, where \underline{x} refers to points on the NEROS grid and $j=1,\dots,10$ refers to the 10 land use types (see P15), compute the exposure class C_e :

$$C_e = \begin{cases} 3, & \sigma_{CT} < 0.2 \\ 2, & 0.2 \leq \sigma_{CT} \leq 0.7 \\ 1, & 0.7 < \sigma_{CT} < 1.0 \\ 0, & \sigma_{CT} = 1.0 \\ -1, & \sigma_{CT} \geq 0.5 \\ -2, & \sigma_{CT} < 0.5 \end{cases} \quad (4-2)$$

} nighttime hours only

In order to account for the nighttime heat fluxes from cities, we will limit the minimum value of C_e to 1 for those cells with "urban" land usage ($j=1$) greater than 30%, i.e.,

$$\text{if } \tau(\underline{x}, 1) > 0.30, C_e(\underline{x}) \geq 1. \quad (4-3a)$$

Similarly, to account approximately for the effects of large bodies of water on the surface heat flux, we assume

$$\text{if } \tau(\underline{x}, 7) \geq 0.6, C_e(\underline{x}) = \begin{cases} -1, & \text{daylight hours} \\ 0, & \text{night.} \end{cases} \quad (4-3b)$$

Now compute the Obukhov length L in the cell at \underline{x} at hour t_m by

$$L = \left[(a_1 S + a_2 S^3) \cdot z_0^{-(b_1 - b_2 |S| + b_3 S^2)} \right]^{-1}, \quad (4-4)$$

where

$$a_1 = 0.004349,$$

$$a_2 = 0.003724,$$

$$b_1 = 0.5034,$$

$$b_2 = 0.2310,$$

$$b_3 = 0.0325.$$

The stability function, S (a digital version of the Pasquill stability category), is expressed as

$$S = -\frac{1}{2}(3 - C_w + |C_e|) \cdot \text{Sign}(C_e),$$

where

$$\text{Sign}(C_e) = \begin{cases} 1, & \text{if } C_e > 0; \\ 0, & \text{if } C_e = 0; \\ -1, & \text{if } C_e < 0, \end{cases}$$

Step 2

Estimate the effective surface roughness z_0 in each cell of the NEROS grid using the following expression

$$z_0(\underline{x}) = \frac{\sum_{n=1}^{10} \Upsilon(\underline{x}, n) z_0(n)}{\sum_{n=1}^{10} \Upsilon(\underline{x}, n)} \quad (4-5)$$

where $\Upsilon(\underline{x}, n)$ is the fraction of the NEROS cell centered at \underline{x} that is in land use category n , with n ($=1, 2, \dots, 10$) referring to the following use types:

- | | |
|---------------------------|---|
| 1. Urban Land | 6. Mixed Forest Land (including Forested Wetland) |
| 2. Agricultural Land | 7. Water |
| 3. Rangeland | 8. Land Falling Outside the Study Area |
| 4. Deciduous Forest Land | 9. Non-Forested Wetland |
| 5. Coniferous Forest Land | 10. Mixed Agricultural Land and Rangeland |

In Eq. 4-5 the surface roughness $z_0(n)$ associated with each land use type are the following (based on the values suggested by Sheih et al., 1979 with modifications as noted below):

$$\begin{aligned} z_0(1) &= 0.7 \text{ m}^{(*1)} \\ (2) &= 0.2 \\ (3) &= 0.1 \\ (4) &= 1.0 \\ (5) &= 1.0 \end{aligned}$$

$$\begin{aligned}(6) &= 0.7 \text{ (*2)} \\(7) &= 0.05 \\(8) &= 0.00 \text{ (*3)} \\(9) &= 0.3 \\(10) &= 0.15 \text{ (*4)}\end{aligned}$$

Notes:

- *1. Sheih, et al. (1979) recommended a value of $z_0=1\text{m}$ for "metropolitan city." In our case the "urban" category includes all "built-up" lands, including residential, industrial, commercial, and other areas characterized by building heights much lower than those characterized as metropolitan. Our choice of 0.7 m for urban areas is an estimated mean value.
- *2. The value for Category 6 represents a rough average between the values suggested.
by Shieh, et al. for marshland and ungrazed forests.
- *3. None of the cells in the NEROS grid fall in this category, i.e., $\tau(x,8)=0$ everywhere, and hence the value assigned to $z_0(8)$ is immaterial.
- *4. Category 10 is a rough average of cropland and rangeland values.

The values of z_0 computed from Eq. (4-5) for each NEROS cell should be recorded in the PIF.

Step 3

Compute the local friction velocity $u_*(x, t_m)$ using

$$u_* = \frac{k |u|}{G(z, L, z_0)} \quad (4-6)$$

where $k = 0.4$ is the von Karman constant; z is the elevation of the surface wind observations above ground--use

$$z=10m; \quad (4-7)$$

and G is the similarity function

$$G = \ln \left[\frac{z+z_0}{z_0} \right] \quad \text{if } L = 0 \quad (4-8a)$$

$$G = \ln \left[\frac{z+z_0}{z_0} \right] + \text{MIN}(5.2 \frac{z}{L}, 5.2) \quad , \text{ if } z \leq 6L \text{ and } L > 0 \quad (4-8b)$$

$$G = 2(\tan^{-1} \xi - \tan^{-1} \xi_0) + \ln \left[\frac{(\xi-1)(\xi_0+1)}{(\xi+1)(\xi_0-1)} \right], \text{ if } L < 0. \quad (4-8c)$$

The Obukhov length L is from (4-4), z_0 is the local surface roughness from (4-5), and

$$\xi = \left(1 - 15 \frac{z+z_0}{L} \right)^{\frac{1}{4}}$$

$$\xi_0 = \left(1 - 15 \frac{z_0}{L} \right)^{\frac{1}{4}}$$

Step 4

Estimate the effective surface kinematic heat flux in each grid cell at hour t_m :

$$Q = - \frac{u_*^3 T_v}{kLg}$$

where T_v is the surface virtual temperature ($^{\circ}\text{K}$) in the given cell obtained by weighting the nearest observations T_{vn} of virtual temperature (provided by P3) as in Step 1 above; and $g = 9.8 \text{ ms}^{-2}$ is the acceleration due to gravity. (Note that the T_{vn} data from P3 are in degrees Celsius.)

Table 4-1 summarizes the input and output variables in each of the three steps that comprise this processor, and Figure 4-1 illustrates the processor and its data interfaces.

Table 4-1 Summary of input and output parameters
in each step of Processor P4.

Input Variable	Description	Source	Step	Output Variable	Description
$\hat{u}_n(t_m)$	east-west surface wind component (ms^{-1}) at surface weather station n, hour t_m .	P3	1	$L(\underline{x}, t_m)$	Obukhov length (meters) in NEROS cell centered at \underline{x} , at hour t_m .
$\hat{v}_n(t_m)$	north-south surface wind component at station n, hour t_m .	P3		$ \underline{u}(\underline{x}, t_m) $	wind speed (m/sec) in NEROS cell centered at \underline{x} , at hour t_m (for use in this Processor <u>only</u>).
\underline{x}_n	location of surface weather station n	PIF			
$\tau(\underline{x}, j)$	land use fraction of category j in NEROS cell centered at \underline{x} .	PIF			
$\sigma_{CT}(\underline{x}, t_m)$	fractional sky coverage, total of all cloud types over cell centered at \underline{x} at hour t_m .	PIF			
$\tau(\underline{x}, j)$	see above	PIF	2	$z_o(\underline{x})$	effective surface roughness (m) of NEROS cell centered at \underline{x} .
$ \underline{u}(\underline{x}, t_m) $	wind speed	Step 1	3	$u_* (\underline{x}, t_m)$	friction velocity (m/s) in NEROS cell centered at \underline{x} , at hour t_m .
$L(\underline{x}, t_m)$	Obukhov length (m)	Step 1			
$z_o(\underline{x})$	surface roughness (m)	Step 2			
$T_{vn}(\underline{x}, t_m)$	surface virtual temperature ($^{\circ}\text{C}$) at surface weather station n, hour t_m .	P3	4	$Q(\underline{x}, t_m)$	surface heat flux ($\text{m}^{\circ}\text{Ks}^{-1}$) in NEROS cell at \underline{x} , at hour t_m .

Table 4-1 Summary of input and output parameters
in each step of Processor P4. (Concluded)

Input Variable	Description	Source	Step	Output Variable	Description
$u_*(\underline{x}, t_m)$	friction velocity (m/s) in cell at \underline{x} at hour t_m .		Step 3		
$L(\underline{x}, t_m)$	Obukhov length (m) in cell at \underline{x} at hour t_m .		Step 1		

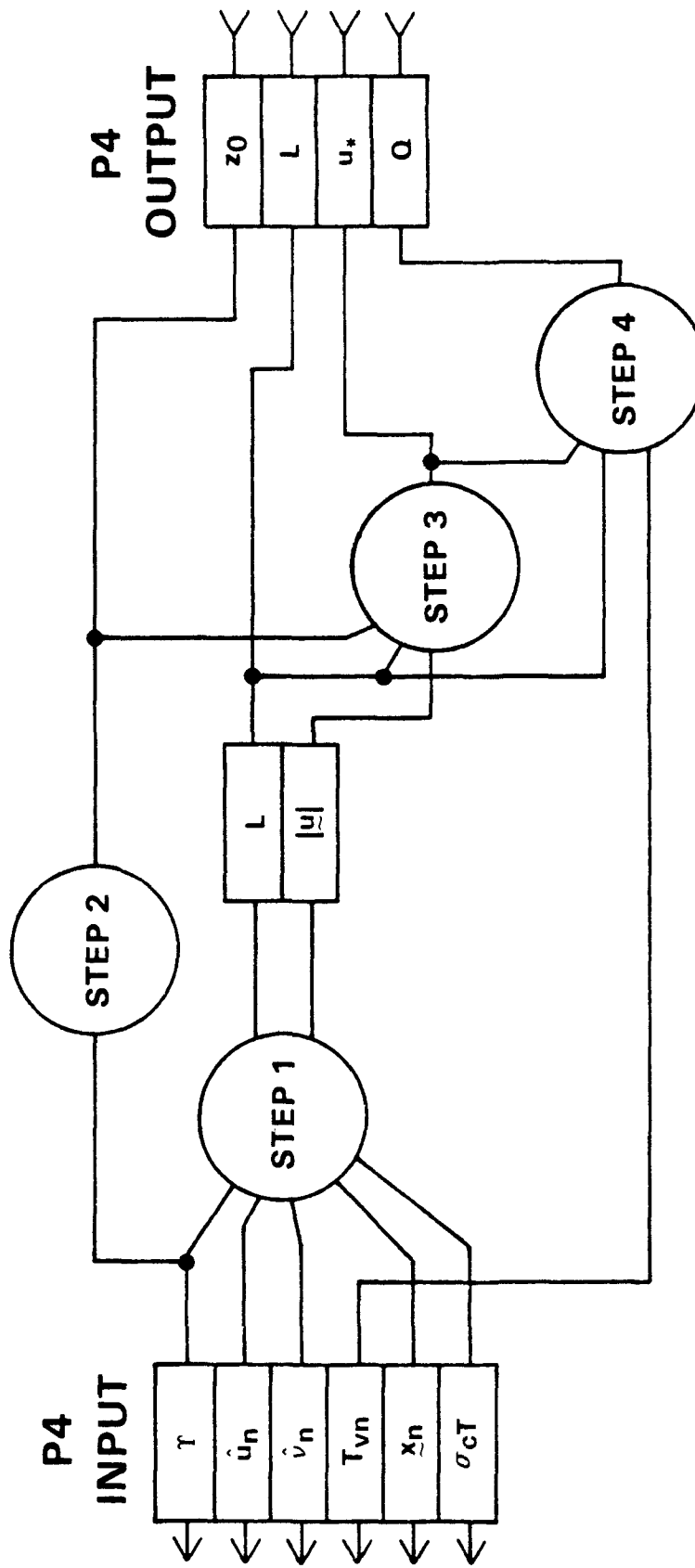


Figure 4-1. Schematic illustration of Processor P4 and its input and output interfaces with the processor network.

SECTION 6
PROCESSOR P7

MOTION OF A VISCOUS, HYDROSTATIC FLUID OF CONSTANT DENSITY OVER IRREGULAR TERRAIN.

We are concerned here with nighttime flow regimes, where winds in the cold air adjacent to the ground, i.e., the radiation inversion layer, are influenced by buoyancy, terrain, warm cities, geostrophic forcing and friction.

We will treat the cold, radiation inversion layer as one of constant density ρ_0 whose upper surface is described by

$$H_{vs}(x,y,z,t) = z_{vs}(x,y,t) - z = 0 \quad (7-1)$$

The subscript "vs" designates that this is also the "virtual surface" of the atmosphere above. We adopt this point of view later in formulating processor P11 which describes the flow field above the inversion layer at night. Figure 7-1 illustrates H_{vs} and other terms that we shall use in the following analyses.

Terrain elevation (MSL) is represented by $z_t(x,y)$ and z is the vertical coordinate whose origin is at sealevel. In keeping with the level of simplicity adopted in formulating the regional diffusion model, we shall treat the cold air layer as a two-dimensional fluid. That is, the horizontal velocity in the cold layer $\underline{u}=(u,v)$ is assumed to be invariant with

respect to z . Keep in mind that during nighttime hours the cold, inversion layer considered here is by definition Layer 1 of the regional model. The flow speed in the atmosphere above the cold layer will be represented by $\underline{U}_m = (U_m, V_m)$ (see P11); and the density in the layer above the inversion will be represented by ρ_m , where $\rho_m < \rho_0$.

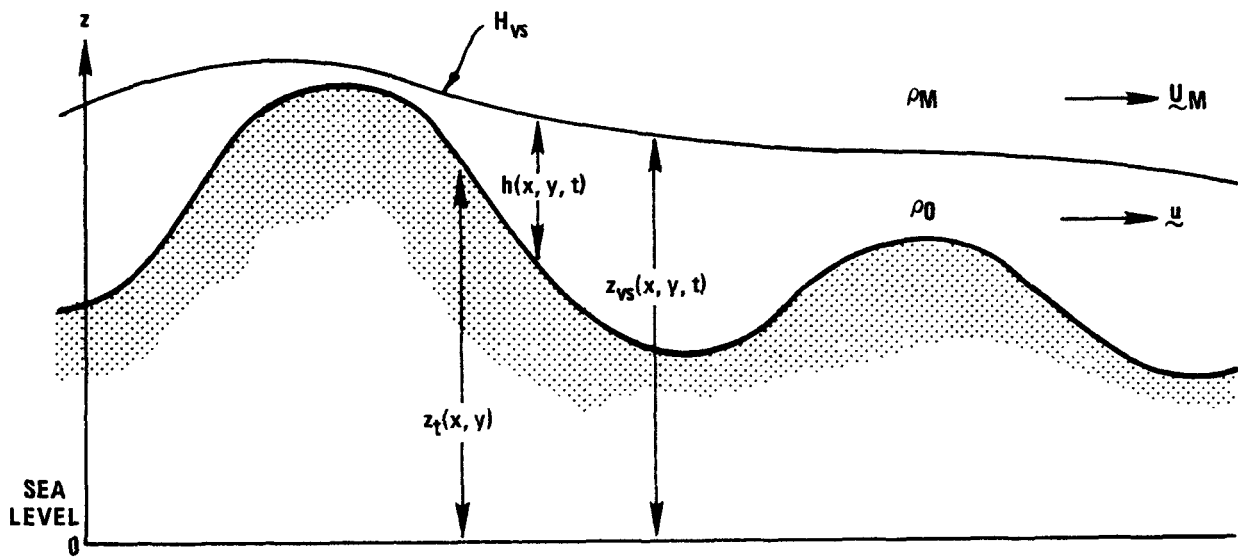


Figure 7-1. Illustration of the variables used in the flow model.

The x -component of the horizontal acceleration of a (2-D) fluid parcel in the cold layer is

$$\frac{d_h u}{dt} \equiv \frac{\partial u}{\partial t} + u \frac{\partial u}{\partial x} + v \frac{\partial u}{\partial y} = \frac{1}{m} [F_{xp} + F_{xc} + F_{xf}] \quad (7-2)$$

where m is the mass of the parcel in question and F_{xp} , F_{xc} , and F_{xf} represent the x -components of the pressure, Coriolis and friction forces, respectively, exerted on the parcel. Consider first the form of pressure force.

The pressure force

We consider the pressure forces acting on the fluid parcel shown in Figure 7-2. Since we assume the flow speed to be uniform in z , we take the parcel to be a vertical column of fluid extending from z_t to the top surface z_{vs} of the cold layer and having horizontal dimensions $(\Delta x, \Delta y)$.

Since the cold fluid and the air above are assumed to be in hydrostatic balance, within the cold layer we have

$$\partial p / \partial z = -\rho_0 g. \quad (7-3)$$

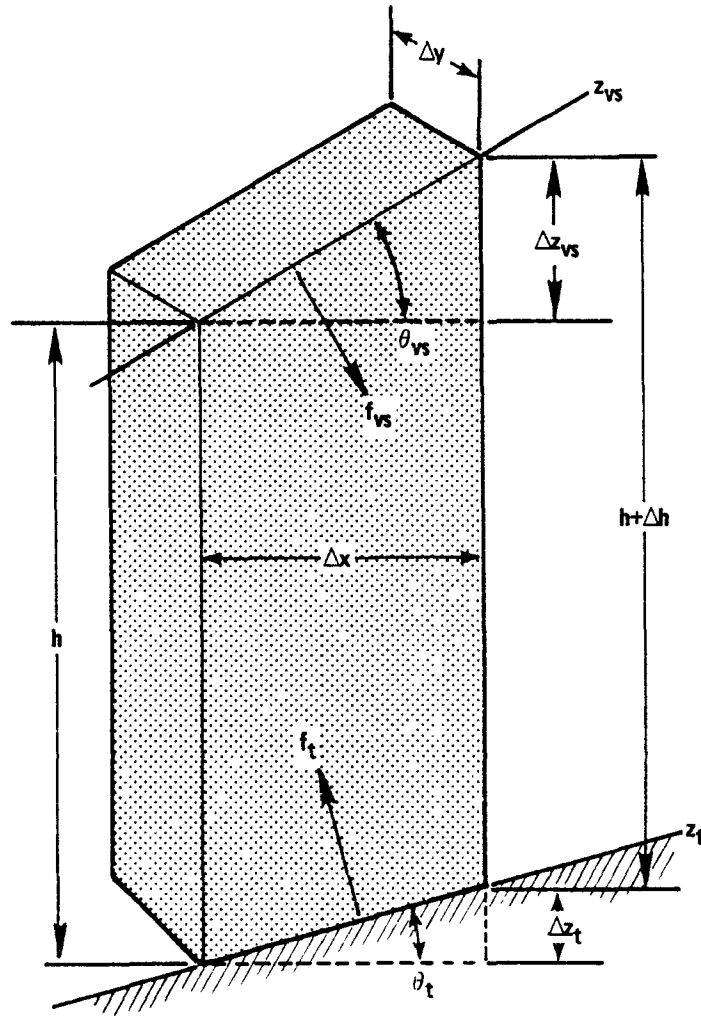


Figure 7-2. Air parcel considered in the force balance analysis.

And since ρ_0 is assumed to be constant, at any level z within the parcel the pressure is

$$p = p_{vs} + \rho_0 g(z_{vs} - z) \quad (7-4)$$

where p_{vs} is the pressure at the top of the parcel, that is on H_{vs} .

The total force on the left face of the parcel due to the hydrostatic pressure is

$$f_{XL} = \Delta y \int_{z_t}^{z_{vs}} p dz.$$

Substituting (7-4) into this expression and making use of the definition

$$h(x,y,t) \equiv z_{vs}(x,y,t) - z_t(x,y) \quad (7-5)$$

we get

$$f_{XL} = p_{vs} h \Delta y + \rho_0 g h^2 \Delta y / 2. \quad (7-6)$$

Keeping in mind that the pressure force is exerted inward on all faces, the force on the right face of the parcel is

$$f_{XR} = - (p_{vs} + \frac{\partial p_{vs}}{\partial z} \Delta z_{vs})(h + \Delta h) \Delta y - \rho_0 g \Delta y (h + \Delta h)^2 / 2 \quad (7-7)$$

The force exerted by the ground on the parcel is directed normal to the lower face which is inclined at an angle θ_t with the horizontal plane and it has a magnitude equal to the total fluid pressure force exerted by the fluid on the ground, i.e.,

$$\begin{aligned}
f_{xt} &= -f_t \sin \theta_t \\
&= -(\rho_0 gh + p_{vs})(\Delta x^2 + \Delta z_t^2)^{\frac{1}{2}} \Delta y \sin \theta_t \\
&= -(\rho_0 gh + p_{vs}) \Delta y \Delta z_t
\end{aligned} \tag{7-8}$$

In a similar manner we find that the force on the top face of the parcel is

$$f_{xvs} = p_{vs} \Delta y \Delta z_{vs}. \tag{7-9}$$

On combining (7-6) - (7-9) and noting that $\partial p_{vs} / \partial z = -\rho_m g$ we obtain the total x-component of the pressure force on the parcel:

$$\begin{aligned}
F_{xp} &= f_{xL} + f_{xR} + f_{xt} + f_{xvs} \\
&= \Delta y (\Delta z_{vs} - \Delta z_t - \Delta h) p_{vs} + \rho_m gh \Delta y \Delta z_{vs} \\
&\quad - \rho_0 gh \Delta y (\Delta h + \Delta z_t)
\end{aligned} \tag{7-10}$$

We can obtain Δh from (7-5) whereupon we can reduce (7-10) to the final form (for small $\Delta x, \Delta y$)

$$F_{xp} = -(\Delta \rho) gh \frac{\partial z_{vs}}{\partial x} \Delta x \Delta y \tag{7-11}$$

where

$$\Delta \rho = \rho_0 - \rho_m \tag{7-12}$$

Now the mass m of the fluid parcel is simply

$$m = \rho_0 gh \Delta x \Delta y,$$

hence

$$\frac{1}{m} F_{xp} = - \frac{\Delta p}{\rho_0} g \frac{\partial z_{vs}}{\partial x} . \quad (7-13a)$$

By analogy the y-component of the pressure induced acceleration is

$$\frac{1}{m} F_{yp} = - \frac{\Delta p}{\rho_0} g \frac{\partial z_{vs}}{\partial y} . \quad (7-13b)$$

Later (see Eqs. 7-34 and 7-35) we will add force components resulting from synoptic scale pressure gradients.

The friction force

The friction force on the fluid parcel is the result of momentum fluxes across the parcel's boundaries. These fluxes are caused by molecular diffusion and by sub-parcel scale velocity fluctuations, or turbulence. For example, at the earth's surface the velocity must be zero, and thus momentum is drained from the fluid in much the same way as heat is removed from a fluid at a cold, constant temperature surface. In the case of our flow where there is no heat transfer into the fluid, the no-slip ground surface acts to transform the bulk kinetic energy of the moving fluid into internal heat energy. The fluid can also be accelerated by influxes of momentum from the atmosphere above.

Referring to Figure 7-3 we note that the viscous force on the left face of the parcel is

$$f_{XL} = \Delta y h \tau_{xx} \quad (7-14)$$

where τ_{xx} is the net flux of x-momentum in the x-direction across the left face of the parcel. The force on the right-hand face is

$$f_{XR} = - \left(\tau_{xx} + \frac{\partial \tau_{xx}}{\partial x} \Delta x \right) \left(h + \frac{\partial z_{vs}}{\partial x} \Delta x \right) \Delta y \quad (7-15)$$

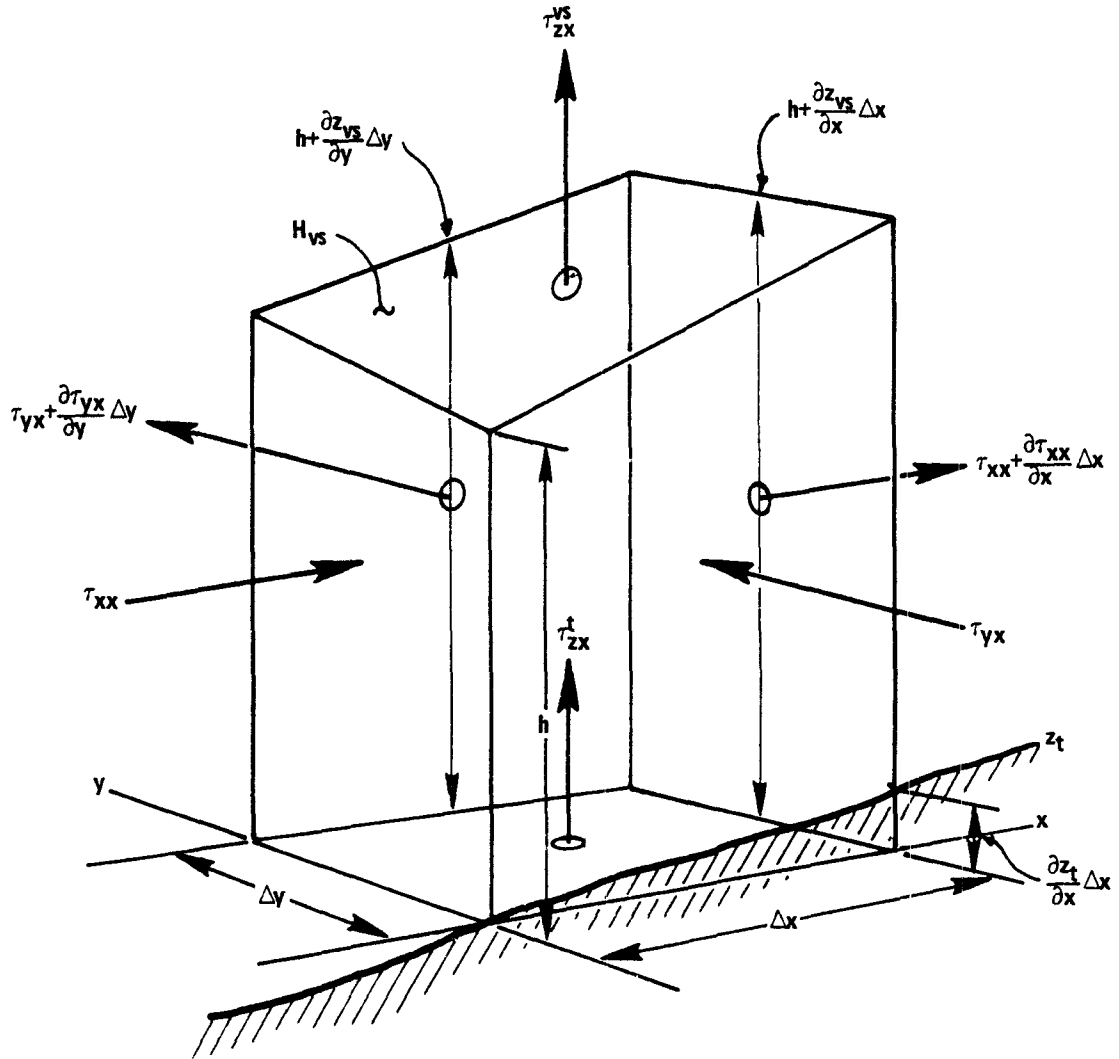


Figure 7-3. Friction forces on a fluid parcel of horizontal dimensions $(\Delta x, \Delta y)$ bounded by z_{vs} and z_t .

Continuing this analysis for each of the other faces and assuming that the slopes of z_t and z_{vs} are small enough that the areas of the bottom and top

faces of the parcel are approximately $\Delta x \Delta y$, we get

$$\begin{aligned}
 F_{xf} = & - \Delta y \left(\frac{\partial \tau_{xx}}{\partial x} h \Delta x + \frac{\partial z_{vs}}{\partial x} \tau_{xx} \Delta x + \frac{\partial \tau_{xx}}{\partial x} \frac{\partial z_{vs}}{\partial x} \Delta x^2 \right) \\
 & - \Delta x \left(\frac{\partial \tau_{yx}}{\partial y} h \Delta y + \frac{\partial z_{vs}}{\partial y} \tau_{yx} \Delta y + \frac{\partial \tau_{yx}}{\partial y} \frac{\partial z_{vs}}{\partial y} \Delta y^2 \right) \\
 & + (\tau_{zx}^t - \tau_{zx}^{vs}) \Delta x \Delta y
 \end{aligned} \tag{7-16}$$

In the limit as Δx and Δy become very small, the mass m of the parcel is

$$m = \rho_0 h \Delta x \Delta y \tag{7-17}$$

and hence

$$\begin{aligned}
 \frac{1}{m} F_{xf} = & - \frac{1}{\rho_0} \left[\frac{\partial \tau_{xx}}{\partial x} + \frac{\partial \tau_{yx}}{\partial y} + \frac{1}{h} (\tau_{zx}^{vs} - \tau_{zx}^t) \right. \\
 & \left. + \tau_{xx} \frac{1}{h} \frac{\partial z_{vs}}{\partial x} + \tau_{yx} \frac{1}{h} \frac{\partial z_{vs}}{\partial y} \right]
 \end{aligned} \tag{7-18}$$

For the lateral stress components τ_{xx} and τ_{yx} we will adopt the gradient transfer forms

$$\frac{1}{\rho_0} \tau_{xx} = - K_{xx} \frac{\partial u}{\partial x} \tag{7-19}$$

$$\frac{1}{\rho_0} \tau_{yx} = - K_{yx} \left(\frac{\partial u}{\partial y} + \frac{\partial v}{\partial x} \right) \tag{7-20}$$

where K_{xx} and K_{yx} are elements of the eddy viscosity tensor, to be defined later. We will treat the stress τ_{zx}^{vs} on the upper surface of the fluid as a prescribed variable. The surface stress τ_{zx}^t will be given later.

By analogy with (7-18) we have

$$\begin{aligned} \frac{1}{m} F_{yf} = & - \frac{1}{\rho_0} \left[\frac{\partial \tau_{xy}}{\partial x} + \frac{\partial \tau_{yy}}{\partial y} + \frac{1}{h} (\tau_{zy}^{vs} - \tau_{zy}^t) \right. \\ & \left. + \tau_{xy} \frac{1}{h} \frac{\partial z_{vs}}{\partial x} + \tau_{yy} \frac{1}{h} \frac{\partial z_{vs}}{\partial y} \right] \end{aligned} \quad (7-21)$$

with

$$\frac{1}{\rho_0} \tau_{xy} = - K_{xy} \left(\frac{\partial u}{\partial y} + \frac{\partial v}{\partial x} \right). \quad (7-22)$$

$$\frac{1}{\rho_0} \tau_{yy} = - K_{yy} \frac{\partial v}{\partial y}. \quad (7-23)$$

The stress τ_{zy}^{vs} is considered to be a prescribed variable; τ_{zy}^t and τ_{zx}^t are given by

$$\tau_{zx}^t = - \rho_0 u_*^2 \cos \theta \quad (7-25a)$$

$$\tau_{zy}^t = - \rho_0 u_*^2 \sin \theta \quad (7-25b)$$

where u_* is the friction velocity which we shall express in the form, following Melgarejo and Deardorff (1974),

$$u_* = C_D (u^2 + v^2)^{\frac{1}{2}}; \quad (7-26)$$

where C_D is the surface drag coefficient and θ is the wind direction,

$$\theta = \tan^{-1} \frac{v}{u}. \quad (7-27)$$

From (7-25) - (7-27) we obtain

$$\frac{1}{\rho_0} \tau_{zx}^t = - C_D^2 (u^2 + v^2)^{\frac{1}{2}} u \quad (7-28a)$$

$$\frac{1}{\rho_0} \tau_{zy}^t = - c_D^2 (u^2 + v^2)^{\frac{1}{2}} v. \quad (7-28b)$$

According to Melgarejo and Deardorff,

$$c_D^2 = k^2 \left[\left(\ln\left(\frac{h}{z_0}\right) - b \right)^2 + a^2 \right]^{-1} \quad (7-29)$$

where z_0 is the local surface roughness, and a and b are functions of h/L , where L is the Obukhov length. (Approximate forms for a and b are given later, 7-89.)

The Coriolis force

The Coriolis force is given simply by

$$\frac{1}{m} F_{xc} = +fv \quad (7-30)$$

$$\frac{1}{m} F_{yc} = -fu \quad (7-31)$$

where f is the Coriolis parameter ($=2\Omega \sin \phi$, where ϕ = latitude and Ω = earth angular speed of rotation $= 2\pi/24 \text{ hr}^{-1}$).

The momentum equations

On combining (7-2), (7-12), (7-18) - (7-20), (7-28a) and (7-30) we obtain the equation governing the u component of the flow speed:

$$\begin{aligned}
\frac{\partial u}{\partial t} + u \frac{\partial u}{\partial x} + v \frac{\partial u}{\partial y} = & -g \frac{\Delta \rho}{\rho_0} \frac{\partial z_{vs}}{\partial x} + fv + K_{xx} \frac{\partial^2 u}{\partial x^2} + K_{yx} \frac{\partial^2 u}{\partial y^2} \\
& + \left[\frac{\partial K_{xx}}{\partial x} + \frac{K_{xx}}{h} \frac{\partial z_{vs}}{\partial x} \right] \frac{\partial u}{\partial x} + \left[\frac{\partial K_{yx}}{\partial y} + \frac{K_{yx}}{h} \frac{\partial z_{vs}}{\partial y} \right] \frac{\partial u}{\partial y} \\
& - \frac{C_D^2}{h} (u^2 + v^2)^{1/2} u + \left[\frac{\partial K_{yx}}{\partial y} \frac{\partial v}{\partial x} + K_{yx} \frac{\partial^2 v}{\partial x^2} \right. \\
& \left. + \frac{K_{yx}}{h} \frac{\partial z_{vs}}{\partial y} \frac{\partial v}{\partial x} - \frac{\tau_{zx}^{vs}}{h \rho_0} \right].
\end{aligned} \tag{7-32}$$

For convenience we will express the shear stress at z_{vs} in the form

$$\frac{1}{\rho_0} \tau_{zx}^{vs} = -\sigma_w^{vs} (U_M - u) \tag{7-33}$$

where σ_w^{vs} is a vertical exchange velocity scale at $z = z_{vs}$ and U_M is the x-component of the "observed" flow in the layer above z_{vs} (see processor P11, Stage UV).

Substituting (7-33) into (7-32) we obtain after rearranging terms

$$\begin{aligned}
\frac{\partial u}{\partial t} + \left[u - \frac{\partial K_{xx}}{\partial x} - \frac{K_{xx}}{h} \frac{\partial z_{vs}}{\partial x} \right] \frac{\partial u}{\partial x} + \left[v - \frac{\partial K_{yx}}{\partial y} - \frac{K_{yx}}{h} \frac{\partial z_{vs}}{\partial y} \right] \frac{\partial u}{\partial y} \\
- K_{xx} \frac{\partial^2 u}{\partial x^2} - K_{yx} \frac{\partial^2 u}{\partial y^2} + \frac{1}{h} \left[C_D^2 (u^2 + v^2)^{1/2} + \sigma_w^{vs} \right] u = \\
\left[-g \left(\frac{\Delta \rho}{\rho_0} \right) \frac{\partial z_{vs}}{\partial x} + fv + \frac{1}{h} \sigma_w^{vs} U_M + \frac{\partial K_{yx}}{\partial y} \frac{\partial v}{\partial x} + K_{yx} \frac{\partial^2 v}{\partial x^2} \right. \\
\left. + \frac{K_{yx}}{h} \frac{\partial z_{vs}}{\partial y} \frac{\partial v}{\partial x} \right] - \frac{1}{\rho_0} \frac{\partial p_s}{\partial x}
\end{aligned} \tag{7-34}$$

Likewise we have

$$\begin{aligned}
& \frac{\partial v}{\partial t} + \left[u - \frac{\partial K_{xy}}{\partial x} - \frac{K_{xy}}{h} \frac{\partial z_{vs}}{\partial x} \right] \frac{\partial v}{\partial x} + \left[v - \frac{\partial K_{yy}}{\partial y} - \frac{K_{yy}}{h} \frac{\partial z_{vs}}{\partial y} \right] \frac{\partial v}{\partial y} \\
& - K_{xy} \frac{\partial^2 v}{\partial x^2} - K_{yy} \frac{\partial^2 v}{\partial y^2} + \frac{1}{h} \left[C_D^2 (u^2 + v^2)^{\frac{1}{2}} + \sigma_w^{vs} \right] v = \\
& \left[-g \left(\frac{\Delta \rho}{\rho_0} \right) \frac{\partial z_{vs}}{\partial y} - fu + \frac{1}{h} \sigma_w^{vs} v_M + \frac{\partial K_{xy}}{\partial x} \frac{\partial u}{\partial y} + K_{xy} \frac{\partial^2 u}{\partial x \partial y} \right. \\
& \left. + \frac{K_{xy}}{h} \frac{\partial z_{vs}}{\partial x} \frac{\partial u}{\partial y} \right] - \frac{1}{\rho_0} \frac{\partial p_{s1}}{\partial y}
\end{aligned} \tag{7-35}$$

In Eqs. (7-34) and (7-35) the last terms on the right-hand side represent the accelerations caused by synoptic scale pressure gradients in the boundary layer, and p_{s1} is the sea-level pressure.

Next we derive an equation for the virtual surface elevation $z_{vs}(x,y,t)$.

The fluid depth equation

Let Q be a point on the virtual surface (cf 7-1)

$$H_{vs}(x,y,z,t) = z_{vs}(x,y,t) - z = 0 \tag{7-36}$$

and let its coordinates at time t_0 be (x_0, y_0, z_0) . If the surface is moving with a velocity $\underline{v}_{vs} = (u_{vs}, v_{vs}, w_{vs})$ at the point Q, then at the later time $t_0 + \Delta t$ Q will have the coordinates

$$(x_1, y_1, z_1) = (x_0 + u_{vs} \Delta t, y_0 + v_{vs} \Delta t, z_0 + w_{vs} \Delta t). \tag{7-37}$$

Since by definition Q lies on the surface H_{vs} at all times we must have

$$H_{vs}(x_0, t_0) = z_{vs}(x_0, y_0, t_0) - z_0 = 0 \quad (7-38)$$

$$H_{vs}(x_1, t_0 + \Delta t) = z_{vs}(x_1, y_1, t_0 + \Delta t) - z_1 = 0 \quad (7-39)$$

If Δt is sufficiently small we can write

$$\begin{aligned} z_{vs}(x_1, y_1, t_0 + \Delta t) \approx & z_{vs}(x_0, y_0, t_0) + \frac{\partial z_{vs}}{\partial x} (x_1 - x_0) \\ & + \frac{\partial z_{vs}}{\partial y} (y_1 - y_0) + \frac{\partial z_{vs}}{\partial t} \Delta t \end{aligned} \quad (7-40)$$

where all derivatives are evaluated at (x_0, y_0, t_0) . Substituting (7-40) into (7-39), subtracting (7-38) from (7-39), and making use of (7-37) we get

$$\frac{\Delta H_{vs}}{\Delta t} = \frac{\partial z_{vs}}{\partial x} u_{vs} + \frac{\partial z_{vs}}{\partial y} v_{vs} + \frac{\partial z_{vs}}{\partial t} - w_{vs} = 0 \quad (7-41)$$

and upon taking the limit $\Delta t \rightarrow 0$ we obtain

$$\frac{dH_{vs}}{dt} \equiv \frac{\partial H_{vs}}{\partial t} + \underline{v}_{vs} \cdot \underline{\nabla} H_{vs} = 0 \quad (7-42)$$

The unit, outward normal vector to the surface H_{vs} at Q is

$$\underline{n} = \frac{-1}{|\underline{\nabla} H_{vs}|} \underline{\nabla} H_{vs} \quad (7-43)$$

where $\underline{\nabla}$ is applied at Q. Let Δs denote the area of the projection on H_{vs} of a horizontal rectangle $(\Delta x, \Delta y)$ centered at the coordinates (x_0, y_0) of Q (see Figure 7-4). It is evident from the figure that for sufficiently small Δx and Δy , the area Δs is

$$\Delta s \approx \Delta x \Delta y \left[\left(\frac{\partial z_{vs}}{\partial x} \right)^2 + 1 \right]^{\frac{1}{2}} \left[\left(\frac{\partial z_{vs}}{\partial y} \right)^2 + 1 \right]^{\frac{1}{2}}. \quad (7-44)$$

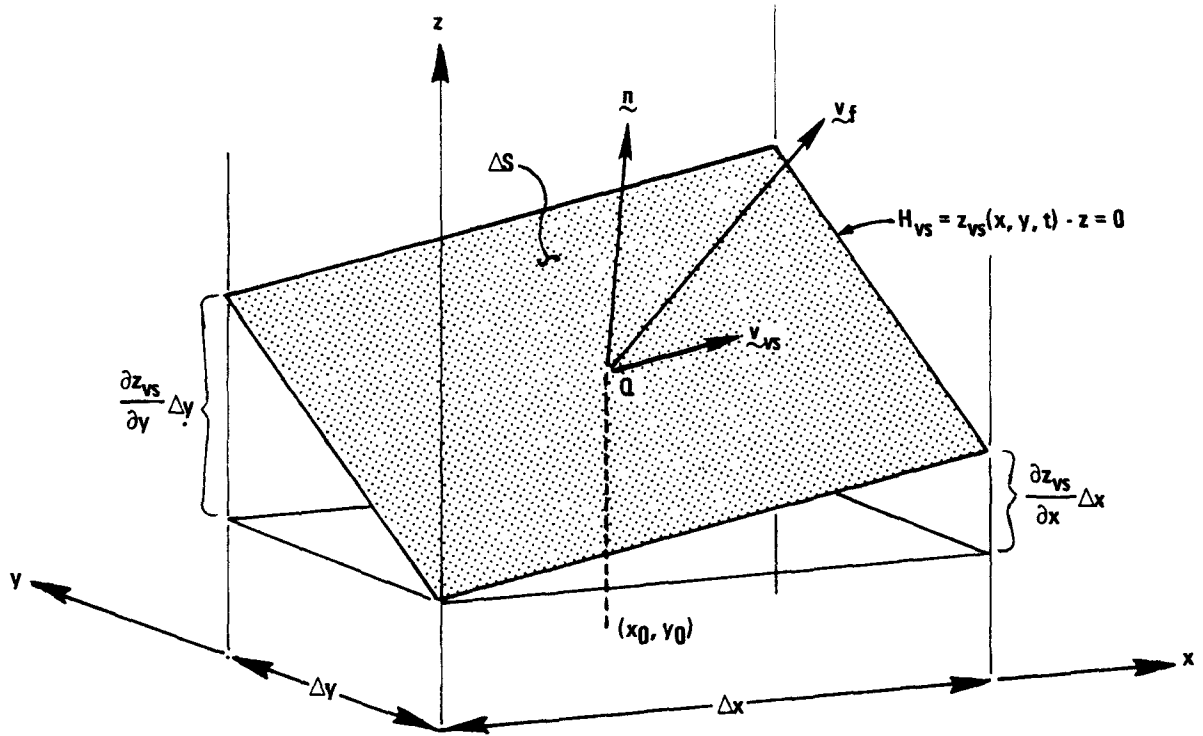


Figure 7-4. Projection of the horizontal rectangle $(\Delta x, \Delta y)$ onto the surface H_{vs} centered at point Q .

If the slope of z_{vs} is small, say

$$\left| \frac{\partial z_{vs}}{\partial x} \right|, \left| \frac{\partial z_{vs}}{\partial y} \right| \ll 1 \quad (7-45)$$

then (7-44) can be approximated by

$$\Delta s \approx \Delta x \Delta y \left[\left(\frac{\partial z_{vs}}{\partial x} \right)^2 + \left(\frac{\partial z_{vs}}{\partial y} \right)^2 + 1 \right]^{\frac{1}{2}}, \text{ if 7-45 holds.} \quad (7-46)$$

Let \underline{v}_f be the velocity of the fluid at the point Q on H_{vs} . Then the normal downward component of the fluid velocity relative to H_{vs} at point Q is

$$\begin{aligned} &= - (\underline{v}_f - \underline{v}_{vs}) \cdot \underline{n} \\ &= \frac{-1}{|\underline{\nabla} H_{vs}|} [\underline{v}_{vs} \cdot \underline{\nabla} H_{vs} - \underline{v}_f \cdot \underline{\nabla} H_{vs}] \end{aligned} \quad (7-47)$$

Making use of (7-42) we can write (7-47) in the equivalent form

$$v = \frac{+1}{|\vec{\nabla}H_{vs}|} \frac{dH_{vs}}{dt} \quad (7-48)$$

where

$$\frac{d}{dt} \equiv \frac{\partial}{\partial t} + \vec{v}_f \cdot \vec{\nabla} \quad (7-49)$$

The total downward volume flux of fluid crossing Δs is $v\Delta s$. Using (7-46), (7-48) and

$$|\vec{\nabla}H_{vs}| = \left(\frac{\partial z_{vs}}{\partial x}\right)^2 + \left(\frac{\partial z_{vs}}{\partial y}\right)^2 + 1 \quad (7-50)$$

we have

$$v\Delta s = \Delta x \Delta y \frac{dH_{vs}}{dt} \quad (7-51)$$

Thus, the net downward flux or fluid per unit horizontal area is

$$\eta_{vs} = \frac{dH_{vs}}{dt} \quad (7-52)$$

or

$$\frac{\partial z_{vs}}{\partial t} + u \frac{\partial z_{vs}}{\partial x} + v \frac{\partial z_{vs}}{\partial y} - w = \eta_{vs} \quad (7-53)$$

where (u, v, w) is the fluid velocity on H_{vs} .

An expression for η_{vs} can be derived from the first law of thermodynamics. Assuming that all sources and sinks of heat are on the boundaries of the fluid, e.g., radiative cooling on H_{vs} and heat transfer to the terrain surface H_t , we can write the first law in the form

$$\frac{d\theta}{dt} = \frac{\partial\theta}{\partial t} + u\frac{\partial\theta}{\partial x} + v\frac{\partial\theta}{\partial y} + w\frac{\partial\theta}{\partial z} = 0 \quad (7-54)$$

where θ is the potential temperature defined as

$$\theta \equiv T\left(\frac{p}{p_0}\right)^{R/c_p} \quad (7-55)$$

where p_0 is a reference pressure (usually 1000 mb) and p is local pressure. Following the procedure described in Part 1, Section 2 for obtaining layer averaged variables, we get from (7-54)

$$\begin{aligned} \frac{\partial}{\partial t} \langle \theta \rangle + \frac{\langle \theta \rangle}{h} \frac{\partial h}{\partial t} + u \frac{\partial \langle \theta \rangle}{\partial x} + v \frac{\partial \langle \theta \rangle}{\partial y} + \frac{1}{h} \left[\overline{\frac{dH_t}{dt}}^t \right. \\ \left. - \langle \theta \rangle \frac{\overline{\mathbf{v} \cdot \nabla H_t}^t}{\overline{\frac{dH_{vs}}{dt}}} - \overline{\frac{dH_{vs}}{dt}}^{vs} + \langle \theta \rangle \frac{\overline{\mathbf{v} \cdot \nabla H_{vs}}^{vs}}{\overline{\frac{dH_{vs}}{dt}}} \right] = 0 \end{aligned} \quad (7-56)$$

where $\overline{\quad}^t$ denotes averaging over the terrain surface H_t , $\overline{\quad}^{vs}$ denotes averaging over the virtual surface H_{vs} ,

$$h(x,y,t) = z_{vs}(x,y,t) - z_t(x,y) \quad (7-57)$$

and

$$\langle \theta \rangle \equiv \frac{1}{h} \int_{A_t}^{z_{vs}} \theta dz da \quad (7-58)$$

and A is the area of a grid cell in the model.

Look at the first term in brackets in (7-56). In analogy with (7-52) we have

$$\frac{dH_t}{dt} = \eta_t \quad (7-59)$$

where η_t is the downward fluid volume flux at the ground. Thus,

$$\frac{\overline{dH}_t}{\overline{\eta}_t} = -\overline{w^T \theta^T}_0 \quad (7-60)$$

where $\overline{w^T \theta^T}_0$ is the kinematic heat flux at the ground.

Consider now the second term in brackets in (7-56). Since $\partial z_t / \partial t = 0$ and since $\overline{\eta}_t = 0$ (there is no net flux of air through the terrain), we have

$$\frac{\overline{dH}_t}{\overline{\eta}_t} = \overline{y \cdot \nabla H}_t = 0. \quad (7-61)$$

The third term in brackets in (7-56) can be written with the aid of (7-52) as

$$\frac{\overline{dH}_{vs}}{\overline{\eta}_{vs}} = \overline{\theta \eta}_{vs} \quad (7-62)$$

and the fourth term becomes, using (7-52) and (7-53),

$$\langle \theta \rangle \overline{y \cdot \nabla H}_{vs} = \langle \theta \rangle \left[\eta_{vs} - \frac{\partial z_{vs}}{\partial t} \right] \quad (7-63)$$

where η_{vs} and z_{vs} are taken to be averages over an area A of a grid cell surrounding any given point.

Substituting (7-60) - (7-63) into (7-56) and collecting terms we get

$$\frac{d_H}{dt} \langle \theta \rangle + \frac{1}{h} \left[-\overline{w^T \theta^T}_0 - \overline{\theta \eta}_{vs} + \langle \theta \rangle \eta_{vs} \right] = 0 \quad (7-64)$$

where

$$\frac{d_H}{dt} \equiv \frac{\partial}{\partial t} + u \frac{\partial}{\partial x} + v \frac{\partial}{\partial y} \quad (7-65)$$

Following Zeman (1979) we shall assume that within the cold fluid, i.e., the nighttime stable boundary layer, the potential temperature has a linear variation with height, namely

$$\theta = \theta_h - (\theta_h - \theta_0)(1 - \frac{z-z_t}{h}) \quad (7-66)$$

where θ_h is the value of θ at the elevation h above ground and θ_0 is the potential temperature at the surface. At elevation h the turbulent heat and momentum fluxes are negligibly small; so if we take this to be the elevation of the virtual surface z_{vs} , then the kinematic heat flux on H_{vs} is simply that due to the motion of the surface itself. In this case we have

$$\overline{\theta \eta}_{vs}^{vs} = \theta_h \eta_{vs} \quad \text{if } \eta_{vs} > 0 \quad (7-67)$$

Also, on integrating (7-66) in the manner of (7-58) we get

$$\langle \theta \rangle = \frac{1}{2} (\theta_h + \theta_0) \quad (7-68)$$

and hence

$$\frac{d_H}{dt} \langle \theta \rangle = \frac{1}{2} \frac{d_H}{dt} \theta_h + \frac{1}{2} \frac{d_H}{dt} \theta_0. \quad (7-69)$$

Substituting (7-67) and (7-68) into (7-64) we obtain

$$\eta_{vs} = \frac{2h}{\theta_h - \theta_0} \frac{d_H}{dt} \langle \theta \rangle - \frac{2\overline{w'\theta_0'}}{\theta_h - \theta_0} \quad (7-70)$$

Making use of (7-69) in this equation we obtain

$$\eta_{vs} = B(h_e - h) \quad (7-71)$$

where

$$B = - \frac{1}{\theta_h - \theta_0} \frac{d_H}{dt} (\theta_h + \theta_0) \quad (7-72a)$$

$$h_e = \frac{2\overline{w'\theta'}_0}{\frac{d_H}{dt}(\theta_h + \theta_0)} \quad (7-72b)$$

It is instructive to compare (7-71) - (7-72) with models of the stable boundary layer developed by others. Earlier efforts have considered only homogeneous surfaces with no mean vertical motion ($w=0$). In this case (7-71) reduces to (see 7-53 and 7-57)

$$\frac{\partial h}{\partial t} = B(h_e - h). \quad (7-73)$$

and $d_H/dt \rightarrow \partial/\partial t$. Nieuwstadt and Tennekes (1981) (NT) recently proposed

$$\frac{\partial h}{\partial t} = B'(h'_e - h) \quad (7-74)$$

where

$$B' = - \frac{4/3}{\theta_h - \theta_0} \frac{\partial \theta_0}{\partial t} \quad (7-75a)$$

$$h'_e = c_4 \frac{2}{\frac{g}{T} \left| \frac{\partial \theta_0}{\partial \tau} \right|} \frac{fG \sin \alpha \cos \alpha}{\quad} \quad (7-75b)$$

where f is the Coriolis parameter, G is the geostrophic wind speed, α is the angle between the geostrophic and the surface winds, and c_4 is a constant whose value is estimated by Nieuwstadt and Tennekes to be about 0.15. Good agreement was found between the predictions of this model and observations of the boundary layer depth h .

On comparing (7-71) - (7-72) with the NT model (7-74) - (7-75) we find that except for the constant 4/3 in B' , the two models are the same, provided

that the surface heat flux satisfies

$$|\overline{w'\theta_0'}| = \frac{0.15}{2} \frac{fG^2 \sin\alpha \cos\alpha}{g/T}. \quad (7-76)$$

To determine whether this is a plausible relationship, we note first that for large values of h/L , where L is the Obukhov length

$$L \equiv - \frac{u_*^3 T}{gk \overline{w'\theta_0'}} \quad (7-77)$$

Brost and Wyngaard (1978) found

$$G^2 \sin\alpha \cos\alpha = u_*^2 \left(\frac{h}{L}\right)^2 \left(\frac{22}{k}\right) \quad (7-78)$$

where $k = 0.4$ is the von Karman constant. Substituting (7-77) and (7-78) into (7-76) we find that (7-76) implies

$$h = 0.8 \left(\frac{u_* L}{f}\right)^{1/2} \quad (7-79)$$

But this is just the formula that Zilitinkevich (1972) derived for h from similarity theory [in particular $h = c_5 \left(\frac{u_* L}{f}\right)^{1/2}$]; and thus we conclude that (7-76) is a plausible expression, at least for large h/L .

Having an expression now for η_{vs} , let us return to (7-53) and consider the vertical velocity w . Since the cold layer is shallow we can approximate the continuity equation by

$$\frac{\partial u}{\partial x} + \frac{\partial v}{\partial y} + \frac{\partial w}{\partial z} = 0. \quad (7-80)$$

Integrating from z_t to z_{vs} and using the assumption that u and v are invariant with respect to z , we get

$$h\left[\frac{\partial u}{\partial x} + \frac{\partial v}{\partial y}\right] = w_t - w_{vs}. \quad (7-81)$$

Since there is no flux F of fluid through the ground, we see from (7-61) that

$$\frac{\partial z_t}{\partial t} + u\frac{\partial z_t}{\partial x} + v\frac{\partial z_t}{\partial y} - w_t = 0 \quad (7-82)$$

Solving (7-82) for w_t and using the result in (7-81) we obtain

$$w_{vs} = u\frac{\partial z_t}{\partial x} + v\frac{\partial z_t}{\partial y} - h\left[\frac{\partial u}{\partial x} + \frac{\partial v}{\partial y}\right] \quad (7-83)$$

where h is given by (7-57). Substituting (7-83) into (7-53) we obtain finally

$$\frac{\partial h}{\partial t} + u\frac{\partial h}{\partial x} + v\frac{\partial h}{\partial y} + h\left[\frac{\partial u}{\partial x} + \frac{\partial v}{\partial y}\right] = \eta_{vs} \quad (7-84a)$$

where

$$h = z_{vs} - z_t \quad (7-84b)$$

This is the model equation that we shall use to obtain z_{vs} .

Simplified model equations

Going back to the momentum equations (7-34) and (7-35) and recalling that z_{vs} is the elevation where vertical heat and momentum fluxes due to turbulence are negligible, we assume that

$$\sigma_w^{vs} \approx 0. \quad (7-85)$$

Let us also assume in this "first generation" model that the lateral eddy

viscosity tensor $\underline{\kappa}$ is also zero. With these assumptions (7-34) and (7-35) reduce to

$$\begin{aligned} \frac{\partial u}{\partial t} + u \frac{\partial u}{\partial x} + v \frac{\partial u}{\partial y} + \frac{u}{h} C_D^2 (u^2 + v^2)^{\frac{1}{2}} = -g \frac{\Delta \rho}{\rho_0} \frac{\partial z_{vs}}{\partial x} \\ - \frac{1}{\rho_0} \frac{\partial p_{s1}}{\partial x} + f v \end{aligned} \quad (7-86)$$

$$\begin{aligned} \frac{\partial v}{\partial t} + u \frac{\partial v}{\partial x} + v \frac{\partial v}{\partial y} + \frac{v}{h} C_D^2 (u^2 + v^2)^{\frac{1}{2}} = -g \frac{\Delta \rho}{\rho_0} \frac{\partial z_{vs}}{\partial y} \\ - \frac{1}{\rho_0} \frac{\partial p_{s1}}{\partial y} - f u \end{aligned} \quad (7-87)$$

where p_{s1} is the sea-level pressure and h and z_{vs} are given by (7-84), which we rewrite here for completeness:

$$\frac{\partial h}{\partial t} + u \frac{\partial h}{\partial x} + v \frac{\partial h}{\partial y} + h \left[\frac{\partial u}{\partial x} + \frac{\partial v}{\partial y} \right] = \eta_{vs} \quad (7-88a)$$

$$h = z_{vs} - z_T. \quad (7-88b)$$

The set of equations (7-86) - (7-88) is a closed system that we can solve for u , v , and h given C_D , $\Delta \rho$, ρ_0 , p_{s1} , z_T and η_{vs} . Earlier we described how η_{vs} is related to the surface heat flux $\overline{w^T \theta_0^T}$ and the temperature distribution θ within the cold layer (see 7-71 and 7-72); and we presented formulas that one might use to derive these variables (see 7-66 and 7-76). Below we summarize the expressions that we propose to use for these and the other parameters listed above in the first generation version of processor P7.

(1) $\eta_{vs} = \text{Eq. 7-71,72 with } \theta_h \text{ and } \theta_o \text{ from surface and upper air meteorological data (Processors P1 and P3); } \overline{w'\theta_o'} = Q = \text{kinematic heat flux at the ground (from Processor P4);}$

(2) $z_T(x,y) = 30 \times 45 \text{ min (lat-lon) smoothed terrain heights (meters, MSL, from P7)}$

$$(3) \quad C_D = k \left\{ \left[\ln\left(\frac{h}{z_o}\right) - b \right]^2 + a^2 \right\}^{-1/2} \quad (7-89a)$$

where $k = 0.4$ is the von Karman constant; h is the local solution of Eq. (7-88); z_o is the surface roughness (m), from P4;

$$a = \begin{cases} 5, & \text{if } L \geq 0, \\ -1, & \text{otherwise;} \end{cases} \quad (7-89b)$$

$$b = \begin{cases} -5, & \text{if } L \geq 0, \\ 4, & \text{otherwise;} \end{cases} \quad (7-89c)$$

and L is the Obukhov length (from P4). Note that L , z_o , h , and hence a , b , and C_D are defined for each grid point in the model domain. (Eq. 89 is based on values given by Melgarejo and Deardorff, 1974.)

$$(4) \quad \frac{\Delta p}{\rho_o} \approx \frac{\Delta \theta}{\langle \theta \rangle} = \frac{\theta_h - \theta_o}{\theta_h + \theta_o}, \quad (7-90a)$$

where θ_h and θ_o are from Processors P1 and P3;

$$(5) \quad \rho_o = \frac{p_{s1}}{RT_v} \quad (7-90b)$$

where p_{s1} is the sea-level pressure (from P3); T_v is the virtual temperature (from P3); and R is the gas constant.

- (6) g and f are gravity (9.8 m sec^{-2}) and the Coriolis parameter ($= 2\Omega \sin\phi$), respectively. Here $\Omega = 2\pi/(24 \cdot 60 \cdot 60) \text{ sec}^{-1}$ and ϕ is the local latitude in radians.

Later we outline the stages of calculations that are needed to compute the parameters listed above and the additional quantities, not used in the flow simulation, that P7 must provide to the model and to other processors in the network.

Solution of the u , v , and z_{vs} equations

Each of the Eqs. (7-86) - (7-88), which govern u , v and z_{vs} , respectively, has the form

$$\frac{\partial \Gamma}{\partial t} + U \frac{\partial \Gamma}{\partial x} + V \frac{\partial \Gamma}{\partial y} + b\Gamma = S \quad (7-91)$$

where U and V are functions of Γ . We will approach the task of solving (7-91) numerically using the technique developed in Section 9 of Part 1. That is, we assume that within each small time interval Δt , the coefficients U and V in (7-91) can be treated as independent variables whose values are determined using the value of Γ at the beginning of the interval, t_0 say. In this case the solution of (7-91) can be expressed in the closed form

$$\begin{aligned} \Gamma(x, t_0 + \Delta t) = & \int p(x, t_0 + \Delta t | x', t_0) \Gamma(x', t_0) dx' \\ & + \iint_{t_0}^{t_0 + \Delta t} p(x, t_0 + \Delta t | x', t') S(x', t') dt' dx' \end{aligned} \quad (7-92)$$

where p is the Green's function of (7-91). In the present instance it has the form

$$p(x,y,t|x',y',t_0) = \delta[x-(x'+\bar{x})]\delta[y-(y'+\bar{y})]e^{-b(t-t_0)} \quad (7-93)$$

where $\delta[x]$ is the delta function and

$$\bar{x} = \bar{x}(t|x',y',t_0) = \int_{t_0}^t U[x' + \bar{x}(t'), y' + \bar{y}(t'), t'] dt' \quad (7-94a)$$

$$\bar{y} = \bar{y}(t|x',y',t_0) = \int_{t_0}^t V[x' + \bar{x}(t'), y' + \bar{y}(t'), t'] dt'. \quad (7-94b)$$

The assumptions that U and V are approximately constant during the time step Δt should be valid provided that Δt is small enough to satisfy

$$\frac{1}{|\bar{u}|} \frac{\partial |\bar{u}|}{\partial t} \Delta t \ll 1. \quad (7-95)$$

From Eqs. 7-86 and 7-87 we find that this condition will be met in general if

$$\max \left\{ \frac{U\Delta t}{L}, \frac{g'H\Delta t}{UL} \right\} \ll 1 \quad (7-96)$$

where $g' = g \Delta\rho/\rho_0$; and U , H , and L are the characteristic speed, depth and length of fluctuations in the flow field. In the stable boundary layers that we plan to model, $g'H$ is typically of the order of $50 \text{ m}^2\text{sec}^{-2}$, $U \sim 5 \text{ m sec}^{-1}$; and thus for disturbances with a horizontal scale of $50 \cdot 10^3 \text{ m}$, which is near the resolution of the regional model, we can use time steps as large as 300 sec and satisfy (7-96). We should add, however, that in regions where the local Froude number

$$F = \frac{U^2}{g'H}$$

exceeds unity, flow discontinuities such as hydraulic jumps will occur, and these will cause considerable problems in the numerical model. We do not expect the nighttime flows that we will simulate to become supercritical often. When it happens, it will occur in isolated portions of the model region and we will be able to anticipate it by monitoring the temporal behavior of the flow. In those grid cells where we predict that the flow is about to become supercritical, we propose to prevent it by applying enhanced eddy viscosity.

A detailed description of the numerical scheme used to solve the flow model equations, specifically equations reducible to the form (7-91), is given in Appendix A of this section. The scheme described there is the same one that is used to solve the transport and diffusion component of the regional pollution model equations. The scheme is an explicit, 5th order space, 1st order time algorithm that permits the model domain to be treated in piece wise fashion. This is a particularly valuable feature in models such as ours that are too large to load entirely into the computer memory.

One of the principal problems associated with the numerical solution of equations like (7-86) - (7-88) is the treatment of the lateral boundary conditions. Since no generally valid method exists for specifying the boundary values required by the difference equations, a common practice in mesoscale flow models is to place the boundaries far from the edges of the spatial domain of interest. Another approach is to imbed the flow model within another one of coarser resolution which provides boundary values.

Neither of these methods of circumventing the boundary problem can be used in our studies because the additional computer storage and time that they would require would make the overall simulation effort impractical. Consequently, we have formulated an approximation of the boundary conditions, described in Appendix B of this section, that is sufficient for treating the limited periods of concern to us in modeling the nighttime boundary layer flow.

Below we outline the various stages of computation that are necessary within processor P7.

Stage ZT

The "raw" topography data available in the PIF will be denoted here by $\hat{z}_t(\lambda, \phi)$. These represent terrain elevations averaged over 5 min x 5 min latitude - longitude sectors. The regional model and the flow model developed in this section require the elevation $z_t(\lambda, \phi)$ averaged over 30 min x 45 min latitude - longitude sectors.

Let $z_t(I, J)$ denote the value of the 30 x 45 min smoothed terrain at grid point (I, J) (column I, row J) of the NEROS region. Then

$$z_t(I, J) = \sum_{i, j \in D(I, J)} \hat{z}_t(i, j) \quad (7-97)$$

where the summation is over the 54, 5 min x 5 min cells surrounding grid point (I, J) (see figure 7-5). Note that the 54 cell smoothing area used in the definition of $z_t(I, J)$ overlaps the smoothing areas associated with the 8 NEROS grid points nearest the point (I, J).

The input and output requirements of Stage ZT are summarized in Table 7-1 later in this section.

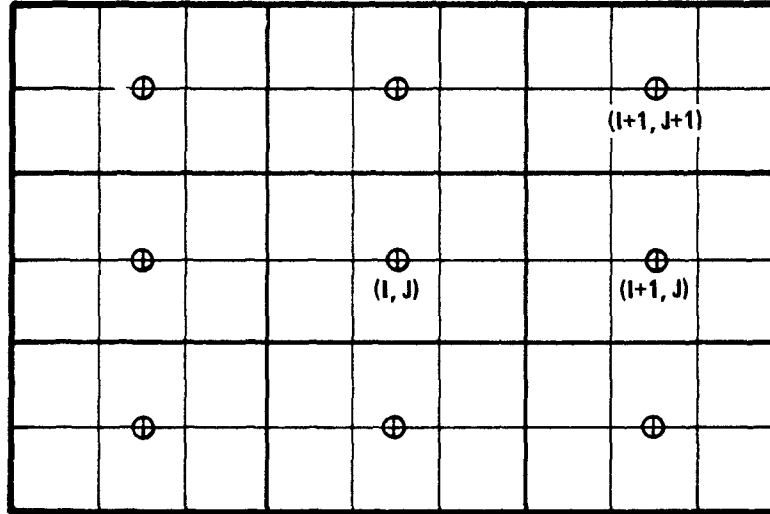


Figure 7-5. Illustration of the 54 5 min x 5 min cells that are used in the calculation of $z_t(I,J)$.

Stage DELR0

The parameter $\Delta\rho_1$ is used in this and other processors as an indicator of the presence of an inversion layer at the ground. This parameter will be a scalar and a function of time only in the first generation model. We define

$$\Delta\rho_1(t_n) = \begin{cases} 1, & \text{if surface inversion is present} \\ & \text{over most of the model region} \\ & \text{at time } t_n; \\ 0, & \text{otherwise.} \end{cases} \quad (7-98)$$

Under this definition the magnitude of $\Delta\rho_1$ is an indicator of the density of

air in Layer 1 relative to that in Layer 2. In the first generation model we will compute $\Delta\rho_1(t_n)$ using the following procedure.

(1) Define

$$\delta\rho_1(t_n) = \begin{cases} +1, & \text{if } \Delta\rho_1(t_n) = 0 \text{ and } \bar{Q}(t_n) \leq 0; \\ -1, & \text{if } \Delta\rho_1(t_n) = 1 \text{ and } \overline{TDEF}(t_n) \leq 0; \\ 0, & \text{otherwise} \end{cases} \quad (7-99)$$

where

$$\bar{Q}(t_n) = \sum_{ij} Q(i,j,t_n)$$

is the surface kinematic heat flux ($^{\circ}\text{K}\text{msec}^{-1}$) summed over all grid points (i,j) of the model domain, and \overline{TDEF} is the mean "temperature deficit" of the cold layer which we approximate by

$$\overline{TDEF}(t_n) = \alpha \sum_{ij} h_{\max}^2(i,j,t_m) - \sum_{ijn=0}^m q(i,j,n) \Delta t. \quad (7-100)$$

In this expression h_{\max} is the depth of the cold layer at the time the surface heat flux reverses, i.e.,

$$h_{\max}(i,j,t_m) = \begin{cases} h(i,j,t_m), & \text{if } Q(i,j,t_m) > 0 \\ & \text{and } Q(i,j,t_{m-1}) \leq 0; \\ 0, & \text{otherwise} \end{cases} \quad (7-101)$$

The value assigned to h_{\max} before the surface heat flux reversal, in this case 0, is immaterial since the value is never used. In (7-100), the variable q is given by

$$q(i,j,t_m) = \begin{cases} Q(i,j,t_m), & \text{if } Q(i,j,t_m) \geq 0; \\ 0, & \text{otherwise} \end{cases} \quad (7-102)$$

The constant α that appears in (7-100) is a temperature gradient that we define in Stage ETA.

(2) With $\delta\rho_1(t_n)$ determined by (7-99) a functional form for $\Delta\rho_1(t_n)$ that is consistent with (7-98) is the following:

$$\Delta\rho_1(t_n) = \Delta\rho_1(t_{n-1}) + \delta\rho_1(t_n) \quad (7-103a)$$

with initial value

$$\Delta\rho_1(t_0) = 0 \quad (7-103b)$$

and

$$t_0 = 1200 \text{ EST.} \quad (7-103c)$$

Under definition (7-103) we assume in effect that an inversion layer forms over the entire model domain at the hour the average surface heat flux over the whole domain becomes negative; and it disappears everywhere at the hour t_n that $\overline{\text{TDEF}}$, defined by (7-100), first becomes negative. This is clearly a crude approximation in a model such as ours which spans 15° of longitude, but to relax it would require an escalation in the complexity of the flow field description that would put the overall modeling effort beyond the scope of the "first generation" effort.

In summary, stage DELR0 computes the single scalar variable $\Delta\rho_1(t_n)$, $n=0,\dots,N$ using Eqs. (7-99) - (7-103). This variable is used throughout processor P7 as an indication of when specific functions are to be performed, and it is an output of P7 that guides the use of the fields generated here in other processors in the model network. A list of all the input and outputs of this stage is given later in Table 7-1.

Stage ETA

This stage operates only during those time steps t_n when $\Delta\rho_1(t_n)=1$ and it operates in unison with Stage FLOMOD, described below, which solves the equation set (7-86) - (7-88). In this stage we compute η_{vs} , using Eqs. (7-71) and (7-72), and $\Delta\rho/\rho_0$, using (7-90a). Both of these calculations require values of the temperature θ_h at the top of the cold layer. Rather than attempt to estimate these from upper air data, which would be a difficult task given the shallow depth of the cold layer and the limited frequency of the upper air measurements, we propose instead to estimate θ_h from the observed ground-level temperatures θ_0 assuming a constant temperature lapse

$$\frac{\partial\theta}{\partial z} = \alpha \quad (7-104)$$

in the cold layer. The observations reported by Godowitch and Ching (1980) of the nighttime surface inversion in rural areas around St. Louis indicate that a typical value is

$$\alpha = 1.2 \text{ } ^\circ\text{C}/100\text{m}. \quad (7-105)$$

Using (7-104) we have

$$\theta_h = \theta_0 + \alpha h \quad (7-106)$$

with α given by (7-105); and hence from (7-90a)

$$\Delta\rho/\rho_0 = \frac{\alpha h}{2\theta_0 + \alpha h} \approx \frac{\alpha h}{2\theta_0}. \quad (7-107)$$

We will estimate the surface temperature θ_0 at each grid point (I,J) using the virtual temperature observations T_{vn} , $n=1,\dots,N$ made at the N surface weather stations. We assume here that the T_{vn} ($^\circ\text{C}$) are available from Processor P3 for each hour. In this case $\theta_0(I,J,t_m)$ is computed as follows:

$$\theta_o(I,J,t_m) = \frac{\sum_{n=1}^N r_n^{-2} [T_{vn}(t_m) + 273]}{\sum_{n=1}^N r_n^{-2}} \quad (7-108)$$

where

$$r_n = [(I\Delta x - x_n)^2 + (J\Delta y - y_n)^2]^{\frac{1}{2}} \quad (7-109)$$

is the distance between grid cell (I,J) and the site (x_n, y_n) of surface station n. Equation (7-108) should be evaluated at each time step t_m that $\Delta\rho_1(t_m)=1$.

The inversion layer growth rate parameter η_{vs} can now be computed from (7-71) and (7-72) for each grid cell and time step. Since the physical assumptions on which the governing equations (7-86) - (7-88) are based do not hold in situations where the fluid is being heated from below, we must limit the minimum value of η_{vs} to zero. The net effect of this is to assume that over warm cities at night, the surface heat flux is never positive. Thus, we have

$$\eta_{vs}(I,J,t_m) = \max \{0, B[h_e - h(I,J,t_m)]\} \quad (7-110)$$

where

$$B = - \frac{1}{\alpha h(I,J,t_m)} \left[2 \frac{\partial \theta_o}{\partial t} + \alpha \frac{\partial h}{\partial t} \right] \quad (7-111a)$$

and

$$h_e = \frac{2Q(I,J,t_m)}{\left(2\frac{\partial\theta_o}{\partial t} + \alpha\frac{\partial h}{\partial t}\right)}. \quad (7-111b)$$

In these expressions we can use the approximations

$$\frac{\partial\theta_o}{\partial t} \approx \frac{\theta_o(I,J,t_m) - \theta_o(I,J,t_{m-1})}{\Delta t} \quad (7-112)$$

$$\frac{\partial h}{\partial t} \approx \frac{h(I,J,t_m) - h(I,J,t_{m-1})}{\Delta t} \quad (7-113)$$

where θ_o is given by (7-108) and h is the solution of Eq. 7-88 provided by Stage FLOMOD.

Note in (7-111b) that we use estimates of the surface heat flux Q in each cell rather than the expression (7-76) discussed earlier in the estimate of h_e . The latter is based on the assumption of homogeneous, flat terrain and homogeneous heat flux and hence estimates of $\overline{w'\theta_o'}$ derived from it using observations of the ageostrophic wind angle α acquired from wind observations would probably be erroneous.

In summary, Stage ETA provides values of $\Delta p/\rho_o$ (using (7-107)) at each grid point and time step that $\Delta p_1 = 1$; values of η_{vs} at the same locations and times using (7-110); and the surface temperature θ_o at all hours. A list of the input and output parameters of this Stage is provided in Table 7-1.

Stage PCD

This stage computes the pressure and drag coefficient terms that are required in the momentum equations (7-86) and (7-87). Therefore, this stage operates only at times t_m when $\Delta\rho_1(t_m) = 1$.

We assume that the sea-level pressure data $p_{sl,n}$ measured at each of the $n=1,2,\dots,N$ surface weather stations is available for each hour t_m that PCD operates. At each of these hours sea-level pressure values should be interpolated at each grid point in the model domain using the following formula:

$$p_{sl}(I,J,t_m) = \frac{\sum_{n=1}^N p_{sl,n}(t_m) r_n^{-1}}{\sum_{n=1}^N r_n^{-1}} \quad (7-114)$$

where

$$r_n = [(I\Delta x - x_n)^2 + (J\Delta y - y_n)^2]^{\frac{1}{2}} \quad (7-115)$$

and N is the number of surface stations at which sea-level pressure values are available. Using the same interpolation formula, derive estimates of the surface air density at each grid point at hour t_m :

$$\rho_0(I,J,t_m) = \frac{\sum_{n=1}^N \rho_n(t_m) r_n^{-1}}{\sum_{n=1}^N r_n^{-1}} \quad (7-116)$$

where r_n is given by (7-115) and ρ_n is the density at surface station n (from P3).

At each grid point we require values of the functions

$$p_x \equiv \frac{1}{\rho_o} \frac{\partial p_{s1}}{\partial x} \quad (7-117a)$$

$$p_y \equiv \frac{1}{\rho_o} \frac{\partial p_{s1}}{\partial y} \quad (7-117b)$$

We will approximate the spatial derivatives that appear in (7-117) using the fourth-order finite difference scheme discussed in the appendix to Section 8. With those expressions we get

$$\begin{aligned} p_x(I, J, t_m) = & A[\rho_o(I, J, t_m)]^{-1} \{ 2/3[p_{s1}(I+1, J, t_m) \\ & - p_{s1}(I-1, J, t_m)] - 1/12[p_{s1}(I+2, J, t_m) \\ & - p_{s1}(I-2, J, t_m)] \} (\Delta x)^{-1} \end{aligned} \quad (7-118)$$

$$\begin{aligned} p_y(I, J, t_m) = & A[\rho_o(I, J, t_m)]^{-1} \{ 2/3[p_{s1}(I, J+1, t_m) \\ & - p_{s1}(I, J-1, t_m)] - 1/12[p_{s1}(I, J+2, t_m) \\ & - p_{s1}(I, J-2, t_m)] \} (\Delta y)^{-1} \end{aligned} \quad (7-119)$$

where Δx and Δy are the x and y separation distances (m) of the grid points nearest (I, J) ; and $A = 100$ is the conversion factor required to transform the sea-level pressure values from units of millibars to $\text{kg m}^{-1}\text{sec}^{-2}$. (Note that ρ_o has units of kg m^{-3} and Δx and Δy have units of meters.) The gridded functions p_x and p_y are outputs of Stage PCD each hour that $\Delta p_1 = 1$; and the sea-level pressure p_{s1} given by (7-114) is an output for all hours.

The computation of the drag coefficient value C_D in each grid cell and hour requires a straightforward implementation of Eq. (7-89). We have

$$C_D(I,J,t_m) = k \{ [\ln(\frac{h(I,J,t_m)}{z_0(I,J)}) - b]^2 + a^2 \}^{-1/2} \quad (7-120)$$

where $k=0.4$; z_0 is the surface roughness (m) of cell (I,J); h is the depth (m) of the surface inversion layer in (I,J) at t_m (from Stage FLOMOD); and

$$a = \begin{cases} 5, & \text{if } L(I,J,t_m) \geq 0; \\ -1, & \text{otherwise} \end{cases}$$

$$b = \begin{cases} -5, & \text{if } L(I,J,t_m) \geq 0; \\ 4, & \text{otherwise.} \end{cases}$$

Here L is the Obukhov length (m) in cell (I,J) at hour t_m (from P4). The coefficient $C_D(I,J,t_m)$ is the third and final output of Stage PCD. (Refer to Table 7-1 for a summary of the inputs and outputs of this Stage.)

Stage IBC

This stage computes boundary and initial values of u , v , and h for use in solving the system of equations (7-86) - (7-88). For this purpose we assume that initially and along the boundaries of the simulation region the velocity field is in equilibrium with the friction, pressure and Coriolis forces. That is, we assume (cf 7-86, 87)

$$\frac{s^2 C_D^2 \cos \theta}{h} = -P_x + fs (\sin \theta) \quad (7-121)$$

$$\frac{s^2 C_D^2 \sin \theta}{h} = -P_y - fs (\cos \theta) \quad (7-122)$$

where $s = (u^2 + v^2)^{\frac{1}{2}}$ is the flow speed and θ is its direction. Cross-multiplying (7-121) by (7-122) we get

$$P_x \sin\theta - P_y \cos\theta = fs \quad (7-123)$$

and on squaring (7-121) and (7-122), adding the results and making use of (7-123) we obtain

$$\frac{s^4 C_D^4}{h^2} + f^2 s^2 - (P_x^2 + P_y^2) = 0. \quad (7-124)$$

Since all parameters except s in (7-124) are known, we can solve this equation for the flow speed s at each grid point and then substitute the results into (7-123) to obtain the corresponding flow directions θ .

Next, we define the time t_{K0} :

$$t_{K0} \equiv \text{time during a given 24-hour period when } \Delta p_1 \text{ changes from 0 to 1.} \quad (7-125)$$

This marks the initial instant at which the equations (7-86) - (7-88) apply, and it is the function of Stage IBC to provide the necessary values of u , v , and h at this time. Thus,

if $t_m = t_{K0}$, Stage IBC computes initial values as follows:

$$h(i, j, t_{K0}) = h_0 = 30m, \quad (7-126)$$

$$u(i, j, t_{K0}) = s(i, j, t_{K0}) \cos\theta(i, j, t_{K0}) \quad (7-127)$$

$$v(i, j, t_{K0}) = s(i, j, t_{K0}) \sin\theta(i, j, t_{K0}) \quad (7-128)$$

where $s(i,j,t_{K0})$ is the solution of (7-124) at grid point (i,j) based on values of P_x , P_y , C_D and h (from 7-126) at that point; and $\theta(i,j,t_{K0})$ is the corresponding solution of Eq. (7-123).

if $t_m > t_{K0}$ and $\Delta p_1(t_m) = 1$, Stage IBC computes
boundary values of u , v , and h as follows:

$$\dot{H}_{BC}(i,j,t_m) = \eta_{vs}(i,j,t_m) \quad (7-129)$$

$$\dot{U}_{BC}(i,j,t_m) = \frac{1}{\Delta t} [u(i,j,t_m) - u(i,j,t_{m-1})] \quad (7-130)$$

$$\dot{V}_{BC}(i,j,t_m) = \frac{1}{\Delta t} [v(i,j,t_m) - v(i,j,t_{m-1})]. \quad (7-131)$$

In these equations (i,j) are boundary points only. Also, η_{vs} is given by Stage ETA and u and v are computed on the boundaries using the same method employed to obtain the initial conditions, (7-127) and (7-128) above. We should point out that in our treatment of the boundary conditions (see Appendix B to this chapter), we give the values of u , v , and h at inflow boundary points in terms of their initial values, i.e., $h(i,j,t_{K0})$ etc., and we require that the subsequent time derivatives of these variables be specified, namely

\dot{H} , \dot{U} , and \dot{V} .

Stage IBC provides the boundary conditions (7-129) - (7-131) at each time step t_m that $\Delta p_1 = 1$. The input and output parameters for this stage are summarized in Table 7-1.

Stage H1H0

This stage performs the final operations in the calculation of the elevation z_1 , of the top surface of Layer 1 of the regional model; and it converts this and other surface elevations into pressure coordinates. The specific operations are defined below.

$$h_1(i,j,t_m) = \begin{cases} h(i,j,t_m), & \text{if } \Delta\rho_1(t_m) = 1; \\ \max\{100, \min\{500, L(i,j,t_m)\}\}, & \text{if } \Delta\rho_1(t_m) = 0. \end{cases} \quad (7-132)$$

Here h is the solution of (7-88), as provided by stage FLOMOD, and L is the Obukhov length, used earlier. The value assigned h_1 by Eq. (7-132) when $\Delta\rho_1 = 0$ is constrained to prevent the Layer 1 depth from approaching zero thickness -- which could happen in extremely unstable conditions when $L \rightarrow 0$ -- and also to prevent Layer 1 from becoming as deep as the mixed layer -- which would force the thickness of Layer 2 to zero. Although these constraints are not necessary in principle, they are applied to prevent numerical problems in the code which might arise as cell thicknesses approach arbitrarily small values.

The virtual surface elevation z_{vs} is computed as follows:

$$z_{vs}(i,j,t_m) = \begin{cases} z_T(i,j) + h_1(i,j,t_m), & \text{if } \Delta\rho_1(t_m) = 1; \\ z_T(i,j), & \text{if } \Delta\rho_1(t_m) = 0. \end{cases} \quad (7-133)$$

Since Z_T is given in meters above sea-level, the values of z_1 and z_{vs} obtained from (7-132) and (7-133) are also in units of m (MSL).

Several other processors require the surface elevations in pressure coordinates. These are computed as follows:

$$p_1(i,j,t_m) = p_{s1}(i,j,t_m) \exp\left[-\frac{z_1(i,j,t_m)g}{R_d T(i,j,t_m)}\right] \quad (7-134)$$

where $g = 9.8 \text{ m sec}^{-2}$, $R_d = 287 \text{ m}^2 \text{ sec}^{-2} \text{ }^\circ\text{K}^{-1}$, $z_1 = z_T + h_1$, and

$$T(i,j,t_m) = \frac{1}{2}[2\theta_0(i,j,t_m) + 0.0065z_t(i,j)] . \quad (7-135)$$

In this expression $0.0065 \text{ }^\circ\text{K m}^{-1}$ is the temperature lapse rate of the Standard Atmosphere which, for altitude calculation purposes, we assume holds between ground elevation and sea-level.

Similarly

$$p_{vs}(i,j,t_m) = \text{Eq. (7-134) with } z_1 \text{ replaced by } z_{vs} \quad (7-136)$$

Finally, in accordance with the analyses presented in Appendix B of Part 1 of this report, we shall prescribe the depth h_0 of Layer 0 to be

$$h_0(i,j,t_m) = h_1(i,j,t_m)/10. \quad (7-137)$$

The inputs and outputs of Stage H1H0 are summarized in Table 7-1.

Stage SIG

This stage estimates the fractions σ_{T1} and σ_{T0} of surfaces $z_1(x,y,t_m)$ and $[z_T(x,y) + h_0(x,y,t_m)]$ that are penetrated by terrain.

Referring to Fig. 7-5 which illustrates the process of computing z_T in Stage ZT, we define

$$\sigma_{T1}(I,J,t_m) = \frac{1}{54} \sum_{i,j \in D(I,J)_m} \lambda(i,j,t_m) \quad (7-138)$$

where λ is defined as

$$\lambda(i,j,t_m) \equiv \begin{cases} 1, & \text{if } \hat{z}_t(i,j) \geq z_1(I,J,t_m); \\ 0, & \text{otherwise} \end{cases} \quad (7-139)$$

and the summation in (7-138) is over all 54 of the 5 min x 5 min subcells contained within the 3 x 3 grid cell area in which $z_T(I,J)$ is defined.

For simplicity in this first generation model we will assume

$$\sigma_{T0}(I,J,t_m) = \sigma_{T1}(I,J,t_m), \quad (7-140)$$

where σ_{T1} is given by (7-138). The inputs and outputs of Stage SIG are summarized in Table. 7-1.

Stage FLOMOD

This stage solves the system of equations (7-86) - (7-88) using the numerical method discussed earlier, beginning on page 79. A detailed description of the numerical procedures used to solve the equations is given in the appendices to this chapter; and the input and output parameters of this stage are summarized in Table 7-1.

A schematic view of the interrelationships among the various stages that comprise Processor P7 is given in Figure 7-6, page 130.

Table 7-1. Summary of the input and output requirements of each stage of Processor P7.

Input Variable	Description	Source	Stage	Output Variable	Description
$Q(i,j,t_n)$	surface kinematic heat flux ($^{\circ}\text{K m s}^{-1}$) at grid cell (i,j) at hour t_n	P4	DELRO	$\Delta\rho_1(t_m)$	surface inversion indicator: = 1 if an inversion is present over the entire model domain at hour t_m ; = 0 otherwise.
$h(i,j,t_n)$	depth of cold layer (m) at grid point (i,j) at hour t_n	Stage FLOMOD			
$\hat{z}_t(\lambda,\phi)$	5 min x 5 min smoothed terrain elevation (m MSL) centered at longitude λ , latitude ϕ .	RAW	ZT	$z_t(i,j)$	30 min x 45 min smoothed terrain centered at NEROS grid cell (i,j).
$T_{vn}(t_m)$	virtual temperature ($^{\circ}\text{C}$) at surface weather station $n=1,\dots,N$ at hour t_m .	P3	ETA (operates only when $\Delta\rho_1=1$)	$\Delta\rho/\rho_0(i,j,t_n)$	buoyancy parameter at grid point (i,j) at time t_n
$h(i,j,t_n)$	depth of cold layer (m) at grid point (i,j) at hour t_n	Stage FLOMOD		$\eta_{vs}(i,j,t_n)$	cold layer growth rate (m s^{-1}) at grid point (i,j) at time t_n .
				$\theta_0(i,j,t_n)$	Surface temperature, $^{\circ}\text{K}$.
$Q(i,j,t_m)$	surface heat flux ($^{\circ}\text{K m sec}^{-1}$)	P4			
$p_{sl,n}(t_m)$	sea-level pressure (mb) at surface station n, hour t_m	P3	PCD	$P_x(I,J,t_m)$	horizontal pressure force term in Eq. (7-86) (see 7-118)
$\rho_n(t_m)$	surface air density (kg m^{-3}) at surface station n, hour m.	P3		$P_y(I,J,t_m)$	horizontal pressure force term in Eq. (7-87) (see 7-119).

Table 7-1. (Continued)

Input Variable	Description	Source	Stage	Output Variable	Description
$h(I,J,t_m)$	depth (meter) of cold surface layer in cell (I,J) at hour m.	Stage FLOMOD	PCD (cont.)	$C_D(I,J,t_m)$	drag coefficient (dimensionless) in cell (I,J) at hour m.
$z_o(I,J)$	surface roughness (m) in cell (I,J)	P4		$p_{sl}(i,j,t_m)$	sea-level pressure in cell (i,j) at hour t
$L(I,J,t_m)$	Obukhov length (m) in cell (I,J) at hour m.	P4			
$P_x(i,j,t_m)$	horizontal pressure force term (see 7-118)	Stage PCD	IBC	$h(i,j,t_{K0})$	initial depth (m) of the cold layer in cell (i,j)
$P_y(i,j,t_m)$	horizontal pressure force term (see 7-119)	Stage PCD		$u(i,j,t_{K0})$	initial east-west ₋₁ flow speed (m sec ⁻¹) component in cell (i,j)
$C_D(i,j,t_m)$	drag coefficient	Stage PCD		$v(i,j,t_{K0})$	initial north-south flow speed component in cell (i,j)
$\eta_{vs}(i,j,t_m)$	cold layer growth rate (m/sec)	Stage ETA		$\dot{H}_{BC}(i,j,t_m)$	time derivative (m/s) of cold layer depth at boundary cell (i,j) at time t_m
				$\dot{U}_{BC}(i,j,t_m)$	time derivative of the east-west flow component on the boundary at time t_m
				$\dot{V}_{BC}(i,j,t_m)$	time derivative of the north-south flow component at boundary point ₋₂ (i,j) (units: m sec ⁻²)
$z_T(i,j)$	elevation (m, MSL) of smoothed terrain in grid cell (i,j)	Stage ZT	H1H0	$h_1(i,j,t_m)$	thickness (m) of Layer 1 in cell (i,j) at time t_m

Table 7-1. (Continued)

Input Variable	Description	Source	Stage	Output Variable	Description
$h(i,j,t_m)$	depth (m) of cold surface layer	Stage FLOMOD	H1H0 (cont.)	$z_{vs}(i,j,t_m)$	elevation (m, MSL) of virtual surface in cell (i,j), hour t_m
$L(i,j,t_m)$	Obukhov length (m)	P4			
$p_{s1}(i,j,t_m)$	sea-level pressure (mb) in cell (i,j) at hour t_m	Stage PCD		$p_1(i,j,t_m)$	elevation of surface z_1 in pressure (mb) coordinates.
$\theta_0(i,j,t_m)$	surface temperature ($^{\circ}$ K) in cell (i,j), hour t_m	Stage ETA		$p_{vs}(i,j,t_m)$	elevation of the virtual surface z_{vs} in pressure (mb) coordinates
$\Delta p_1(t_m)$	indicator of presence of cold surface layer	Stage DELRO		$h_0(i,j,t_m)$	depth (m) of Layer 0 in cell (i,j) at hour t_m .
$z_t(i,j)$	smoothed terrain elevations (m, MSL)	Stage ZT	SIG	$\sigma_{T1}(i,j,t_m)$	fraction ($0 \leq \sigma_{T1} \leq 1$) of surface z_1 penetrated by terrain in cell (i,j) at hour t_m
$\hat{z}_t(i,j)$	5 min x 5 min averaged terrain elevation (m, MSL) of cell (i,j)	RAW		$\sigma_{T0}(i,j,t_m)$	fraction ($0 \leq \sigma_{T0} \leq 1$) of top surface of Layer 0 that is penetrated by terrain.
$z_1(i,j,t_m)$	elevation (m, MSL) of top surface of Layer 1.	Stage H1H0			
$z_t(i,j)$	smoothed terrain elevation	Stage ZT	FLOMOD	$h(i,j,t_m)$	depth of cold layer at time t_m in cell (i,j)
$P_x(i,j,t_m)$	see stage PCD output	Stage PCD		$\langle u(i,j,t_m) \rangle_{vL}$	cell averaged east-west flow speed component (m/sec) at time t_m in the cold layer
$P_y(i,j,t_m)$	see stage PCD output	Stage PCD			

Table 7.1. (Concluded)

Input Variable	Description	Source	Stage	Output Variable	Description
$C_D(i,j,t_m)$	drag coefficient	Stage PCD		$\langle v(i,j,t_m) \rangle_{vL}$	same as $\langle u \rangle_{vL}$ except north-south component
$\Delta\rho/\rho_0(i,j,t_m)$	buoyancy parameter	Stage ETA			
$\eta_{vs}(i,j,t_m)$	cold layer growth rate	Stage ETA			
$\Delta\rho_1(t_m)$	indicator of presence of cold surface layer	Stage DELRO			
$\left. \begin{matrix} h(i,j,t_{K0}) \\ u(i,j,t_{K0}) \\ v(i,j,t_{K0}) \end{matrix} \right\}$	initial values of h, u, and v	Stage IBC			
$\dot{h}_{BC}(i',j',t_m)$	time rate of change ($m \text{ sec}^{-1}$) of cold layer depth at boundary point (i',j') at time t_m	Stage IBC			
$\dot{u}_{BC}(i',j',t_m)$	acceleration ($m \text{ sec}^{-2}$) of east-west flow component at boundary point (i',j') at time t_m .	Stage IBC			
$\dot{v}_{BC}(i',j',t_m)$	same as \dot{u}_{BC} except north-south flow component.	Stage IBC			

Appendix A to Section 7.

Here we describe a numerical procedure for deriving solutions of differential equations of the form

$$\frac{\partial \Gamma}{\partial t} + U \frac{\partial \Gamma}{\partial x} + V \frac{\partial \Gamma}{\partial y} + b\Gamma = K \frac{\partial^2 \Gamma}{\partial x^2} + K \frac{\partial^2 \Gamma}{\partial y^2} + S \quad (7-A1)$$

where all coefficients are functions of time and all except K and b are functions of (x,y,t). We pointed out in Eq. 7-92 that the solution of (7-A1) can be expressed in the form

$$\begin{aligned} \Gamma(x, t_1) = & \int p(x, t_1 | x', t_0) \Gamma(x', t_0) dx' \\ & + \iint_{t_0}^{t_1} p(x, t_1 | x', t') S(x', t') dt' dx' \end{aligned} \quad (7-A2)$$

where

$$p(x, t | x', t') = \frac{1}{2\pi\sigma^2} \exp \left[-\frac{(x-x'-\bar{x})^2}{2\sigma^2} - \frac{(y-y'-\bar{y})^2}{2\sigma^2} - \int_{t'}^t b(t'') dt'' \right] \quad (7-A3)$$

$$\bar{x} = \bar{x}(t | x', y', t') = \int_{t'}^t U(x' + \bar{x}(t''), y' + \bar{y}(t''), t'') dt'' \quad (7-A4)$$

$$\bar{y} = \bar{y}(t | x', y', t') = \int_{t'}^t V(x' + \bar{x}(t''), y' + \bar{y}(t''), t'') dt'' \quad (7-A5)$$

and

$$\sigma^2 = 2K(t-t'). \quad (7-A6)$$

In both our flow model and in the regional model we are interested in the values of the dependent variable Γ only at the grid points

$$\underline{x} = (I\Delta x, J\Delta y), \quad I, J = 1 \dots I_{MAX}, J_{MAX};$$

and only at the discrete time intervals $t_n = n\Delta t$, $n = 1, \dots$. Furthermore, in the situations of concern to us the spatial variations in S are of a scale much larger than $U_{MAX}\Delta t$ or $V_{MAX}\Delta t$ and the temporal variations are generally slower than the time step Δt . Under these conditions we can express (7-A2) in the approximate form

$$\Gamma_{IJ}^{n+1} = \int p(I\Delta x, J\Delta y, t_{n+1} | \underline{x}', t_n) F(\underline{x}', t_n) d\underline{x}' \quad (7-A7)$$

where

$$\Gamma_{IJ}^n = \Gamma(I\Delta x, J\Delta y, t_n) \quad (7-A8)$$

and

$$F(\underline{x}', t_n) = \Gamma(\underline{x}', t_n) + S(\underline{x}', t_n)\Delta t. \quad (7-A9)$$

Eq. 7-A7 expresses the value of Γ at grid point (I, J) at the future time t_{n+1} in terms of its known values at the present time t_n . Since the kernel p has the form (7-A3), we can evaluate (7-A7) analytically if we express $F(\underline{x}', t_n)$ in polynomial form (or in a Fourier series).

To do this we note first that the kernel p in (7-A7) has a maximum value at the point

$$\left. \begin{aligned} x' &= x^* = I\Delta x - \bar{x} \\ y' &= y^* = J\Delta y - \bar{y} \end{aligned} \right\} \quad (7-A10)$$

and it decreases to zero rather rapidly away from this point. In fact, if $K=0$, p has the delta function form given earlier by (7-93). Thus, the polynomial that we use to represent F in (7-A7) should have maximum accuracy in the vicinity of the point $\underline{x}' = (x^*, y^*)$, which we can find by solving the transcendental equations (7-A10). In the simple case where the spatial variations in U and V are much larger than Δx and Δy and the temporal changes in U and V are slow compared to Δt , (7-A10) yields the approximate solutions (cf 7-94)

$$\left. \begin{aligned} x^* &= I\Delta x - U(I\Delta x, J\Delta y, t_{n+1})\Delta t \\ y^* &= J\Delta y - V(I\Delta x, J\Delta y, t_{n+1})\Delta t \end{aligned} \right\} \quad (7-A11)$$

The points (x^*, y^*) and $(I\Delta x, J\Delta y)$ are illustrated in Figure 7-A1.

Using computer programming notation (to facilitate comparisons of the theory presented here with the actual computer code), we define

$$IST = [IFIX(x^*/\Delta x) + 0.5]\Delta x \quad (7-A12)$$

$$JST = [IFIX(y^*/\Delta y) + 0.5]\Delta y \quad (7-A13)$$

As illustrated in Figure 7-A1, (IST, JST) is the grid cell center closest to (x^*, y^*) (taking the grid points (I, J) to lie at the corners of each grid cell). In preparation for the expansion of $F(\underline{x}', t_n)$ in polynomial form, we define the new coordinates

$$\eta = \frac{x' - IST}{(\Delta x/2)} \quad (7-A14)$$

$$\xi = \frac{y' - JST}{(\Delta y/2)} \quad (7-A15)$$

Note that the origin of the (η, ξ) system is the cell center (IST, JST) . We can

now express $F(\tilde{x}', t_n)$ by the biquintic (5th order) Lagrange polynomial

$$F(\tilde{x}', t_n) = \sum_{i=1}^6 \sum_{j=1}^6 [F_{ij}^n \frac{\prod_{k=1}^6 (\eta - a_k)}{\prod_{k=1}^6 (a_i - a_k)} \frac{\prod_{l=1}^6 (\xi - b_l)}{\prod_{l=1}^6 (b_j - b_l)}] \quad (7-A16)$$

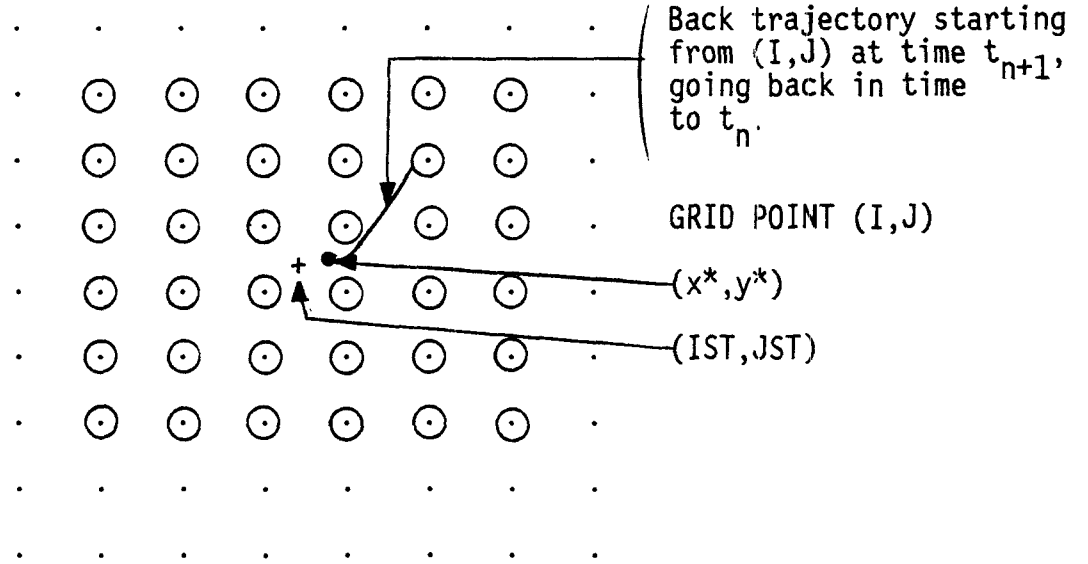


Figure 7-A1. Illustration of the points used in the numerical solution of Eq. 7-A1. Circled grid points are those from which values of Γ and S are taken to derive a biquintic expansion of $F(\tilde{x}', t_n)$ about the point (IST, JST) (see Eq. 7-A9).

where

$$\left. \begin{aligned} a_1 &= b_1 = -5 \\ a_2 &= b_2 = -3 \\ a_3 &= b_3 = -1 \\ a_4 &= b_4 = 1 \\ a_5 &= b_5 = 3 \\ a_6 &= b_6 = 5 \end{aligned} \right\} \quad (7-A17)$$

$$F_{ij}^n = F(i\Delta x/2 + IST, j\Delta y/2 + JST, t_n) \quad (7-A18)$$

and

$$\prod_{k=1}^6 () = \text{product over all } k \text{ except } k=i,$$

$$\prod_{l=1}^6 () = \text{product over all } l \text{ except } l=j.$$

Note that (a_i, b_j) , $i, j=1 \dots 6$ are the coordinates in (η, ξ) space of the grid points at which the F_{ij}^n are evaluated. These are the circled grid points shown in Figure 7-A1.

To simplify (7-A16) let

$$X_i = \prod_{k=1}^6 (\eta - a_k) \quad (7-A19)$$

$$Y_j = \prod_{l=1}^6 (\xi - b_l) \quad (7-A20)$$

$$L_i = \prod_{k=1}^6 (a_i - a_k) \quad (7-A21)$$

$$M_j = \prod_{l=1}^6 (b_j - b_l). \quad (7-A22)$$

The last two parameters can be evaluated directly using (7-A17). We get

$$\left. \begin{array}{l} L_1 = M_1 = -3840 \\ L_2 = M_2 = 768 \\ L_3 = M_3 = -384 \\ L_4 = M_4 = 384 \\ L_5 = M_5 = -768 \\ L_6 = M_6 = 3840 \end{array} \right\} \quad (7-A23)$$

Now (7-A16) can be written

$$F(\tilde{x}', t_n) = \sum_{i=1}^6 \sum_{j=1}^6 F_{ij}^n \frac{X_i Y_j}{L_i M_j} \quad (7-A24)$$

Now look at the expansion of X_i :

$$X_1 = \eta^5 - 5\eta^4 - 10\eta^3 + 50\eta^2 + 9\eta - 45 \quad (7-A25)$$

$$X_2 = \eta^5 - 3\eta^4 - 26\eta^3 + 78\eta^2 + 25\eta - 75 \quad (7-A26)$$

$$\vdots$$

$$X_6 = \eta^5 + 5\eta^4 - 10\eta^3 - 50\eta^2 + 9\eta + 45. \quad (7-A27)$$

Thus, we can express the X_i in the alternate form

$$X_i = \sum_{\alpha=0}^5 a_{i\alpha} \eta^\alpha \quad (7-A28)$$

where the coefficients $a_{i\alpha}$ are the known values given in (7-A25 - A27).

Similarly

$$Y_j = \sum_{\beta=0}^5 a_{j\beta} \xi^\beta. \quad (7-A29)$$

Substituting (7-A28) and (7-A29) into (7-A24) and we obtain

$$F(\tilde{x}', t_n) = \sum_{\alpha=0}^5 \sum_{\beta=0}^5 A_{\alpha\beta}^n \eta^\alpha \xi^\beta \quad (7-A30)$$

where

$$A_{\alpha\beta}^n = \sum_{i=1}^6 \sum_{j=1}^6 F_{ij}^n \frac{a_{i\alpha} a_{j\beta}}{L_i M_j}. \quad (7-A31)$$

We now have the polynomial expansion of $F(\underline{x}', t_n)$ that we need to evaluate (7-A7), but first we must change the integration variables in (7-A7) from \underline{x}' to (η, ξ) . We get

$$\Gamma_{IJ}^{n+1} = \left(\frac{\Delta x}{2}\right) \left(\frac{\Delta y}{2}\right) \int_{-\infty}^{\infty} \int_{-\infty}^{\infty} \phi_x(I, x', t_{n+1}, t_n) \phi_y(J, y', t_{n+1}, t_n) e^{-b^* \Delta t} F(\eta, \xi, t_n) d\eta d\xi \quad (7-A32)$$

where

$$\phi_x = \frac{1}{\sqrt{2\pi}\sigma} \exp \left[-\frac{(I\Delta x - x' - \bar{x})^2}{2\sigma^2} \right] \quad (7-A33)$$

$$\phi_y = \frac{1}{\sqrt{2\pi}\sigma} \exp \left[-\frac{(J\Delta y - y' - \bar{y})^2}{2\sigma^2} \right] \quad (7-A34)$$

(see Eq. 7-A3); and $b^* = b(x^*, y^*, t_n)$.

Let

$$\epsilon_x = x^* - IST \quad (7-A35)$$

$$\epsilon_y = y^* - JST. \quad (7-A36)$$

Then, representing x' in (7-A33) in terms of η we obtain (from 7-A14 and 7-A10)

$$\phi_x = \frac{2}{\sqrt{2\pi}\hat{\sigma}\Delta x} \exp \left[-\frac{(\eta + \hat{\epsilon}_x)^2}{2\hat{\sigma}^2} \right] \quad (7-A37)$$

where

$$\hat{\varepsilon}_x = \varepsilon_x / (\Delta x / 2) \quad (7-A38)$$

$$\hat{\sigma} = \sigma / (\Delta x / 2) \quad (7-A39)$$

An expression similar to (7-A37) describes ϕ_y .

Substituting (7-A30), (7-A37) and the analogous expression for ϕ_y into (7-A32) we obtain

$$\Gamma_{IJ}^{n+1} = \sum_{\alpha=0}^5 \sum_{\beta=0}^5 A_{\alpha\beta}^n e^{-b^* \Delta t} \lambda_{\alpha} v_{\beta} \quad (7-A40)$$

where

$$\lambda_{\alpha} = \frac{1}{\sqrt{2\pi\hat{\sigma}}} \int_{-\infty}^{\infty} \eta^{\alpha} \exp \left[-\frac{(\eta + \hat{\varepsilon}_x)^2}{2\hat{\sigma}^2} \right] d\eta \quad (7-A41)$$

$$v_{\beta} = \frac{1}{\sqrt{2\pi\hat{\sigma}}} \int_{-\infty}^{\infty} \xi^{\beta} \exp \left[-\frac{(\xi + \hat{\varepsilon}_y)^2}{2\hat{\sigma}^2} \right] d\xi \quad (7-A42)$$

These last two integrals can be evaluated analytically and we get

$$\begin{aligned} \lambda_0 &= 1 \\ \lambda_1 &= \hat{\varepsilon}_x \\ \lambda_2 &= \hat{\varepsilon}_x^2 + \hat{\sigma}^2 \\ \lambda_3 &= \hat{\varepsilon}_x^3 + 3\hat{\varepsilon}_x \hat{\sigma}^2 \\ \lambda_4 &= \hat{\varepsilon}_x^4 + 6\hat{\varepsilon}_x^2 \hat{\sigma}^2 + 3\hat{\sigma}^4 \\ \lambda_5 &= \hat{\varepsilon}_x^5 + 10\hat{\varepsilon}_x^3 \hat{\sigma}^2 + 15\hat{\varepsilon}_x \hat{\sigma}^4 \end{aligned} \quad (7-A43)$$

Similar expressions give v_β , $\beta=1,\dots,6$, except $\hat{\epsilon}_x$ is replaced by $\hat{\epsilon}_y$.

In summary, the value of the dependent variable Γ governed by (7-A1) is obtained at time level $n+1$ at grid point (I,J) from (7-A40) where $A_{\alpha\beta}^n$ is derived from (7-A31) using known values of Γ at time level n ; and where the λ and v parameters are given by (7-A43).

Appendix B to Section 7

Here we describe the scheme we have developed to provide the boundary values that the numerical analogues of the differential equations (7-86) - (7-88) require but which the differential equations themselves do not need.

The essence of our method is that we divide the u , v , and h fields into a base state and a perturbation component, and then in the governing equations we set all sources of the perturbation fields to zero outside the region in which the prognostic equations are applied. In addition we assume that perturbations do not exist outside inflow points of the modeling domain. At outflow points, we extrapolate interior values to estimate u , v , and h outside the boundary, but these estimates are only included in the advection and diffusion terms of the equation and are excluded from the forcing terms.

Rewriting the governing equations (7-86, 87, and 88) for future reference and manipulation, we have

$$\frac{\partial u}{\partial t} + u \frac{\partial u}{\partial x} + v \frac{\partial u}{\partial y} + \frac{u}{h} C_D^2 (u^2 + v^2)^{\frac{1}{2}} = \quad (7-B1)$$

$$-g' \left(\frac{\partial h}{\partial x} + \frac{\partial z_t}{\partial x} \right) - p_x + fv + K \frac{\partial^2 u}{\partial x^2} + K \frac{\partial^2 u}{\partial y^2}$$

$$\frac{\partial v}{\partial t} + u \frac{\partial v}{\partial x} + v \frac{\partial v}{\partial y} + \frac{v}{h} C_D^2 (u^2 + v^2)^{\frac{1}{2}} = \quad (7-B2)$$

$$-g' \left(\frac{\partial h}{\partial y} + \frac{\partial z_t}{\partial y} \right) - p_y - fu + K \frac{\partial^2 v}{\partial x^2} + K \frac{\partial^2 v}{\partial y^2}$$

$$\frac{\partial h}{\partial t} + u \frac{\partial h}{\partial x} + v \frac{\partial h}{\partial y} + h \left(\frac{\partial u}{\partial x} + \frac{\partial v}{\partial y} \right) = \eta + K_h \frac{\partial^2 h}{\partial x^2} + K_h \frac{\partial^2 h}{\partial y^2} \quad (7-B3)$$

where

$$p_x = \frac{1}{\rho_0} \frac{\partial p}{\partial x}, \quad p_y = \frac{1}{\rho_0} \frac{\partial p}{\partial y}, \quad g' = g \frac{\Delta \rho}{\rho_0}. \quad (7-B4)$$

Let

$$u = \bar{u} + u' \quad (7-B5a)$$

$$v = \bar{v} + v' \quad (7-B5b)$$

$$h = \bar{h} + h' \quad (7-B5c)$$

where barred variables refer to the base state and primed variables denote fluctuations from this state. Our aim is to absorb the effects of the given large scale forcing terms p_x and p_y as well as initial and boundary conditions in the base state variables $(\bar{u}, \bar{v}, \bar{h})$, and to let (u', v', h') represent the perturbations from this state that arise as a result of forcing by the terrain z_t and cooling η within the simulated domain. Substituting (7-B5a) into (7-B1) we get

$$\begin{aligned} & \frac{\partial \bar{u}}{\partial t} + \frac{\partial u'}{\partial t} + \bar{u} \frac{\partial \bar{u}}{\partial x} + \bar{u} \frac{\partial u'}{\partial x} + u' \frac{\partial \bar{u}}{\partial x} + u' \frac{\partial u'}{\partial x} \\ & + \bar{v} \frac{\partial \bar{u}}{\partial y} + \bar{v} \frac{\partial u'}{\partial y} + v' \frac{\partial \bar{u}}{\partial y} + v' \frac{\partial u'}{\partial y} \\ & + \frac{u}{h} C_D^2 (u^2 + v^2)^{\frac{1}{2}} = -g' \left(\frac{\partial \bar{h}}{\partial x} + \frac{\partial h'}{\partial x} + \frac{\partial z_t}{\partial x} \right) \\ & - p_x + f \bar{v} + f v' + K \left[\frac{\partial^2 \bar{u}}{\partial x^2} + \frac{\partial^2 \bar{u}}{\partial y^2} + \frac{\partial^2 u'}{\partial x^2} + \frac{\partial^2 u'}{\partial y^2} \right] \end{aligned} \quad (7-B6)$$

Now let \bar{u} and \bar{v} be solutions of

$$\frac{\bar{u}}{h} C_D^2 (\bar{u}^2 + \bar{v}^2)^{\frac{1}{2}} = -p_x + f \bar{v} \quad (7-B7a)$$

$$\frac{\bar{v}}{\bar{h}} C_D^2 (\bar{u}^2 + \bar{v}^2)^{\frac{1}{2}} = -p_y - f\bar{u}. \quad (7-B7b)$$

and assume

$$\frac{\partial \bar{u}}{\partial t} = \frac{\partial \bar{v}}{\partial t} \approx 0 \approx K \left[\frac{\partial^2 \bar{u}}{\partial x^2} + \frac{\partial^2 \bar{u}}{\partial y^2} \right] \quad (7-B8)$$

Subtract (7-B7a) from (7-B6) and use (7-B8):

$$\begin{aligned} \frac{\partial u'}{\partial t} + (\bar{u} + u') \frac{\partial u'}{\partial x} + (\bar{v} + v') \frac{\partial u'}{\partial y} + \frac{u}{\bar{h}} C_D^2 (u^2 + v^2)^{\frac{1}{2}} - \frac{\bar{u}}{\bar{h}} C_D^2 (\bar{u}^2 + \bar{v}^2)^{\frac{1}{2}} \\ + u' \frac{\partial \bar{u}}{\partial x} = - \left(\bar{u} \frac{\partial \bar{u}}{\partial x} + \bar{v} \frac{\partial \bar{u}}{\partial y} \right) - g' \left(\frac{\partial \bar{h}}{\partial x} + \frac{\partial z_t}{\partial x} \right) \\ - g' \frac{\partial h'}{\partial x} - v' \left(\frac{\partial \bar{u}}{\partial y} - f \right) \\ + K \left[\frac{\partial^2 u'}{\partial x^2} + \frac{\partial^2 u'}{\partial y^2} \right] \end{aligned} \quad (7-B9)$$

From (7-B2) and (7-B5b) we have

$$\begin{aligned} \frac{\partial \bar{v}}{\partial t} + \frac{\partial v'}{\partial t} + \bar{u} \frac{\partial \bar{v}}{\partial x} + \bar{u} \frac{\partial v'}{\partial x} + u' \frac{\partial \bar{v}}{\partial x} + u' \frac{\partial v'}{\partial x} \\ + \bar{v} \frac{\partial \bar{v}}{\partial y} + \bar{v} \frac{\partial v'}{\partial y} + v' \frac{\partial \bar{v}}{\partial y} + v' \frac{\partial v'}{\partial y} + \frac{v}{\bar{h}} C_D^2 (u^2 + v^2)^{\frac{1}{2}} = \\ - g' \left(\frac{\partial \bar{h}}{\partial y} + \frac{\partial h'}{\partial y} + \frac{\partial z_t}{\partial y} \right) - p_y - f\bar{u} - fu' + K \left[\frac{\partial^2 \bar{v}}{\partial x^2} \right. \\ \left. + \frac{\partial^2 \bar{v}}{\partial y^2} + \frac{\partial^2 v'}{\partial x^2} + \frac{\partial^2 v'}{\partial y^2} \right] \end{aligned} \quad (7-B10)$$

Using (7-B7b) and (7-B8) we can reduce (7-B10) to

$$\begin{aligned}
& \frac{\partial v'}{\partial t} + (\bar{u}+u')\frac{\partial v'}{\partial x} + (\bar{v}+v')\frac{\partial v'}{\partial y} + \frac{v}{h} C_D^2(u^2+v^2)^{\frac{1}{2}} - \frac{\bar{v}}{\bar{h}} C_D^2(\bar{u}^2+\bar{v}^2)^{\frac{1}{2}} \\
& + v'\frac{\partial \bar{v}}{\partial y} = - [\bar{u}\frac{\partial \bar{v}}{\partial x} + \bar{v}\frac{\partial \bar{v}}{\partial y}] - g'(\frac{\partial \bar{h}}{\partial y} + \frac{\partial z_t}{\partial y}) \\
& - g'\frac{\partial h'}{\partial y} - u'(\frac{\partial \bar{v}}{\partial x} + f) + K[\frac{\partial^2 v'}{\partial x^2} + \frac{\partial^2 v'}{\partial y^2}]
\end{aligned} \tag{7-B11}$$

Now combine (7-B5c) and (7-B3):

$$\begin{aligned}
& \frac{\partial \bar{h}}{\partial t} + \frac{\partial h'}{\partial t} + \bar{u}\frac{\partial \bar{h}}{\partial x} + \bar{v}\frac{\partial \bar{h}}{\partial y} + u'\frac{\partial \bar{h}}{\partial x} + v'\frac{\partial \bar{h}}{\partial y} \\
& + \bar{u}\frac{\partial h'}{\partial x} + \bar{v}\frac{\partial h'}{\partial y} + u'\frac{\partial h'}{\partial x} + v'\frac{\partial h'}{\partial y} + h(\frac{\partial \bar{u}}{\partial x} + \frac{\partial \bar{v}}{\partial y}) \\
& + \bar{h}(\frac{\partial u'}{\partial x} + \frac{\partial v'}{\partial y}) + h'(\frac{\partial \bar{u}}{\partial x} + \frac{\partial \bar{v}}{\partial y}) + h'(\frac{\partial u'}{\partial x} + \frac{\partial v'}{\partial y}) = \\
& \bar{\eta} + \eta' + K_h[\frac{\partial^2 \bar{h}}{\partial x^2} + \frac{\partial^2 \bar{h}}{\partial y^2} + \frac{\partial^2 h'}{\partial x^2} + \frac{\partial^2 h'}{\partial y^2}]
\end{aligned} \tag{7-B12}$$

where

$$\bar{\eta} = \frac{1}{A} \int_A \eta dx \tag{7-B13}$$

and A is the model domain. We define

$$\frac{\partial \bar{h}}{\partial t} = \bar{\eta}. \tag{7-B14}$$

Subtracting this equation from (7-B12) we have

$$\begin{aligned}
& \frac{\partial h'}{\partial t} + (\bar{u}+u')\frac{\partial h'}{\partial x} + (\bar{v}+v')\frac{\partial h'}{\partial y} + h' \left[\frac{\partial \bar{u}}{\partial x} + \frac{\partial u'}{\partial x} + \frac{\partial \bar{v}}{\partial y} + \frac{\partial v'}{\partial y} \right] = \\
& - \left[\bar{u} \frac{\partial \bar{h}}{\partial x} + \bar{v} \frac{\partial \bar{h}}{\partial y} \right] - \left[u' \frac{\partial \bar{h}}{\partial x} + v' \frac{\partial \bar{h}}{\partial y} \right] - \bar{h} \left[\frac{\partial \bar{u}}{\partial x} + \frac{\partial \bar{v}}{\partial y} \right] \\
& - \bar{h} \left(\frac{\partial u'}{\partial x} + \frac{\partial v'}{\partial y} \right) + \eta' + K_h \left[\frac{\partial^2 h'}{\partial x^2} + \frac{\partial^2 h'}{\partial y^2} \right]
\end{aligned} \tag{7-B15}$$

where we have assumed

$$\frac{\partial^2 \bar{h}}{\partial x^2} + \frac{\partial^2 \bar{h}}{\partial y^2} \approx 0. \tag{7-B16}$$

Now we write the basic equations (7-B9), (7-B11) and (7-B15) in the following forms:

$$\frac{\partial u'}{\partial t} + (\bar{u}+u')\frac{\partial u'}{\partial x} + (\bar{v}+v')\frac{\partial u'}{\partial y} + u'(\bar{\beta}_u + \beta'_u) = + \bar{S}_u + S'_u + K \left(\frac{\partial^2 u'}{\partial x^2} + \frac{\partial^2 u'}{\partial y^2} \right) \tag{7-B17}$$

$$\frac{\partial v'}{\partial t} + (\bar{u}+u')\frac{\partial v'}{\partial x} + (\bar{v}+v')\frac{\partial v'}{\partial y} + v'(\bar{\beta}_v + \beta'_v) = + \bar{S}_v + S'_v + K \left(\frac{\partial^2 v'}{\partial x^2} + \frac{\partial^2 v'}{\partial y^2} \right) \tag{7-B18}$$

$$\frac{\partial h'}{\partial t} + (\bar{u}+u')\frac{\partial h'}{\partial x} + (\bar{v}+v')\frac{\partial h'}{\partial y} + h'(\bar{\beta}_h + \beta'_h) = + \bar{S}_h + S'_h + K_h \left(\frac{\partial^2 h'}{\partial x^2} + \frac{\partial^2 h'}{\partial y^2} \right) \tag{7-B19}$$

where

$$\bar{\beta}_u = \partial \bar{u} / \partial x \tag{7-B20}$$

$$\bar{\beta}_v = \partial \bar{v} / \partial y \tag{7-B21}$$

$$\bar{\beta}_h = \partial \bar{u} / \partial x + \partial \bar{v} / \partial y \tag{7-B22}$$

$$\beta'_u = \begin{cases} \frac{C_D^2}{u'} \left[\frac{u}{\bar{h}} (u^2 + v^2)^{\frac{1}{2}} - \frac{\bar{u}}{\bar{h}} (\bar{u}^2 + \bar{v}^2)^{\frac{1}{2}} \right], & \text{if } u' \neq 0; \\ \frac{C_D^2}{\bar{h}} (\bar{u}^2 + \bar{v}^2)^{\frac{1}{2}}, & \text{otherwise} \end{cases} \quad (7-B23)$$

$$\beta'_v = \begin{cases} \frac{C_D^2}{v'} \left[\frac{v}{\bar{h}} (u^2 + v^2)^{\frac{1}{2}} - \frac{\bar{v}}{\bar{h}} (\bar{u}^2 + \bar{v}^2)^{\frac{1}{2}} \right], & \text{if } v' \neq 0; \\ \frac{C_D^2}{\bar{h}} (\bar{u}^2 + \bar{v}^2)^{\frac{1}{2}}, & \text{otherwise.} \end{cases} \quad (7-B24)$$

$$\beta'_n = \frac{\partial u'}{\partial x} + \frac{\partial v'}{\partial y} \quad (7-B25)$$

$$\bar{s}_u = -\left[\bar{u} \frac{\partial \bar{u}}{\partial x} + \bar{v} \frac{\partial \bar{u}}{\partial y} + g' \left(\frac{\partial \bar{h}}{\partial x} + \frac{\partial z_t}{\partial x} \right) \right] \quad (7-B26)$$

$$\bar{s}_v = -\left[\bar{u} \frac{\partial \bar{v}}{\partial x} + \bar{v} \frac{\partial \bar{v}}{\partial y} + g' \left(\frac{\partial \bar{h}}{\partial y} + \frac{\partial z_t}{\partial y} \right) \right] \quad (7-B27)$$

$$\bar{s}_h = -\left[\bar{u} \frac{\partial \bar{h}}{\partial x} + \bar{v} \frac{\partial \bar{h}}{\partial y} + \bar{h} \left(\frac{\partial \bar{u}}{\partial x} + \frac{\partial \bar{v}}{\partial y} \right) - \eta' \right] \quad (7-B28)$$

$$s'_u = -\left[g' \frac{\partial h'}{\partial x} + v' \left(\frac{\partial \bar{u}}{\partial y} - f \right) \right] \quad (7-B29)$$

$$s'_v = -\left[g' \frac{\partial h'}{\partial y} + u' \left(\frac{\partial \bar{v}}{\partial x} + f \right) \right] \quad (7-B30)$$

$$s'_h = -\left[u' \frac{\partial \bar{h}}{\partial x} + v' \frac{\partial \bar{h}}{\partial y} + \bar{h} \left(\frac{\partial u'}{\partial x} + \frac{\partial v'}{\partial y} \right) \right] \quad (7-B31)$$

and \bar{h} satisfies (7-B14); \bar{u} and \bar{v} satisfy (7-B7a, B7b) and (7-B8); and u , v and h are defined by (7-B5).

We require only first-order derivatives in evaluation of the β 's and S 's.
We use the notation

$$\Delta_x(g_{I,J}) = \left. \frac{\partial g}{\partial x} \right|_{\substack{x=I\Delta x \\ y=J\Delta y}} \quad \Delta_y(g_{I,J}) = \left. \frac{\partial g}{\partial y} \right|_{\substack{x=I\Delta x \\ y=J\Delta y}}$$

We define several different Δ_x and Δ_y operators, each of different orders of accuracy.

$$\begin{aligned} 6\Delta_x(g_{I,J}) \equiv & [45(g_{I+1,J} - g_{I-1,J}) - 9(g_{I+2,J} - g_{I-2,J}) \\ & + (g_{I+3,J} - g_{I-3,J})]/(60\delta_x) \end{aligned} \quad (7-B32)$$

$$4\Delta_x(g_{I,J}) = [8(g_{I+1,J} - g_{I-1,J}) - (g_{I+2,J} - g_{I-2,J})]/(12\delta_x) \quad (7-B33)$$

$$2\Delta_x(g_{I,J}) = (g_{I+1,J} - g_{I-1,J})/(2\delta_x) \quad (7-B34)$$

$$\begin{aligned} 6\Delta_y(g_{I,J}) = & [45(g_{I,J+1} - g_{I,J-1}) - 9(g_{I,J+2} - g_{I,J-2}) \\ & + (g_{I,J+3} - g_{I,J-3})]/(60\delta_y) \end{aligned} \quad (7-B35)$$

$$4\Delta_y(g_{I,J}) = [8(g_{I,J+1} - g_{I,J-1}) - (g_{I,J+2} - g_{I,J-2})]/(12\delta_y) \quad (7-B36)$$

$$2\Delta_y(g_{I,J}) = (g_{I,J+1} - g_{I,J-1})/(2\delta_y) \quad (7-B37)$$

where δ_x and δ_y are the grid mesh dimensions.

The following operators are used to compute first derivatives on boundaries:

$$W_x^{\Delta}(g_{I,J}) = [-171g_{I,J} + 169g_{I+1,J} + 105g_{I+2,J} - 160g_{I+3,J} + 65g_{I+4,J} - 9g_{I+5,J} + g_{I+6,J}]/(120\delta_x) \quad (7-B38)$$

$$S_y^{\Delta}(g_{I,J}) = [-171g_{I,J} + 169g_{I,J+1} + 105g_{I,J+2} - 160g_{I,J+3} + 65g_{I,J+4} - 9g_{I,J+5} + g_{I,J+6}]/(120\delta_y) \quad (7-B39)$$

$$E_x^{\Delta}(g_{I,J}) = [171g_{I,J} - 169g_{I-1,J} - 105g_{I-2,J} + 160g_{I-3,J} - 65g_{I-4,J} + 9g_{I-5,J} - g_{I-6,J}]/(120\delta_x) \quad (7-B40)$$

$$N_y^{\Delta}(g_{I,J}) = [171g_{I,J} - 169g_{I,J-1} - 105g_{I,J-2} + 160g_{I,J-3} - 65g_{I,J-4} + 9g_{I,J-5} - g_{I,J-6}]/(120\delta_y) \quad (7-B41)$$

The operators defined above are used to compute the variables $\bar{\beta}_u, \bar{\beta}_v, \dots, S'_h$ defined by Eqs. (7-B20) - (7-B31) in the sequence illustrated by the flow chart in Figure 7B-1. Following are descriptions of the operations indicated in the flow chart.

Although the model domain is a grid of 60 x 42 cells, we use an array of 66 x 48 cells in solving the governing equations (7B-1, 2 and 3) in FLOMOD. The extra cells comprise a "frame" 3 cells wide around the 60 x 42 modeling domain. Values of all parameters within this frame of cells are specified whereas those within the modeling domain are predicted using the governing equations. Specification of the BAR variables $\bar{\beta}_u, \bar{\beta}_v, \bar{\beta}_h, \bar{S}_u, \bar{S}_v$ and \bar{S}_h within the frame is straightforward since the variables $\bar{u}, \bar{v}, \bar{h}$, etc. on which they depend are given at all points in the 66 x 48 cell region. Specification of the PRIME variables $\beta'_u, \beta'_v, \beta'_h, S'_u, S'_v$, and S'_h within the frame region is guided by the desire to avoid the spurious generation of disturbances just outside the modeling region that can subsequently enter the area of interest.

The prime variables u' , v' , and h' represent perturbations from the "base" state represented by $(\bar{u}, \bar{v}, \bar{h})$. We assume that all sources of perturbation energy, such as terrain z_t , cooling η' , etc. are within the 60×42 model region. Therefore, we assign zero value to all prime variables outside this region, namely in the boundary frame area. This is a key feature of our boundary scheme. Finally, specification of u' , v' , and h' in the frame zone must be done arbitrarily. The prognostic equations (7-B1, B2, B3) cannot be applied in the frame region because that would require values of all parameters outside the 66×48 domain. A common method of estimating the values of the dependent variables outside the modeling area is to extrapolate values from the interior of the simulation area. We have found that even crude extrapolation techniques give acceptable results when used with the advection-diffusion equation. But the same methods generally fail when utilized with systems of equations like (7-B1, etc.) because the errors in the extrapolated values outside the simulation region give rise to disturbances that spoil the accuracy of the solutions obtained within the model region. We attempt to alleviate this problem by setting all source terms that involve the dependent variables equal to zero outside the model domain (the 60×42 region) but we extrapolate values of these variables for use in the advection and diffusion terms of the equation. In particular, if a given point on the edge of the 60×42 region is a point of inflow, then we assume $u' = v' = h' = 0$ at all 3 cells of the frame zone adjacent to this point. For example,

$$\left. \begin{aligned} u'(1,J) &= u'(2,J) = u'(3,J) = 0 \\ v'(1,J) &= v'(2,J) = v'(3,J) = 0 \\ h'(1,J) &= h'(2,J) = h'(3,J) = 0 \end{aligned} \right\} \text{ if } [\bar{u}(4,J) + u'(4,J)] \geq 0$$

At points of outflow, we use the following extrapolation, illustrated for the case of point (4,J):

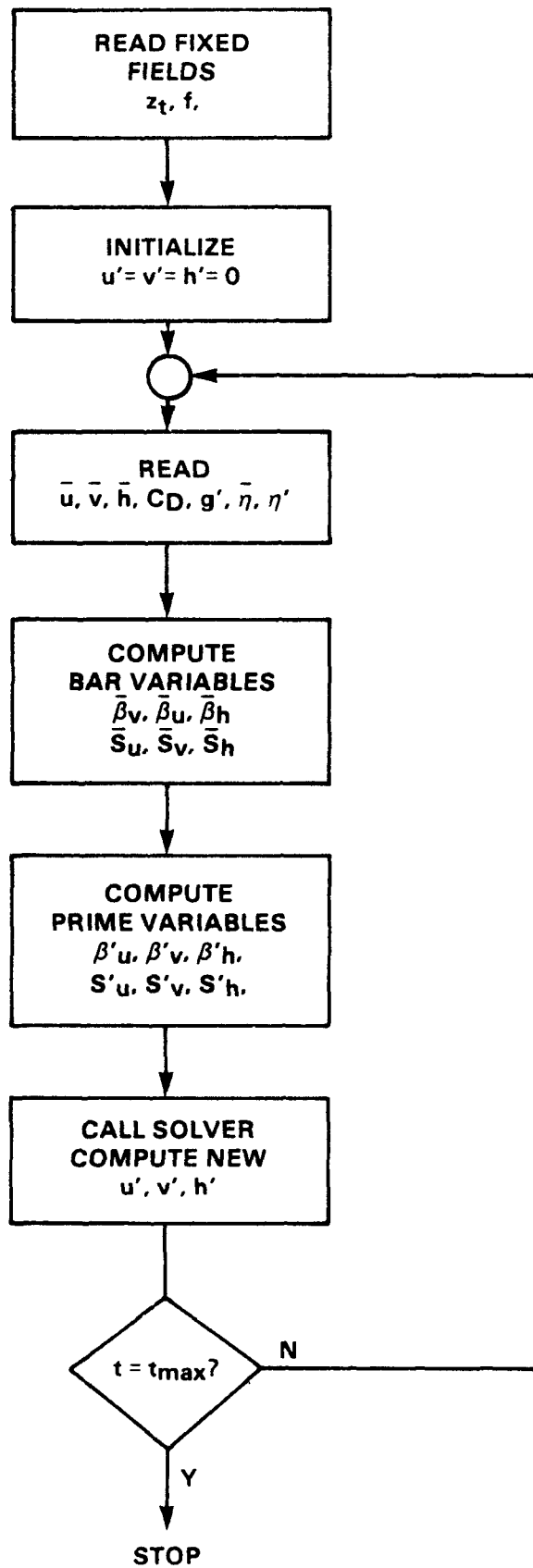


Figure 7B-1. Flow chart of FLOMOD operations.

$$\left. \begin{aligned} u'(1,J) &= u'(2,J) = u'(3,J) = \xi_u \\ v'(1,J) &= v'(2,J) = v'(3,J) = \xi_v \\ h'(1,J) &= h'(2,J) = h'(3,J) = \xi_h \end{aligned} \right\} \text{ if } [\bar{u}(4,J) + u'(4,J)] < 0$$

where

$$\xi_u = -2u'(5,J) + (1/2)u'(6,J) + (5/2)u'(4,J)$$

etc.

Calculation of the BAR variables.

Figure 7B-2 shows the grid on which the BAR variables $\bar{\beta}_u$, $\bar{\beta}_v$, etc. are to be evaluated and the derivative operators that are to be employed at each point.

From (7-B20) - (7-B22)

$$\bar{\beta}_u(I,J) = \Delta_x(\bar{u}_{I,J}) \quad (7-B42)$$

$$\bar{\beta}_v(I,J) = \Delta_y(\bar{v}_{I,J}) \quad (7-B43)$$

$$\bar{\beta}_h(I,J) = \bar{\beta}_u(I,J) \div \bar{\beta}_v(I,J) \quad (7-B44)$$

and from (7-B26) - (7-B28)

$$\begin{aligned}\bar{S}_u(I,J) = & \bar{u}_{I,J} \Delta_x(\bar{u}_{I,J}) + \bar{v}_{I,J} \Delta_y(\bar{u}_{I,J}) \\ & + g'_{I,J} [\Delta_x(\bar{h}_{I,J} + z_{tI,J})]\end{aligned}\quad (7-B45)$$

$$\begin{aligned}\bar{S}_v(I,J) = & \bar{u}_{I,J} \Delta_x(\bar{v}_{I,J}) + \bar{v}_{I,J} \Delta_y(\bar{v}_{I,J}) \\ & + g'_{I,J} [\Delta_y(\bar{h}_{I,J} + z_{tI,J})]\end{aligned}\quad (7-B46)$$

$$\begin{aligned}\bar{S}_h(I,J) = & \bar{u}_{I,J} \Delta_x(\bar{h}_{I,J}) + \bar{v}_{I,J} \Delta_y(\bar{h}_{I,J}) \\ & + \bar{h}_{I,J} [\Delta_x(\bar{u}_{I,J}) + \Delta_y(\bar{v}_{I,J})] - \eta'_{I,J}\end{aligned}\quad (7-B47)$$

In evaluating the six expressions above, the operators Δ_x and Δ_y should be selected as follows (see Fig. 7B-2):

$$\Delta_x(\bar{\xi}_{I,J}) = \begin{cases} w\Delta_x & , \text{ if } I=1; \\ E\Delta_x & , \text{ if } I=66; \\ 2\Delta_x & , \text{ if } I=2 \text{ or } I=65; \\ 4\Delta_x & , \text{ if } I=3 \text{ or } I=64; \\ 6\Delta_x & , \text{ if } I=4-63. \end{cases}\quad (7-B48)$$

$$\Delta_y(\bar{\xi}_{I,J}) = \begin{cases} S\Delta_y & , \text{ if } J=1; \\ N\Delta_y & , \text{ if } J=48; \\ 2\Delta_y & , \text{ if } J=2 \text{ or } J=47 \\ 4\Delta_y & , \text{ if } J=3 \text{ or } J=46 \\ 6\Delta_y & , \text{ if } J=4-45 \end{cases}\quad (7-B49)$$

where $2\Delta_x$, $2\Delta_y$, etc. are defined by (7-B32) - (7-B41).

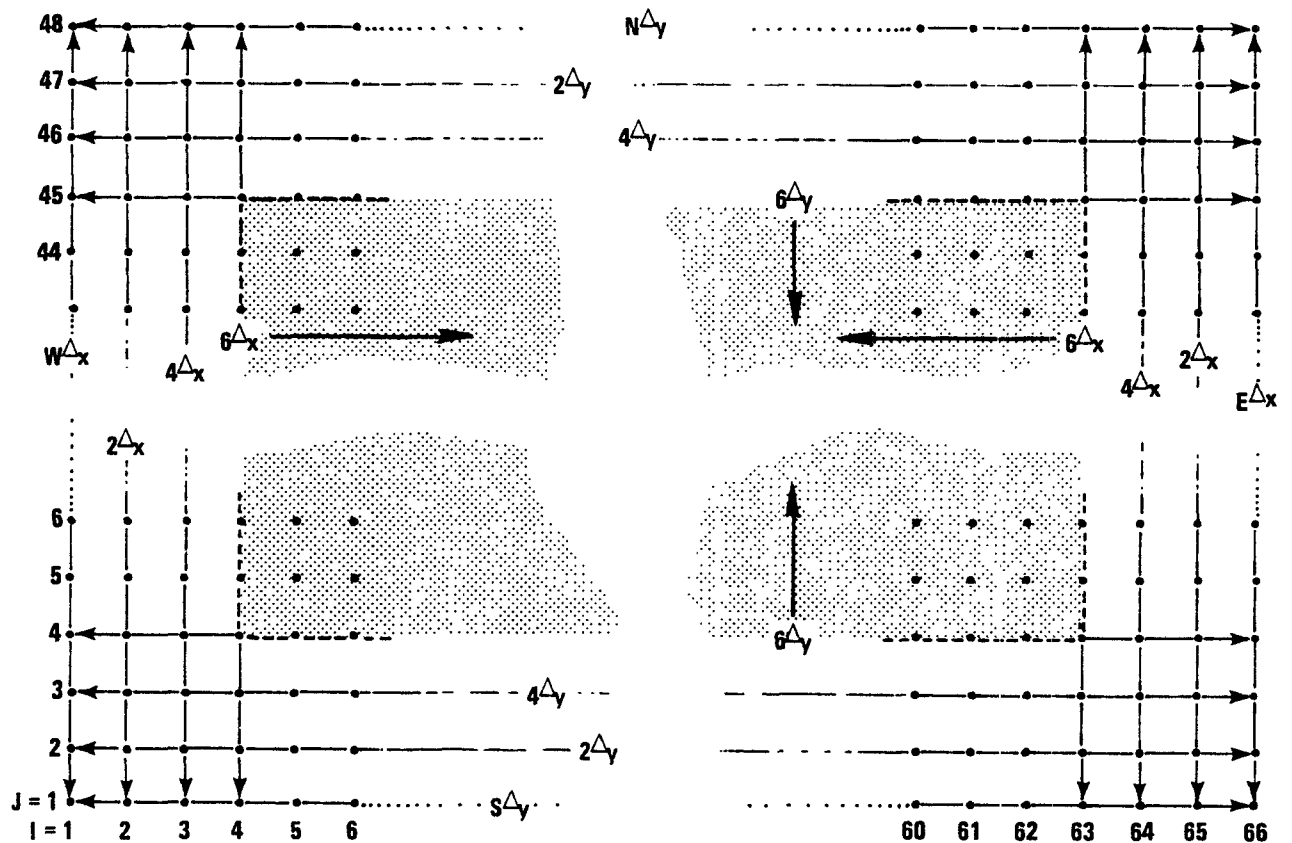


Figure 7B-2. Grid network on which $\bar{\beta}_u$, $\bar{\beta}_v$, $\bar{\beta}_h$, \bar{S}_u , \bar{S}_v , and \bar{S}_h are computed. Different spatial derivative operators Δ_x and Δ_y are required in these calculations as indicated.

Calculation of the PRIME variables

The PRIME variables β'_u , β'_v , ..., S'_h are defined on the same 66 x 48 grid system as the BAR variables but the calculation procedure is different. As we noted earlier all PRIME variables are set to zero outside the 60 x 42 cell simulation area. Thus, we assume

$$\beta'_u(I,J) = \beta'_v(I,J) = \beta'_h(I,J) = S'_u(I,J) = S'_v(I,J) = S'_h(I,J) = 0, \quad (7-B50)$$

if $I = 1, 2, 3, 64, 65$, or 66 ; or $J = 1, 2, 3, 46, 47$, or 48 .

At all other grid points, namely $I=4-63$, $J=4-45$ compute the PRIME variables as follows:

$$\beta'_u(I,J) = \begin{cases} 0 & , \text{ if } u'_{I,J} = 0; \\ \frac{C_{DI,J}^2}{u'_{I,J}} \left[\frac{u_{I,J}}{h_{I,J}} (u_{I,J}^2 + v_{I,J}^2)^{\frac{1}{2}} - \frac{\bar{u}_{I,J}}{\bar{h}_{I,J}} (\bar{u}_{I,J}^2 + \bar{v}_{I,J}^2)^{\frac{1}{2}} \right], & \text{ if } u'_{I,J} \neq 0 \end{cases} \quad (7-B51)$$

where

$$u_{I,J} = \bar{u}_{I,J} + u'_{I,J} ;$$

$$\beta'_v(I,J) = \begin{cases} 0, & \text{ if } v'_{I,J}=0; \\ \frac{C_{DI,J}^2}{v'_{I,J}} \left[\frac{v_{I,J}}{h_{I,J}} (u_{I,J}^2 + v_{I,J}^2)^{\frac{1}{2}} - \frac{\bar{v}_{I,J}}{\bar{h}_{I,J}} (\bar{u}_{I,J}^2 + \bar{v}_{I,J}^2)^{\frac{1}{2}} \right] & \end{cases} \quad (7-B52)$$

where

$$v_{I,J} = \bar{v}_{I,J} + v'_{I,J} ;$$

$$\beta'_h(I,J) = \Delta_x(u'_{I,J}) + \Delta_y(v'_{I,J}) \quad (7-B53)$$

$$S'_u(I,J) = g'_{I,J} \Delta_x(h'_{I,J}) + v'_{I,J} [\Delta_y(\bar{u}_{I,J}) - f_J] \quad (7-B54)$$

$$S'_v(I,J) = g'_{I,J} \Delta_y(h'_{I,J}) + u'_{I,J} [\Delta_x(\bar{v}_{I,J}) + f_J] \quad (7-B55)$$

$$S_h^i(I,J) = u_{I,J}^i \Delta_x(\bar{h}_{I,J}) + v_{I,J}^i \Delta_y(\bar{h}_{I,J}) + \bar{h}_{I,J} \beta_h^i(I,J) \quad (7-B56)$$

In equations (7-B53,...,7-B56) the derivative operators Δ_x and Δ_y should be selected as follows when they operate on PRIME variables:

$$\Delta_x(\xi_{I,J}^i) = \begin{cases} w\Delta_x & \text{if } I=4; \\ E\Delta_x & \text{if } I=63; \\ 2\Delta_x & \text{if } I=5 \text{ or } I=62; \\ 4\Delta_x & \text{if } I=6 \text{ or } I=61; \\ 6\Delta_x & \text{if } I=7-60. \end{cases} \quad (7-B57)$$

$$\Delta_y(\xi_{I,J}^i) = \begin{cases} S\Delta_y & \text{if } J=4; \\ N\Delta_y & \text{if } J=45; \\ 2\Delta_y & \text{if } J=5 \text{ or } J=44; \\ 4\Delta_y & \text{if } J=6 \text{ or } J=43; \\ 6\Delta_y & \text{if } J=7-42. \end{cases} \quad (7-B58)$$

In Eqs. (7-B53,...,7-B56) use $6\Delta_x$ and $6\Delta_y$ in all applications to the BAR variables \bar{u} , \bar{v} , and \bar{h} . In this regard it should be repeated that Eqs. (7-B51,...,7-B56) are applied only to columns $I=4-63$ and to rows $J=4-45$, and at these points the 6-th order operators can be applied to BAR variables (see 7-B48 and 7-B49). At all other points the PRIME variables are set to zero (see 7-B50).

Calculation of the dependent variables u^i , v^i , and h^i .

The three dependent variables are computed at each time step using the prognostic equations (7-B17,...,7-B19) within the 60×42 cell modeling region bounded by columns $I=4$ and 63 and by rows $J=4$ and 45 . These calculations are done in the following steps.

First we define the function

$$A(I,J) = \text{SOLVER}(I,J,\text{IST},\text{JST},\xi_{6 \times 6},K) \quad (7-B59)$$

which represents the biquintic algorithm described in Appendix 7A that is used to solve the differential equations numerically. In Eq. (7-B59), IST and JST are given functions of I,J,u' and v' (see 7-A12, A13); $\xi_{6 \times 6}$ is an array of 36 variables at grid points surrounding (IST,JST) which we specify below (see also Fig. 7-A1); and K is the diffusivity. The function SOLVER can be used to predict the next values of u', v', and h' at each of the 60 x 42 points defined above. Consider each of the 3 variables in turn.

1. $u'(I,J,N+1)$ in 60 x 42 model domain.

Step 1.

$$B^*(I,J) = \text{SOLVER}(I,J,\text{IST},\text{JST},\xi_{6 \times 6},0)$$

where

$$\xi_{6 \times 6} = \bar{\beta}_u + \beta'_u$$

Step 2.

$$C^*(I,J) = \text{SOLVER}(I,J,\text{IST},\text{JST},\xi_{6 \times 6},K)$$

where

$$\xi_{6 \times 6} = u'(N) + \Delta t(\bar{S}_u + S'_u)$$

Step 3.

$$u'(I,J,N+1) = C^*(I,J) \cdot \exp(-B^*(I,J))$$

2. $v'(I,J,N+1)$ in 60 x 42 model domain.

Same steps as in u' calculation except replace $\bar{\beta}_u$, β'_u , $u'(N)$, \bar{S}_u and S'_u by $\bar{\beta}_v$, β'_v , $v'(N)$, \bar{S}_v and S'_v , respectively.

3. $h'(I,J,N+1)$ in 60×42 model domain.

Same steps as u' , except replace $\bar{\beta}_u$, β'_u , $u'(N)$, \bar{S}_u , and S'_u by $\bar{\beta}_h$, β'_h , $h'(N)$, \bar{S}_h and S'_h , respectively. Replace K by K_h . In order to avoid the problems that zero or negative fluid depth predictions would cause, perform the following operation after each time step:

$$\text{IF}((h'(N+1) + \bar{h}(N+1)).\text{LT}.1.0) \ h' (N+1) = 1.0 - \bar{h}(N+1)$$

As we noted earlier, values of the dependent variables in the boundary frame region are assigned zero values at all inflow points and are predicted by simple extrapolation of the interior values at points of outflow. Consider first the western boundary zone.

4. $u'(N+1)$, $v'(N+1)$ and $h'(N+1)$ in western boundary zone $I=1-3$, $J=4-45$.

If $(\bar{u}(4,J,N) + u'(4,J,N)) \geq 0$, then

$$u'(1,J,N+1) = u'(2,J,N+1) = u'(3,J,N+1) = 0$$

Same holds for v' and h' .

If $(\bar{u}(4,J,N) + u'(4,J,N)) < 0$, then

$$\begin{aligned} u'(1,J,N+1) &= u'(2,J,N+1) = u'(3,J,N+1) \\ &= -2u'(5,J,N) + (1/2)u'(6,J,N) + (5/2)u'(4,J,N) \end{aligned}$$

Similar expressions are used for v' and h' .

5. $u'(N+1)$, $v'(N+1)$ and $h'(N+1)$ in the eastern boundary zone $I=64-66$, $J = 4-45$.

If $(\bar{u}(63,J,N) + u'(63,J,N)) \leq 0$, then

$$u'(64,J,N+1) = u'(65,J,N+1) = u'(66,J,N+1) = 0$$

Same holds for v' and h' .

If $(\bar{u}(63,J,N) + u'(63,J,N)) \leq 0$, then

$$\begin{aligned} u'(66,J,N+1) &= u'(65,J,N+1) = u'(64,J,N+1) \\ &= (1/2)u'(61,J,N) - 2u'(62,J,N) + (5/2)u'(63,J,N) \end{aligned}$$

Similar expressions hold for v' and h' .

6. $u'(N+1)$, $v'(N+1)$ and $h'(N+1)$ in the southern zone $I=4-63$, $J=1-3$.

If $(\bar{v}(I,4,N) + v'(I,4,N)) \geq 0$, then

$$u'(I,1,N+1) = u'(I,2,N+1) = u'(I,3,N+1) = 0.$$

Same holds for v' and h' .

If $(\bar{v}(I,4,N) + v'(I,4,N)) < 0$, then

$$\begin{aligned} u'(I,1,N+1) &= u'(I,2,N+1) = u'(I,3,N+1) = \\ &-2u'(I,5,N) + (1/2)u'(I,6,N) + (5/2)u'(I,4,N). \end{aligned}$$

Similar expressions hold for v' and h' .

7. $u'(N+1)$, $v'(N+1)$ and $h'(N+1)$ in the northern boundary zone

$$I = 4-63, J = 46-48.$$

If $(\bar{v}(I,45,N) + v'(I,45,N)) \leq 0$, then

$$u'(I,46,N+1) = u'(I,47,N+1) = u'(I,48,N+1) = 0$$

Same holds for v' and h' .

If $(\bar{v}(I,45,N) + v'(I,45,N)) > 0$, then

$$u'(I,48,N+1) = u'(I,47,N+1) = u'(I,46,N+1) =$$

$$(1/2)u'(I,43,N) - 2u'(I,44,N) + (5/2)u'(I,45,N)$$

Similar expressions hold for v' and h' .

The specifications of u' , v' and h' given in steps 4-7 above give the dependent variables at time step $N+1$ at all boundary zone areas except the 4 corner zones. The southwest corner zone is illustrated in Figure 7B-3. In each of the four corner zones we will assign the dependent variables the average of the values computed on the edges of these zones, as illustrated in the Figure. For example, referring to Figure 7B-3 and keeping in mind that

$$u'(4,1,N) = u'(4,2,N) = u'(4,3,N),$$

and similarly for v' and h' ; and that

$$u'(1,4,N) = u'(2,4,N) = u'(3,4,N),$$

and similarly for v' and h' , we assume in the southwest corner zone that

$$u'(I,J,N+1) = 1/2[u'(4,1,N+1) + u'(1,4,N+1)]$$

$$I=1,2,3 \text{ and } J=1,2,3.$$

and similarly for v' and h' . We use a similar method to compute the dependent variables in the northwest, northeast, and southeast corner zones.

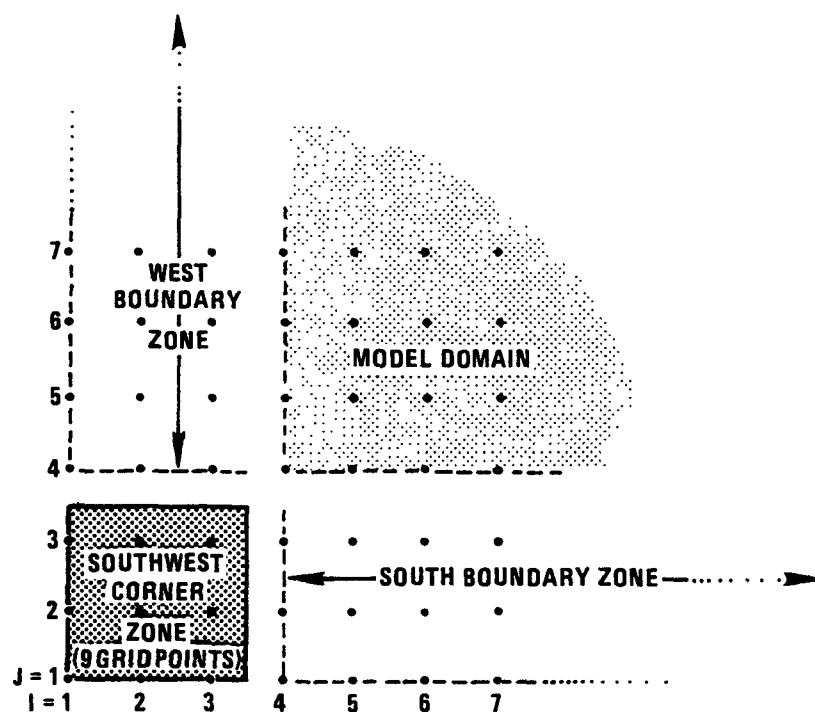


Figure 7B-3. Illustration of the southwest corner zone and the west and south boundary zones of the model domain.

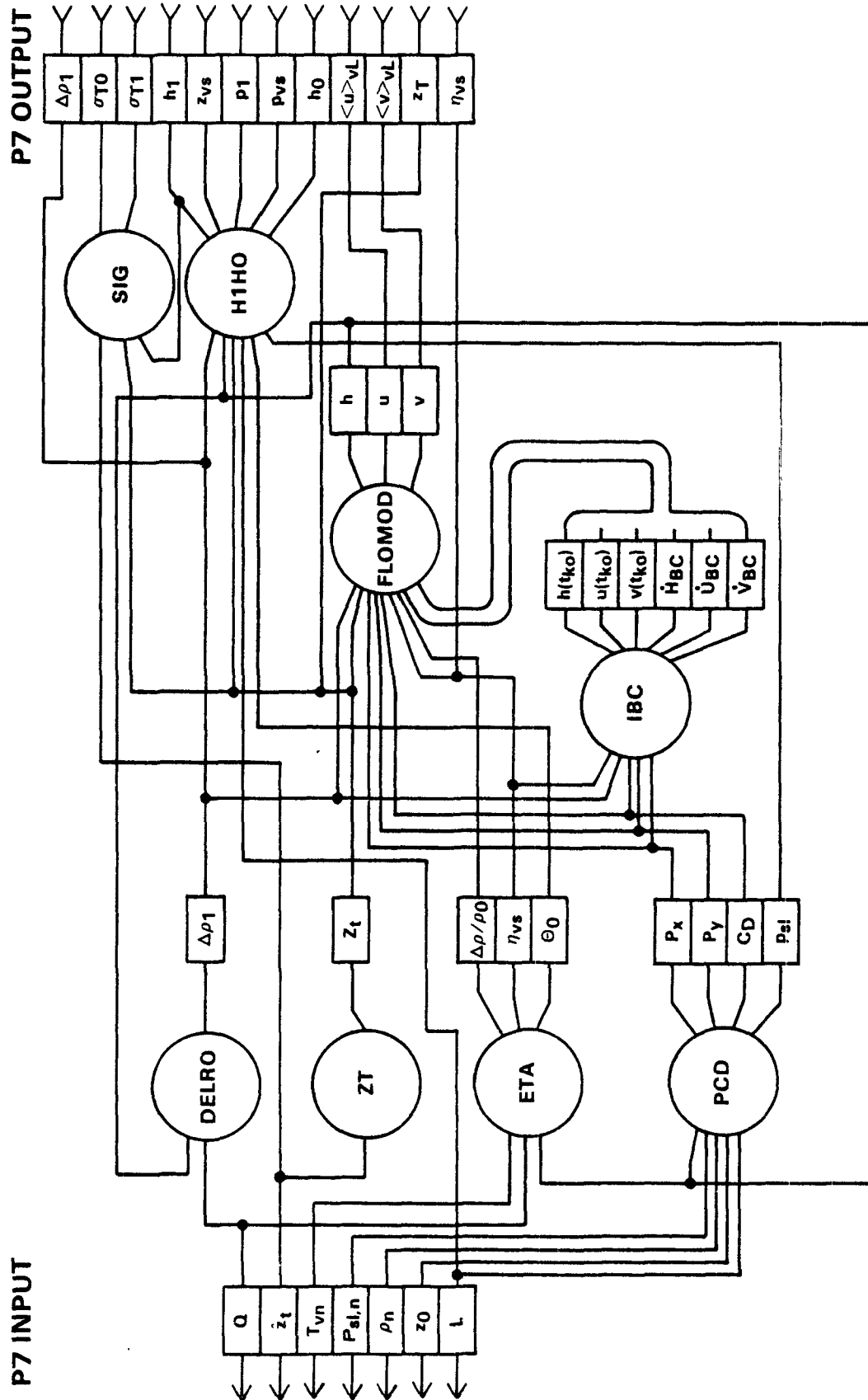


Figure 7-6. Schematic illustration of Processor P7 and its input and output interfaces with the processor network.

SECTION 7

PROCESSOR P8

INTRODUCTION

This processor determines the top surfaces H_2 and H_3 of layers 2 and 3 of the regional model, it computes mean vertical velocities on these surfaces, and it estimates convective cloud updraft speeds and other parameters required in the specification of pollutant fluxes across surfaces H_2 and H_3 . All of these quantities play important roles in the regional model, but unfortunately none of them is directly measurable. In this section we outline a procedure for deriving estimates of these parameters that are consistent both with observational data and physical principles.

DERIVATION OF BASIC EQUATIONS

Recall from Part 1 that

$$H_2(x,y,z,t) = z_2(x,y,t) - z \quad (8-1)$$

where z_2 is nominally the elevation of the top of the mixed layer. During clear daylight hours, z_2 is the highest elevation that nonbuoyant pollutants can reach. When convective clouds are present, we take z_2 to be the elevation of cloud bases, specifically, the so-called lifting condensation level (LCL). In this case pollutants entering the updrafts that feed individual cumulus clouds can rise above elevation z_2 and proceed as far as the elevation of the cloud tops, which we define to be the elevation z_3 of the top of Layer 3.

When convective clouds are absent, z_3 is defined to be $z_2 + h_3$, where h_3 is some constant depth of order 100 meters. Figure 8-1 illustrates the surfaces H_2 and H_3 in a regional domain in the typical condition where cumulus clouds are present over only a portion of the modeling region.

We showed in Part 1, Eq. (4-20) that z_2 satisfies the differential equation

$$\frac{\partial z_2}{\partial t} + \overline{v_{2H} \cdot \nabla_H z_2} = \frac{w_2 - \sigma_C w_C}{1 - \sigma_C} + w_e. \quad (8-2)$$

Here w_e is the entrainment velocity (represented in Part 1 by $f\theta/\Delta\theta$); w_2 is the cell averaged vertical air speed at elevation z_2 ; w_C is the effective, cell averaged cumulus updraft velocity at cloud base (i.e., at z_2); v_{2H} is the horizontal wind velocity at elevation z_2 ; and σ_C is the fractional area covered by convective (cumulus) clouds. The last parameter is measurable from

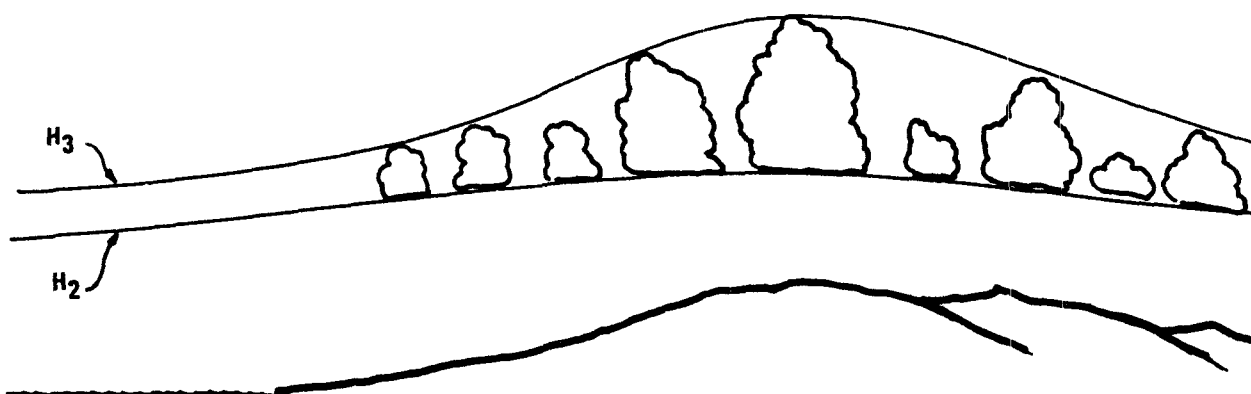


Figure 8-1. Illustration of surfaces H_2 and H_3 during situations in which convective clouds cover only a portion of the modeling region.

satellite photographs and it is the only variable in (8-2) that can be estimated reliably. We will assume that $\sigma_c(x,y,t)$ is an input to this processor.

All the other variables in (8-2) must be inferred through comparisons of this equation with certain measured data and other physical principles. This is the task we undertake in this section.

An auxiliary relationship that will aid in the estimation of w_c is the water vapor mass conservation equation. Using Eq. 2-29 of Part 1 we can express the layer averaged water vapor mixing ratio q in the form

$$\frac{\partial}{\partial t} \langle q \rangle_j + \langle q \rangle_j \frac{\partial \ln V_j}{\partial t} + \underline{v}_{jH} \cdot \underline{\nabla}_H \langle q \rangle_j + \frac{A}{V_j} [F_{j-1,j} - F_{j,j}] = 0 \quad (8-3)$$

where $\langle q \rangle_j$ is the cell averaged mixing ratio in layer j , A is the horizontal area of a cell, V_j is the volume of a cell lying in layer j and $F_{j,k}$ is the flux of material across surface H_j to or from layer k . To arrive at (8-3), we dropped the horizontal flux terms in (2-29) of Part 1 that represent the effects of subgrid scale variations in the horizontal wind \underline{v}_{jH} . Our interest is in $\langle q \rangle_3$ during periods when cumulus clouds are present (i.e., $\sigma_c \neq 0$). If we assume that the advection term in (8-3) is negligible in these conditions compared to the other terms, we obtain with the aid of Eqs. (4-3) and (4-21b) of Part 1

$$\begin{aligned} \frac{\partial}{\partial t} \langle q \rangle_3 + \frac{\langle q \rangle_3}{z_3 - z_2} [\dot{z}_3 - \dot{z}_2] + \frac{1}{z_3 - z_2} [\sigma_c \left(\frac{w_2 - w_c}{1 - \sigma_c} + \right. \\ \left. w_e \right) (q_c - \langle q \rangle_3) + \langle q \rangle_3 \dot{z}_2 - (q_\infty - \langle q \rangle_3) \dot{H}_3 \\ \left. - \langle q \rangle_3 \dot{z}_3] = 0 \end{aligned} \quad (8-4)$$

where $\dot{z}_2 = \partial z_2 / \partial t$, $\dot{z}_3 = \partial z_3 / \partial t$ and

$$\dot{H}_3 = \dot{z}_3 + \underline{v}_{3H} \cdot \underline{\nabla}_H z_3 - w_3. \quad (8-5)$$

Also, q_c represents the mixing ratio in cumulus clouds and q_∞ is the mixing ratio just above the elevation of cloud tops, i.e., just above z_3 . If we assume that the horizontal advection term in (8-5) is negligible, we can reduce (8-4) to

$$\begin{aligned} \frac{\partial}{\partial t} \langle q \rangle_3 + \frac{1}{z_3 - z_2} [\sigma_c \left(\frac{w_2 - w_c}{1 - \sigma_c} + w_e \right) (q_c - \langle q \rangle_3) \\ - (q_\infty - \langle q \rangle_3) (\dot{z}_3 - w_3)] = 0, \end{aligned} \quad (8-6)$$

and after multiplying by $(z_3 - z_2)$ and rearranging terms we obtain

$$\begin{aligned} \frac{q_c \sigma_c}{1 - \sigma_c} w_c = \frac{\partial M_3}{\partial t} + [w_2 + (1 - \sigma_c) w_e] [\langle q \rangle_3 + \frac{q_c \sigma_c}{1 - \sigma_c}] \\ - q_\infty \dot{z}_3 + w_3 (q_\infty - \langle q \rangle_3) \end{aligned} \quad (8-7)$$

where

$$M_3(\underline{x}, t) = \int_{z_2(\underline{x}, t)}^{z_3(\underline{x}, t)} q(\underline{x}, z, t) dz \quad (8-8)$$

and

$$\langle q \rangle_3 = \frac{M_3}{z_3 - z_2} \quad (8-9)$$

At each of the sites \underline{x}_m of rawin stations we have available measurements of $q(z)$, $\underline{v}_{2H}(z)$ and $\theta(z)$ at each observation time. We also know σ_c and z_3 (where $\sigma_c \neq 0$) everywhere from satellite data. Using all this information we can derive estimates of all the parameters in (8-7) except w_c and w_e , and

thereby we can derive a relationship that w_c and w_e must satisfy at each rawin site x_m . This relationship can subsequently be employed in conjunction with (8-2) to obtain estimates of z_2 , w_c and w_e throughout the modeling domain.

In order to use the rawin data and Eq. 8-7 in this way, it is convenient to integrate (8-7) between each set of measurement times. Let t_0 and t_1 denote two successive times when rawin observations are gathered at a given station. Ordinarily, t_1 and t_0 will be 12 hours apart, but shorter intervals are possible. Integrating (8-7) we get

$$\begin{aligned} \int_{t_0}^{t_1} \left[\frac{q_c \sigma_c}{1 - \sigma_c} w_c - w_e (1 - \sigma_c) \langle q \rangle_3 - w_e q_c \sigma_c \right] dt = M_3(t_1) - M_3(t_0) \\ + \int_{t_0}^{t_1} \left[w_2 (\langle q \rangle_3 + \frac{q_c \sigma_c}{1 - \sigma_c}) - q_\infty \dot{z}_3 + w_3 (q_\infty - \langle q \rangle_3) \right] dt \end{aligned} \quad (8-10)$$

where all variables are evaluated at a given rawin site x_m . We assume that only w_c and w_e are unknowns in this equation. For all other parameters we can use the following expressions.

First, we adopt the approximation

$$q_c \approx q(z_2). \quad (8-11)$$

Then

$$q_c(t) \approx q(z_2, t_0) + \dot{q}_c(t - t_0) \quad (8-12)$$

where

$$\dot{q}_c = [q(z_2, t_1) - q(z_2, t_0)](t_1 - t_0)^{-1} \quad (8-13)$$

and

$$q(z_2, t_0) = q(x_m, z=z_2(t_0), t_0).$$

Next, we approximate z_2 and z_3 by

$$z_2(t_n) = F(q(x_m, z, t_n), \theta(x_m, z, t_n)) \quad n=0,1 \quad (8-14)$$

where F is a function that is defined later; and

$$z_3(t_n) = \begin{cases} z_2(t_n) + 100 \text{ meters, if } \sigma_c(x_m, t_n)=0; \\ \text{from satellite data, otherwise} \end{cases} \quad n=0,1 \quad (8-15)$$

$$\dot{z}_3(t) = [z_3(t_1) - z_3(t_0)](t_1 - t_0)^{-1}. \quad (8-16)$$

Since (8-4) bears the implicit assumption that $\dot{H}_3 \geq 0$, which we adopted in anticipation of application to situations where convective clouds are present and growing, we must ensure that the value of \dot{z}_3 given by (8-16) satisfies

$$\dot{z}_3 \geq 0. \quad (8-17)$$

This constraint is most likely to be violated when $\sigma_c = 0$ either at observation time t_0 or at t_1 , but not both.

In this instance we can adjust the estimate of z_2 at the hour that $\sigma_c = 0$ to achieve $\dot{z}_3 \geq 0$. Adjusting z_2 is consistent with the position adopted later that only a range of z_2 values can be estimated with confidence from the measured data at any rawin site and time.

We approximate the temporal variations in q_∞ by

$$q_\infty \approx q(z_3), \quad (8-18)$$

and from this we assume in analogy with the form we adopted for q_c , i.e., Eq. 8-12,

$$q_\infty(t) = q(z_3, t_0) + \dot{q}_\infty(t-t_0) \quad (8-19a)$$

where

$$\dot{q}_\infty = [q(z_3, t_1) - q(z_3, t_0)] (t_1 - t_0)^{-1}. \quad (8-19b)$$

From (8-8) we get

$$M_3(\tilde{x}_m, t_1) = \int_{z_2(\tilde{x}_m, t_1)}^{z_3(\tilde{x}_m, t_1)} q(\tilde{x}_m, z, t_1) dz \quad (8-20)$$

and

$$M_3(\tilde{x}_m, t_0) = \int_{z_2(\tilde{x}_m, t_0)}^{z_3(\tilde{x}_m, t_0)} q(\tilde{x}_m, z, t_0) dz \quad (8-21)$$

Similarly,

$$\langle q(t) \rangle_3 = \langle q(t_0) \rangle_3 + \langle \dot{q} \rangle_3 (t - t_0) \quad (8-22)$$

where

$$\langle \dot{q} \rangle_3 = [\langle q(t_1) \rangle_3 - \langle q(t_0) \rangle_3] / (t_1 - t_0) \quad (8-23)$$

and

$$\langle q(t_n) \rangle_3 = \frac{M_3(t_n)}{z_3(t_n) - z_2(t_n)}, \quad n=0,1 \quad (8-24)$$

The vertical air speeds w_2 and w_3 that enter into (8-10) will be approximated by

$$w_2(x_m, t) = w(x_m, z_2(t), t) \quad , \quad t_0 \leq t \leq t_1; \quad (8-25)$$

$$w_3(x_m, t) = w(x_m, z_3(t), t) \quad , \quad t_0 \leq t \leq t_1; \quad (8-26)$$

where $w(x, z, t)$ is the vertical air speed at site x , elevation z (MSL) at hour t . There are various methods of determining w from the set of rawin data but we will not consider any of them here. We will simply assume that some means of estimating w exists and we will leave it to the model user to choose a feasible scheme. [In implementating the present regional model, we used the method developed by Bullock (1983)]. The elevations $z_2(t)$ and $z_3(t)$ at which $w(t)$ is evaluated in (8-25) and (8-26) are taken to be

$$z_2(t) = z_2(x_m, t_0) + \dot{z}_2(t-t_0) \quad t_0 \leq t \leq t_1 \quad (8-27)$$

where

$$\dot{z}_2 = [z_2(x_m, t_1) - z_2(x_m, t_0)] / (t_1 - t_0);$$

$$z_3(t) = z_3(x_m, t_0) + \dot{z}_3(t-t_0) \quad (8-28)$$

with \dot{z}_3 given by (8-16).

Now that we have formulated approximate expressions for each of the parameters in (8-10) except w_c and w_e , we can define a constant \bar{w}_c which satisfies

$$\begin{aligned} \bar{w}_c \int_{t_0}^{t_1} \frac{q_c \sigma_c}{1 - \sigma_c} dt &= \int_{t_0}^{t_1} [\langle q \rangle_3 + \sigma_c (q_c - \langle q \rangle_3)] w_e dt \\ &+ A(x_m; t_0, t_1) \end{aligned} \quad (8-29)$$

where $\bar{w}_c = \bar{w}_c(x_m; t_0, t_1)$ and

$$A(x_m; t_0, t_1) = M_3(t_1) - M_3(t_0) + \int_{t_0}^{t_1} [w_2(\langle q \rangle_3 + \frac{q_c \sigma_c}{1 - \sigma_c}) - q_\infty \dot{z}_3 + w_3(q_\infty - \langle q \rangle_3)] dt. \quad (8-30)$$

The parameter \bar{w}_c is the effective cumulus cloud updraft speed w_c characteristic of the air mass in the vicinity of the rawin site x_m during the interval $t_0 \leq t \leq t_1$ between observations. In other words, in the vicinity of x_m we assume

$$w_c(x, t) = \bar{w}_c(x_m; t_0, t_1) \quad t_0 \leq t \leq t_1, \text{ and} \quad (8-31)$$

$$|x - x_m| < \delta$$

where \bar{w}_c satisfies (8-29). Note that (8-29) relates \bar{w}_c to the unknown entrainment speed w_e , which we consider next.

Continuing our examination of the region around x_m , let us look at the air parcel trajectory that ends at x_m at time t_1 . Figure 8-2 depicts it beginning from its position at time t_0 . Writing Eq. (8-2) in the form

$$\frac{dz}{dt} = \frac{w}{1 - \sigma_c} - w_c \frac{\sigma_c}{1 - \sigma_c} + w_e \quad (8-32)$$

and integrating it from t_0 to t_1 along the trajectory ending at x_m at time t_1 we get

$$\begin{aligned}
z_2(\tilde{x}_m, t_1) - z_2(\tilde{x}'_m, t_0) = & \oint_{t_0}^{t_1} \frac{w_2}{1-\sigma_c} dt - \oint_{t_0}^{t_1} w_c \frac{\sigma_c}{1-\sigma_c} dt \\
& + \oint_{t_0}^{t_1} w_e dt
\end{aligned}
\tag{8-33}$$

where \oint indicates that all parameters in the integrand are evaluated at space-time points along the trajectory between \tilde{x}'_m and \tilde{x}_m (see Figure 8-2). Since \tilde{x}_m is the site of a rawin station and t_1 is an observation time, we can get $z_2(\tilde{x}_m, t_1)$, or more precisely a range of values in which we expect z_2 to lie, from (8-14). But \tilde{x}'_m is generally not the location of meteorological measurements so $z_2(\tilde{x}'_m, t_0)$ can only be estimated from interpolation procedures. Let us suppose that through a combination of measurements and interpolation we are able to say with confidence that

$$\begin{aligned}
z_2(\tilde{x}_m, t_1) - z_2(\tilde{x}'_m, t_0) = \Delta z_2(\tilde{x}_m; t_1, t_0) \pm \\
\delta z_2(\tilde{x}_m; t_1, t_0)
\end{aligned}
\tag{8-34}$$

where Δz_2 and δz_2 are known, partly from (8-14). We can now write (8-33) in the form

$$\Delta z_2 \pm \delta z_2 = \oint_{t_0}^{t_1} \frac{w_2}{1-\sigma_c} dt - \bar{w}_c \oint_{t_0}^{t_1} \frac{\sigma_c}{1-\sigma_c} dt + \oint_{t_0}^{t_1} w_e dt.
\tag{8-35}$$

The cloud cover fraction $\sigma_c(\tilde{x}, t)$ is known everywhere and we assume that w_2 is also available at all points and hours. Thus, (8-35) contains only 2 unknowns: \bar{w}_c and w_e .



Figure 8-2. Illustration of the air parcel trajectory that arrives at point x_m at hour t_1 . Point x'_m denotes the parcel's location at time $t_0 < t_1$.

Following a number of previous investigators (see, for example, the review by Artoz and Andre, 1980) we shall assume that the kinematic heat flux at z_2 is proportional to that at the ground, namely

$$\overline{w'\theta'}_{z=z_2} = aQ \quad (8-36)$$

where Q is the known surface heat flux and a is a constant. Recall that

$$w_e = \frac{\overline{w'\theta'}_{z=z_2}}{\Delta\theta} \quad (8-37)$$

where $\Delta\theta$ is the effective jump in potential temperature across the elevation z_2 . By comparing simple mixed-layer growth rate formulas with measurements,

Artoz and Andre (1980) found that a simple, reasonably accurate expression is

$$w_e \approx \frac{1.4Q}{\gamma h} \quad (8-38)$$

where $\gamma = d\theta/dz$ evaluated at $z=z_2+\varepsilon$ and $h=z_2-z_t$, where z_t is the local terrain elevation. Eq. (8-38) suggests that within the vicinity of rawin station x_m we can approximate w_e by

$$w_e(x,t) = G(x_m; t_0, t_1) Q(x,t) \quad , \quad t_0 \leq t \leq t_1; \\ x - x_m < \delta \quad (8-39)$$

where G is an unknown function that we suspect from (8-38) is of the order

$$G(x_m; t_0, t_1)^{-1} \sim \left[\frac{\partial}{\partial z} \theta(x_m, z=z_2+\varepsilon, \tau) \right] [z_2(x_m, \tau) - \\ z_t(x_m)] \quad (8-40)$$

where τ is some instant in the interval t_0 to t_1 .

Substituting (8-39) into (8-35) we obtain

$$\Delta z_2 \pm \delta z_2 = \oint_{t_0}^{t_1} \frac{w_2}{1-\sigma_c} dt - \bar{w}_c \oint_{t_0}^{t_1} \frac{\sigma_c}{1-\sigma_c} dt + G \oint_{t_0}^{t_1} Q dt, \quad (8-41)$$

where the integrals are all along the trajectory shown in Fig. 8-2. Making use of (8-39) in (8-29) and substituting the result into (8-41) we get

$$\Delta z_2 \pm \delta z_2 = \oint_{t_0}^{t_1} \frac{w_2}{1-\sigma_c} dt - \frac{1}{\tilde{q}_c} [G \int_{t_0}^{t_1} [\langle q \rangle_3 + \sigma_c(q_c - \langle q \rangle_3)]$$

(8-42)

$$Q(x_m, t)dt + A] + G \oint_{t_0}^{t_1} Q dt$$

where

$$\tilde{q}_c = \frac{\int_{t_0}^{t_1} \frac{q_c \sigma_c}{1-\sigma_c} dt}{\int_{t_0}^{t_1} \frac{\sigma_c}{1-\sigma_c} dt}.$$

(8-43)

We repeat that in our notation $\int_{t_0}^{t_1} \zeta dt$ denotes integration of ζ evaluated at the fixed point x_m while $\oint_{t_0}^{t_1} \zeta dt$ denotes integration of $\zeta(x, t)$ along the space-time coordinates illustrated in Figure 8-2.

In expression (8-42), G is the only unknown parameter. For each number Δz_2 in the interval indicated on the left-hand side of (8-42), i.e.,

$$\Delta z_2 - \delta z_2 \leq \Delta z_2 \leq \Delta z_2 + \delta z_2 \quad (8-44)$$

there corresponds a G given by

$$G = [\Delta z_2 - \oint_{t_0}^{t_1} \frac{w_2}{1-\sigma_c} dt + \frac{1}{\tilde{q}_c} A] \{ \oint_{t_0}^{t_1} Q dt - \frac{1}{\tilde{q}_c} \int_{t_0}^{t_1} [\langle q \rangle_3 + \sigma_c(q_c - \langle q \rangle_3)]$$

(8-45)

$$Q(x_m, t)dt \}^{-1}$$

Let us assume that the set of G associated through (8-45) with the set of ΔZ_2 defined by (8-44) lies on the interval

$$G_{\min} \leq G \leq G_{\max} \quad (8-46)$$

Only positive values of G are physically meaningful because both w_e and Q are positive during convective conditions. Therefore, if the interval¹ defined by (8-46) contains only negative values, one or more of the parameters entered in (8-45) have erroneous values. When this situation arises in practice, we propose to alter the values of the various terms in (8-45) until the resulting G interval at least contains positive values. At the most we would want the largest positive values of G to be consistent with (8-40). Alterations of the parameters in (8-45) should proceed according to a fixed rule in which the parameter suspected of being the most inaccurate is altered first, and succeeding terms in the hierarchy are modified only after adjustments to the least accurate terms have failed to produce the desired values of G . The alterations made in the value of any one parameter should be confined to the smallest interval in which one could reasonably assume that the correct value lies. Regarding the order in which the parameters in (8-45) should be altered, we propose the following hierarchy based solely on intuition:

$$q_c, \tilde{q}_c, \langle q \rangle_3, Q, w_2, \Delta Z_2, \sigma_c. \quad (8-47)$$

Suppose that through a process like that described above we have managed to extract from (8-45) an interval of G that contains some positive values. Our interest is only in the positive values, i.e., the G in the interval

$$\max[0, G_{\min}] \leq G \leq G_{\max} \quad (8-48)$$

To each G in this interval there corresponds a \bar{w}_c through relationship (8-29), namely

$$\bar{w}_c = \left[\tilde{q}_c \int_{t_0}^{t_1} \frac{\sigma_c}{1-\sigma_c} dt \right]^{-1} \{ A + G \int_{t_0}^{t_1} [\langle q \rangle_3 + \sigma_c (q_c - \langle q \rangle_3)] Q(x_m, t) dt \} \quad (8-49)$$

Let the interval defined by (8-48) and (8-49) be represented by

$$\hat{\bar{w}}_c - \delta \bar{w}_c \leq \bar{w}_c \leq \hat{\bar{w}}_c + \delta \bar{w}_c . \quad (8-50)$$

Like G , \bar{w}_c is intrinsically a positive quantity. Therefore, if (8-50) does not lie at least partially on the positive, real axis, we must perform alterations on parameter values in (8-49) until the interval (8-50) contains some positive values. The procedure should be similar to that used to obtain positive G values, except in the case of \bar{w}_c we should alter only those parameters in (8-49) that do not appear in the expression for G . Otherwise, we would cause changes in the G values as well. Thus, the suggested hierarchy of parameters that should be modified, if necessary, to achieve positive \bar{w}_c values is the following:

$$q_\infty, M_3, w_3, z_3. \quad (8-51)$$

At the conclusion of this operation we obtain a positive set of \bar{w}_c values and a positive set of G values, both of which apply only to the time interval $t_0 \leq t \leq t_1$ and within the vicinity of rawin station m . The next step is to apply the same procedures to the rawin observations made at station $m+1$ at hours t_0 and t_1 to obtain the corresponding sets of \bar{w}_c and G values for that

site. Once values have been obtained for all rawin stations for the interval $t_0 \leq t \leq t_1$, we can interpolate values for \bar{w}_c and G at all grid points in the model domain. With these fields and the known wind fields $u_2(x,t)$, $w_2(x,t)$, and the cloud cover distribution σ_c , we can solve (8-2) for z_2 at each grid point and each hour t in the interval $t_0 \leq t \leq t_1$. By repeating the entire process for the next observation interval $t_1 \leq t \leq t_2$, we can obtain z_2 and all the other necessary fields during this period.

Before outlining the specific sequence of steps necessary to implement the procedure described above, let us comment briefly on the philosophy of this approach. Many prognostic models have been developed in recent years for predicting the mixed-layer depth z_2 given the surface heat flux Q , the mean vertical velocity w_2 and other physical quantities. These models are not well suited to our needs for several reasons.

First, nearly all these models are one-dimensional and therefore they do not take into account advection and horizontal variations in z_2 , w_2 , Q and the other governing fields.

Second, our interest in regional modeling is with historical situations where available observations exist from which z_2 can be inferred, at least approximately, not only at the initial moment t_0 of the simulation period but also at discrete intervals throughout it. In general, the z_2 predictions of a model initialized at t_0 will become increasingly inconsistent with later observations due to deficiencies in the model and errors in the input data. Our position is that the values of z_2 inferred from meteorological observations made during the simulation period are more credible than the predictions

made by a model. Therefore, in our approach the physical principles on which models are based are employed in the role of interpolating and extrapolating the discrete observations. This is the essence of the roles performed by Eqs. (8-2), (8-45) and (8-49) in our scheme above.

At this time, the proposed procedure has not been tested. Therefore, it should be viewed as the starting point in the development of a scheme capable of providing the various required parameter fields.

In the remainder of this section we present the detailed steps needed to produce an operational processor.

Stage Z0

As noted in the introduction, when cumulus clouds are not present during daylight hours, z_2 is the highest elevation that dry thermals produced by surface heating can reach; however, once cumulus clouds form, z_2 is defined to be the lifting condensation level. In either case, z_2 can be inferred, at least approximately, from radiosonde data and we expressed this in the form (8-14) of a function F that relates z_2 to the potential temperature and mixing ratio vertical profiles. Our first task here is to develop an explicit form for F .

Our approach stems from the realization that turbulence acts to destroy spatial variations in scalar quantities. According to the empirical K-theory

description of turbulent mixing, the rate at which spatial fluctuations are eliminated is inversely proportional to the square of the size λ of the fluctuation. This is evident from the Fourier transform of the classical diffusion equation

$$\frac{\partial c}{\partial t} = K \frac{\partial^2 c}{\partial z^2}. \quad (8-52)$$

From this equation one finds that the Fourier amplitude A of spatial variation in the scalar c of wave number $k = 2\pi/\lambda$ decays in time at the rate

$$\frac{\partial A}{\partial t} = -Kk^2 A. \quad (8-53)$$

Sources of c can generate small scale variations but turbulence always destroys them.

These observations suggest that if second and higher order derivatives of a conservative, scalar quantity remain large for an extended period of time at points in the fluid that are far from sources, the intensity of turbulent mixing at these points, as manifested in the diffusivity K in Eqs. (8-52) and (8-53), must be very small. Otherwise, the small-scale variations that cause large values of these derivatives would be eradicated.

Thus, our basic premise is that in cloud free conditions we can estimate the elevation at which the vertical diffusivity becomes vanishingly small by examining the vertical profiles of the second, and perhaps higher, order derivatives of the mixing ratio and potential temperature, both of which are (approximately) conservative quantities that can be derived from the radiosonde measurements.

Consider for example the classical profiles of mixing ratio q and potential temperature θ in dry, convective conditions illustrated in Figure 8-3a. In Figure 8-3b we show the corresponding profiles of d^2q/dz^2 and $d^2\theta/dz^2$. In this idealized example, the product of these derivatives has a large negative value at the top of the mixed layer, i.e.,

$$\left(\frac{d^2\theta}{dz^2}\right)\left(\frac{d^2q}{dz^2}\right) \lll 0 \text{ at } z = z_2. \quad (8-54)$$

We can estimate the derivatives of a given parameter ζ measured at discrete points in space by representing the parameter values measured in the vicinity of the point of interest by a polynomial. Suppose that we want an estimate of $d^2\zeta/dz^2$ at the point $z=z''$ but that ζ is known only at discrete points z_1, z_2, \dots, z_I that are not necessarily equally spaced. Let us denote the ζ values at these points by

$$\zeta_i = \zeta(x_m, z_i, t_0) \quad , \quad i=1,2,\dots,I \quad (8-55)$$

where we assume that ζ is a parameter measured at rawin station m at time t_0 . We can estimate the second derivative of ζ as well as other properties of interest at the desired elevation z'' by expanding ζ in a polynomial about z'' . Thus, let

$$\zeta(z) = a_0 + a_1\eta + a_2\eta^2 + a_3\eta^3 \quad (8-56)$$

where

$$\eta = z - z''. \quad (8-57)$$

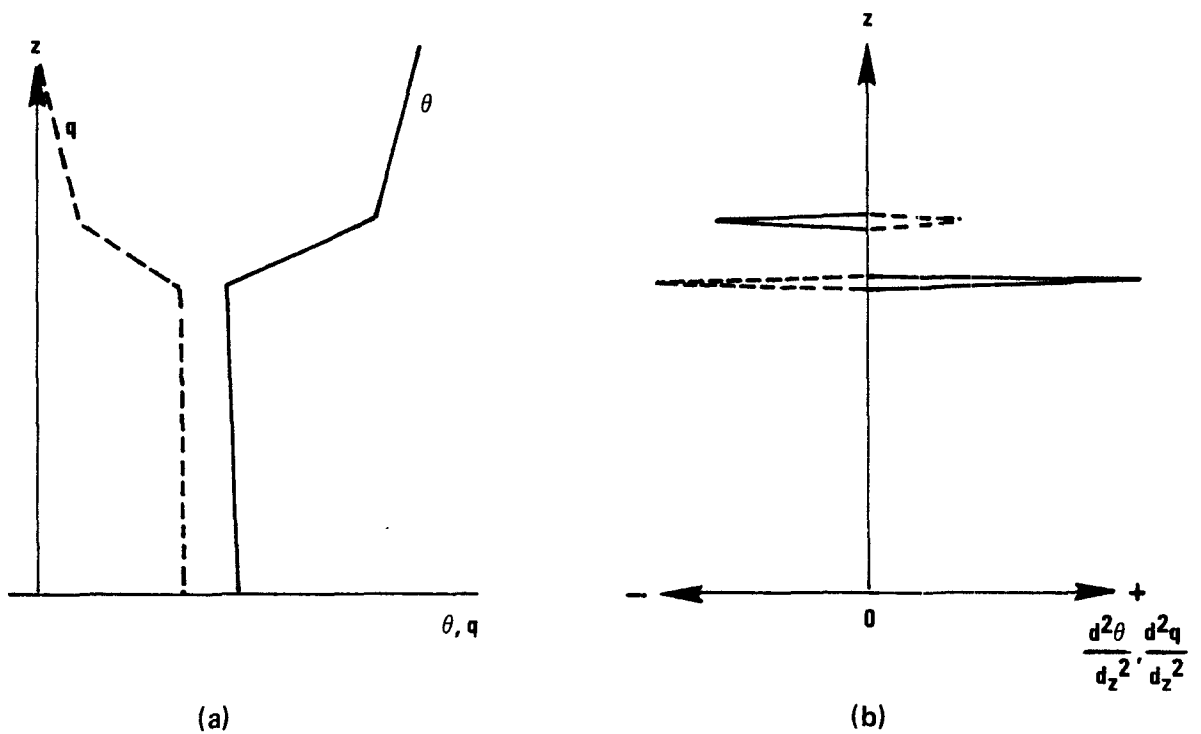


Figure 8-3. (a) Idealized profiles of mixing ratio q and potential temperature θ in dry, convective conditions.
 (b) Second derivatives of the profiles illustrated in panel a.

We can obtain the four constants a_0, \dots, a_3 in (8-56) from four values of ζ and their corresponding measurement locations z_i . The most accurate

representation is obtained by using the four successive measurements of ζ , shown in Figure 8-4, that straddle the point z'' . Two of these are from elevations below z'' and two are from higher elevations. For convenience, let us denote these four points by z_1, z_2, z_3 and z_4 , as indicated in the Figure; and let the associated ζ measurements be designated $\zeta_1 \dots \zeta_4$. In this notation we have from (8-56)

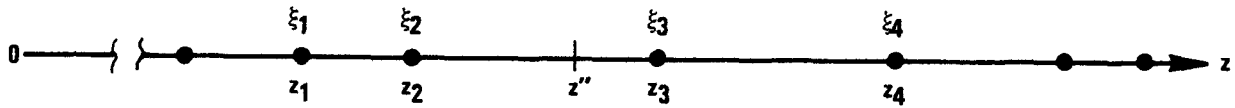


Figure 8-4. Illustration of the points (dots) at which measurements of ζ are available; and the point z'' at which a measure of $d^2\zeta/dz^2$ is desired. Values of ζ measured at the points $z_i, i=1, \dots, 4$ centered at z'' are used to approximate $\zeta(z)$ in a polynomial about z'' .

$$\begin{aligned} \zeta_1 &= a_0 + a_1\eta_1 + a_2\eta_1^2 + a_3\eta_1^3 \\ &\vdots \\ \zeta_4 &= a_0 + a_1\eta_4 + a_2\eta_4^2 + a_3\eta_4^3 \end{aligned} \tag{8-58}$$

where

$$\eta_i = z_i - z'' \tag{8-59}$$

Solving the system of equations (8-58) for the a 's is straightforward and we obtain

$$a_2 = \frac{B_1 A_{12} - B_2 A_{11}}{A_{21} A_{12} - A_{11} A_{22}} \quad (8-60)$$

$$a_1 = \frac{B_1 - a_2 A_{21}}{A_{11}} \quad (8-61)$$

$$a_3 = \frac{(\zeta_1 - \zeta_2) - a_1(\eta_1 - \eta_2) - a_2(\eta_1^2 - \eta_2^2)}{(\eta_1^3 - \eta_2^3)} \quad (8-62)$$

$$a_0 = \zeta_1 - a_1 \eta_1 - a_2 \eta_1^2 - a_3 \eta_1^3 \quad (8-63)$$

$$A_{11} = (\eta_1 - \eta_2)(\eta_2^3 - \eta_3^3) - (\eta_2 - \eta_3)(\eta_1^3 - \eta_2^3) \quad (8-64)$$

$$A_{12} = (\eta_2 - \eta_3)(\eta_3^3 - \eta_4^3) - (\eta_3 - \eta_4)(\eta_2^3 - \eta_3^3) \quad (8-65)$$

$$A_{21} = (\eta_1^2 - \eta_2^2)(\eta_2^3 - \eta_3^3) - (\eta_2^2 - \eta_3^2)(\eta_1^3 - \eta_2^3) \quad (8-66)$$

$$A_{22} = (\eta_2^2 - \eta_3^2)(\eta_3^3 - \eta_4^3) - (\eta_3^2 - \eta_4^2)(\eta_2^3 - \eta_3^3) \quad (8-67)$$

$$B_1 = (\zeta_1 - \zeta_2)(\eta_2^3 - \eta_3^3) - (\zeta_2 - \zeta_3)(\eta_1^3 - \eta_2^3) \quad (8-68)$$

$$B_2 = (\zeta_2 - \zeta_3)(\eta_3^3 - \eta_4^3) - (\zeta_3 - \zeta_4)(\eta_2^3 - \eta_3^3) \quad (8-69)$$

The coefficients a_0, \dots, a_3 provide the following useful properties of ζ :

$$\zeta(z=z'') = a_0 \quad (8-70)$$

$$\left. \frac{\partial \zeta}{\partial z} \right|_{z=z''} = a_1 \quad (8-71)$$

$$\left. \frac{\partial^2 \zeta}{\partial z^2} \right|_{z=z''} = 2a_2 \quad (8-72)$$

$$\left. \frac{\partial^3 \zeta}{\partial z^3} \right|_{z=z''} = 6a_3 \quad (8-73)$$

$$\int_{z''-\delta z}^{z''+\delta z} \zeta(z) dz = 2(\delta z)a_0 + \frac{2}{3}(\delta z)^3 a_2 \quad (8-74)$$

Now that we have formulated a method of estimating the derivatives of parameters measured at discrete points, we can proceed to estimate z_2 .

Let

$$q_{zz} = \frac{\partial^2 q}{\partial z^2} \quad (8-75)$$

$$\theta_{zz} = \frac{\partial^2 \theta}{\partial z^2} . \quad (8-76)$$

The steps for Stage ZQ are as follows:

- (1) Applying the procedure outlined above for estimating derivatives. [specifically (8-60) - (8-69) and (8-72)] to the mixing ratio and potential temperature soundings $q_m(z, t_0)$ and $\theta_m(z, t_0)$, respectively, compute

$$\left. \begin{array}{l} q_{zz}(x_m, z_k, t_0) \\ \theta_{zz}(x_m, z_k, t_0) \end{array} \right\} \quad k = 1, \dots, 60$$

at rawin station m ($=1$ on the first pass through this stage) at hour t_0 , where

$$z_k = z_t(\tilde{x}_m) + 25m + k\Delta z \quad (8-77)$$

and $\Delta z = 50 \text{ m.}$

(2) Next form the products

$$P_k = q_{zz}(z_k) \cdot \theta_{zz}(z_k) , k = 1, \dots 60 \quad (8-78)$$

and from this find

$$P = \max_k (-P_k). \quad (8-79)$$

This value of P pertains to the site \tilde{x}_m of rawin station m and to hour t_0 of the sounding.

(3) Next we estimate z_2 to be (units of m MSL).

$$\begin{aligned} z_2(\tilde{x}_m, t_0) &= F(q(\tilde{x}_m, t_0), \theta(\tilde{x}_m, t_0)) \\ &= z_t(\tilde{x}_m) + 25 + 50k^* \end{aligned} \quad (8-80)$$

where k^* is the smallest integer for which

$$P_{k^*} = -P. \quad (8-81)$$

(4) We also need for use in Eq. 8-34 an estimate of the range $\pm \delta z_2$ of elevations in which the actual elevation z_2 of the mixed layer top is likely to lie.

We anticipate that a measure of δz_2 is the width of the interval centered at $z=z_{k*}$ in which P_k has a magnitude of, say, 60% of its peak value . Examination of the third order derivatives of q and θ might also provide a useable measure of δz_2 . At this time, no information is available on which to base a quantitative rule for estimating the range of z_2 values. Therefore, we will assume for now that

$$\delta z_2 = 100\text{m (interim assumption)} \quad (8-82)$$

and after we have gained experience with actual soundings, we will attempt to formulate an empirical rule for estimating δz_2 .

- (5) Compute the lifting condensation level (LCL) at each surface weather station $n=1, \dots, N$ at the hour t_0 of the upper air observations used above in step 3 to estimate z_2 . The elevation of the LCL is found first in pressure coordinates as follows.

Let q_n and θ_n be the mixing ratio (dimensionless) and potential temperature ($^{\circ}\text{K}$), respectively, at surface weather station n .

These data are available from Processor P3. If a parcel of air originally at ground level in the vicinity of the station is lifted without mixing with ambient air, both the mixing ratio and potential temperature will be conserved. Thus, at any altitude $p(\text{mb})$ the vapor pressure in the air parcel will be

$$e = \frac{pq_n}{0.622 + q_n} \quad (8-83a)$$

(cf Eq. 3-2a), and its temperature will be

$$T = \theta_n \left(\frac{1000}{p} \right)^{-0.286} \quad (8-83b)$$

(cf Eq. 3-6). The elevation p_{LCL} of the lifting condensation level is defined as the altitude where the parcel's vapor pressure e is the saturation vapor pressure e_s . The latter is a function of temperature alone, namely

$$e_s = e_0 \exp \left[\frac{L}{R} \left(\frac{1}{T_0} - \frac{1}{T} \right) \right] \quad (8-83c)$$

where $e_0 = 40\text{mb}$, $T_0 = 302^\circ\text{K}$, $L = 2500 \text{ joule g}^{-1}$, and $R = 0.461 \text{ joule g}^{-1} \text{ } ^\circ\text{K}^{-1}$. Hence, p_{LCL} is the solution of the equation

$$\frac{pq_n}{0.622 + q_n} = e_0 \exp \left[\frac{L}{R} \left(\frac{1}{302} - \frac{1}{T} \right) \right] \quad (8-83d)$$

where T is given by (8-83b). Eq. (8-83d) can be solved approximately by substituting successively smaller values of p into the equation, beginning with the surface pressure; and considering the solution p_{LCL} to be the pressure at which the left side of (8-83d) first exceeds the right side.

Using the pressure-height functions $p_m(z, t_0)$ available from processor P1, convert p_{LCL} into elevation z_{LCL} (m MSL) as follows

$$z_{LCL}(x_n, t_0) = z^* \quad (8-84)$$

where z^* is the elevation for which

$$p(x_n, z^*, t_0) = p_{LCL}(x_n, t_0). \quad (8-85)$$

The function on the left side of (8-85) can be obtained by applying an inverse r weighting interpolation to the set of $p_m(z, t_0)$ profiles, namely

$$p(x_n, z, t_0) = \frac{\frac{1}{M} \sum_{m=1}^M (|x_n - x_m|)^{-1} p_m(z, t_0)}{\frac{1}{M} \sum_{m=1}^M (|x_n - x_m|)^{-1}}. \quad (8-86)$$

At the end of this step we have values of $z_{LCL}(t_0)$ at all N surface weather stations. The M rawin stations whose soundings we are using to determine z_2 are a subset of the N surface stations.

- (6) At this step we must decide whether z_2 is to be the elevation given by (8-80) or the elevation z_{LCL} given by (8-84). As we noted earlier, the decision rests solely on whether $\sigma_c(x_m, t_0)$ is greater than or equal to zero. In particular

$$z_2(x_m, t_0) = \begin{cases} z_2^1(x_m, t_0) & \text{if } \sigma_c(x_m, t_0) = 0; \\ z_{LCL}(x_m, t_0) & \text{(Eq. 8-84), otherwise.} \end{cases} \quad (8-87)$$

where

$$z_2^1(x_m, t_0) = \text{value given by Eq. 8-80.} \quad (8-88)$$

There are two situations here that signal the presence of an error in our estimates of z_2^1 and/or z_{LCL} . The first is

$$\sigma_c(x_m, t_0) = 0 \text{ and } z_{LCL}(x_m, t_0) < [z_2^1(x_m, t_0) - \delta z_2]; \quad (8-89)$$

and the second is

$$\sigma_c(\tilde{x}_m, t_0) \neq 0 \text{ and } z_{LCL}(\tilde{x}_m, t_0) > [z_2^1(\tilde{x}_m, t_0) + \delta z_2]. \quad (8-90)$$

The first condition indicates that clouds are not forming even though our estimates of z_{LCL} and the mixed layer depth indicate that they should; and (8-90) implies the opposite, namely, that clouds are forming even though our estimates indicate that they should not. If either (8-89) or (8-90) is true at site \tilde{x}_m at hour t_0 this should be recorded for output from Stage ZQ. Frequent occurrences of these conditions would indicate some systematic error in the calculation procedures.

(7) Next we compute z_3 . As we noted earlier (see Eq. 8-15)

$$z_3(\tilde{x}_m, t_0) = \begin{cases} z_2(\tilde{x}_m, t_0) + 100 & , \text{ if } \sigma_c(\tilde{x}_m, t_0) = 0; \\ z_{TCU}(\tilde{x}_m, t_0) & , \text{ otherwise} \end{cases} \quad (8-91)$$

where z_{TCU} is the average elevation (m MSL) of the tops of cumulus clouds, an input to P8 derived from satellite data.

(8) From (8-11) and (8-70)

$$q_c(\tilde{x}_m, t_0) = q(\tilde{x}_m, z_2, t_0) = a_{0,q}(z_2, t_0) \quad (8-92)$$

where $a_{0,q}$ is the coefficient a_0 of the expansion of q about the point $z''=z_2$. This coefficient is found from the mixing ratio sounding and Eqs. (8-60) - (8-69).

(9) From (8-18) and (8-70)

$$q_{\infty}(\tilde{x}_m, t_0) = q(\tilde{x}_m, z_3, t_0) = a_{0,q}(z_3, t_0) \quad (8-93)$$

where $a_{0,q}$ is obtained as in step (8-8) except the expansion is about the elevation $z''=z_3$.

(10) From (8-8) and (8-74) we have

$$M_3(\tilde{x}_m, t_0) = \sum_{k=k_2}^{k_3} [\Delta z a_{0,q}(z_k, t_0) + \frac{1}{12} (\Delta z)^3 a_{2,q}(z_k, t_0)] \quad (8-94)$$

where k_2 is the altitude interval given by (8-77) that is nearest $z_2(\tilde{x}_m, t_0)$, i.e.,

$$|z_2(\tilde{x}_m, t_0) - (z_t(\tilde{x}_m) + 25 + k_2 \Delta z)| = \text{minimum} \quad (8-95)$$

and similarly k_3 is the integer that minimizes

$$|z_3(\tilde{x}_m, t_0) - (z_t(\tilde{x}_m) + 25 + k_3 \Delta z)| = \text{minimum}; \quad (8-96)$$

and $\Delta z = 50\text{m}$ as in (8-77). The coefficients $a_{0,q}$ and $a_{2,q}$ in (8-94) are derived from the q sounding data using formulas (8-60) - (8-69).

(11) From (8-9)

$$\langle q(\tilde{x}_m, t_0) \rangle_3 = \frac{M_3(\tilde{x}_m, t_0)}{z_3(\tilde{x}_m, t_0) - z_2(\tilde{x}_m, t_0)} \quad (8-97)$$

(12) Repeat steps 1-8 at rawin station m for the next observation hour t_1 to obtain $z_2(\tilde{x}_m, t_1)$, $z_3(\tilde{x}_m, t_1)$, $q_c(\tilde{x}_m, t_1)$, $q_{\infty}(\tilde{x}_m, t_1)$, $M_3(\tilde{x}_m, t_1)$ and $\langle q(\tilde{x}_m, t_1) \rangle_3$. (In general, $t_1 = t_0 + \Delta t_m$, where Δt_m is

the interval between observations at station m ; so we should actually write t_{1m} rather than t_1 to designate the second observation time. However, this distinction is not important because in the analyses that follow, we treat the observations on a station-by-station basis and interpolate hourly values of the desired quantities at each site.)

- (13) Construct linear functions of q_c , q_∞ and $\langle q \rangle_3$ for use in integrating these values with respect to time from t_0 to t_1 . That is

$$\left. \begin{aligned} q_c(x_m, t) &= q_c(x_m, t_0) + \dot{q}_c(t-t_0) \\ q_\infty(x_m, t) &= q_\infty(x_m, t_0) + \dot{q}_\infty(t-t_0) \\ \langle q(x_m, t) \rangle_3 &= \langle q(x_m, t_0) \rangle_3 + \langle \dot{q} \rangle_3(t-t_0) \end{aligned} \right\} t_0 \leq t \leq t_1 \quad (8-98)$$

where

$$\dot{q}_c = [q_c(x_m, t_1) - q_c(x_m, t_0)](t_1 - t_0)^{-1} \quad (8-99)$$

with similar expressions for \dot{q}_∞ and $\langle \dot{q} \rangle_3$ [see (8-19b) and (8-23)].

- (14) Repeat steps 1-10 above for each of the M rawin stations, and then repeat all steps for each observation interval in the period for which the regional model is to be operated. The observation interval is usually not the same at each upper air station. Figure 8-5 illustrates a hypothetical situation in which the model simulation period is of length T beginning at hour t_0 and the stations make soundings at a variety of intervals.

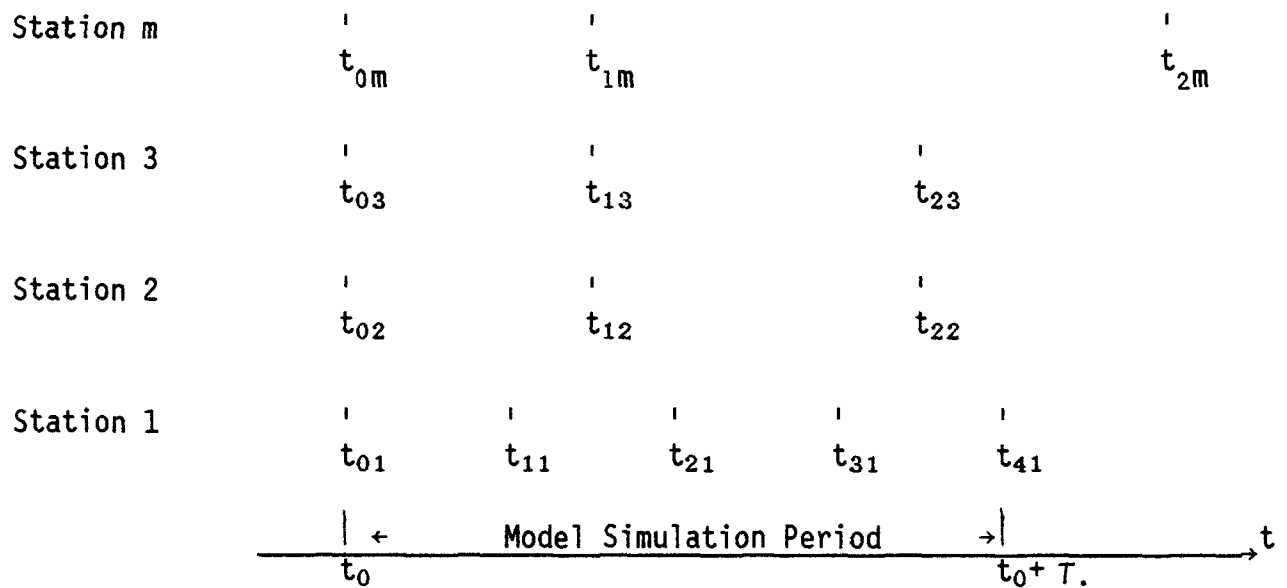


Figure 8-5. Illustration of possible relationships among the intervals at which upper air soundings are made at a set of rawin stations.

At the end of the operations in Stage ZQ there should be values of z_2 , δz_2 , z_3 , q_c , q_∞ , $\langle q \rangle_3$ and M_3 for each station $m=1, \dots, M$ and for each observation interval in the model simulation period T illustrated in Figure 8-5.

Stage PATH

In Stage ZQ we derived estimates of the parameters required to evaluate the fixed point time integrals that enter in Eqs. (8-45) and (8-49). In this stage we estimate the trajectories necessary to evaluate the path integrals \oint that enter into these equations.

We are still considering the time interval $t_0 \leq t \leq t_1$ and we require the backward trajectories that begin at each of the rawin stations at hour t_1 and go back in time to t_0 . That is, we need to know the location $x(t; x_m, t_1)$ during the interval $t_0 \leq t \leq t_1$ of the air parcel that arrives at station x_m at hour t_1 . By definition

$$x(t_1; x_m, t_1) = x_m \quad (8-100)$$

and by previous declaration (see Figure 8-2)

$$x(t_0; x_m, t_1) = x'_m(t_0, t_1). \quad (8-101)$$

We will compute the trajectories using the horizontal velocities u_{2H} measured in the vicinity of z_2 . These velocities control the rate of advection of the mixed layer height (see Eq. 8-2); but the effective path along which the surface heat flux Q is determined is more likely fixed by the vertically averaged horizontal flow beneath z_2 . In actuality the temperature of a vertical column of air of depth $z_2 - z_t$ at x_m at time t_1 is affected by the surface heat flux in a plume-shaped area whose width σ_y increases from zero at x_m at $t=t_1$ to a value of the order

$$\sigma_y(x'_m) \sim (t_1 - t_0) \Delta v \quad (8-102)$$

at the upstream starting point of the trajectory that ends at x_m at t_1 . In (8-102) Δv is the magnitude of the vertically integrated horizontal wind shear in the mixed layer. Since we are representing the heating rate of the column as an unknown function G multiplied by the surface heat flux variations along the trajectory between x'_m and x_m , we can assume that the difference in the integrated heat flux along the trajectory extracted from the winds u_{2H} at the level z_2 and that along the "correct" trajectory is absorbed in the function G .

To compute the trajectory \underline{x}_m' to \underline{x}_m we will assume that there exists a routine, or stage, which we will call WV, which returns an estimate of the vertical wind speed w and the horizontal wind vector \underline{v}_H at any given space-time point (\underline{x}, z, t) in the NEROS domain. Thus, when we write $w(\underline{x}, z, t)$ or $\underline{v}_H(\underline{x}, z, t)$ it will be understood that these values are available from the routine WV which we will not specify here. (In the first generation model we will employ the scheme developed by Bullock (1983) in the role of stage WV.) For later reference let us signify this in equation form:

$$\left. \begin{array}{l} w(\underline{x}, z, t) \\ \underline{v}_H(\underline{x}, z, t) \end{array} \right\} \text{ from Stage WV} \quad (8-103)$$

The trajectories can now be generated using the following recursive formula:

$$\begin{aligned} \underline{x}(t_1 - (I+1)\Delta t; \underline{x}_m, t_1) = & \underline{x}(t_1 - I\Delta t; \underline{x}_m, t_1) \\ & - \Delta t \underline{v}_H(\underline{x}(t_1 - I\Delta t; \underline{x}_m, t_1), z_2, t_1 - I\Delta t) \end{aligned} \quad (8-104)$$

where Δt is a time step of order 30 minutes. Execution of (8-104) is the first step in the operation of Stage PATH, i.e.,

- (1) Solve (8-104) for the trajectories $\underline{x}(t; \underline{x}_m, t_1)$, $t_0 \leq t \leq t_1$ at each of the M upper air stations.

In the next steps we use these trajectories to evaluate the path integrals in (8-45) and (8-49).

- (2) Determine the variations in w_2 , σ_c , and Q along each of the M trajectories generated in step 1 for the period $t_0 \leq t \leq t_1$ and express the results in the following functional forms:

$$w_{2m}(t) = w(\underline{x}(t; \underline{x}_m, t_1), \bar{z}_{2m}, t) \quad (8-105)$$

$$\sigma_{cm}(t) = \sigma_c(\underline{x}(t; \underline{x}_m, t_1), t) \quad (8-106)$$

$$Q_m(t) = Q(\underline{x}(t; \underline{x}_m, t_1), t) \quad (8-107)$$

where

$$\bar{z}_{2m} = \frac{1}{2}[z_2(\underline{x}_m, t_0) + z_2(\underline{x}_m, t_1)]. \quad (8-108)$$

- (3) Now compute the following path integrals:

$$\oint_{t_0}^{t_1} \frac{w}{1-\sigma_c} dt \approx I_{wm}(t_1) = \Delta t \sum_{j=0}^J \frac{w_{2m}(t_1-j\Delta t)}{1-\sigma_{cm}(t_1-j\Delta t)} \quad (8-109)$$

$$\oint_{t_0}^{t_1} \frac{\sigma_c}{1-\sigma_c} dt \approx I_{om}(t_1) = \Delta t \sum_{j=0}^J \frac{\sigma_{cm}(t_1-j\Delta t)}{1-\sigma_{cm}(t_1-j\Delta t)} \quad (8-110)$$

$$\oint_{t_0}^{t_1} Q dt \approx I_{Qm}(t_1) = \Delta t \sum_{j=0}^J Q_m(t_1-j\Delta t) \quad (8-111)$$

where

$$J = (t_1 - t_0)/\Delta t \quad (8-112)$$

- (4) Repeat the three steps above for each of the M rawin stations and

for each of the observation intervals within the model simulation period (see Figure 8-5). At the end of Stage PATH, there should be values of the path integrals I_w , I_σ and I_Q (Eqs. 8-109 - 8-111) for each rawin station for each observation interval in the simulation period T .

Stage WEWC

Here we attempt to solve (8-45) for the function $G(\underline{x}_m; t_1, t_0)$, which will provide the entrainment velocity field $w_e(\underline{x}, t)$ through (8-39); and equation (8-49) for $\bar{w}_c(\underline{x}_m; t_1, t_0)$ which will provide the cumulus updraft speed $\bar{w}_c(\underline{x}, t)$.

- (1) Using the estimates (8-98) of the temporal variations in q_c , and $\langle q \rangle_3$ at each upper air site \underline{x}_m in the period $t_0 \leq t \leq t_1$, and the surface heat flux $Q(\underline{x}_m, t)$ in this period, compute the following integral:

$$I(\underline{x}_m; t_1, t_0) = \Delta t \sum_{j=0}^J [\langle q(\underline{x}_m, t_1 - j\Delta t) \rangle_3 + \sigma_c(\underline{x}_m, t_1 - j\Delta t) \cdot (q_c(\underline{x}_m, t_1 - j\Delta t) - \langle q(\underline{x}_m, t_1 - j\Delta t) \rangle_3)] Q(\underline{x}_m, t_1 - j\Delta t) \quad (8-113)$$

- (2) Compute the parameter (see 8-43):

$$\tilde{q}_c(\underline{x}_m; t_1, t_0) = [I_{\sigma m}(t_1)]^{-1} \Delta t \sum_{j=0}^J \frac{q_c(\underline{x}_m, t_1 - j\Delta t) \sigma_c(\underline{x}_m, t_1 - j\Delta t)}{1 - \sigma_c(\underline{x}_m, t_1 - j\Delta t)} \quad (8-114)$$

where $I_{\sigma m}(t_1)$ is from Stage PATH, Eq. 8-110.

In Eq. 8-45, Δz_2 is a measure of the change in z_2 between the starting point x_m' and the end point x_m of the trajectory that arrives at x_m at time t_1 . As we noted earlier, we have an estimate of z_2 at x_m at t_1 but no measurement of z_2 at x_m' at t_0 .

Let us assume that t_0 is the initial instant of the time period in which data for the regional model are required and that t_0 is also an hour at which rawin data are routinely collected. At this initial moment we must use some objective analysis method to determine z_2 in the model domain. Subsequently, we can use the prognostic equation 8-2 to obtain z_2 . Thus, to estimate z_2 at x_m' at time t_0 , we first estimate z_2 at each of the m rawin stations using (8-87) (Stage ZQ), and we estimate the likely error bounds $\pm \delta z_2(x_m, t_0)$ on this estimate at each x_m (see step 4 of Stage ZQ). Next, we apply the r^{-1} interpolation formula to obtain $z_2(x_m', t_0)$. To do this we must take into account the possibility that cumulus clouds are present between rawin stations. In this instance the z_2 estimates obtained at the station sites x_m will not represent the lifting condensation level, which is the altitude of z_2 wherever $\sigma_c(x, t_0) \neq 0$. Thus, we assign $z_2(x_m', t_0)$ values according to the following rule:

$$z_2(x_m', t_0) = \begin{cases} \frac{\sum_{i=1}^M |r_{im}|^{-1} z_2(x_i, t_0)}{\sum_{i=1}^M |r_{im}|^{-1}}, & \text{if } \sigma_c(x_m', t_0) = 0; \\ \frac{\sum_{j=1}^N |r_{jm}|^{-1} z_{LCL}(x_j, t_0)}{\sum_{j=1}^N |r_{jm}|^{-1}}, & \text{otherwise} \end{cases} \quad \begin{matrix} (8-115a) \\ (8-115b) \end{matrix}$$

where

$$r_{nm} = [(x_n - x'_m)^2 + (y_n - y'_m)^2]^{1/2}, \quad (8-116)$$

z_{LCL} is given by (8-84), $z_2(x_i, t_0)$ is given by (8-87) and the summations in (8-115a) are over all M rawin stations while in (8-115b) they are over all N surface weather stations.

We apply the same $|r|^{-1}$ interpolation formula to estimate δz_2 at x'_m . At all times $t = t_1, t_2$, etc. after t_0 , we will have estimates of $z_2(x, t)$ from the prognostic equation 8-2 (output of Stage W_2 described below). In this case $z_2(x'_m, t)$ must be assumed to be exact (i.e., $\delta z_2(x'_m, t) = 0$). Errors are allowed only at the end points of the time intervals that we treat. For example, in $t_1 \leq t \leq t_2$, we assume $\delta z_2(t_1) = 0$ but we allow finite values of $\delta z_2(t_2)$ at each rawin station.

Thus, step 3 of this stage (WEWC) is as follows:

- (3) a. If t_0 is the initial instant of the regional model simulation period, determine $z_2(x_m, t_0), m=1, \dots, M$ from (8-87) (Stage ZQ) and $z_2(x'_m, t_0)$ from (8-115). Then estimate $\delta z_2(x_m, t_0), m=1, \dots, M$ (see step 4, Stage ZQ) and subsequently $\delta z_2(x'_m, t_0)$ using these values and (8-115).
- b. If t_0 is not the initial instant of the model simulation, then $z_2(x, t_0)$ is available at all grid points x from Stage Z2, described below; and $\delta z_2(x'_m, t_0) = 0$ everywhere.
- (4) We can now estimate the range of values (8-44) in which the parameter ΔZ_2 that enters in (8-45) lies. Recall from (8-34)

that ΔZ_2 is the difference in the z_2 values measured at (x'_m, t_0) and (x_m, t_1) . We find after some thought that

$$\Delta Z_2(x_m, t_1)_{\min} = [z_2(x_m, t_1) - \delta z_2(x_m, t_1)] - [z_2(x'_m, t_0) + \delta z_2(x'_m, t_0)] \quad (8-117)$$

$$\Delta Z_2(x_m, t_1)_{\max} = [z_2(x_m, t_1) + \delta z_2(x_m, t_1)] - [z_2(x'_m, t_0) - \delta z_2(x'_m, t_0)] \quad (8-118)$$

(5) We now solve (8-45) for the minimum and maximum values of G (see 8-46) in the vicinity of x_m during the interval $t_0 \leq t \leq t_1$.

$$G(x_m, t_1)_{\min} = \begin{cases} [\Delta Z_2(x_m, t_1)_{\min} - I_{wm}(t_1) + \frac{A}{\tilde{q}_c}] [I_{Qm}(t_1)]^{-1}, \\ \text{if } I_{om}(t_1) \text{ or } \tilde{q}_c(x_m) = 0 \text{ and } I_{Qm} \neq 0; \\ [\Delta Z_2(x_m, t_1)_{\min} - I_{wm}(t_1) + \frac{A}{\tilde{q}_c}] [I_{Qm}(t_1) - \\ I(x_m; t_1, t_0) / \tilde{q}_c(x_m; t_1, t_0)]^{-1}, \text{ if} \\ I_{om}(t_1) \text{ and } \tilde{q}_c(x_m) \text{ and } I_{Qm} \neq 0; \\ 0, \text{ if } I_{Qm}(t_1) \leq 0. \end{cases} \quad (8-119)$$

$$G(x_m, t_1)_{\max} = (8-119) \text{ with } \Delta Z_2(x_m, t_1)_{\min} \text{ replaced by } \Delta Z_2(x_m, t_1)_{\max}. \quad (8-120)$$

In Eq. (8-119), $\Delta Z_2(\)_{\min}$ is from (8-117), $\Delta Z_2(\)_{\max}$ is from (8-118), $I_{wm}(t_1)$ is from (8-109), $I_{Qm}(t_1)$ is from (8-111), $I_{om}(t_1)$ is from (8-110), $I(\)$ is from (8-113), $\tilde{q}_c(\)$ is from (8-114), and A is given by (8-30).

(6) Next we must check whether the upper bound G_{\max} on G is positive. If it is not, we must return to Stage ZQ and alter the value of q_c and, if necessary, the other parameters listed in (8-47) until the resulting integrals I , \tilde{q}_c , etc. in (8-120) yield a value for G_{\max} that is positive, and preferably of an order of magnitude consistent with (8-40). The procedure for altering the variables in (8-47) must be developed through experimentation (refer again to the paragraphs preceding (8-47)) and therefore we will not attempt to define it here. Thus, if $G(\tilde{x}_m, t_1)_{\max} > 0$, go to step 7; otherwise return to Stage ZQ and begin modification of q_c , etc. as described above.

(7) We can arrive at this step only after the previous analyses have produced a range of G values that lies at least partially on the positive, real axis. We assume, therefore, that

$$G_0 \leq G(\tilde{x}_m, t_1) \leq G(\tilde{x}_m, t_1)_{\max} \quad (8-121)$$

where

$$G_0 = \max[0, G(\tilde{x}_m, t_1)_{\min}]. \quad (8-122)$$

We now compute limiting values for the cloud updraft velocity parameter \bar{w}_c .

$$\bar{w}_c(\tilde{x}_m, t_1)_{\min} = \begin{cases} [A(\tilde{x}_m, t_1) + G_0 I(\tilde{x}_m; t_1, t_0)] [\tilde{q}_c(\tilde{x}_m; t_1, t_0) \cdot \\ I_{om}(t_1)]^{-1}, & \text{if } \tilde{q}_c \text{ and } I_{om} \neq 0; \\ 0, & \text{if } \tilde{q}_c(\tilde{x}_m; t_1, t_0) \text{ or } I_{om}(t) = 0 \end{cases} \quad (8-123)$$

where

$$\begin{aligned}
 A(\tilde{x}_m, t_1) = & M_3(\tilde{x}_m, t_1) - M_3(\tilde{x}_m, t_0) + \Delta t \sum_{j=0}^J \{ w(\tilde{x}_m, \bar{z}_{2m}, \\
 & t_1 - j\Delta t) [\langle q(\tilde{x}_m, t_1 - j\Delta t) \rangle_3 + \\
 & \frac{q_c(\tilde{x}_m, t_1 - j\Delta t) \sigma_c(\tilde{x}_m, t_1 - j\Delta t)}{1 - \sigma_c(\tilde{x}_m, t_1 - j\Delta t)}] - q_\infty(\tilde{x}_m, t_1 - j\Delta t) \cdot \\
 & (\frac{z_3(\tilde{x}_m, t_1) - z_3(\tilde{x}_m, t_0)}{t_1 - t_0}) + w(\tilde{x}_m, \bar{z}_{3m}, t_1 - j\Delta t) \cdot \\
 & [q_\infty(\tilde{x}_m, t_1 - j\Delta t) - \langle q(\tilde{x}_m, t_1 - j\Delta t) \rangle_3] \} \quad (8-124)
 \end{aligned}$$

In this expression M_3 is from (8-94); z_3 is from (8-91); $\langle q \rangle_3$, q_c , and q_∞ are from (8-98); $w(\tilde{x}, z, t)$ is the vertical velocity function solution or stage WV defined earlier just before (8-103); and \bar{z}_{2m} is defined by (8-108) with a similar definition for \bar{z}_{3m} .

$$\begin{aligned}
 \bar{w}_c(\tilde{x}_m, t_1)_{\max} = & \text{Eq. (8-123) with } G_0 \text{ replaced by} \\
 & G(\tilde{x}_m, t_1)_{\max} \quad (8-125)
 \end{aligned}$$

- (8) If $\bar{w}_c(\tilde{x}_m, t_1)_{\max} \leq 0$ and $I_{om}(t_1)$ and $\tilde{q}_c(\tilde{x}_m; t_1, t_0) > 0$, then return to Stage ZQ and alter q_∞ and, if necessary, the other parameters in list (8-51) until Eq. (8-125) yields a positive value for $\bar{w}_c(\tilde{x}_m, t_1)_{\max}$. The alteration process is similar to that discussed earlier in connection with the calculation of G (see the paragraph preceding (8-51) and step 6 above. When a range $\bar{w}_c(\)_{\min} \leq \bar{w}_c \leq \bar{w}_c(\)_{\max}$ has been found that lies at least partially on the positive real axis, proceed to step 9.

- (9) At this point a range of values of $G(\bar{x}_m, t_1)$ has been established (in step 7, Eqs. 8-121 and 8-122); and a range of $\bar{w}_c(\bar{x}_m, t_1)$ has been computed in steps 7 and 8, namely

$$\bar{w}_c(\bar{x}_m, t_1)_{\min} \leq \bar{w}_c(\bar{x}_m, t_1) \leq \bar{w}_c(\bar{x}_m, t_1)_{\max} \quad (8-126)$$

where the upper bound is positive. We now select from these ranges the following values for site \bar{x}_m for the interval t_0 to t_1 :

$$G(\bar{x}_m, t_1) = \text{value in the range (8-121) that satisfies (8-40) closest;} \quad (8-127)$$

$$\bar{w}_c(\bar{x}_m, t_1) = \text{solution of (8-49) with } G \text{ given by (8-127) and all other parameters with values determined in step 8.} \quad (8-128)$$

We assume that these values are constant at \bar{x}_m during the entire interval $t_0 \leq t \leq t_1$, specifically, we assume

$$\left. \begin{aligned} G(\bar{x}_m, t) &= G(\bar{x}_m, t_1) \\ \bar{w}_c(\bar{x}_m, t) &= \bar{w}_c(\bar{x}_m, t_1) \end{aligned} \right\} t_0 \leq t \leq t_1 \quad (8-129)$$

These values should be recorded for each hour in the interval t_0 to t_1 for site \bar{x}_m . Note that t_1 , which is the hour of the rawin observation following that at t_0 , is not necessarily the same hour for all rawin stations. (See Figure 8-5). This does not pose a problem because we apply (8-129) to each station separately to obtain hourly estimates of G and \bar{w}_c .

- (10) Repeat step 9 for each interval in the model simulation period. This will produce hourly values of G and \bar{w}_c at rawin station m throughout the simulation period t_0 to $t_0 + T$.
- (11) Repeat steps 1-10 for each rawin station $m=1, \dots, M$. At the conclusion of Stage WEWC, there will be hourly values of G and \bar{w}_c at every rawin station throughout the simulation period.

Stage W2

We now begin to assemble the information gathered in the previous stages to solve the prognostic equation (8-2) for z_2 over the model space-time domain. First, we construct the entrainment velocity field.

- (1) Starting at the initial instant t_0 of the simulation period, collect the G values at this hour generated in Stage WEWC at each of the M rawin stations and interpolate them onto the NEROS grid using the r^{-1} weight:

$$G(\underline{x}, t_0) = \frac{\sum_{m=1}^M |\underline{x} - \underline{x}_m|^{-1} G(\underline{x}_m, t_0)}{\sum_{m=1}^M |\underline{x} - \underline{x}_m|^{-1}} \quad (8-130)$$

where \underline{x} ranges over all grid points.

- (2) Convert the G field into the w_e field as follows (see 8-39):

$$w_e(\underline{x}, t_0) = G(\underline{x}, t_0) Q(\underline{x}, t_0) (=f\theta/\Delta\theta) \quad (8-131)$$

where Q is the surface heat flux in the grid cell centered at \underline{x} at time t_0 . Note that $w_e(\underline{x}, t)$ (designated $f\theta/\Delta\theta$ in Part 1), $t_0 \leq t \leq t_0 + T$ is an output of this processor, P8, for each grid point in the regional model domain.

- (3) We construct the initial z_2 field at each grid point using the interpolation scheme (8-115) employed earlier in Stage PATH. Specifically,

$$z_2(\underline{x}, t_0) = \begin{cases} \text{Eq. 8-115a, if } \sigma_c(\underline{x}, t_0) = 0; \\ \text{Eq. 8-115b, otherwise} \end{cases} \quad (8-132)$$

where \underline{x} ranges over all grid points in the model region.

- (4) Interpolation of the cloud updraft velocities \bar{w}_c estimated at the rawin stations in Stage WEWC requires caution because it may often happen that cumulus clouds are present in isolated areas that do not contain an upper air station, or are present at station locations between observation times. To handle these situations we propose to compile a semi-empirical relationship between \bar{w}_c and cloud depth using all \bar{w}_c , z_2 and z_{TCU} estimated in the earlier analyses during the simulation period T . This function can be based on field data. For now compute the average of the \bar{w}_c values obtained in Stage WEWC for various values of the cloud thickness $h_3 = z_{TCU} - z_2$, say values of h_3 at intervals of 200m; and call the resulting function $w(h_3)$. Then we assume

$$\begin{aligned} \bar{w}_c(\underline{x}, t_0) = & (1-\alpha(\underline{x}))w(z_{TCU}(\underline{x}, t_0)-z_2(\underline{x}, t_0)) \\ & + \alpha(\underline{x})\bar{w}_{cLOCAL}(\underline{x}, t_0) \end{aligned} \quad (8-133)$$

where

$$w(h_3) = \bar{w}_c \text{ for clouds of depth } h_3 \text{ (an empirical function);} \quad (8-134)$$

$$\begin{aligned} \alpha(x) &= \text{distance weighting function} \\ &= \exp[-|x-x_m|/\text{SIG}] \end{aligned} \quad (8-135)$$

x_m is the rawin site closest to x where $\bar{w}_c \neq 0$; SIG is a distance constant, e. g., 50km; and

$$\bar{w}_{c\text{LOCAL}}(x, t_0) = \bar{w}_c(x_m, t_0). \quad (8-136)$$

Formula (8-133) is an heuristic expression that assigns \bar{w}_c a value that is determined partly by any \bar{w}_c estimates that have been derived for that location in the earlier stages and partly by the assumed empirical relationship between cloud depth and updraft velocity.

Note that $\bar{w}_c(x, t)$, with x ranging over all grid points and t over all hours in the simulation period T , is an output of this processor, P8.

- (5) For the advection velocity field v_{2H} required in Eq. (8-2) at time t_0 , we will use

$$v_{2H}(x, t_0) = [z_2(x, t_0) - z_t(x)]^{-1} \int_{z_t(x)}^{z_2(x, t_0)} v_H(x, z, t_0) dz \quad (8-137)$$

where $v(x, z, t)$ is the horizontal wind at level z from the routine WV described earlier. The horizontal velocities that WV provides

should be those that are used to compute the vertical velocity $w(\underline{x}, z, t)$ and they should be interpolated from the wind observation stations to each grid point \underline{x} using an interpolation scheme that maintains a consistent relationship between $w(\underline{x}, z, t)$ and the horizontal winds $\underline{v}_H(\underline{x}, z, t)$ at elevations $z_t \leq z' \leq z$.

- (6) The vertical air speed at each grid point \underline{x} at the initial moment t_0 is obtained from the function routine WV as before, namely

$$w_2(\underline{x}, t_0) = w(\underline{x}, z_2(\underline{x}, t_0), t_0) \quad (8-138)$$

where the function on the right side is a part of routine WV.

- (7) We now solve (8-2) for $z_2(\underline{x}, t_0 + \Delta t)$ using the difference scheme described in Appendix A to Processor P7. With this scheme we have

$$z_2(\underline{x}, t_0 + \Delta t) = \int p(\underline{x}, t_0 + \Delta t | \underline{x}', t_0) [z_2(\underline{x}', t_0) + \Delta t S(\underline{x}', t_0)] d\underline{x}' \quad (8-139)$$

where

$$S(\underline{x}', t_0) = [w_2(\underline{x}', t_0) - \sigma_c(\underline{x}', t_0) \bar{w}_c(\underline{x}', t_0)] \cdot (1 - \sigma_c(\underline{x}', t_0)) + w_e(\underline{x}', t_0) \quad (8-140)$$

where $\sigma_c(\underline{x}, t_0)$ is the known fractional coverage of cumulus clouds at time t_0 in the grid cell centered at \underline{x} ; w_2 is from (8-138); \bar{w}_c is from (8-133); w_e is from (8-131); and

$$p(\underline{x}, t | \underline{x}', t') = \text{known function of } \underline{v}_{2H}. \quad (\text{see Chapter 9, Part 1}) \quad (8-141)$$

- (8) At this point we have computed $z_2(\underline{x}, t_0 + \Delta t)$. From this field we construct z_3 in the manner of (8-91), namely

$$z_3(\underline{x}, t_0 + \Delta t) = \begin{cases} z_2(\underline{x}, t_0 + \Delta t) + 100, & \text{if } \sigma_c(\underline{x}, t_0 + \Delta t) = 0; \\ z_{TCU}(\underline{x}, t_0 + \Delta t), & \text{otherwise} \end{cases} \quad (8-142)$$

where z_{TCU} is the known elevation of cumulus tops. This calculation should be performed at all grid points \underline{x} and the results retained for output from P8.

- (9) The material surface flux \dot{H}_3 across surface H_3 must be computed at each grid point at time $t_0 + \Delta t$ as follows:

$$\dot{H}_3(\underline{x}, t_0 + \Delta t) = \dot{z}_3(\underline{x}, t_0 + \Delta t) + \underline{v}_{3H} \cdot \underline{\nabla}_H z_3 - w(\underline{x}, z_3(\underline{x}, t_0 + \Delta t), t_0 + \Delta t) \quad (8-143)$$

where

$$\dot{z}_3(\underline{x}, t_0 + \Delta t) = \frac{z_3(\underline{x}, t_0 + \Delta t) - z_3(\underline{x}, t_0)}{\Delta t} \quad (8-144)$$

$$\underline{v}_{3H}(\underline{x}, t_0 + \Delta t) = \underline{v}(\underline{x}, z_3(\underline{x}, t_0 + \Delta t), t_0 + \Delta t) \quad (8-145)$$

and

$$\underline{v}_{3H} \cdot \underline{\nabla}_H z_3 = \text{calculated from } \underline{v}_{3H} \text{ and } z_3 \text{ in the manner of (8-A2). See the Appendix to this section.} \quad (8-146)$$

In (8-143), $w(\)$ denotes the function routine WV. The same applies to $\underline{v}(\)$ in (8-145). The flux \dot{H}_3 is an output of processor P8 but it is not used in the calculations performed within this processor. At the initial moment t_0 , assume

$$\dot{H}_3(\underline{x}, t_0) = \dot{H}_3(\underline{x}, t_0 + \Delta t) \quad (8-147)$$

(10) We must also output the local time derivative \dot{z}_2 at each grid point and each hour:

$$\dot{z}_2(\underline{x}, t_0 + \Delta t) = \frac{z_2(\underline{x}, t_0 + \Delta t) - z_2(\underline{x}, t_0)}{\Delta t} . \quad (8-148)$$

assume

$$\dot{z}_2(\underline{x}, t_0) = \dot{z}_2(\underline{x}, t_0 + \Delta t) . \quad (8-149)$$

These fields are outputs of P8 at each hour.

(11) Compute the thickness of Layer 3 at each grid point at time $t_0 + \Delta t$:

$$h_3(\underline{x}, t_0 + \Delta t) = z_3(\underline{x}, t_0 + \Delta t) - z_2(\underline{x}, t_0 + \Delta t) \quad (8-150)$$

where z_3 is from (8-142) and z_2 is from (8-139). Evaluate (8-150) for output only when $t_0 + \Delta t$ is an integral number of hours.

(12) Compute the thickness of Layer 2 for output:

$$h_2(\underline{x}, t_0 + \Delta t) = z_2(\underline{x}, t_0 + \Delta t) - z_T(\underline{x}) - h_1(\underline{x}, t_0 + \Delta t) \quad (8-151)$$

where z_2 is from (8-139) and z_T and h_1 are inputs to Processor P8. Compute (8-151) only at integral hours.

(13) Compute the elevation of surface z_3 in pressure coordinates.

$$p_3(\underline{x}, t_0 + \Delta t) = p(\underline{x}, z_3(\underline{x}, t_0 + \Delta t), t_0 + \Delta t) \quad (8-152)$$

where $p(\underline{x}, z, t)$, which is given by (8-86), is the pressure (mb) at elevation z (m MSL) over site \underline{x} at hour t . This function is interpolated from the pressure-height functions $p_m(\underline{x}, t)$ that are inputs from Processor P1. The field p_3 is an output of this processor, P8, at each grid point and hour.

- (14) Compute the elevation of surface z_2 in pressure coordinates:

$$p_2(\underline{x}, t_0 + \Delta t) = p(\underline{x}, z_2(\underline{x}, t_0 + \Delta t), t_0 + \Delta t) \quad (8-153)$$

where p is given by (8-86). The field p_2 is an output of this processor at each hour of the simulation period.

- (15) In Part 1, Eq. 5-44, we defined the function $\Psi(\underline{x}, t)$ to be the fraction of the volume flux entering cumulus clouds in the grid cell centered at \underline{x} at time t that originates in Layer 0. Here we compute an interim estimate Ψ' of this parameter based strictly on heuristic notions. In Processor P12 we test whether the Ψ' values derived here satisfy criterion (5-47) of Part 1. If they meet this condition they become the final estimate of the parameter Ψ . Otherwise $\Psi(\underline{x}, t)$ is given the largest value that satisfies (5-47).

As a rough, heuristic approximation we shall assume

$$\Psi'(\underline{x}, t_0 + \Delta t) = 0.5 \exp \left\{ - \left[\frac{2h_3(\underline{x}, t_0 + \Delta t)}{z_2(\underline{x}, t_0 + \Delta t) - z_T(\underline{x})} \right]^2 \right\} + 0.1 \quad (8-154)$$

Under this assumption, $\Psi \rightarrow 0.1$ as the depth of cumulus clouds becomes large compared to the depth $(z_2 - z_T)$ of the subcloud layer. For shallow cumulus, $\Psi \rightarrow 0.6$. The Ψ' field is an output of Processor P8 each hour.

Stage WV

This stage is in effect a function routine that provides vertical and horizontal wind speeds at any grid cell and elevation, and horizontal divergence between any two surfaces in any grid cell.

As with nearly all of the input parameters required in the regional model, the variables just cited can be estimated by a number of methods. Solutions of the omega equation, isentropic analyses, and differentiation of functions fit to wind data are several approaches. Our intent here is not to prescribe the use of one particular technique but rather to specify which quantities are required for subsequent use in this and other processors in the network, and in the regional model itself. Selection of specific techniques is left to the "user". Indeed, one of the reasons for structuring the model system in a modular form was to facilitate the use of various techniques interchangeably. In the "first generation" processor network we plan to employ in this stage, WV, the method developed by Bullock (1983).

In order to insure compatibility between the horizontal divergences $\langle \delta \rangle$ required in Processor P11 and the vertical velocities w_n required in this and other processors, it is advantageous to compute all these fields in this one stage. Following is a list of the divergences that must be computed each hour for output to Processor P11:

$$\langle \delta(x,y,t) \rangle_3 = \frac{1}{p_3 - p_2} \int_{p_2(x,y,t)}^{p_3(x,y,t)} (\nabla_H \cdot \underline{v}) dp \quad (8-155)$$

$$\langle \delta(x,y,t) \rangle_2 = \begin{cases} \frac{1}{p_2 - p_{vs}} \int_{p_{vs}(x,y,t)}^{p_2(x,y,t)} (\nabla_H \cdot \underline{v}) dp & , \text{ if } \Delta p_1(t) = 1; \\ \frac{1}{p_2 - p_1} \int_{p_1(x,y,t)}^{p_2(x,y,t)} (\nabla_H \cdot \underline{v}) dp & , \text{ if } \Delta p_1(t) = 0 \end{cases} \quad (8-156)$$

$$\langle \delta(x,y,t) \rangle_1 = \frac{1}{p_1 - p_{vs}} \int_{p_{vs}(x,y,t)}^{p_1(x,y,t)} (\nabla_H \cdot \underline{v}) dp \quad , \text{ defined only when } \Delta p_1 = 0 \quad (8-157)$$

Since the input wind data are in z coordinates, it will be necessary to convert them to p coordinates using the function $p_m(z,t)$ available from P1. Note also that since $p_3 < p_2$, $p_2 < p_1$ or p_{vs} , and $p_1 < p_{vs}$, the integrals in all three of the expressions above are negative when $(\nabla_H \cdot \underline{v}) > 0$ and the reciprocals of the pressure differences that appear outside these integrals are also negative. The net result is that $\langle \delta \rangle$ has the same sign as $\nabla_H \cdot \underline{v}$. We leave the method of computing the divergences $(\nabla_H \cdot \underline{v})$ to the user.

The layer averaged divergences $\langle \delta \rangle_n$ given by (8-155, 156 and 157) are related to the vertical velocity \bar{w}^n on the pressure surfaces p_n that bound each layer by (see Eqs. 11-1b and 11-40)

$$\langle \delta(x,y,t) \rangle_n = \frac{1}{\Delta p_n} [\bar{w}^n(x,y,t) - \bar{w}^{n-1}(x,y,t)] \quad (8-158)$$

where

$$\Delta p_n = |p_n(x,y,t) - p_{n-1}(x,y,t)| \quad (8-159)$$

and \bar{w}^n denotes the vertical velocity in pressure coordinates (mb sec^{-1}) averaged over the surface p_n within the grid cell centered at (x,y) . We shall assume that the spatial variations in w have such large scales that

$$\bar{w}^n(x,y,t) \approx w_n(x,y,t) \quad (8-160)$$

where w_n denotes the local value of w on pressure surface p_n at the cell center (x,y) .

By definition

$$w \equiv \frac{\partial p}{\partial t} + \mathbf{v}_H \cdot \nabla_H p + w \frac{\partial p}{\partial z} \quad (8-161)$$

where p is pressure and w is the vertical velocity in z coordinates at the point where p is measured. Making use of the hydrostatic approximation and (8-161), we can write

$$w_n = \frac{\partial}{\partial t} p_n + \mathbf{v}_n \cdot \nabla_H p_n - w_n \rho_n g. \quad (8-162)$$

Two of the fields that we need in this processor, P8, are w_3 and w_2 , the vertical velocities in z coordinates (m sec^{-1}) on the top surfaces of Layers 3 and 2. Eqs. (8-158), (8-160), and (8-162) provide a means of estimating these velocities in terms of the measured horizontal winds and their divergence.

We must distinguish between the two cases $\Delta p_1=1$ and $\Delta p_1=0$. Recall from (7-98) that $\Delta p_1(t)=1$ if a surface inversion is present over the modeling region at time t and it is zero otherwise. When an inversion is present the effective ground surface for the flow aloft is the "virtual surface" p_{vs} defined as the top of the inversion layer.

Mode 0: $\Delta p_1 = 0$.

In this case the virtual surface coincides with the terrain. Using (8-158) and (8-159) we can express w_3 in the form

$$w_3 = \Delta p_3 \langle \delta \rangle_3 + \Delta p_2 \langle \delta \rangle_2 + \Delta p_1 \langle \delta \rangle_1 + w_0 \quad (8-163)$$

where w_0 is the value of w at ground level.

To estimate w_0 we note first that the vertical velocity w_0 at ground level is

$$w_0 \cong \underline{v}_0 \cdot \underline{\nabla}_H z_T \quad (8-164)$$

where z_T is the terrain height and \underline{v}_0 is the horizontal wind velocity near the ground. Since horizontal gradients in terrain level are generally much larger than those of the synoptic scale pressure field p_0 , we expect that the last term on the right side of (8-162) will have a much larger magnitude than the term involving $\underline{\nabla}_H \cdot p_0$. We also expect the last term to exceed the magnitude of the local time rate of change of p_0 . Thus, to good approximation we can assume

$$w_0 \approx -p_0 g \underline{v}_0 \cdot \underline{\nabla}_H z_T. \quad (8-165)$$

Combining (8-162), (8-163), and (8-165) we have

$$w_3 = \frac{1}{\rho_3 g} \left[\frac{\partial p_3}{\partial t} + \underline{v}_3 \cdot \underline{\nabla}_H p_3 - \Delta p_3^{<\delta>}_3 - \Delta p_2^{<\delta>}_2 - \Delta p_1^{<\delta>}_1 + \rho_0 g \underline{v}_0 \cdot \underline{\nabla}_H z_T \right], \quad \text{mode 0.} \quad (8-166)$$

where

$$\Delta p_1 = |p_1(x,y,t) - p_{vs}(x,y,t)|, \quad \text{mode 0.} \quad (8-166a)$$

We assume the velocity and divergence fields required to evaluate this equation have been extracted from the wind data that are inputs to this processor. The pressure surfaces p_n are specified by those stages within P8 that call stage WV for w estimates.

To estimate the densities ρ_3 and ρ_0 , we use

$$\rho_n(\underline{x}, t) = \frac{p_n(\underline{x}, t)}{RT_n(\underline{x}, t)} \quad (8-167)$$

where R is the gas constant and T_n is the temperature at pressure level p_n and grid point $\underline{x} = (x,y)$. The temperature fields will be an input to this processor. To evaluate $\underline{\nabla}_H p_3$ and $\underline{\nabla}_H z_T$ in Eq. (8-166), it will be necessary to fit a polynomial of at least 3-rd order to the pressure and terrain data (see Appendix to this chapter).

The expression for w_2 is obtained in the same manner that (8-166) was derived. We get

$$w_2 = \frac{1}{\rho_2 g} \left[\frac{\partial p_2}{\partial t} + \underline{v}_2 \cdot \underline{\nabla}_H p_2 - \Delta p_2 \langle \delta \rangle_2 - \Delta p_1 \langle \delta \rangle_1 + \rho_o g \underline{v}_o \cdot \underline{\nabla}_H z_T \right], \text{ mode 0} \quad (8-168)$$

Also in mode 0 we require for direct use in the regional model the component of the vertical velocity w_1 on surface p_1 that is due to horizontal divergence of the flow in Layer 1 (see Eq. 3.1b of Part 1). We denote this velocity component by \bar{w}_{D1} where

$$w_1 = w_{T1} + \bar{w}_{D1} = \frac{1}{\rho_1 g} \left[\frac{\partial p_1}{\partial t} + \underline{v}_1 \cdot \underline{\nabla}_H p_1 - \Delta p_1 \langle \delta \rangle_1 + \rho_o g \underline{v}_o \cdot \underline{\nabla}_H z_T \right]. \quad (8-169)$$

Since by definition \bar{w}_{D1} is the divergence induced vertical motion on p_1 , the terrain induced component is just the right side of (8-169) with $\langle \delta \rangle_1 = 0$. Thus,

$$\bar{w}_{D1}^i = - \frac{\Delta p_1}{\rho_1 g} \langle \delta \rangle_1, \text{ mode 0.} \quad (8-170)$$

and Δp_1 is given by (8-166a). In order to emphasize that this value applies in mode 0 only, we designate it \bar{w}_{D1}^i at the output of P11. Processor P12 will take this field as input and generate the final, complete function \bar{w}_{D1} .

Mode 1: $\Delta p_1 = 1$

In this state an inversion layer is present at the ground and the effective bottom of the flow aloft is the virtual surface p_{vs} , which coincides with terrain features that extend up through the inversion layer but which otherwise is the top of the inversion layer itself. In this situation the expression for w_3 becomes

$$w_3 = \Delta p_3 \langle \delta \rangle_3 + \Delta p_2 \langle \delta \rangle_2 + w_{vs}. \quad (8-171)$$

In order to obtain an estimate of w_{vs} that is consistent with the model used in P7 to simulate flow in the ground level inversion, we must impose the constraint that the volume flux across p_{vs} is continuous.

Just below the top z_{vs} of the cold inversion layer the downward volume flux is

$$\left. \frac{dH_{vs}}{dt} \right|_{z_{vs} - \epsilon} = \frac{\partial z_{vs}}{\partial t} + u_0 \frac{\partial z_{vs}}{\partial x} + v_0 \frac{\partial z_{vs}}{\partial y} - w_0 = \eta_{vs} \quad (8-172)$$

where (u_0, v_0, w_0) is the fluid velocity in the cold layer; and η_{vs} is the cooling rate, a known function of space and time. Just above z_{vs} , i.e., at the base of Layer 2, the downward volume flux is

$$\left. \frac{dH_{vs}}{dt} \right|_{z_{vs} + \epsilon} = \frac{\partial z_{vs}}{\partial t} + u_{vs} \frac{\partial z_{vs}}{\partial x} + v_{vs} \frac{\partial z_{vs}}{\partial y} - w_{vs}. \quad (8-173)$$

Continuity of the flux across H_{vs} requires that (8-172) and (8-173) be equal, which is true if

$$w_{vs} = \frac{\partial z_{vs}}{\partial t} + u_{vs} \frac{\partial z_{vs}}{\partial x} + v_{vs} \frac{\partial z_{vs}}{\partial y} - \eta_{vs}. \quad (8-174)$$

If we assume that the spatial gradients in z_{vs} are also much larger than those in the synoptic pressure field, we can make use of the earlier approximation (8-165) to obtain

$$w_{vs} \approx -\rho_{vs} g w_{vs} \quad (8-175)$$

where w_{vs} is given by (8-174).

Combining (8-162), (8-171), (8-174), and (8-175) we get

$$\begin{aligned} w_3 = & \frac{1}{\rho_3 g} \left[\frac{\partial p_3}{\partial t} + \underline{v}_3 \cdot \underline{\nabla}_H p_3 - \Delta p_3 \langle \delta \rangle_3 - \Delta p_2 \langle \delta \rangle_2 \right] \\ & + \frac{\rho_{vs}}{\rho_3} \left[\frac{\partial z_{vs}}{\partial t} + \underline{v}_{vs} \cdot \underline{\nabla}_H z_{vs} - \eta_{vs} \right], \text{ mode 1} \end{aligned} \quad (8-176)$$

and similarly

$$\begin{aligned} w_2 = & \frac{1}{\rho_2 g} \left[\frac{\partial p_2}{\partial t} + \underline{v}_2 \cdot \underline{\nabla}_H p_2 - \Delta p_2 \langle \delta \rangle_2 \right] \\ & + \frac{\rho_{vs}}{\rho_3} \left[\frac{\partial z_{vs}}{\partial t} + \underline{v}_{vs} \cdot \underline{\nabla}_H z_{vs} - \eta_{vs} \right], \text{ mode 1} \end{aligned} \quad (8-177)$$

In both (8-176) and (8-177)

$$\Delta p_2 = |p_2(x, y, t) - p_{vs}(x, y, t)|, \text{ mode 1} \quad (8-178)$$

In mode 1 no estimate of w at the top of layer 1 is required because in this situation the volume flux is given by η_{vs} .

The input requirements and outputs of Stage WV are summarized in Table 8-1. Figure 8-6 illustrates processor P8 and its data interfaces schematically.

Table 8-1. Summary of the input and output requirements of each stage of Processor P8.

Input Variable	Description	Source	Stage	Output Variable	Description
$q_m(z,t)$	mixing ratio at elevation z (m MSL) at hour t over rawin station m .	P1	ZQ	$z_2(\tilde{x}_m,t)$	elevation (m MSL) of top surface of model layer 2 over rawin site \tilde{x}_m at times t of rawin soundings
$\theta_m(z,t)$	potential temperature ($^{\circ}\text{K}$) at elevation z (m MSL) at hour t over rawin station m .	P1		$\delta z_2(\tilde{x}_m,t)$	expected range of values, centered at at which actual mixture layer top lies over rawin site \tilde{x}_m at times t of rawin soundings.
$z_t(\tilde{x})$	mean terrain elevation (m MSL) in grid cell centered at \tilde{x} .	P7		$z_3(\tilde{x}_m,t)$	elevation (m MSL) of top surface of model Layer 3 over rawin station m at times t of rawin soundings.
$q_n(t)$	mixing ratio (dimensionless) at surface weather station n at time t .	P3		$q_c(\tilde{x}_m,t)$	estimated water mixing ratio entering cumulus clouds over rawin station m at time t (available at 30 minute intervals).
$\theta_n(t)$	potential temperature ($^{\circ}\text{K}$) at surface weather station n at time t .	P3			
$p_m(z,t)$	pressure (mb) at elevation z (m MSL) at time t over rawin station m .	P1		$q_{\infty}(\tilde{x}_m,t)$	estimated water mixing ratio above Layer 3 at rawin station m at time t (available at 30 minute intervals).
$\sigma_c(\tilde{x},t)$	fraction of sky covered by cumulus clouds in grid cell centered at \tilde{x} at time t .	RAW		$M_3(\tilde{x}_m,t)$	vertically integrated water mixing ratio in Layer 3 over rawin site m (units=m, see Eq. 8-20) at times t of rawin soundings.

Table 8-1. (continued)

Input Variable	Description	Source	Stage	Output Variable	Description
$z_{TCU}(\tilde{x}, t)$	elevation (m MSL) of highest cumulus cloud tops in grid cell centered at \tilde{x} at time t.	RAW	ZQ, (Cont.)	$\langle q(\tilde{x}_m, t) \rangle_3$	average mixing ratio in Layer 3 over rawin site m at time t (available at 30 min. intervals).
				$z_{LCL}(\tilde{x}_n, t)$	elevation (m MSL) of the lifting condensation level over surface station n at time t (required only at the hours t of rawin observations)
$v_H(\tilde{x}, z, t)$	horizontal wind vector (m/sec) at site \tilde{x} , elevation z (m MSL) at time t.	Stage WV	PATH	$I_{wm}(t)$	path integral of w leading to rawin site m at time t (see 8-109) units = m.
$w(\tilde{x}, z, t)$	vertical air speed (m/sec) at site \tilde{x} , elevation z (m MSL) at time t.	Stage WV		$I_{om}(t)$	path integral of cumulus cloud cover fraction leading to rawin site m at hour t (see 8-110) units = sec.
$Q(\tilde{x}, t)$	surface kinematic \sim_1 heat flux ($m^{\circ}K \text{ sec}^{-1}$) in cell at \tilde{x} at time t.	P4		$I_{Qm}(t)$	path integral of kinematic surface heat flux leading to site \tilde{x}_m at time t (see 8-111) units = $m^{\circ}K$.
$\sigma_c(\tilde{x}, t)$	fraction of sky covered by cumulus clouds in grid cell centered at \tilde{x} at time t.	RAW			
$z_2(\tilde{x}_m, t)$	elevation of top surface of Layer 2 at rawin station m.	Stage ZQ			

Table 8-1. (continued)

Input Variable	Description	Source	Stage	Output Variable	Description
$\langle q(\tilde{x}_m, t) \rangle_3$	average mixing ratio in Layer 3 over rawin station m at time t (available at 30 min. intervals).	Stage ZQ	WEWC	$G(\tilde{x}_m, t)$	entrainment velocity scale factor (units $^{\circ}\text{K}^{-1}$) (see 8-39) at rawin site \tilde{x}_m at <u>hourly</u> intervals t.
$q_c(\tilde{x}_m, t)$	mixing ratio entering cumulus clouds over site \tilde{x}_m at time t (available at 30 min. intervals).	Stage ZQ		$\bar{w}_c(\tilde{x}_m, t)$	cumulus updraft velocity scale (m/sec) at rawin site \tilde{x}_m at <u>hourly</u> intervals t.
$Q(\tilde{x}, t)$	surface kinematic heat flux ($\text{m } ^{\circ}\text{K sec}^{-1}$) in grid cell at \tilde{x} at time t (at hourly intervals).	P4			
$\sigma_c(\tilde{x}, t)$	fractional coverage of cumulus clouds	RAW			
$I_{\text{om}}(t)$	cumulus cover path integral	Stage PATH			
$z_2(\tilde{x}_m, t)$	elevation of top surface of Layer 2 at rawin site \tilde{x}_m at times t of rawind soundings.	Stage ZQ			
$z_{\text{LCL}}(\tilde{x}_n, t)$	lifting condensation level at surface weather station n at times t of rawin soundings.	Stage ZQ			
$I_{\text{wm}}(t)$	w path integral leading to rawind site \tilde{x}_m at time t of rawin sounding	Stage PATH			
$I_{\text{Qm}}(t)$	surface heat flux path integral leading to site \tilde{x}_m at hour t of rawin sounding.	Stage PATH			

Table 8-1. (continued)

Input Variable	Description	Source	Stage	Output Variable	Description
$M_3(\tilde{x}_m, t)$	vertically integrated water mixing ratio in Layer 3 over rawin site \tilde{x}_m (at sounding hours t only).	Stage ZQ	WEWC (Cont.)		
$w(\tilde{x}, z, t)$	vertical air speed (m/sec) at (\tilde{x}, z, t)	Stage WV			
$q_\infty(\tilde{x}_m, t)$	water mixing ratio above Layer 3 at rawin site \tilde{x}_m (at $t = 30$ min intervals).	Stage ZQ			
$z_3(\tilde{x}_m, t)$	elevation of top of Layer 3 at rawin station m at sounding times t .	Stage ZQ			
$\delta z_2(\tilde{x}_m, t)$	expected range of z_2 at rawin site \tilde{x}_m at observation hour t .	Stage ZQ			
$G(\tilde{x}_m, t)$	hourly values of the entrainment velocity scale factor at rawin site \tilde{x}_m .	Stage WEWC	W2	$w_e(\tilde{x}, t) = f\theta/\Delta\theta(\tilde{x}, t)$	entrainment velocity at hour t at grid cell centered at \tilde{x} (m/sec)
$\bar{w}_c(\tilde{x}_m, t)$	hourly values of the cumulus updraft speed (m/sec) at site \tilde{x}_m .	Stage WEWC		$\bar{w}_c(\tilde{x}, t)$	cumulus updraft speed (m/sec) at hour t in grid cell centered at \tilde{x} .
$z_{TCU}(\tilde{x}, t)$	cumulus top elevation at hour t in grid cell centered at \tilde{x} .	RAW		$w_2(\tilde{x}, t)$	vertical air speed (m/sec) on surface H_2 at grid cell centered at \tilde{x} at hour t .
$z_2(\tilde{x}_m, t)$	estimated top of Layer 2 at rawin site \tilde{x}_m at sounding time t .	Stage ZQ		$z_2(\tilde{x}, t)$	elevation (m MSL) of surface H_2 (top of Layer 2) in grid cell centered at \tilde{x} at hour t .

Table 8-1. (continued)

Input Variable	Description	Source	Stage	Output Variable	Description
$z_t(\underline{x})$	mean terrain elevation (m MSL) in grid cell centered at \underline{x} .	P7	W2 (Cont.)	$z_3(\underline{x},t)$	elevation (m MSL) of surface H_3 (top of Layer 3) in grid cell centered at \underline{x} at hour t .
$\underline{v}_H(\underline{x},z,t)$	horizontal wind vector (m/sec) at site \underline{x} , elevation z , time t .	Stage WV		$\dot{H}_3(\underline{x},t)$	volume flux (m/sec) through top surface Layer 3 in grid cell at \underline{x} at hour t .
$w(\underline{x},z,t)$	vertical air speed (m/sec) at site \underline{x} , elevation z (MSL) at time t .	Stage WV		$\dot{z}_2(\underline{x},t)$	local time derivative of elevation z_2 (m/sec) at grid cell centered at \underline{x} at hour t .
$p_m(z,t)$	pressure (mb) at elevation z (m MSL) at hour t over rawin station m .	P1		$h_3(\underline{x},t)$	thickness (m) of Layer 3 at hour t in grid cell centered at \underline{x} .
$h_1(\underline{x},t)$	depth (m) of Layer 1 in grid cell centered at \underline{x} at time t .	P7		$h_2(\underline{x},t)$	thickness (m) of Layer 2 at hour t in grid cell centered at \underline{x} .
				$p_3(\underline{x},t)$	pressure (mb) at elevation of top of Layer 3 at hour t in grid cell centered at \underline{x} .
				$p_2(\underline{x},t)$	pressure (mb) at elevation of top of Layer 2 at hour t in grid cell centered at \underline{x} .
				$\Psi'(\underline{x},t)$	interim estimate of the cumulus flux partition function (see Eq. 5-44 of Part 1) at hour t in grid cell at \underline{x} (non-dimensional)

Table 8-1. (continued)

Input Variable	Description	Source	Stage	Output Variable	Description
$z_T(\underline{x})$	terrain elevation (m MSL) in grid cell centered at \underline{x} .	P7	WV	$\underline{v}_H(\underline{x}, z, t)$	horizontal wind vector (m/sec) [$\underline{v}_H = (u, v)$] at (arbitrary) elevation z (m MSL), time t at site \underline{x} .
$\hat{u}_m(z, t)$	observed east-west wind component (m/sec) at elevation z (m MSL) at observation hour t at rawind station m .	P1		$w(\underline{x}, z, t)$	vertical air speed (m/sec) at (arbitrary) elevation z (m MSL) at time t at site \underline{x} .
$\hat{v}_m(z, t)$	same as \hat{u}_m except north-south wind component	P1		$\bar{w}_{D1}^I(\underline{x}, t)$	divergence induced vertical air speed (m/sec) on top surface of Layer 1 (Defined for daytime hours only)
$\hat{u}_n(t)$	observed east-west wind component (m/sec) at observation hour t at surface weather station n .	P3		$\langle \delta(\underline{x}, t) \rangle_3$	average horizontal wind divergence (sec ⁻¹) in Layer 3 in grid cell centered at (\underline{x}) at hour t .
$\hat{v}_n(t)$	same as $\hat{u}_n(t)$ except north-south wind component.	P3			same as $\langle \delta \rangle_3$ except applies to Layer 2.
$\Delta p_1(t)$	surface inversion indicator (see 7-98).	P7			Same as $\langle \delta \rangle_3$ except applies to Layer 1 (values of this quantity are computed only for daytime hour)
$p_m(z, t)$	elevation (m MSL) at pressure level p (mb) at rawin station m at hour t .	P1		$\langle \delta(\underline{x}, t) \rangle_2$	same as $\langle \delta \rangle_3$ except applies to Layer 2.
$p_3(\underline{x}, t)$	elevation in pressure coordinates (mb) of top surface of Layer 3 in grid cell at \underline{x} at time t .	Stage W2		$\langle \delta(\underline{x}, t) \rangle_1$	same as $\langle \delta \rangle_3$ except applies to Layer 1 (values of this quantity are computed only for daytime hour)
$p_2(\underline{x}, t)$	same as p_3 except elevation of top of Layer 2.	Stage W2			

Table 8-1 (Concluded)

Input Variable	Description	Source	Stage	Output Variable	Description
$p_1(\underline{x}, t)$	same as p_3 except top of Layer 1.	P7			
$p_{vs}(\underline{x}, t)$	same as p_3 except top of radiation inversion	P7			
$z_{vs}(\underline{x}, t)$	elevation (m MSL) of virtual surface in cell at (\underline{x}) at hour t . Note: $z_{vs} = z_T$ when $\Delta p_1 = 0$.	P7			
$\eta_{vs}(\underline{x}, t)$	growth rate (m/sec) of the radiation inversion layer depth.	P7			

Appendix to Section 8

Some of the equations in this Processor, such as (8-166), contain terms of the form

$$\underline{v} \cdot \underline{\nabla}_H p \quad (8-A1)$$

that must be evaluated at each grid point (I,J) of the regional model domain. In (8-A1) both \underline{v} and p are variables represented in discrete form at each grid point of the model region. To fourth-order accuracy we can represent (8-A1) at grid point (I,J) by

$$(\underline{v} \cdot \underline{\nabla}_H p)_{I,J} = u_{I,J} \Delta_x(p_{I,J}) + v_{I,J} \Delta_y(p_{I,J}) \quad (8-A2)$$

where

$$\Delta_x(p_{I,J}) = \frac{2}{3} (p_{I+1,J} - p_{I-1,J}) - \frac{1}{12} (p_{I+2,J} - p_{I-2,J})$$

and

$$\Delta_y(p_{I,J}) = \frac{2}{3} (p_{I,J+1} - p_{I,J-1}) - \frac{1}{12} (p_{I,J+2} - p_{I,J-2}).$$

Here $p_{I,J}$ is the value of p at point (I,J), i.e., column I, row J, with rows parallel to the x axis and columns parallel to y .

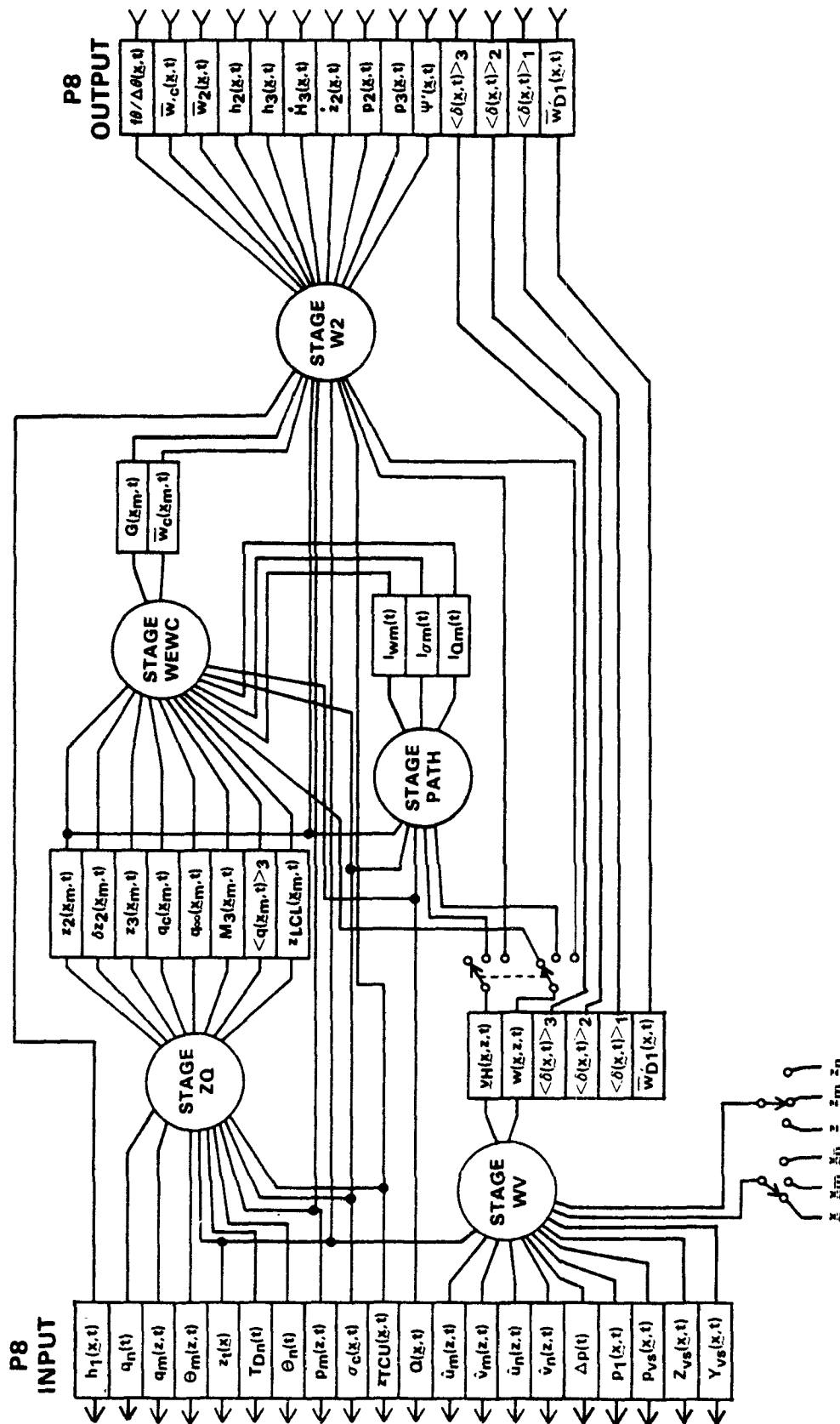


Figure 8-6. Schematic illustration of Processor P8 and its input and output interfaces with the processor network.

SECTION 8
PROCESSOR P9

DEVELOPMENT

This processor prepares the information necessary to correct the chemical rate constants for variations in atmospheric density, temperature, cloud cover, and solar zenith angle. Often the top of the regional model will lie near the middle of the troposphere and therefore significant variations in air density and temperature can exist between each of the model's layers. All rate constants for the intermolecular reactions are affected by density and many are strongly sensitive to temperature as well. The photolytic rate constants are affected by the variations in solar radiation induced by cloud scattering and absorption, and by the variations in radiation that accompany changes in the solar zenith angle. We treat the density and temperature correction terms in Stage DEN, and the cloud and zenith corrections in Stage ZEN.

Stage DEN

The easiest way to handle the effects of atmospheric density variation on the pollutant concentrations is to work with the species mass continuity equation in its mixing ratio form. Thus let

$$\gamma(x,t) \equiv c(x,t)/\rho(x,t) \quad (9-1)$$

be the mixing ratio of a given species, where c is the species concentration, say, moles m^{-3} , and ρ is the local air density in the same units. The mixing ratio γ is dimensionless and is often expressed in terms of parts per million (ppm). Making use of (9-1) in the species mass continuity equation (Eq. 2-1 of Part 1) we have

$$\frac{\partial}{\partial t} (\gamma \rho) + \nabla_H \cdot (\gamma \rho \mathbf{v}) + \frac{\partial}{\partial z} (\gamma p w) = S + R - W. \quad (9-2)$$

The mass continuity equation for the atmosphere has a similar form, namely

$$\frac{\partial}{\partial t} \rho + \nabla_H \cdot (\rho \mathbf{v}) + \frac{\partial}{\partial z} (\rho w) = 0. \quad (9-3)$$

Multiplying (9-3) by γ and subtracting the result from (9-2) we obtain

$$\frac{\partial \gamma}{\partial t} + \nabla_H \cdot (\gamma \mathbf{v}) + \frac{\partial}{\partial z} (\gamma w) = \frac{S}{\rho} + \frac{R}{\rho} - \frac{W}{\rho}. \quad (9-4)$$

Thus, the equation governing the mixing ratio γ has the same form as the equation governing the concentration c (i.e., Eq. 2-1 of Part 1) except that the inhomogeneous terms S , R and W are divided by the local air density. Notice that Eq. 9-4 indicates that material is well-mixed (i.e., $\partial \gamma / \partial t = 0$) vertically when the mixing ratio is constant in z . However, the concentration form of the continuity equation yields the contradictory result that the well-mixed state is achieved only when the concentration c is independent of height. The latter is in error because it fails to take into account the effects of gravity on the mass distribution of material in the atmosphere. The mixing ratio form of the equation handles this effect implicitly through the link with the air density ρ . In short, Eq. (9-4) is the proper form of the continuity equation for use in applications to atmospheric layers deep enough ($\gtrsim 10^3 m$) that air density variations are important.

Normalization of the emissions function S by the air density is performed by Processor P10. Here we are concerned with the normalization of the chemical reaction term R , which has the general form

$$R = kcd + k_1c \quad (9-5)$$

where d is the concentration of a species with which the given pollutant reacts, k is the rate constant (units of $\text{mole}^{-1}\text{m}^3\text{sec}^{-1}$) of this second-order reaction, and k_1 is the rate constant for a first-order reaction that consumes species c . We can write (9-5) in the form

$$\frac{R}{\rho} = (\rho k)\left(\frac{c}{\rho}\right)\left(\frac{d}{\rho}\right) + k_1\left(\frac{c}{\rho}\right) = k^*\gamma\gamma_d + k_1\gamma \quad (9-6)$$

where

$$\gamma_d = d/\rho$$

is the mixing ratio of species d . Substituting (9-6) into (9-4) we have the equation governing γ . In it the second-order rate constants have the form

$$k^* = k\rho. \quad (9-7)$$

but the first-order rate constants are unchanged. In order for the model equations to predict mixing ratio, we must supply the kinetics algorithm with effective air densities for each layer so that the rate constants k can be modified in the manner of (9-7). For this purpose, and also for normalizing the emission strengths S in Processor P10, we compute in this stage average air densities for each of the model's four layers. Concurrently, we compute average temperatures for each cell and layer for use within the model itself to make temperature corrections on the rate constants. The rationale for supplying temperature data to the model rather than temperature corrected rate constants is to avoid any procedure that would "hard wire" a particular chemical kinetics scheme into the model or the input processor network.

Let $T_{vm}(z,t)$ and $\rho_n(z,t)$ be the virtual temperature and density, respectively, at elevation z (MSL) at hour t over rawin station m , and let \hat{z}_m be the elevation (m MSL) of that station. Now define

$$\langle \rho \rangle_{0m} = \frac{b}{h_{0m}} \int_{\hat{z}_m}^{\hat{z}_m + h_{0m}} \rho_m(z) dz \quad (9-8)$$

$$\langle \rho \rangle_{1m} = \frac{b}{h_{1m}} \int_{\hat{z}_m + h_{0m}}^{\hat{z}_m + h_{0m} + h_{1m}} \rho_m(z) dz \quad (9-9)$$

$$\langle \rho \rangle_{2m} = \frac{b}{h_{2m}} \int_{\hat{z}_m + h_{0m} + h_{1m}}^{\hat{z}_m + h_{0m} + h_{1m} + h_{2m}} \rho_m(z) dz \quad (9-10)$$

$$\langle \rho \rangle_{3m} = \frac{b}{h_{3m}} \int_{\hat{z}_m + \dots + h_{2m}}^{\hat{z}_m + \dots + h_{3m}} \rho_m(z) dz \quad (9-11)$$

where

$$b = \frac{1000}{28.97}$$

is the factor necessary to change the units of density from (kg m^{-3}) , the units of $\rho_m(z)$ as supplied by P1, to (moles m^{-3}) , the units in which the chemical rate constants that we will modify are expressed. In (9-8) - (9-11) h_{jm} is the thickness of model layer j in the grid cell that contains rawin station m .

The integrals on the right-hand side of Eqs. (9-8) - (9-11) can be evaluated by subdividing the integration interval into 50m subintervals that coincide with the intervals at which $T_{vm}(z)$ and $\rho_m(z)$ are available (from P1). Similarly, we define

$$\langle T \rangle_{1m} = \frac{1}{h_{1m}} \int_{\hat{z}_m + h_{om}}^{\hat{z}_m + h_{om} + h_{1m}} T_{vm}(z) dz \quad (9-12)$$

$$\vdots \quad \vdots \quad (9-13)$$

$$\langle T \rangle_{3m} = \frac{1}{h_{3m}} \int_{\hat{z}_m + h_{om} + h_{1m} + h_{2m}}^{\hat{z}_m + \dots + h_{3m}} T_{vm}(z) dz \quad (9-14)$$

The temperature and density profiles T_{vm} and ρ_m are available from P1 each hour but they give values only at the measurement station sites x_m . Therefore, the layer averaged density and temperature values derived from (9-8) - (9-14) must be interpolated to each grid cell location. Use the r^{-1} weighting scheme as follows:

$$\langle \rho(I, J, t_k) \rangle_n = \frac{10^{-6} \sum_{m=1}^M r_m^{-1} \langle \rho(t_k) \rangle_{nm}}{\sum_{m=1}^M r_m^{-1}} \quad n = 0, 1, 2, 3 \quad (9-15)$$

$$\langle T(I, J, t_k) \rangle_n = \frac{\sum_{m=1}^M r_m^{-1} \langle T(t_k) \rangle_{nm}}{\sum_{m=1}^M r_m^{-1}} \quad n = 1, 2, 3 \quad (9-16)$$

where

$$r_m = [(I\Delta x - x_m)^2 + (J\Delta y - y_m)^2]^{\frac{1}{2}}. \quad (9-17)$$

The factor 10^{-6} in the density equation (9-15) is necessary when the mixing ratio γ is expressed as parts per million (ppm). The factors $\langle \rho \rangle_n$ generated by this stage will pass through the B-matrix compiler (BMC) unchanged and will be used in the model to modify the second-order rate constants k in the manner described above in Eq. (9-7), namely

$$k_n^* = k \langle \rho \rangle_n \quad (9-18)$$

where k_n^* is the modified rate constant in Layer n . (Keep in mind that the first-order constants are not modified by the density.) As we noted above, we assume that the second-order rate constants k are expressed in units of $(\text{moles m}^{-3})^{-1} \text{sec}^{-1}$. (Consistency of the concentration units throughout the model should be confirmed by comparing the parameters generated in this processor, the source strength functions provided by Processor P10, the initial concentration fields produced by Processor P2, and the rate constants contained in the chemical kinetics subroutine CHEM that operates in unison with the model.)

The layer averaged temperature values $\langle T \rangle_n$ given by (9-16) above also pass unmodified into the model at operation time. These data are made available there for temperature corrections to those rate constants that require it.

The input-output summary of stage DEN is given in Table 9-1, and the processor is illustrated schematically in Figure 9-1.

Stage ZEN

All of the photolytic rate constants require adjustments for the local solar zenith angle ϕ_s and cloud cover. We assume following Jones, et al (1981) that these "constants" can be expressed in the form

$$k_{\alpha}^* = k_{\alpha}(\phi_s) \Xi(cc) \quad (9-19)$$

where $k_{\alpha}(\phi_s)$ is the "clear sky" photolytic rate constant for reaction α and $\Xi(cc)$ is an empirical function of the cloud cover $cc = cc(h)$, which is the fraction ($0 \leq cc \leq 1$) of the sky covered by clouds of height h . We assume further that the clear sky constants k_{α} are contained in the chemical kinetics subroutine of the regional model code in the functional forms $k_{\alpha}(\phi_s)$ and that the solar zenith angle ϕ_s must be supplied for each grid cell and hour to evaluate them (note that ϕ_s is virtually independent of altitude). Thus, Processor, P9, particularly Stage ZEN, must supply the following fields to the model by way of the model input file MIF:

$$\phi_s(I,J,t_m) = \text{solar zenith angle in cell (I,J) at hour } t_m \text{ (units of degrees of arc);} \quad (9-20)$$

and

$$\Xi(I,J,t_m) = \text{cloud cover correction factor for photolytic rate constants in cell (I,J) at hour } t_m \text{ (dimensionless).} \quad (9-21)$$

The zenith angle ϕ_s can be obtained from standard astronomical formulas given the latitude ($J\Delta\phi$) and longitude ($I\Delta\lambda$) of cell (I,J), and the date and hour t_m of the period of interest. The factor Ξ is obtained from the formulas given in Jones, et al (1981) using the observed cloud cover $cc(h)$ in cell (I,J) at hour t_m . We will not elaborate on the computation of ϕ_s and Ξ here.

In summary, the solar zenith angle ϕ_s is used in each grid cell and hour to determine the clear sky rate constant k_α for each photolytic reaction α . These values are multiplied in turn by the cloud cover factor Ξ for that cell and hour to arrive at the corrected rate constant

$$k_\alpha^*(I, J, t_m) = k_\alpha(\phi_s(I, J, t_m))\Xi(I, J, t_m). \quad (9-22)$$

The photolytic constants are not modified by the density correction terms $\langle \rho \rangle_n$ generated in Stage DEN.

The inputs and outputs of Stage ZEN are summarized in Table 9-1.

Table 9-1. Summary of the input and output variables of each stage of Processor P9 and their sources.

Input Variable	Description	Source	Stage	Output Variable	Description
$T_{vm}(z, t_k)$	virtual temperature ($^{\circ}\text{C}$) at elevation z (m MSL) at hour t_k over rawin station $m(=1, \dots, M)$	P1	DEN	$\langle \rho(I, J, t_k) \rangle_0$	density correction for rate constants in Layer 0, cell (I, J) hour t_k (units: 10^{-6} moles m^{-3})
				$\langle \rho(I, J, t_k) \rangle_1$	same as $\langle \rho \rangle_0$ except applies to Layer 1
$\rho_m(z, t_k)$	same as T_{vm} except density (kgm^{-3})	P1		$\langle \rho(I, J, t_k) \rangle_2$	same as $\langle \rho \rangle_0$ except applies to Layer 2
\hat{z}_m	elevation (m MSL) of rawin station m	RAW		$\langle \rho(I, J, t_k) \rangle_3$	same as $\langle \rho \rangle_0$ except applies to Layer 3
$h_0(I, J, t_k)$	thickness (m) of Layer 0 at time t_k in grid cell (I, J)	P7		$\langle T(I, J, t_k) \rangle_1$	average temperature ($^{\circ}\text{C}$) in Layer 1, cell (I, J), hour t_k (for temperature correction of rate constants in model)
$h_1(I, J, t_k)$	same as h_0 except Layer 1	P7		$\langle T(I, J, t_k) \rangle_2$	same as $\langle T \rangle_1$ except Layer 2
$h_2(I, J, t_k)$	same as h_0 except Layer 2	P8		$\langle T(I, J, t_k) \rangle_3$	same as $\langle T \rangle_1$ except Layer 3
$h_3(I, J, t_k)$	same as h_0 except Layer 3	P8			
$cc(x_n, h, t_m)$	fractional sky coverage of clouds of height h (low, middle, and high) at surface weather station n at hour t_m	RAW	ZEN	$\phi_s(I, J, t_m)$	solar zenith angle (degrees) at grid cell (I, J) at hour t_m (used to obtain photolytic rate constant values).
				$\Xi(I, J, t_m)$	cloud cover correction factor (dimensionless) for photolytic rate constants in cell (I, J) at hour t_m

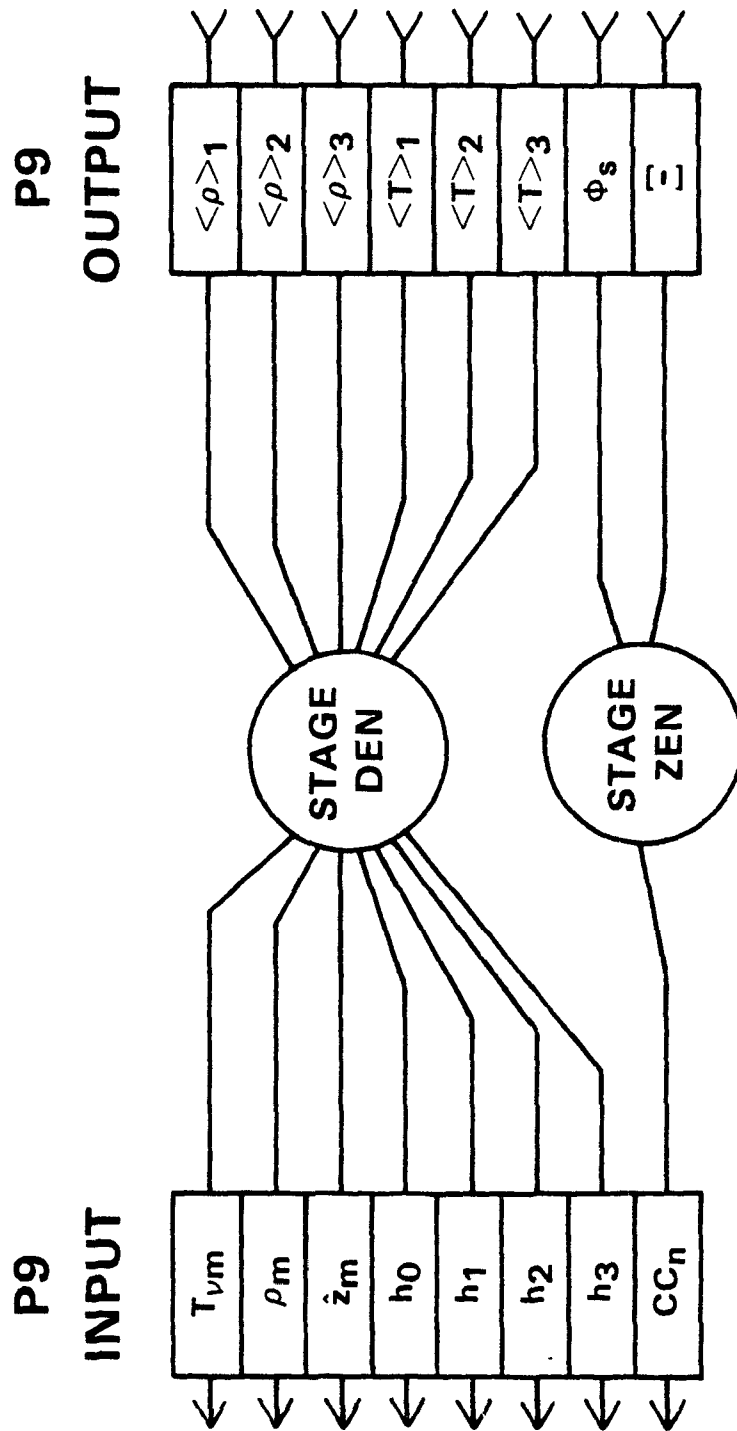


Figure 9-1. Schematic illustration of Processor P9 and its interfaces with the porcessor network.

SECTION 9

PROCESSOR P10

DEVELOPMENT

Processor P10 transforms the emissions inventory into the source strength functions \tilde{S} , S_1 and S_2 . It is assumed that the emissions data have already been structured to provide the following information: (1) total emission rate (moles hr^{-1}) of each primary pollutant from all mobile and minor stationary sources in each of the model's grid cells, at each hour of the simulation period; (2) emission rate (moles hr^{-1}) of each primary pollutant each hour for all major point sources; and (3) the physical parameters necessary to determine in which grid cell each major point source lies and what its effective source height will be under given meteorological conditions. Here "major" point source refers to any point source whose discharge rate of a given pollutant exceeds some prespecified threshold. This processor also computes the plume volume fraction ζ which is used in the Layer 0 equations to parameterize subgrid scale chemistry effects.

The three basic tasks involved in computing the source strengths are estimating the effective heights of the major point sources; partitioning the point and area source emissions among the three layers 0, 1, and 2; and converting the results to units of ppm. The first of these operations is performed in Stage DELH -- the last two are done in Stage S. We should add here that the units conversion is necessary because concentration must be

expressed in ppm in the governing equations in order to account for the variation of atmospheric density with elevation (see the discussion presented with the description of Processor P9). The calculation of the parameter ξ in this processor is performed in Stage ZTA.

Stage DELH

Suppose that there are a total of K major point sources in the entire modeling region, and let the subscript "k" designate any one of them. We compute the plume rise $\Delta h_k(t_m)$ of the k-th source at hour t_m as follows.

Let $[I(k), J(k)]$ be the grid cell (column I, row J) in which the k-th source lies. Then

$$\Delta h_k(t_m) = \begin{cases} 0, & \text{if } L[I(k), J(k), t_m] \leq 0; \\ 3 \left(\frac{F_k}{u_s} \right)^{1/3}, & \text{otherwise.} \end{cases} \quad (10-1)$$

Here $L[I, J, t_m]$ is the Obukhov length (meters) in cell (I, J) at hour t_m , and

$$F_k = g \left[\frac{T_k - T_{ak}}{T_k + 273} \right] \left(\frac{1}{4} \right) D_k^2 w_k^2. \quad (10-2)$$

In this expression T_k is the exhaust temperature ($^{\circ}\text{C}$) of the stack, D_k is the stack diameter (m), w_k its exhaust velocity (m sec^{-1}), $g = 9.8 \text{ m sec}^{-2}$ is gravity, and

$$T_{ak} = \frac{\sum_{n=1}^N r_{nk}^{-2} T_{vn}(t_m)}{\sum_{n=1}^N r_{nk}^{-2}} \quad (10-3)$$

is the estimated surface air temperature ($^{\circ}\text{C}$) at the location of source k . In (10-3)

$$r_{nk}^2 = [(x_n - x_k)^2 + (y_n - y_k)^2],$$

(x_n, y_n) is the location of surface weather station n and T_{vn} is the virtual temperature ($^{\circ}\text{C}$) measured at that station at hour t_m .

In Eq. (10-1)

$$u = [(\langle u(I(k), J(k), t_m) \rangle_1)^2 + (\langle v(I(k), J(k), t_m) \rangle_1)^2]^{\frac{1}{2}} \quad (10-4)$$

where $\langle u \rangle_1$ and $\langle v \rangle_1$ are the Layer 1 averaged wind components (m sec^{-1}). Finally, the parameter s in (10-1) is approximated by

$$s = \frac{g^2}{c_p (T_{ak} + 273)} \quad (10-5)$$

where $c_p = 1003 \text{ m}^2 \text{ sec}^{-2} \text{ }^{\circ}\text{K}^{-1}$. This expression for the stability parameter s assumes an isothermal temperature lapse rate throughout the depth of the layer that the buoyant source emissions traverse.

The effective height of source k at hour t_m is now estimated to be

$$H_k(t_m) = z_{sk} + \Delta h_k(t_m) \quad (10-6)$$

where z_{sk} is the stack height (m) of source k .

By virtue of the assumption embodied in (10-1) for the case of negative L , expression (10-6) yields effective source heights equal to the actual stack

height z_s under neutral and unstable atmospheric conditions. Although plume rise does occur under these conditions, it is not particularly important in our regional scale grid model because under these conditions vertical mixing is so strong that pollutants are nearly uniformly spread through the mixed layer before horizontal transport has moved them out of the grid cell in which they were released.

For example, with a horizontal grid size of 18,000 m and a horizontal wind speed of 4 m sec^{-1} , material has a residence time of 4500 sec in a grid cell. The time scale of vertical mixing during unstable conditions is on the order of $2h/w_*$. Typical values of the mixed layer depth h and velocity scale w_* are 1500 and 1.5 m sec^{-1} , respectively. Hence, vertical mixing is completed within the time material is resident in the cell surrounding the source and consequently the actual height of the emission is not significant. (A much more important factor in this instance is the lack of complete horizontal mixing of point source plumes within a grid cell. Although the material is well mixed vertically, it may occupy a volume only 1 km wide whereas the grid model treats the emissions as though they fill the entire cell uniformly. This discrepancy is a subgrid scale phenomenon that the current regional model does not treat in Layers 1, 2 and 3. It is potentially a source of considerable error in the photochemical reaction simulations that should be considered in future modeling applications.)

In stable conditions, vertical mixing is very weak or nonexistent and in that case point source emissions must be placed in the proper layer.

Table 10-1 summarizes the input and output parameters associated with Stage DELH.

Stage S

Having estimated the effective discharge heights of the major point sources in Stage DELH, we can now compute the source strength functions \tilde{S} , S_1 and S_2 .

In this task we must take into account that the ground surface can extend into Layers 1 and 2 where hills penetrate the model layer surfaces H_0 and H_1 . Figure 10-1 illustrates the relationships between the layer interfaces and the terrain. (See Fig. 4-7 of Part 1. Recall that σ_{T1} is the fraction of surface H_1 that is penetrated by terrain, and that σ_{T0} is the corresponding fraction for surface H_0 .)

Let $E_k(t_m)$ be the emission rate (moles h^{-1}) of a given primary pollutant from the k -th major point source at hour t_m , and let $E(I,J,t_m)$ be the total emission rate (moles hour $^{-1}$) of that pollutant from all other sources in grid cell (I,J) at time t_m . The source strength functions for each primary pollutant have the following forms.

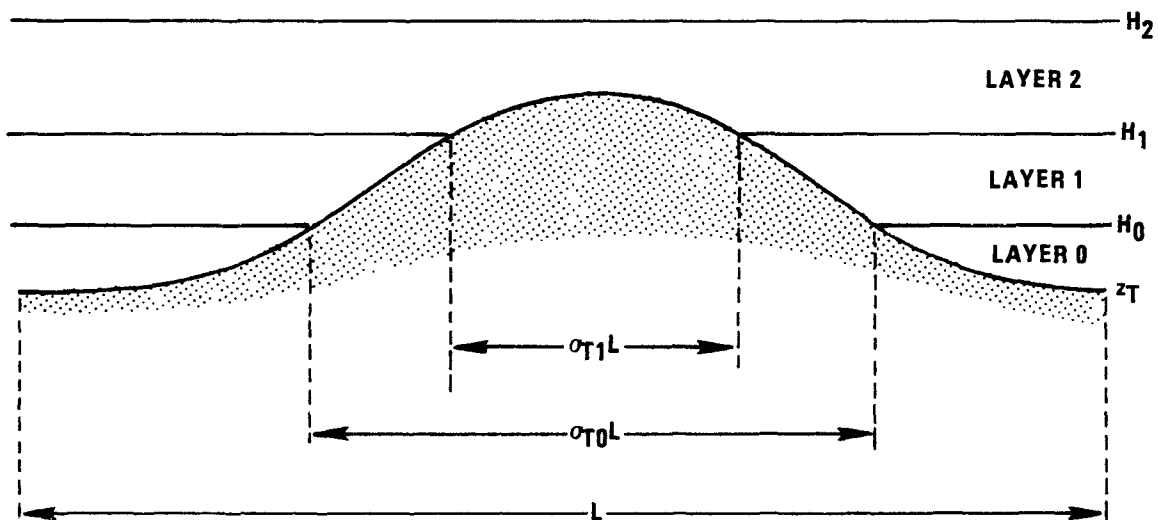


Figure 10-1. Illustration of the influence of terrain on model layers 0, 1 and 2 for given values of the penetration fractions σ_{T1} and σ_{T0} .

$$\langle S(I, J, t_m) \rangle_2 = [\sigma_{T1} E + \sum_{k=1}^K E_k U_{k2}] / (A_2 h_2) \quad (10-7)$$

$$\langle S(I, J, t_m) \rangle_1 = [(\sigma_{T0} - \sigma_{T1}) E + \sum_{k=1}^K E_k U_{k1}] / (A_1 h_1) \quad (10-8)$$

$$\tilde{S}(I, J, t_m) = [(1 - \sigma_{T0}) E + \sum_{k=1}^K E_k U_{k0}] / A_0 \quad (10-9)$$

where σ_{T0} , σ_{T1} , E , h_1 , and h_2 are functions of (I, J, t_m) ; and E_k and U_{kj} depends on t_m . The latter is defined by

$$U_{kj}(t_m) = \begin{cases} 1, & \text{if } (z_{j-1} - z_T) \leq H_k \leq (z_j - z_T) \\ 0, & \text{otherwise.} \end{cases} \quad (10-10)$$

where

$$z_{-1} = z_T(I(k), J(k)).$$

$$z_0 = h_0(I(k), J(k), t_m) + z_T(I(k), J(k))$$

$$z_1 = h_1(I(k), J(k), t_m) + z_0$$

$$z_2 = h_2(I(k), J(k), t_m) + z_1$$

and h_n is the thickness of Layer n . Also

$$A_2 = A \quad (10-11)$$

$$A_1 = (1 - \sigma_{T1})A \quad (10-12)$$

$$A_0 = (1 - \sigma_{T0})A \quad (10-13)$$

$$A = a^2(\cos\phi_J)(\delta\lambda)(\delta\phi) \quad (10-14)$$

$$a = 6,367,333 \text{ m} = \text{earth radius}$$

$$\delta\lambda = 1/4\left(\frac{2\pi}{360}\right) = \text{longitude grid interval}$$

$$\delta\phi = 1/6\left(\frac{2\pi}{360}\right) = \text{latitude grid interval}$$

and ϕ_J is the latitude of row J. In the evaluation of Eq. 10-9, the total number of major point sources lying in Layer 0 should be determined in each grid cell for later use in Stage ZTA. Let us denote this variable $N_{mJ}(I, J, t_m)$.

The source strength functions derived from (10-7) and (10-8) have units of $(\text{moles m}^{-3} \text{ hr}^{-1})$ and (10-9) gives \tilde{S} in units of $(\text{moles m}^{-2} \text{ hr}^{-1})$. These must be converted to units of (ppm sec^{-1}) and (ppm m sec^{-1}) , respectively. This is done as follows:

$$S_2(I, J, t_m) = \frac{\langle S(I, J, t_m) \rangle_2}{\langle \rho(I, J, t_m) \rangle_2} \cdot \frac{1}{3600} \quad (\text{ppm/sec}) \quad (10-15)$$

$$S_1(I, J, t_m) = \frac{\langle S(I, J, t_m) \rangle_1}{\langle \rho(I, J, t_m) \rangle_1} \cdot \frac{1}{3600} \quad (\text{ppm/sec}) \quad (10-16)$$

$$\tilde{S}(I, J, t_m) = \frac{\tilde{S}(I, J, t_m)}{\langle \rho(I, J, t_m) \rangle_0} \cdot \frac{1}{3600} \quad (\text{ppm m/sec}) \quad (10-17)$$

where $\langle \rho(I, J, t_m) \rangle_n$ is the average air density (units = $10^{-6} \text{ moles m}^{-3}$) in Layer n, time t_m in cell (I, J). Eqs. (10-15) - (10-17) should be evaluated

for each primary pollutant at each hour, level and grid cell; the results should be recorded in the MIF. The inputs and outputs of Stage S and their sources and destinations are summarized in Table 10-1.

Stage ZTA

The plume volume fraction parameter $\xi(I,J)$ is used in the Layer 0 equations to parameterize subgrid scale chemistry effects (see Chapters 5 and 8 of Part 1). Here we use a very simple approximation to estimate it.

Let $L(I,J)$ be the total length (m) of major line sources in cell (I,J) , let $N_{mp}(I,J)$ be the total number of minor point sources in cell (I,J) , and let $N_{mj}(I,J)$ be the total number of major point sources that lie in Layer 0 in cell (I,J) (from Stage S). Then we assume

$$\xi(I,J,t_m) = [(N_{mp} + N_{mj})(h_o)^2 + L h_o]/A \quad (10-18)$$

where h_o is the depth of Layer 0 in cell (I,J) at hour t_m and A is given by (10-14). (This is Eq. 8-7 in Part 1.)

Input and output information for this stage are summarized in Table 10-1, and a schematic illustration of the relationship among the stages and I/O is provided in Figure 10-2.

Table 10-1. Summary of input and output parameters for Processor P10 and their sources.

Input Variable	Description	Source	Stage	Output Variable	Description
$L(I,J,t_m)$	Obukhov length (m) in cell (I,J) at hour t_m	P4	DELH	$H_k(t_m)$	effective source height (m) of k-th major point source at hour t_m .
$T_{vn}(t_m)$	virtual temperature ($^{\circ}\text{C}$) at surface weather station n at time t_m .	P3			
$\langle u(I,J,t_m) \rangle_1$	Layer 1 averaged east-west wind (m/sec) in cell (I,J), hour t_m .	P11			
$\langle v(I,J,t_m) \rangle_1$	same as $\langle u \rangle_1$ except north-south component	P11			
$T_k(t_m)$	temperature ($^{\circ}\text{C}$) of exhaust gas of major point source k at hour t_m .	RAW			
D_k	diameter (m) of stack k.	RAW			
$w_k(t_m)$	exhaust velocity (m/sec) of stack k.	RAW			
$[I(k),J(k)]$	grid cell coordinates (row J, column I) of major point source k.	RAW			
z_{sk}	stack height (m) of source k	RAW			
$E_k(t_m;\alpha)$	emission rate (moles/hr) of species α at time t_m from major point source k	RAW	S	$\tilde{S}(I,J,t_m;\alpha)$	emission rate (ppm m/sec) of species α at hour t_m from <u>all</u> sources in Layer 0, cell (I,J).

Table 10-1. (Continued)

Input Variable	Description	Source	Stage	Output Variable	Description
$E(I,J,t_m;\alpha)$	emission rate (moles/hr) of species α from all except major point sources in grid cell (I,J,) at hour t_m	RAW	S (Cont.)	$S_1(I,J,t_m;\alpha)$	emission rate (ppm sec^{-1}) of species α at hour t_m from all sources in Layer 1, cell (I,J).
$\sigma_{T0}(I,J,t_m)$	fraction (non-dimensional) of model surface H_0 penetrated by terrain.	P7		$S_2(I,J,t_m;\alpha)$	emission rate (ppm sec^{-1}) of species α at hour t_m from all sources in Layer 2, cell (I,J).
$\sigma_{T1}(I,J,t_m)$	same as σ_{T0} except applies to surface H_1 .	P7		$N_{mj}(I,J,t_m)$	total number of major point sources in Layer 0, cell (I,J) at hour t_m .
$z_t(I,J)$	average terrain elevation (m,MSL) in cell (I,J).	P7			
$h_0(I,J,t_m)$	thickness (m) of Layer 0 at hour t_m in cell (I,J)	P7			
$h_1(I,J,t_m)$	thickness (m) of Layer 1 at time t_m , cell (I,J).	P7			
$h_2(I,J,t_m)$	same as h_1 except applies to Layer 2.	P8			
$H_k(t_m)$	effective source height of major point source k	DELH			
$\langle \rho(I,J,t_m) \rangle_2$	mean air density (moles m^{-3}) in Layer 2 at hour t_m , cell (I,J)	P9			
$\langle \rho(I,J,t_m) \rangle_1$	same as $\langle \rho \rangle_2$ except applies to Layer 1.	P9			

Table 10-1. (Completed)

Input Variable	Description	Source	Stage	Output Variable	Description
$\langle \rho(I,J,t_m) \rangle_0$	same as $\langle \rho \rangle_2$ except applies to Layer 0.	P9			
$L(I,J)$	total length (m) of major line sources in cell (I,J)	RAW	ZTA	$\xi(I,J,t_m)$	fraction ($0 \leq \xi \leq 1$) of Layer 0 in cell (I,J,) filled by line and point source plume at hour t_m .
$N_{mp}(I,J)$	number of minor point sources in cell (I,J).	RAW			
$N_{mj}(I,J,t_m)$	total number of major point sources in Layer 0, cell (I,J) at hour t_m	Stage S			
$h_o(I,J,t_m)$	depth (m) of Layer 0 in cell (I,J) at time t_m .	P7			

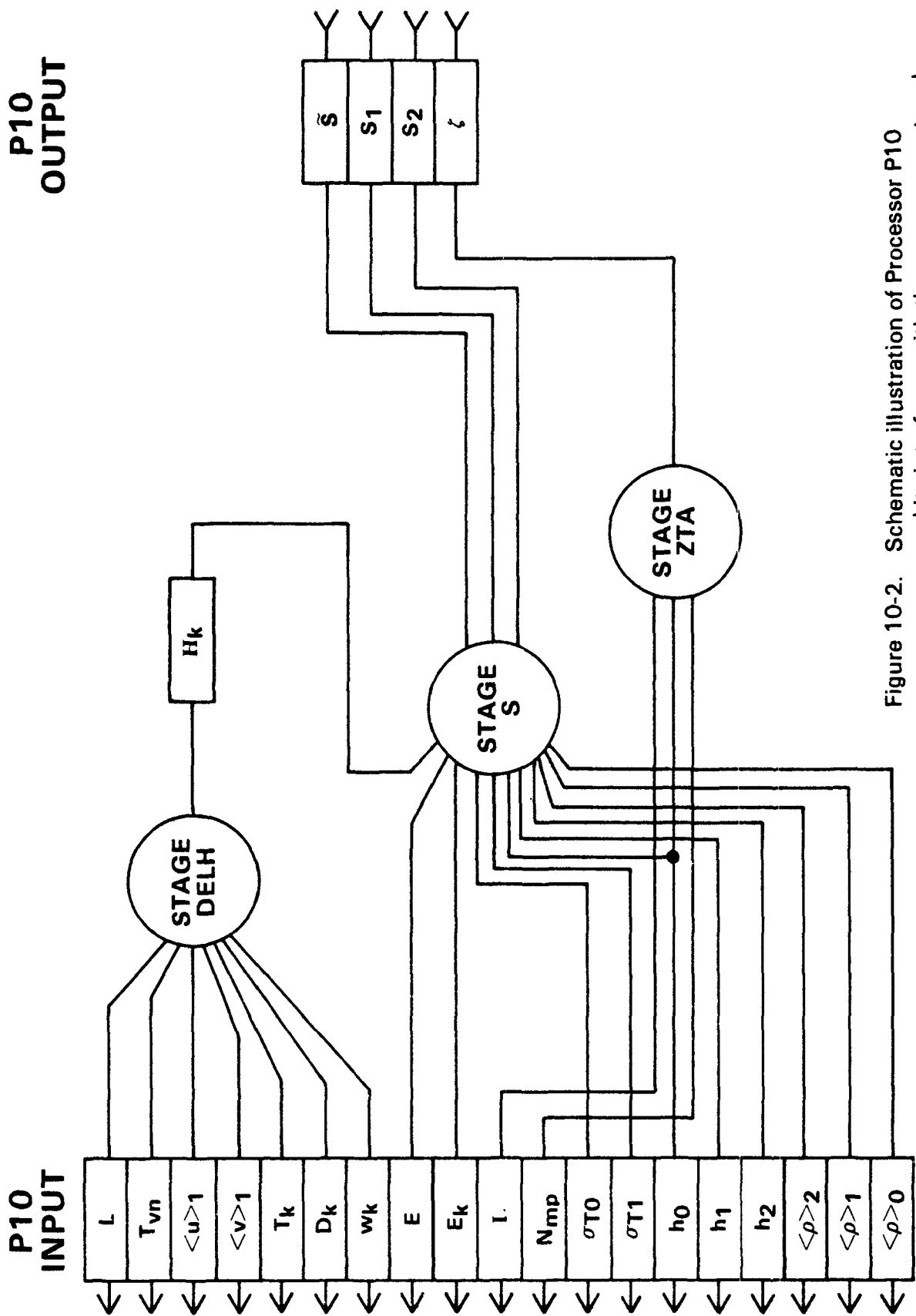


Figure 10-2. Schematic illustration of Processor P10 and its interfaces with the processor network.

SECTION 10

PROCESSOR P11

SUMMARY

Processor P11 generates families of vertically integrated horizontal winds for each of the model's layers. During daytime hours, namely times when the surface heat flux is positive, this processor produces wind fields for each of the model's three layers. However, at night when surface inversions exist, it provides winds for Layers 2 and 3 only. In this case the flow field in Layer 1 is generated in Processor P7, and the results are passed into Processor P11 for amalgamation with the wind fields derived here.

INTRODUCTION

Previous air pollution models have represented the wind fields either by continuous functions fit to discrete meteorological data, or by flow fields derived from mesoscale meteorological models. In this study we use neither of these approaches. Following the consideration presented in Chapters 6 and 7 of Part 1 of this report and in Lamb (1983a), we use wind observations and physical principles jointly to define a set or family of flow fields each member of which is a possible description of the flow that existed during the time that the observations were made. In the aforementioned papers it is argued that in the case of the atmosphere, observations and physical laws together are inadequate to specify flow patterns to within better than a set of functions. The ability of so-called objective analysis schemes to produce a single functional description of a given discrete set of data stems from the imposition of additional constraints that are not founded in physical laws and which therefore lack universal validity. In the more sophisticated of these schemes, use is made of empirical data such as spatial auto-correlation functions of the flow in the given region. Our position is that this type of empirical information is of great value, but its proper role is in estimating the probabilities of the members of the set of possible flows that specific observations and physical principles together define. These members of the wind field set that have finite probability constitute an ensemble of wind fields. For a given distribution of pollutant sources, there is a one-to-one correspondence, through the equation of species mass conservation and chemical reaction, between each member of the flow ensemble and each member of a concentration ensemble. In other words, having defined the ensemble of flow fields one can generate the ensemble of concentration fields associated with a

given emissions distribution by "driving" the air pollution model with each member of the flow ensemble and recording the outcomes. Ensemble statistics of the concentration can then be derived by performing averages of the desired quantity over the ensemble set, weighting each member of the set by the probability of the flow field from which that particular concentration distribution was derived.

This approach to pollution modeling is much more costly than the conventional method of formulating differential equations that yield the desired statistics directly. However, our approach has at least two advantages that in our judgement compensate several fold for the added cost. The first is that by deriving ensemble properties from a subset of the ensemble itself, we avoid major sources of error associated with the assumptions that one must invoke to formulate a set of differential equations that describe a particular statistical property. In the case of modeling the long range transport of photochemical pollutants, the nonlinear character and interaction of the processes involved are so complex that it is very unlikely that a single set of equations exist that would yield accurate estimates of even the simplest statistical properties under all conditions.

A second advantage of our approach is that it provides direct access to all of the statistical properties of concentration, such as the mean, variance, frequency distribution, spectrum, etc., whereas the conventional method gives only those limited properties, usually only the mean, for which equations have been hypothesized. Following we describe the basic mathematical steps implemented in this processor for deriving the ensemble of flow fields in each of the model's layers.

AVERAGE HORIZONTAL WINDS IN A LAYER BOUNDED BY TWO ARBITRARY PRESSURE SURFACES

In this section we develop a general method for deriving vertically averaged winds in a given layer. Later we will apply it to each of the model's three layers to obtain the necessary horizontal flow fields.

As in Part I we define the cell averaged value between two pressure surfaces p_α and p_β ($p_\alpha > p_\beta$, i.e., surface α has the lower elevation)

$$\langle \phi(x,y) \rangle_\beta \equiv \frac{1}{V_{\alpha\beta}} \int_A \int_{p_\alpha(x',y')}^{p_\beta(x',y')} \phi(x',y',p) dp dx' dy' \quad (11-1a)$$

where A denotes the rectangular domain $x - \frac{\Delta x}{2} \leq x' \leq x + \frac{\Delta x}{2}$, $y - \frac{\Delta y}{2} \leq y' \leq y + \frac{\Delta y}{2}$ of a model grid cell; and ϕ is an arbitrary scalar or vector function. The averaging volume $V_{\alpha\beta}$ is given by

$$V_{\alpha\beta}(x,y) \equiv \int_A \int_{p_\alpha(x',y')}^{p_\beta(x',y')} dp dx' dy' \quad (11-1b)$$

Note that since $p_\alpha > p_\beta$, both $V_{\alpha\beta}$ and the integrals in (11-1a) are negative (assuming $\phi > 0$).

Suppose that observations of \underline{u} are available at N arbitrary sites on surface p_α , i.e.,

$$\hat{v}_{\alpha n}(t) = v(x_n, y_n, p_\alpha(x_n, y_n, t), t) \quad (11-2)$$

$$n=1, 2, \dots, N.$$

where (x_n, y_n) denotes the location of observation n . (Throughout this section, we shall use the caret (^) to signify observed values of a parameter.) Suppose further that we have measurements of v and other meteorological parameters along vertical lines between surfaces p_α and p_β at a total of M locations, i.e., we have

$$\hat{v}_m(p, t) = v(x_m, y_m, p, t), \quad m=1, 2, \dots, M. \quad (11-3)$$

These surface observations and sounding sites are illustrated in Figure 11-1. In general the number N of surface stations must equal or exceed the number of soundings, i.e.,

$$N \geq M. \quad (11-4)$$

Later we would like the option of supplementing the rather sparse upper air data with estimates of the flow aloft extrapolated from the numerous surface measuring stations. Toward this end we define the function $g_\alpha(x, y, p, t)$ to be the ratio of the wind velocity at (x, y, p, t) to the value at (x, y, p_α, t) where α is any pressure level. Specifically, we have $g_\alpha = (g_{u\alpha}, g_{v\alpha})$ where

$$g_{u\alpha}(x, y, p, t) \equiv \frac{u(x, y, p, t)}{u(x, y, p_\alpha, t)} \quad (11-5a)$$

$$g_{v\alpha}(x, y, p, t) \equiv \frac{v(x, y, p, t)}{v(x, y, p_\alpha, t)}. \quad (11-5b)$$

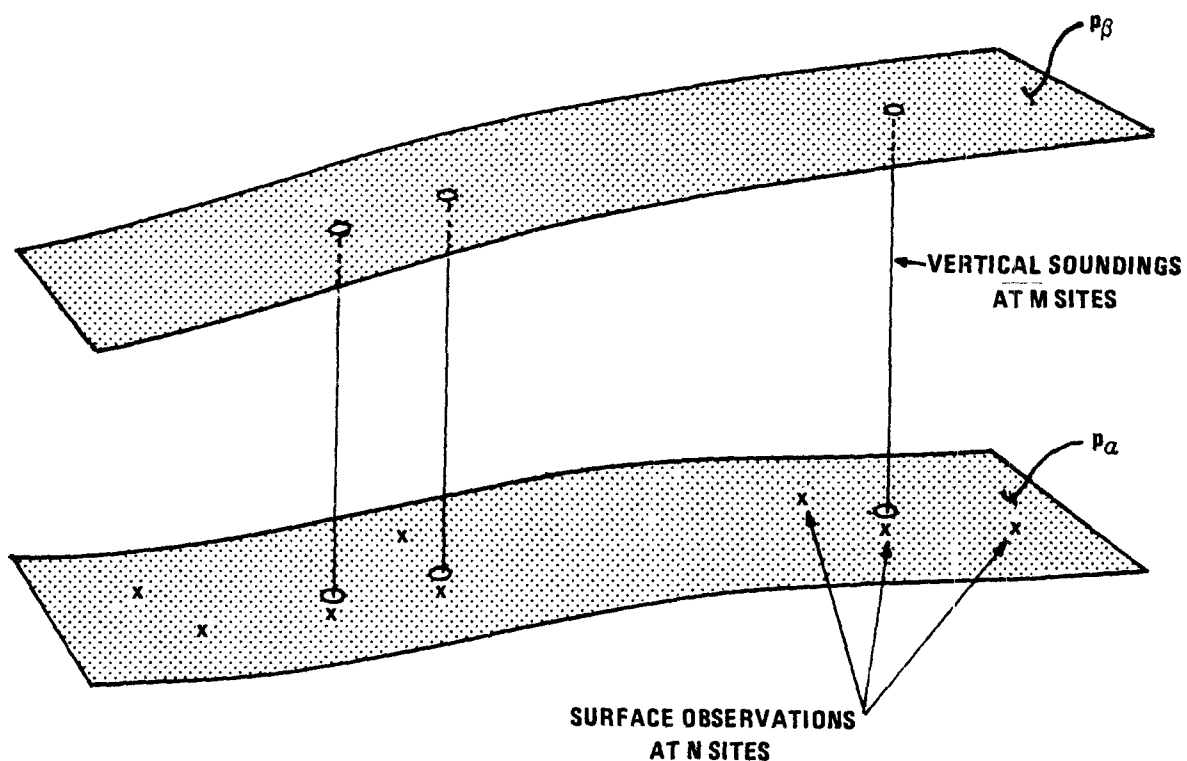


Figure 11-1 Surfaces Bounding Layer β in which M Soundings of the Horizontal Wind are Available. N Observations of the Wind on are also Available on the Bottom Surface p_α of Layer β .

Assuming that \underline{g} and \underline{v} vary by only small fractions of themselves as (x,y) ranges over the area A of any grid cell, we get from (11-1) and (11-5)

$$\langle \underline{v}(x,y,t) \rangle_\beta \cong \frac{\underline{v}_\alpha(x,y,t)}{p_\alpha - p_\beta} \int_{p_\alpha}^{p_\beta} \underline{g}_\alpha(x,y,p,t) dp \quad (11-6)$$

or

$$\langle \underline{v}(x,y,t) \rangle_\beta \cong \underline{v}_\alpha(x,y,t) \langle \underline{g}_\alpha(x,y,t) \rangle_\beta \quad (11-7)$$

where

$$\underline{v}_\alpha(x,y,t) \equiv \underline{v}(x,y,p_\alpha,t), \quad (11-8)$$

and $\langle \underline{g}_\alpha \rangle_\beta$ is defined as in (11-1).

At the M sites of the measurements of the vertical wind profile, we can evaluate $\langle \underline{g} \rangle_\beta$. We have

$$\langle \hat{g}_{u\alpha}(x_m, y_m, t) \rangle_\beta \equiv \langle \hat{g}_{u\alpha m}(t) \rangle_\beta = \frac{\langle \hat{u}(x_m, y_m, t) \rangle_\beta}{\hat{u}(x_m, y_m, p_\alpha, t)} \quad (11-9a)$$

$$\langle \hat{g}_{v\alpha m}(t) \rangle_\beta = \frac{\langle \hat{v}(x_m, y_m, t) \rangle_\beta}{\hat{v}(x_m, y_m, p_\alpha, t)} \quad (11-9b)$$

We will approximate the value of $\langle \underline{g}_\alpha \rangle_\beta$ at each point (x,y) in space by interpolation of the "observed" values $\langle \hat{g}_{\alpha m} \rangle_\beta$. That is, we assume

$$\langle \underline{g}_\alpha(x, y, t) \rangle_\beta \approx \frac{\sum_{m=1}^M \langle \hat{g}_{\alpha m}(t) \rangle_\beta W_m(\underline{r})}{\sum_{m=1}^M W_m(\underline{r})} \quad (11-10)$$

where $W_m(\underline{r})$ is a weighting function, e.g., \underline{r}^{-2} , to be selected later, and \underline{r} is the vector separation of (x,y) and the observation site (x_m, y_m) . Using (11-10) and the N ($\geq M$) observations \hat{v}_α of the wind on surface p_α , we can approximate the layer average winds at all those points (x_n, y_n) , $n \neq m$, where wind observations are available only on the surface p_α . In other words, we use the horizontally interpolated $\langle \underline{g} \rangle_\beta$ function to approximate layer averaged winds at points where only surface wind observations are available. Thus, we define

$$\langle \underline{v}(x_n, y_n, t) \rangle_{OB, \beta} = \langle \underline{g}_\alpha(x_n, y_n, t) \rangle_\beta \hat{v}_{\alpha n}(t) \quad (11-11)$$

where

$$\hat{v}_{\alpha n}(t) = \hat{v}(x_n, y_n, p_\alpha, t),$$

$\langle \underline{g}_\alpha \rangle_\beta$ is given by (11-10), and the vector product on the right side of (11-11) is defined by

$$\underline{a} \underline{b} \equiv (a_x b_y - a_y b_x)$$

where $\underline{a} = (a_x, a_y)$ and $\underline{b} = (b_x, b_y)$.

We will work later with the stream function and velocity potential which are functions of the vorticity and divergence, respectively, of the wind field. The vertical component of vorticity ζ is defined by

$$\zeta \equiv \underline{k} \cdot \nabla \times \underline{v} = \underline{k} \cdot \begin{vmatrix} \underline{i} & \underline{j} & \underline{k} \\ \frac{\partial}{\partial x} & \frac{\partial}{\partial y} & \frac{\partial}{\partial p} \\ u & v & w \end{vmatrix} = \frac{\partial v}{\partial x} - \frac{\partial u}{\partial y}; \quad (11-12)$$

and the horizontal divergence δ is

$$\delta \equiv \frac{\partial u}{\partial x} + \frac{\partial v}{\partial y}. \quad (11-13)$$

Since we are concerned with layer averaged winds $\langle \underline{v} \rangle$, we must determine how $\langle \zeta \rangle$ and $\langle \underline{v} \rangle$ are related and how $\langle \delta \rangle$ and $\langle \underline{v} \rangle$ are related. From (11-1) and (11-12)

$$\langle \zeta \rangle = \left\langle \frac{\partial v}{\partial x} \right\rangle - \left\langle \frac{\partial u}{\partial y} \right\rangle. \quad (11-14)$$

From Part I, page 21, we have

$$\left\langle \frac{\partial v}{\partial x} \right\rangle = \frac{\partial}{\partial x} \langle v \rangle + \frac{A}{V_{\alpha\beta}} \left(\overline{v \frac{\partial p_\alpha}{\partial x}} - \overline{v \frac{\partial p_\beta}{\partial x}} \right) + \langle v \rangle \frac{\partial}{\partial x} \ln (V_{\alpha\beta}) \quad (11-15a)$$

$$\left\langle \frac{\partial u}{\partial y} \right\rangle = \frac{\partial}{\partial y} \langle u \rangle + \frac{A}{V_{\alpha\beta}} \left(\overline{u \frac{\partial p_\alpha}{\partial y}} - \overline{u \frac{\partial p_\beta}{\partial y}} \right) + \langle u \rangle \frac{\partial}{\partial y} \ln (V_{\alpha\beta}) \quad (11-15b)$$

where A is the horizontal area on which $\langle \rangle$ is defined; $V_{\alpha\beta}$ is defined by (11-1b);

and

$$\overline{(\phi)}^\alpha \equiv \frac{1}{A} \iint_A \phi(x', y', p_\alpha(x', y')) dx' dy' \quad (11-16)$$

with a similar definition of the surface average $\overline{(\phi)}^\beta$.

Assumption: On p_α , $\underline{v}(x, y, p_\alpha) \approx \langle \underline{v}(x, y) \rangle$ and on p_β ,

$$\underline{v}(x, y, p_\beta) \approx \langle \underline{v}(x, y) \rangle. \quad (11-17)$$

In this case we have

$$\overline{\left(v \frac{\partial p_\alpha}{\partial x} \right)}^\alpha \approx \frac{\langle v \rangle}{A} \iint \frac{\partial p_\alpha}{\partial x'} dx' dy', \quad (11-18a)$$

$$\overline{\left(v \frac{\partial p_\beta}{\partial x} \right)}^\beta \approx \frac{\langle v \rangle}{A} \iint \frac{\partial p_\beta}{\partial x'} dx' dy'. \quad (11-18b)$$

Note that

$$\begin{aligned}
 \langle v \rangle \frac{\partial}{\partial x} \ln(V_{\alpha\beta}) &= \frac{\langle v \rangle}{V_{\alpha\beta}} \frac{\partial}{\partial x} \int_A \int \int \frac{p_{\beta}(x',y')}{p_{\alpha}(x',y')} dp dx' dy' \\
 &= \frac{\langle v \rangle}{V_{\alpha\beta}} \frac{\partial}{\partial x} \int_A [p_{\beta}(x',y') - p_{\alpha}(x',y')] dx' dy' \quad (11-19)
 \end{aligned}$$

where the domain A is a function of x inasmuch as $A = x - \Delta x/2 \leq x' \leq x + \Delta x/2$, etc.

Thus, using Leibniz' rule on (11-19) we obtain

$$\begin{aligned}
 \langle v \rangle \frac{\partial}{\partial x} \ln(V_{\alpha\beta}) &= \frac{\langle v \rangle}{V_{\alpha\beta}} \int [p_{\beta}(x+\Delta x, y') - p_{\beta}(x-\Delta x, y') - p_{\alpha}(x+\Delta x, y') \\
 &\quad + p_{\alpha}(x-\Delta x, y')] dy'
 \end{aligned}$$

or

$$\langle v \rangle \frac{\partial}{\partial x} \ln(V_{\alpha\beta}) = \frac{\langle v \rangle}{V_{\alpha\beta}} \int_A \left[\frac{\partial p_{\beta}}{\partial x'} - \frac{\partial p_{\alpha}}{\partial x'} \right] dx' dy' \quad (11-20)$$

Combining (11-15a), (11-18) and (11-20) we get, under the constraint of assumption (11-17),

$$\left\langle \frac{\partial v}{\partial x} \right\rangle \simeq \frac{\partial}{\partial x} \langle v \rangle.$$

Thus, from this result and (11-14) we conclude that

$$\langle \xi \rangle \simeq \frac{\partial \langle v \rangle}{\partial x} - \frac{\partial \langle u \rangle}{\partial y} \quad (\text{given (11-17)}) \quad (11-21)$$

and similarly

$$\langle \delta \rangle \simeq \frac{\partial \langle u \rangle}{\partial x} + \frac{\partial \langle v \rangle}{\partial y} \quad (\text{given (11-17)}) \quad (11-22)$$

Using Helmholtz theorem that any vector can be written as the sum of a rotational and a divergent component we can write

$$\underline{v} = \underline{v}_\psi + \underline{v}_\chi \quad (11-23)$$

from which we have

$$\langle \underline{v} \rangle = \langle \underline{v}_\psi \rangle + \langle \underline{v}_\chi \rangle. \quad (11-24)$$

Since by definition \underline{v}_ψ is nondivergent, we can express it in terms of the stream function Ψ :

$$\langle \underline{v}_\psi \rangle = \underline{k} \times \nabla \Psi \quad (11-25)$$

and since \underline{v}_χ is irrotational we can express it in terms of the velocity potential χ :

$$\langle \underline{v}_\chi \rangle = \nabla \chi. \quad (11-26)$$

From (11-25) we get

$$\langle \underline{v}_\psi \rangle = \begin{vmatrix} \underline{i} & \underline{j} & \underline{k} \\ 0 & 0 & 1 \\ \frac{\partial \Psi}{\partial x} & \frac{\partial \Psi}{\partial y} & \frac{\partial \Psi}{\partial p} \end{vmatrix} = \left(-\frac{\partial \Psi}{\partial y}\right) \underline{i} - \left(-\frac{\partial \Psi}{\partial x}\right) \underline{j} \quad (11-27)$$

and from (11-26)

$$\langle \underline{v}_\chi \rangle = \frac{\partial \chi}{\partial x} \underline{i} + \frac{\partial \chi}{\partial y} \underline{j}. \quad (11-28)$$

Combining (11-24), (11-27), and (11-28) we get

$$\langle \underline{u} \rangle = -\frac{\partial \Psi}{\partial y} + \frac{\partial \chi}{\partial x} + \bar{u} \quad (11-29a)$$

$$\langle v \rangle = \frac{\partial \Psi}{\partial x} + \frac{\partial \chi}{\partial y} + \bar{v} . \quad (11-29b)$$

where \bar{u} and \bar{v} are the average values of $\langle u \rangle$ and $\langle v \rangle$ over the entire model region and are known functions of time only.

Differentiating these expressions in the manner of (11-21), (11-22), we get

$$\langle \xi \rangle = \nabla^2 \Psi \quad (11-30a)$$

$$\langle \delta \rangle = \nabla^2 \chi . \quad (11-30b)$$

We seek the functional forms of Ψ and χ that are consistent both with physical laws and with our observations $\langle \underline{v}(x_n, y_n, t) \rangle_{0B, n=1 \dots N}$ (see Equation 11-11). (We assume that the wind observations are error free.)

Our observation set might represent a time period in the past for which we would like to determine the origin of pollutants responsible for an episode; or it might represent so-called worst-case meteorological conditions for which we wish to test a control strategy; or so on.

We will consider only two of the physical laws as constraints on the flow fields that we consider, the momentum law and the mass conservation principle. In pressure coordinates these are expressed, respectively, by

$$\frac{\partial \underline{v}}{\partial t} + (\underline{v} \cdot \nabla_H) \underline{v} + \omega \frac{\partial \underline{v}}{\partial p} + f \underline{k} \times \underline{v} = - \nabla \Phi + K \nabla^2 \underline{v} + \underline{F}_H \quad (11-31)$$

$$\nabla_H \cdot \underline{v} + \partial \omega / \partial p = 0 \quad (11-32)$$

where w is the "vertical velocity" in pressure coordinates, i.e.,

$$w \equiv \frac{\partial p}{\partial t} + \underline{v} \cdot \underline{\nabla}_H p + w \frac{\partial p}{\partial z} \quad (11-33)$$

Φ is the geopotential height, f the Coriolis parameter, K the "eddy viscosity", F_H represents the viscous source of negative momentum, and $\underline{v} = (u, v)$ as before. Expanding (11-31) into its two components and using (11-13) we get

$$\frac{\partial u}{\partial t} + u \frac{\partial u}{\partial x} + v \frac{\partial u}{\partial y} + w \frac{\partial u}{\partial p} - f v = - \frac{\partial \Phi}{\partial x} + K \left[\frac{\partial^2 u}{\partial x^2} + \frac{\partial^2 u}{\partial y^2} \right] + F_{Hx} \quad (11-34)$$

$$\frac{\partial v}{\partial t} + u \frac{\partial v}{\partial x} + v \frac{\partial v}{\partial y} + w \frac{\partial v}{\partial p} + f u = - \frac{\partial \Phi}{\partial y} + K \left[\frac{\partial^2 v}{\partial x^2} + \frac{\partial^2 v}{\partial y^2} \right] + F_{Hy} \quad (11-35)$$

$$\delta = - \partial w / \partial p \quad (11-36)$$

It is useful to convert (11-34) and (11-35) into the vorticity equation, partly as a means of eliminating explicit dependence of the velocity on Φ . Guided by (11-12) we differentiate (11-35) with respect to x and (11-34) with respect to y and then subtract the two equations to get

$$\begin{aligned} \frac{\partial \zeta}{\partial t} + u \frac{\partial \zeta}{\partial x} + v \frac{\partial \zeta}{\partial y} + w \frac{\partial \zeta}{\partial p} + (\zeta + f) \delta + \frac{\partial f}{\partial y} v + \\ \left[\frac{\partial w}{\partial x} \frac{\partial v}{\partial p} - \frac{\partial w}{\partial y} \frac{\partial u}{\partial p} \right] = K \left[\frac{\partial^2 \zeta}{\partial x^2} + \frac{\partial^2 \zeta}{\partial y^2} \right] + \frac{\partial F_{Hy}}{\partial x} - \frac{\partial F_{Hx}}{\partial y} \end{aligned} \quad (11-37)$$

The equation governing $\langle \delta \rangle$ is found by averaging (11-36) in the manner of (11-1):

$$\langle \delta \rangle = - \frac{1}{V_{\alpha\beta}} \iiint_A \int_{p_\alpha}^{p_\beta} \frac{\partial w}{\partial p} dp dx' dy' \quad (11-38)$$

$$\langle \delta \rangle = \frac{1}{V_{\alpha\beta}} \int_A [\omega_\alpha(x', y') - \omega_\beta(x', y')] dx' dy' \quad (11-39)$$

where ω_α denotes $\omega(x', y', p_\alpha)$. Using (11-16) we can write (11-39) in the final form

$$\langle \delta \rangle = \frac{A}{V_{\alpha\beta}} [\bar{\omega}^\alpha - \bar{\omega}^\beta]. \quad (11-40)$$

Later when we apply (11-40) we will describe approximations of $\bar{\omega}^\alpha$, etc.

Turning next to the vorticity equation (11-37) and the derivation of the equation governing $\langle \zeta \rangle$, we see that under assumption (11-17) we can write

$$\frac{\partial v}{\partial p}, \frac{\partial u}{\partial p} \simeq 0. \quad (\text{under assumption 11-17}) \quad (11-41)$$

This permits the term in brackets in (11-37) to be neglected. (This term represents the generation of ζ by the rotation of horizontal vorticity.) We will also omit the "beta" term $\partial f / \partial y$ in (11-37). With these approximations we can write (11-37) in the simpler form

$$\begin{aligned} \frac{\partial \zeta}{\partial t} + u \frac{\partial \zeta}{\partial x} + v \frac{\partial \zeta}{\partial y} + \frac{\partial}{\partial p} (\zeta w) + (2\zeta + f)\delta = K \left[\frac{\partial^2 \zeta}{\partial x^2} + \frac{\partial^2 \zeta}{\partial y^2} \right] \\ - g \frac{\partial}{\partial p} \left[\frac{\partial \tau_{zy}}{\partial x} - \frac{\partial \tau_{zx}}{\partial y} \right] \end{aligned} \quad (11-42)$$

where we have used the approximation (see Haltiner 1971, page 151)

$$F_H = - g \frac{\partial \tau}{\partial p} \quad (11-43)$$

and τ is the shear stress.

Averaging (11-42) in the manner of (11-1) we generate the following terms, expressed following the analyses of Part I:

$$\begin{aligned} \left\langle \frac{\partial \zeta}{\partial t} \right\rangle = \frac{\partial}{\partial t} \langle \zeta \rangle + \langle \zeta \rangle \frac{\partial}{\partial t} \ln(V_{\alpha\beta}) + \\ \frac{A}{V} \left[\overline{\zeta \dot{p}_\alpha^\alpha} - \overline{\zeta \dot{p}_\beta^\beta} \right] \end{aligned} \quad (11-44)$$

$$\begin{aligned} \left\langle \frac{\partial}{\partial x} u \zeta \right\rangle = \frac{\partial}{\partial x} \langle u \zeta \rangle + \langle u \zeta \rangle \frac{\partial}{\partial x} \ln(V_{\alpha\beta}) + \\ \frac{A}{V} \left[\overline{u \zeta \frac{\partial p_\alpha^\alpha}{\partial x}} - \overline{u \zeta \frac{\partial p_\beta^\beta}{\partial x}} \right] \end{aligned} \quad (11-45)$$

$$\begin{aligned} \left\langle \frac{\partial}{\partial y} v \zeta \right\rangle = \frac{\partial}{\partial y} \langle v \zeta \rangle + \langle v \zeta \rangle \frac{\partial}{\partial y} \ln(V_{\alpha\beta}) + \\ \frac{A}{V} \left[\overline{v \zeta \frac{\partial p_\alpha^\alpha}{\partial y}} - \overline{v \zeta \frac{\partial p_\beta^\beta}{\partial y}} \right] \end{aligned} \quad (11-46)$$

$$\left\langle \frac{\partial}{\partial p} \omega \zeta \right\rangle = \frac{A}{V_{\alpha\beta}} [\overline{\omega \zeta}^{\beta} - \overline{\omega \zeta}^{\alpha}] \quad (11-47)$$

The terms like $\left\langle \frac{\partial^2 \zeta}{\partial x^2} \right\rangle$ are quite complex and we will approximate them simply by

$$\left\langle \frac{\partial^2 \zeta}{\partial x^2} \right\rangle \approx \frac{\partial^2}{\partial x^2} \langle \zeta \rangle \quad (11-48)$$

Combining all the above and assuming $\langle \zeta \delta \rangle = \langle \zeta \rangle \langle \delta \rangle$, we get

$$\begin{aligned} \frac{\partial \langle \zeta \rangle}{\partial t} + \langle \underline{u} \rangle \cdot \underline{\nabla}_H \langle \zeta \rangle + \langle \zeta \rangle \left[\frac{\partial}{\partial t} \ln V_{\alpha\beta} + \langle \underline{u} \rangle \cdot \underline{\nabla}_H \ln V_{\alpha\beta} + 2 \langle \delta \rangle \right] \\ = -f \langle \delta \rangle + \frac{A}{V_{\alpha\beta}} \left[\overline{\zeta \frac{dp}{dt}}^{\beta} - \overline{\zeta \frac{dp}{dt}}^{\alpha} \right] - \underline{\nabla}_H \cdot \langle \underline{u}' \zeta' \rangle \end{aligned} \quad (11-49)$$

$$+ g \frac{A}{V_{\alpha\beta}} \left[\overline{\frac{\partial \tau_{zy}}{\partial x}} - \overline{\frac{\partial \tau_{zx}}{\partial y}} \right] + K \left[\frac{\partial^2}{\partial x^2} + \frac{\partial^2}{\partial y^2} \right] \langle \zeta \rangle - \langle \underline{u}' \zeta' \rangle \cdot \underline{\nabla}_H \ln V_{\alpha\beta}$$

where

$$\langle \underline{u}' \zeta' \rangle = \langle \underline{u} \zeta \rangle - \langle \underline{u} \rangle \langle \zeta \rangle \quad (11-50)$$

$$\langle \underline{u} \rangle = (\langle u \rangle, \langle v \rangle) \quad (11-51)$$

$$p_{\alpha} = p_{\alpha}(x, y, t) - p \quad (11-52)$$

and

$$\frac{d}{dt} \equiv \frac{\partial}{\partial t} + u \frac{\partial}{\partial x} + v \frac{\partial}{\partial y} + \omega \frac{\partial}{\partial p} \quad (11-53)$$

In deriving (11-49) we assumed that $\tau_z = 0$ on p_{β} in anticipation of the eventual use of this equation in applications where the upper surface p_{β} is above the friction layer. We will use Haltiner's approximation (page 152) for τ_z , namely

$$\tau_z = \rho_0 C_D \langle \underline{u} \rangle \quad (11-54)$$

where ρ_0 is air density in layer α, β , in particular the mixed layer; C_D is the drag coefficient and $\langle \underline{u} \rangle$ is the layer averaged wind vector given by (11-51).

It is convenient to group the terms in (11-49) according to whether they represent sources or sinks of $\langle \zeta \rangle$. The terms involving ζ' do not fall into either category, but for now we will combine them with the source terms and write (11-49) in the form

$$\frac{\partial}{\partial t} \langle \zeta \rangle + \langle u \rangle \frac{\partial}{\partial x} \langle \zeta \rangle + \langle v \rangle \frac{\partial}{\partial y} \langle \zeta \rangle + \langle \zeta \rangle G - K \left[\frac{\partial^2}{\partial x^2} + \frac{\partial^2}{\partial y^2} \right] \langle \zeta \rangle = H \quad (11-55)$$

where

$$G \equiv \frac{\partial}{\partial t} \ln V_{\alpha\beta} + \langle \underline{u} \rangle \cdot \nabla_H \ln(V_{\alpha\beta}) + 2\langle \delta \rangle \quad (11-56)$$

$$H \equiv -f\langle \delta \rangle + \frac{A}{V_{\alpha\beta}} \left[\zeta \frac{dP}{dt}^\beta - \zeta \frac{dP}{dt}^\alpha + g\rho_0 C_D \zeta_0 \right] - \nabla_H \cdot \langle \underline{u}' \zeta' \rangle - \langle \underline{u}' \zeta' \rangle \cdot \nabla_H \ln V_{\alpha\beta} \quad (11-57)$$

$$\zeta_0 = \frac{\partial \langle v \rangle_0}{\partial x} - \frac{\partial \langle u \rangle_0}{\partial y} \quad (11-58)$$

We are now ready to collect the equations that we will use to generate the ψ and χ fields. First, let the superscript denote the time variable, i.e.,

$$\phi^J \equiv \phi(x,y,J\Delta t). \quad (11-59)$$

Now express (11-55) in the difference form

$$\begin{aligned} \frac{1}{\Delta t} [\langle \xi \rangle^{J+1} - \langle \xi \rangle^J] + \langle u \rangle^J \frac{\partial}{\partial x} \langle \xi \rangle^J + \langle v \rangle^J \frac{\partial}{\partial y} \langle \xi \rangle^J + \langle \xi \rangle^J G^J \\ - K \left[\frac{\partial^2}{\partial x^2} + \frac{\partial^2}{\partial y^2} \right] \langle \xi \rangle^J = H^J \end{aligned} \quad (11-60)$$

Let ξ^J be the complex Fourier transform of $\langle \xi \rangle^J$, i.e.,

$$\langle \xi \rangle^J = \frac{1}{4\pi^2} \iint_{-\infty}^{\infty} \xi^J(\underline{k}) e^{i\underline{k} \cdot \underline{x}} d\underline{k}_x d\underline{k}_y \quad (11-61a)$$

$$\xi^J = \iint_{-\infty}^{\infty} \langle \xi(\underline{x}) \rangle^J e^{-i\underline{k} \cdot \underline{x}} d\underline{x} d\underline{y} \quad (11-61b)$$

where $\underline{k} = (k_x, k_y)$ and $\underline{x} = (x, y)$. We will represent transform pairs by

$$\xi^J \leftrightarrow \langle \xi \rangle^J, \quad (11-62)$$

and will make use of the convolution theorem

$$g(\underline{x})f(\underline{x}) \leftrightarrow \frac{1}{(2\pi)^2} \int_{-\infty}^{\infty} F(\underline{k}') G(\underline{k} - \underline{k}') d\underline{k}' \quad (11-63)$$

where \underline{x} and \underline{k} are 2-D and

$$g(\underline{x}) \leftrightarrow G(\underline{k})$$

$$f(\underline{x}) \leftrightarrow F(\underline{k}).$$

Note from (11-61a) that

$$\frac{\partial}{\partial x} \langle \xi \rangle^J = \frac{i}{4\pi^2} \iint_{-\infty}^{\infty} k_x \xi^J(\underline{k}) e^{i \underline{k} \cdot \underline{x}} dk_x dk_y, \quad (11-64)$$

$$\frac{\partial^2}{\partial x^2} \langle \xi \rangle^J = \frac{-1}{4\pi^2} \iint_{-\infty}^{\infty} k_x^2 \xi^J(\underline{k}) e^{i \underline{k} \cdot \underline{x}} dk_x dk_y, \quad (11-65)$$

and in general

$$\frac{\partial^n}{\partial x^n} \langle \xi \rangle^J \leftrightarrow (ik_x)^n \xi^J \quad (11-66)$$

Now, replacing each term in (11-60) by its Fourier transform and making use of (11-63) and (11-66) we get

$$\begin{aligned} & \frac{(2\pi)^2}{\Delta t} [\xi^{J+1} - \xi^J] - i \iint_{-\infty}^{\infty} k'_x \xi^J(\underline{k}') u^J(\underline{k} - \underline{k}') dk'_x dk'_y \\ & - i \iint_{-\infty}^{\infty} k'_y \xi^J(\underline{k}') v^J(\underline{k} - \underline{k}') dk'_x dk'_y + K(k_x^2 + k_y^2) \xi^J (2\pi)^2 \\ & + \iint_{-\infty}^{\infty} \xi^J(\underline{k}') G^J(\underline{k} - \underline{k}') dk'_x dk'_y = 4\pi^2 H^J \end{aligned} \quad (11-67)$$

where

$$G^J \leftrightarrow G^J \quad (11-68a)$$

$$H^J \leftrightarrow H^J \quad (11-68b)$$

$$u^J \leftrightarrow \langle u \rangle^J \quad (11-69a)$$

$$v^J \leftrightarrow \langle v \rangle^J \quad (11-69b)$$

We want equations for Ψ and χ . Thus, we obtain from (11-30a) and (11-66)

$$\xi^J = - (k_x^2 + k_y^2) A^J \quad (11-70)$$

where

$$\Psi^J(\underline{x}) \leftrightarrow A^J(\underline{k}). \quad (11-71)$$

Using (11-70) in (11-67) we obtain one of the equations governing Ψ , namely

$$\begin{aligned} A^{J+1}(\underline{k}) = & A^J(\underline{k}) [1 - (k_x^2 + k_y^2)K\Delta t] - \frac{H^J(\underline{k})\Delta t}{k_x^2 + k_y^2} \\ & + \frac{\Delta t}{(2\pi)^2(k_x^2 + k_y^2)} \iint_{-\infty}^{\infty} (k_x'^2 + k_y'^2) A^J(\underline{k}') [ik_x' u^J(\underline{k} - \underline{k}') \\ & + ik_y' v^J(\underline{k} - \underline{k}') - G^J(\underline{k} - \underline{k}')] dk_x' dk_y' . \end{aligned} \quad (11-72)$$

The transforms u^J and v^J of the velocity components $\langle u \rangle^J$ and $\langle v \rangle^J$ can now be expressed in the form (see 11-29)

$$u^J = -ik_y A^J + ik_x B^J + \bar{u}^J \delta(\underline{k}) \quad (11-73a)$$

$$v^J = ik_x A^J + ik_y B^J + \bar{v}^J \delta(\underline{k}) \quad (11-73b)$$

where

$$x^J(\underline{x}) \leftrightarrow B^J(\underline{k}) \quad (11-73c)$$

and $\delta(\underline{k})$ is the delta function of the wave number vector \underline{k} . Then from (11-30b), (11-40), and (11-66) we find that B^J must satisfy

$$B^J(\underline{k}) = -\frac{\mathcal{D}^J(\underline{k})}{k_x^2 + k_y^2} \quad (11-74)$$

where

$$\mathcal{D}^J(\underline{k}) \leftrightarrow \langle \delta \rangle = \frac{A}{V_{\alpha\beta}(\underline{x})} [\bar{w}^\alpha(\underline{x}, J\Delta t) - \bar{w}^\beta(\underline{x}, J\Delta t)] \quad (11-75)$$

and w is considered to be a known variable.

Finally, the observations $\langle v(x_n) \rangle_{0B}$ given by (11-11) must be satisfied. Hence, from (11-29), (11-61a), (11-66), and (11-11) we have

$$\frac{i}{(2\pi)^2} \iint_{-\infty}^{\infty} [-k_y A^J(\underline{k}) + k_x B^J(\underline{k})] e^{i\mathbf{k} \cdot \mathbf{x}_n} d\underline{k} = \langle u(x_n, J\Delta t) \rangle_{0B} - \bar{u}(J\Delta t) \quad (11-76)$$

$n=1, 2, \dots, N;$

$$\frac{i}{(2\pi)^2} \iint_{-\infty}^{\infty} [k_x A^J(\underline{k}) + k_y B^J(\underline{k})] e^{i\underline{k} \cdot \underline{x}_n} d\underline{k} = \langle v(\underline{x}_n, J\Delta t) \rangle_{OB} - \bar{v}(J\Delta t) \quad (11-77)$$

$n=1, 2, \dots, N$

where $\underline{x}_n = (x_n, y_n)$ are the observation sites described above, and \bar{u} and \bar{v} are the averaged observed winds in the entire model domain at time $t = J\Delta t$.

Equations (11-72, 74, 76 and 77) comprise a set of $2N + 2$ relationships that the transforms A and B , or equivalently $\langle u \rangle$ and $\langle v \rangle$, must satisfy. A fundamental difference between this system of equations and the system currently used in meteorological modeling is the presence of the $2N$ equations (11-76, 77) associated with the wind observations made at time $J\Delta t$. In conventional meteorological models, the observed data are transformed through ad hoc means into a description of an initial velocity field; and using it, the two equations (11-72 and 74) are solved as an initial value problem. As we shall discuss below, this practice is not supportable on scientific grounds, and when it is employed, the velocity field that one obtains is largely an artifact of the ad hoc procedure that was used in the formulation of the initial state.

The fact is that the N observations of the wind velocity at any instant $J\Delta t$, say, do not uniquely determine the velocity distribution at that moment. Rather, these measurements, specifically (11-76, 77), together with the continuity equation (11-74) define a hyperplane in the phase space of wind velocity. Each point on this plane represents an entire vector function $[u(\underline{x}, J\Delta t), v(\underline{x}, J\Delta t)]$, $\underline{x} \in D$. We pointed out in Section 6 of Part 1 that each of

these functions in a possible description of the actual velocity field that existed at the moment $t = J\Delta t$ that the observations contained in Eqs. (11-76) and (11-77) were made. If we had to choose from this set of possible velocity functions the one that we thought described the flow that actually existed at the moment the observations were made, our choice would be guided by whatever previous wind data we had seen for the region in question and on our knowledge of the nature of atmospheric motion generally. On this basis we would declare many of the possible functions to be "unlikely" descriptions because they have characteristics that are incompatible with our knowledge. For example, even though all functions in the set satisfy the observations and the continuity equation (11-74) exactly, some contain hurricane force winds between the observation stations; some contain intense vortices and jets; and so on. However, even after all these are dismissed, there remains a virtually infinite set of functions no one of which can be ruled out as a plausible description of the actual flow.

This suggests that we should assign to each point on the hyperplane of possible flow descriptions a weight p , say, whose magnitude is a measure of our conviction that that particular function is the one that describes the flow field that existed when the observations were made (at time $J\Delta t$). To those bizarre functions mentioned above, we would assign the weight $p=0$; and to the remainder of the points on the hyperplane of possible descriptions we would assign weights $1 > p > 0$. Without going into details, we point out that the weight p is synonymous with the "probability" of occurrence of the flow field to which the p is assigned (see Lamb, 1983c).

The problem is to formulate a quantitative rule for assigning the weights. Clearly, we cannot examine every function on the hyperplane of possible flows and assign it a weight subjectively. We need a mathematical procedure.

In Lamb (1983c) several approaches to this problem are proposed. It is shown in that paper that in effect the method that has been employed to date in both diffusion and meteorological modeling studies has been to assign a zero value of p to all of the possible flows except one and to assign the value $p=1$ to that single function. This is equivalent to declaring that we know the correct description of the flow field at $t=J\Delta t$ without any doubt. This "correct" description is obtained using one of the so-called objective analysis formulas. But many such formulas exist -- no formula of this type can be universally valid -- and therefore it is illogical to label any one description of the flow the "correct" description. The point is that there is no scientific basis whatever for assigning unit weight to only one function in the set of possible flows and zero weights to all others.

One rational method of assigning p is the following. It has been theorized that in 2-D fluids kinetic energy is partitioned among the spatial fluctuations in the flow in proportion to $|\underline{k}|^{-3}$, where \underline{k} is the wave number vector of the fluctuation. To a large extent this theory is supported by measurements of kinetic energy in the free atmosphere. Thus, let Q represent the manifold in velocity phase space of functions whose Fourier transform is consistent with an energy spectrum of the form $E(\underline{k}) \sim |\underline{k}|^{-3}$. And let Ω represent the manifold formed by the intersection of Q and the hyperplane of possible flow descriptions. We now advance the hypothesis:

$$p(\underline{v}(\underline{x}, J\Delta t), \underline{x} \in D) = \begin{cases} q(\underline{v}), & \text{if } \underline{v} \in \Omega; \\ 0 & , \text{ otherwise} \end{cases} \quad (11-78a)$$

where $1 > q(\underline{v}) > 0$ is a function of the entire velocity field $\underline{v}(\underline{x}, J\Delta t)$, $\underline{x} \in D$ that we have yet to specify. Hypothesis (11-78a) is simply a statement of our a priori belief that the description of the true velocity field at time $J\Delta t$ is a member of the subset Ω of the hyperplane of possible flows. Observations of the flow field at times following $J\Delta t$ and observations of the rate of dispersion of material in the flow might force us a posteriori to reject this hypothesis.

To supplement (11-78a) we might advance the following hypothesis:

$$q(\underline{v}) \sim \bar{E}(\underline{v})^{-1} \quad (11-78b)$$

where \bar{E} is the kinetic energy of the flow field \underline{v} integrated over the entire model domain D . In practice one can treat only a finite number of the velocity fields contained in Ω . For example, in accordance with (11-78b) we might select, say, the 20 members of Ω that contain the least kinetic energy, namely the 20 points in Ω closest to the origin of the phase space; and assign p values to each using (11-78b) and the constraint that the sum of the 20 p 's be unity.

In hypothesis (11-78a,b), and in the conventional approach discussed earlier, consideration is given only to the observations made at the single time $J\Delta t$. However, observations made after $J\Delta t$ provide valuable information that can be used by way of the momentum equation (11-72) to obtain a better approximation of the probabilities p of the flow fields at $J\Delta t$ than we can

obtain from empirical-theoretical considerations alone. To implement this approach requires rather complicated dynamic programming procedures. We plan to utilize this method in the "second generation" regional model.

For the present we shall replace Eq. (11-72) with the much simpler, and much weaker, diagnostic constraint

$$\int_D \langle \xi(\underline{x}, t) \rangle d\underline{x} = C(t) \quad (11-79)$$

where $C(t)$ is the circulation around the perimeter of the modeling region D . This equation is a statement of Gauss' theorem. We will derive estimates of $C(t)$ from observed winds and treat it as a known function of time.

We see from (11-30a) that Eq. 11-79 is a constraint on the stream function, and hence on A (See 11-71). Substituting (11-30a) into (11-79) and making use of (11-71) and Stoke's theorem, we can express (11-79) in terms of the transform of the stream function:

$$\frac{1}{4\pi^2} \iint A(\underline{k}) [(e^{ik_x L_x} - 1)(e^{ik_y L_y} - 1) \left(\frac{k_x^2 + k_y^2}{k_x k_y} \right)] dk_x dk_y = c(t) \quad (11-80)$$

Thus, the initial version of processor P11 will be based on the equation set

$$\left. \begin{array}{l} \text{Eq. (11-81)} \\ \text{Eq. (11-74)} \\ \text{Eq. (11-76)} \\ \text{Eq. (11-77)} \end{array} \right\} \Rightarrow A^J(\underline{k}), B^J(\underline{k}) \quad (11-81)$$

Each solution set $[A^J(k), B^J(k)]$ derived from (11-81) yields layer averaged winds $[<u(x, J\Delta t)>, <v(x, J\Delta t)>]$ through the following equations, whose origin is (11-29):

$$<u(x, J\Delta t)> = \frac{i}{(2\pi)^2} \iint_{-\infty}^{\infty} [-k_y A^J(k) + k_x B^J(k)] e^{ik \cdot x} dk + \bar{u}(J\Delta t) \quad (11-82a)$$

$$<v(x, J\Delta t)> = \frac{i}{(2\pi)^2} \iint_{-\infty}^{\infty} [k_x A^J(k) + k_y B^J(k)] e^{ik \cdot x} dk + \bar{v}(J\Delta t) \quad (11-82b)$$

In the first generation model we will derive between ten and twenty flow fields from (11-81, 82) for each hour of the model simulation period and assign weights p to each using hypothesis (11-78) above. Let us call this finite ensemble of flow fields at hour $t=J\Delta t$ W^J . (We should add that even though the members of W^J are not explicitly related to those of W^K , $K \neq J$, due to our replacing the momentum equation (11-72) with the simple diagnostic expression (11-79), there is implicit coupling of these ensembles by virtue of the fact that each of them is defined in terms of the actual winds observed at each hour.) We generate a corresponding finite ensemble C of concentrations (containing $M=10$ to 20 members) associated with a given emissions distribution $S(x, t)$, $x \in D$, $0 \leq t \leq T$, by "driving" the dispersion model with M wind fields $[<u(x, J\Delta t)>, <v(x, J\Delta t)>]_{\mu}$, $x \in D$, $J=0, 1, \dots, J_{MAX}$, $\mu=1, \dots, M$. Each of the M flow fields is created by selecting a $<u(x, J\Delta t)>$ and a $<v(x, J\Delta t)>$ at random from the ensembles W^J for each hour $J=1, \dots, J_{MAX}$ in the period of interest. Either ensemble mean values of the concentration or the frequency distribution of concentration or any other statistical quantity of interest can be computed

directly from the ensemble C for any desired receptor sites and times. Details will be presented in a future report. (See also Lamb 1983 a,b,c).

Below we outline the basic structure of Processor P11 which utilizes the techniques described above to compute the layer averaged winds $\langle \tilde{v} \rangle_k$ for each of the regional model's three layers. Winds are determined for Layers 2 and 3 at all hours and in Layer 1 during the day only. The nighttime air flow in Layer 1 is simulated in Processor P7 and passed into Processor P11 in the form $(\langle u \rangle_{VL}, \langle v \rangle_{VL})$ for amalgamation with the flow fields computed here.

STAGE UV11

This stage computes layer averages of the measured winds aloft that are used as the observations in solving Eq. (11-76) and (11-77). Consider first the calculations required for Layer 3.

- (1) At each of the M upper air weather stations compute the layer averaged horizontal wind components as follows:

$$\begin{aligned} \langle u(x_m, t) \rangle_{OB,3} &= \frac{1}{p_3 - p_2} \int_{p_2(x_m, t)}^{p_3(x_m, t)} \hat{u}(x_m, p, t) dp \\ \langle v(x_m, t) \rangle_{OB,3} &= \frac{1}{p_3 - p_2} \int_{p_2(x_m, t)}^{p_3(x_m, t)} \hat{v}(x_m, p, t) dp \end{aligned} \quad \left. \begin{array}{l} m=1, 2, \dots, M \\ \text{mode 0 and} \\ \text{mode 1} \end{array} \right\} \quad (11-83)$$

where \hat{u} and \hat{v} are the measured wind profiles. Since the input winds (\hat{u} , \hat{v}) are in z coordinates, it will be necessary to transform them to p coordinates, e.g., $\hat{u}(x_m, p, t)$, using the pressure-height function $p_m(z, t)$.

- (2) Since the bottom surface of Layer 2 is p_{VS} in mode 1 and p_1 in mode 0, the corresponding expression for the Layer 2 observed winds is

$$\begin{aligned}
\langle u(\tilde{x}_m, t) \rangle_{OB,2} &= \frac{1}{p_2 - p_B} \int_{p_B(\tilde{x}_m, t)}^{p_2(\tilde{x}_m, t)} \hat{u}(\tilde{x}_m, p, t) dp \\
\langle v(\tilde{x}_m, t) \rangle_{OB,2} &= \frac{1}{p_2 - p_B} \int_{p_B(\tilde{x}_m, t)}^{p_2(\tilde{x}_m, t)} \hat{v}(\tilde{x}_m, p, t) dp
\end{aligned}
\left. \vphantom{\begin{aligned} \langle u(\tilde{x}_m, t) \rangle_{OB,2} \\ \langle v(\tilde{x}_m, t) \rangle_{OB,2} \end{aligned}} \right\} \begin{array}{l} m=1,2,\dots,M, \\ \text{mode 0 and} \\ \text{mode 1} \end{array} \quad (11-84)$$

where

$$p_B(\tilde{x}, t) = \begin{cases} p_{vs}(\tilde{x}, t), & \text{mode 1;} \\ p_1(\tilde{x}, t), & \text{mode 0.} \end{cases} \quad (11-85)$$

(Recall that mode 1 applies when $\Delta p_1=1$, and mode 0 applies when $\Delta p_1=0$.)

(3) Processor P11 is not used in Layer 1 during mode 1 conditions. In that case the flow field in Layer 1 is generated in P7. During mode 0 conditions, the depth of Layer 1 is set in P7 to a value that is approximately the top of the shear layer. Assuming, then, that the flow speed and direction in Layer 1 are roughly uniform we adopt the following expressions for $\langle \tilde{v} \rangle_{OB,1}$:

$$\begin{aligned}
\langle u(\tilde{x}_n, t) \rangle_{OB,1} &= \hat{u}(\tilde{x}_n, t) \\
\langle v(\tilde{x}_n, t) \rangle_{OB,1} &= \hat{v}(\tilde{x}_n, t)
\end{aligned}
\left. \vphantom{\begin{aligned} \langle u(\tilde{x}_n, t) \rangle_{OB,1} \\ \langle v(\tilde{x}_n, t) \rangle_{OB,1} \end{aligned}} \right\} \begin{array}{l} n=1,2,\dots,N \\ \text{mode 0 only} \end{array} \quad (11-86)$$

where \tilde{x}_n , $n=1,\dots,N$ are the sites of the N surface weather stations.

(4) Optional. In order to supplement the sparse upper air data on which the observations in Layers 2 and 3 are based, we define the following "shear functions" for use in estimating the flow in Layer 2 over surface wind stations.

$$\left. \begin{aligned} \langle \hat{g}_{um}(t) \rangle_2 &= \frac{\langle u(x_m, t) \rangle_{OB,2}}{\bar{u}(x_m, p_{vs}(x_m, t), t)} \\ \langle \hat{g}_{vm}(t) \rangle_2 &= \frac{\langle v(x_m, t) \rangle_{OB,2}}{\bar{v}(x_m, p_{vs}(x_m, t), t)} \end{aligned} \right\} \begin{array}{l} m=1, \dots, M \\ \text{mode 0 only} \end{array} \quad (11-87)$$

In mode 0, p_{vs} coincides with the ground surface and hence the function $\langle \hat{g} \rangle_2$ is the ratio of the measured vertically averaged wind in layer 2 to the observed wind at ground level.

Next we interpolate values of $\langle g_u \rangle_2$ and $\langle g_v \rangle_2$ at each of the N surface stations from the values given by (11-87) for the rawin station sites as follows:

$$\langle g_u(x_n, t) \rangle_2 = \frac{\sum_{m=1}^M \langle \hat{g}_{um}(t) \rangle_2 W(r_{nm})}{\sum_{m=1}^M W(r_{nm})} \quad (11-88)$$

where

$$W(r_{nm}) = [(x_n - x_m)^2 + (y_n - y_m)^2]^{-1}. \quad (11-89)$$

A similar operation yields $\langle g_v \rangle_2$. We can now define pseudo Layer 2 winds over each surface station as follows

$$\begin{aligned} \langle u(x_n, t) \rangle_{OB,2} &\cong \langle g_u(x_n, t) \rangle_2 \hat{u}(x_n, t) \\ \langle v(x_n, t) \rangle_{OB,2} &\cong \langle g_v(x_n, t) \rangle_2 \hat{v}(x_n, t) \end{aligned} \quad \begin{array}{l} n=1, \dots, N \\ \text{mode 0 only.} \\ \text{optional} \end{array} \quad (11-90)$$

This optional method of supplementing the upper air data can be implemented as desired.

Stage PHLOB

This portion of Processor P11 solves the equation set (11-81) to obtain members of the flow field ensemble. When a surface inversion is not present (mode 0), this stage computes averaged winds for all three layers of the model. Otherwise (Mode 1) simulations are performed only for layers 2 and 3, and the corresponding Layer 1 flow is assigned the values

$$\left. \begin{array}{l} \langle u \rangle_1 = \langle u \rangle_{VL} \\ \langle v \rangle_1 = \langle v \rangle_{VL} \end{array} \right\} \text{ mode 1}$$

where $\langle u \rangle_{VL}$ and $\langle v \rangle_{VL}$ are the wind components in the cold inversion layer generated by Processor P7 at each grid cell and at each hour that the inversion (mode 1) exists.

The input requirements of Processor P11 are summarized in Table 11-1 and its outputs are listed in Table 11-2. Processor P11 and its interfaces with the processor network are illustrated in Figure 11-2.

Table 11-1 Input Requirements of Processor P11 and Their Sources

Variable	Description	Source
$p_3(x, t)$	top surface of Layer 3 in pressure (mb) coordinates	P8
$p_2(x, t)$	same as above, except top of Layer 2	P8
$p_{vs}(x, t)$	pressure (mb) at the virtual surface	P7
$p_1(x, t)$	top surface of Layer 1 in pressure (mb) coordinates	P7
$\hat{u}(x_m, z, t)$	observed east-west wind speed component (m/sec) at rawin station $m(=1, \dots, M)$ at hour t at elevation z (m MSL)	P1
$\hat{v}(x_m, z, t)$	same as above, except north-south wind component	P1
$\hat{u}(x_n, t)$	observed east-west wind component (m/sec) at surface station $n(=1, \dots, N)$ at hour t	P3
$\hat{v}(x_n, t)$	same as above, except north-south wind component	P3
$p_m(z, t)$	pressure (mb) at elevation z (m MSL) over rawin station $m(=1, \dots, M)$ at hour t .	P1
$\langle \delta(x, t) \rangle_3$	average horizontal wind divergence (sec^{-1}) in Layer 3 in grid cell centered at x at hour t .	P8
$\langle \delta(x, t) \rangle_2$	Same as $\langle \delta \rangle_3$ except applies to Layer 2	P8
$\langle \delta(x, t) \rangle_1$	Same as above except applies to Layer 1	P8
$\langle u(x, t) \rangle_{VL}$	Average east-west wind component in Layer 1 during mode 0 (generally night-time) hours (m/sec)	P7
$\langle v(x, t) \rangle_{VL}$	Same as above except north-south wind component	P7

Table 11-2 Outputs of Processor P11

Variable	Description
$\langle u(\underline{x}, t) \rangle_3$	Vertically averaged wind (m/sec) in Layer 3 at grid cell centered at \underline{x} at hour t (east-west component)
$\langle v(\underline{x}, t) \rangle_3$	same as above, except north-south wind component
$\langle u(\underline{x}, t) \rangle_2$	Vertically averaged wind (m/sec) in Layer 2 at grid cell centered at \underline{x} at hour t (east-west component)
$\langle v(\underline{x}, t) \rangle_2$	same as above, except north-south wind component
$\langle u(\underline{x}, t) \rangle_1$	Layer 1 averaged wind (m/sec) in grid cell centered at \underline{x} at hour t (east-west component)
$\langle v(\underline{x}, t) \rangle_1$	same as above, except north-south wind component

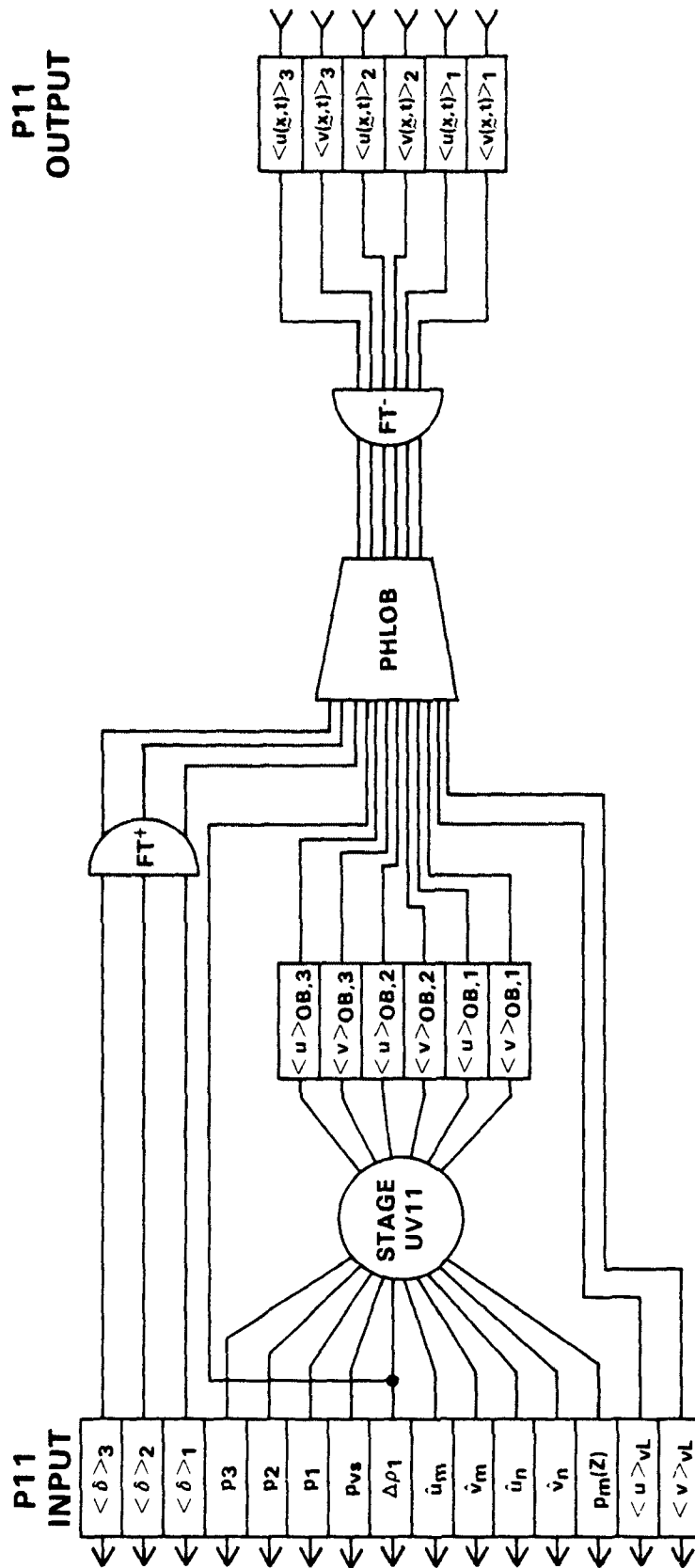


Figure 11-2. Illustration of Processor P11 and its input and output interfaces with the processor network. Stages FT^+ and FT^- perform Fourier transforms and inverse Fourier transforms, respectively.

SECTION 11

PROCESSOR P12

DEVELOPMENT

Processor P12 calculates parameter fields required in the description of interfacial material fluxes between Layer 0 and Layer 1 and between Layer 1 and Layer 2. It also provides estimates of the horizontal eddy diffusivities in all layers. The mathematical expressions for the parameters we require were presented in Part 1 of this report. Below we provide detailed descriptions of the implementation of these expressions and further commentary on their meanings and origin. The discussion is divided by stages just as the calculations within P12 are divided.

Stage K

This stage computes estimates of the horizontal eddy diffusivity $K_n(I,J,t_m)$ at each grid point (I,J) at each hour t_m , for each of the model's three layers $n = 1, 2$, and 3 . Here eddy diffusivity refers to the action of the small scale wind fluctuations generally associated with turbulence. These include wind fluctuations generated by wind shear at the earth's surface and across the top of the mixed layer, and lateral fluctuations induced by convective thermals, principally at the top of the mixed layer and at the ground. (The effects of small scale vertical fluctuations are handled by parameters like w_1 that we consider later.)

It is important to keep in mind the role that the eddy diffusivity will play in the regional model. In conventional studies, the magnitude of the horizontal diffusivity controls the rate at which a plume expands about its "centerline" and this in turn affects the magnitude of the "mean" concentration that the model predicts. In the present model the eddy diffusivity plays a lesser role. As we discussed in Part 1, Chapter 7, and in the description of Processor P11 in this report, the regional model will be applied to simulation of the ensemble averaged concentration. This requires the model to be run a number of times, each time using a different flow field [$\langle u \rangle_n$, $\langle v \rangle_n$] from the ensemble of flow fields described in Processor P11 following (11-77) but using the same eddy diffusivity K_n in each case. The results of all the individual simulations are eventually superposed to arrive at the ensemble averaged concentration properties. In the case of a point source plume, the superposition of the individual realizations within the ensemble might appear as shown in Figure 12-1. Note that K_n controls the rate of expansion of the plume in each realization, but the spatial variability of the wind fields within the flow ensemble are what govern the envelope of the superposed results and hence it is these larger scale variations in the flow that dominate the ensemble mean concentration. In this case it can be shown that K_n affects the mean square concentration. This in turn affects the rates of second-order chemical reactions and also the expected deviation of the mean concentration the model predicts from the actual concentration values that one might measure.

Another way of viewing the role of the eddy diffusivity in the regional model is to consider that between the largest turbulent fluctuations represented by the diffusivity K and the smallest perturbations in the

subsynoptic flow that our network of wind sensors can resolve, there lies a range of "mesoscale" wind fluctuations that are not accounted for either in the K 's or in the "transport flow". And it is these fluctuations that give the ensemble averaged plume the width Σ illustrated in Figure 12-1.

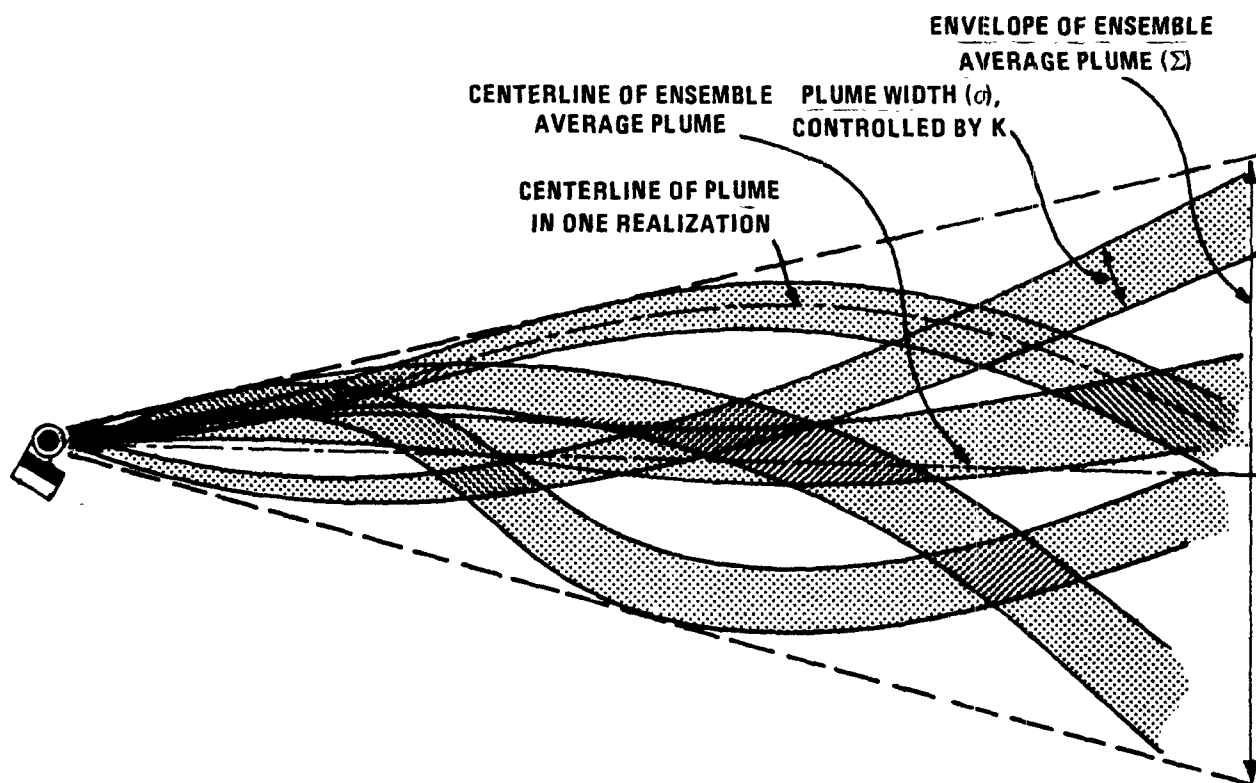


Figure 12-1. Illustration of the superposition of five hypothetical realizations of an ensemble of point source plumes. The width Σ of the ensemble of plumes is controlled by the character of the flow field ensemble. The width σ of the plumes in the ensemble is controlled by the turbulent, eddy diffusivity K .

On the basis of the points raised above, we expect that the values assigned to K_n in the regional model will directly affect the mean square concentration values more than the mean. However, they may have a significant indirect effect on the mean concentration through the influence that they will have on photochemical reaction rates. We can only determine through test

calculations just how large these effects can be. For now we will postulate simple forms for the lateral diffusivities K_h that we can use in the first generation model.

Lacking a firm basis on which to estimate the eddy diffusivity, we will use heuristic arguments to formulate expressions for K_h . Our first assumption is that the lateral eddy diffusivity is effectively zero during nighttime hours when convection is absent and/or stable stratification damps shear generated velocity fluctuations. Our second assumption is that during the day, convection is the primary source of horizontal wind fluctuations. Let D be the horizontal scale of convective cells, or rolls, and let H be the depth of air in which the convection is confined (usually by a stable layer an elevation H above the ground). We will base our parameterization on the concept that convective circulations have a toroidal shape with rising motion along the axis of the toroid, outward horizontal motion along the top, sinking motion along the outer surface of the toroid, and horizontal motion at its bottom directed in toward the axis. In this picture the outer diameter of the toroid is D and its height is H . If the circulation were indeed this simple, then a particle would receive a horizontal displacement of order D in the time Δt required for the particle to traverse the depth H of the circulation.

We imagine that each convection toroid is surrounded by others and that a particle in any one toroid can escape into an adjacent one during the time the particle is moving downward along the outer edges of the toroid or during times when the convective cell is dying. If these migrations of particles from one cell to another occur at random, then as a rough approximation we can treat them as a classical random walk process. In this case the effective

diffusivity K is

$$K \sim D^2/\Delta t. \quad (12-1)$$

(Incidentally, the random walk and the gradient transfer, or K theory, models of diffusion are essentially equivalent.)

It has been found in empirical studies of dry convection in the planetary boundary layer that $D \approx 1.5H$. If we represent the transit time Δt by

$$\Delta t = H/W, \quad (12-2)$$

where W is a characteristic velocity scale of the convective motion, then we get from (12-1) and (12-2)

$$K \sim WH \quad (12-3)$$

which we could have guessed at the outset on purely dimensional grounds. In dry convection $W = w_*$, where

$$w_* = (HQg/\theta)^{1/3} \quad (12-4)$$

where Q is the kinematic heat flux at the ground and θ is the mean temperature in the mixed layer. When cumulus clouds are present (moist convection), the appropriate measures of W and H are unknown. In this initial work we shall assume that when convective clouds are present

$$W = w_c$$

where w_c is the average upward air speed within clouds and

$$H = H_2 + H_3 \quad (12-5)$$

where H_2 is the depth of the convective layer below cloud base and H_3 is the depth of the layer occupied by clouds. These estimates will be tested in future studies.

Based on the considerations presented above, we propose the expressions summarized in Table 12-1 for the diffusivities K_n in each of the model's layers.

Horizontal Diffusivity	$L(i,j,t_m)$		
	>0	≤ 0 and $\sigma_c = 0$	≤ 0 and $\sigma_c \neq 0$
$K_1(i,j,t_m)$	0	$.1w_*H_2$	$.1w_*H_2$
$K_2(i,j,t_m)$	0	$.1w_*H_2$	$.1w_c(H_2+H_3)$
$K_3(i,j,t_m)$	0	0	$.1w_c(H_2+H_3)$

Table 12-1 Summary of the expressions used to estimate the horizontal eddy diffusivity K_n in each of the model's three layers.

The relationships between H_2 and H_3 and the thickness h_n of the model layers, which are inputs to P12, are as follows:

$$H_2 = h_1 + h_2 \quad (12-6a)$$

$$H_3 = h_3 \quad (12-6b)$$

In Table 12-1, σ_c is the fraction of the sky covered by cumulus clouds in a given grid cell at a given hour. The velocity $w_c(i,j,t_m)$ required in the expressions for K_n is an input parameter to processor P12; and w_* should be computed by

$$w_* = (H_2 Q g / \theta_o)^{1/3} \quad (12-7)$$

where H_2 is given by (12-6a); Q is the surface heat flux, an input parameter; $g = 9.8 \text{ m sec}^{-2}$; and θ_o is the surface temperature interpolated from the surface virtual temperature measurements T_{vn} as follows (compare with Eq. 7-108)

$$\theta_o(i,j,t_m) = \frac{\sum_{n=1}^N r_n^{-2} [T_{vn}(t_m) + 273]}{\sum_{n=1}^N r_n^{-2}} \quad (12-8)$$

where

$$r_n = [(i\Delta x - x_n)^2 + (j\Delta y - y_n)^2]^{1/2} \quad (12-9)$$

and (x_n, y_n) are the coordinates of surface weather station n . The values of w_* obtained from (12-7) will be needed again in stage WW1 below.

The input and output requirements of Stage K are summarized in Table 12-2.

Stage WWO

Here we calculate parameters λ_+ , w_+ , w_- and w associated with turbulence phenomena in Layer 0 and on the surface H_0 that separates Layers 0 and 1. The definitions of these parameters were developed in Part 1.

First we compute the vertical velocity variance on surface H_0 :

$$\sigma_{w0}^2 = u_*^2 \left[\frac{\phi_m - \xi}{1.2 f_m} \right]^{2/3} \quad (12-10)$$

where

$$\xi = h_0/L \quad (12-11)$$

$$\phi_m = \begin{cases} (1 - 16\xi)^{-1/4}, & \text{if } \xi < 0; \\ 1 + 5\xi & \text{if } \xi \geq 0 \end{cases} \quad (12-12)$$

$$f_m = \begin{cases} 0.4 [0.4 + 0.6 \exp(4\xi)], & \text{if } \xi < 0; \\ 0.4 [1.0 + 3.4\xi - 0.25\xi^2], & \text{if } \xi \geq 0. \end{cases} \quad (12-13)$$

and u_* is the friction velocity. In Eqs. (12-10) - (12-12), the variables σ_{w0} , u_* , and ξ are all functions of (i,j,t_m) .

Next we approximate the time derivative of h_0 by

$$\dot{h}_0(i,j,t_m) = [h_0(i,j,t_m) - h_0(i,j,t_{m-1})](\Delta t)^{-1} \quad (12-14)$$

where $\Delta t = 3600$ sec is the time interval at which h_0 and other variables in the processor network are available.

With these preliminary variables computed at each grid point and hour t_m , we can now calculate the following output parameters (see Eqs. 8-10, 8-12, and 8-13 of Part 1).

$$\lambda_+(i,j,t_m) = \frac{1}{2} \left[1 - \operatorname{erf} \left(\frac{\dot{h}_o(i,j,t_m)}{\sqrt{2}\sigma_{wo}(i,j,t_m)} \right) \right] \quad (12-15)$$

where erf is defined by

$$\operatorname{erf}(x) = \frac{2}{\sqrt{\pi}} \int_0^x e^{-\lambda^2} d\lambda. \quad (12-16)$$

$$w_+(i,j,t_m) = \frac{\sigma_{wo}}{\sqrt{2\pi}} \exp\left(-\frac{\dot{h}_o^2}{2\sigma_{wo}^2}\right) - \frac{\dot{h}_o}{2} \left[1 - \operatorname{erf} \left(\frac{\dot{h}_o}{\sqrt{2}\sigma_{wo}} \right) \right] \quad (12-17)$$

where σ_{wo} , given by (12-10), and \dot{h}_o , given by (12-14), are functions of (i,j,t_m) .

$$w_-(i,j,t_m) = \dot{h}_o(i,j,t_m) + w_+(i,j,t_m) \quad (12-18)$$

$$v(i,j,t_m) = u_*(i,j,t_m) \quad (12-19)$$

The parameter v is the entrainment velocity of ambient air into plumes from surface emissions and is discussed in detail in Chapters 5 and 8 of Part 1.

At this point it is advantageous to determine the values of the cumulus flux partition parameter Ψ defined in Part 1, Eq. 5-44. Interim values Ψ' of this parameter were developed in Processor P8, but we must test whether they satisfy criterion (5-47) of Part 1, namely

$$\Psi' \leq \frac{w_+ \lambda_+ (1 - \sigma_{T0})}{\sigma_c V_c} \quad (12-20)$$

where w_+ and λ_+ are the parameters that we just computed in (12-17) and 12-15) above, and where

$$V_c = - \frac{\bar{w}_2 - \bar{w}_c}{1 - \sigma_c} - f_\theta / \Delta\theta \quad (12-21)$$

(see Eq. 5-45 of Part 1). All of the variables in (12-20, 21) are functions of space and time and each of them, except w_+ and λ_+ , is an input to this processor. Consult Table 12-2 for definitions.

To obtain the final values of Ψ for output to the model, proceed as follows. First, at each grid point (i,j) and at each hour t_m compute the variable $V(i,j,t_m)$ defined by (12-21) using the input fields $\bar{w}_2(i,j,t_m)$, $\bar{w}_c(i,j,t_m)$, etc. Next, compute

$$\Psi''(i,j,t_m) = \frac{w_+(i,j,t_m) \lambda_+(i,j,t_m) [1 - \sigma_{T0}(i,j,t_m)]}{\sigma_c(i,j,t_m) V_c(i,j,t_m)} \quad (12-22)$$

where w_+ and λ_+ are from (12-17) and (12-15) and σ_{T0} and σ_c are inputs to this processor. Finally, we have

$$\Psi(i,j,t_m) = \min\{\Psi'(i,j,t_m), \Psi''(i,j,t_m)\} \quad (12-23)$$

where Ψ' is the interim estimate of Ψ that is input from processor P8. The values of Ψ should be recorded in the model input file MIF. This parameter is also required in the next stage of this processor.

Parameter summaries for Stage WW0 are given in Table 12-2.

Stage WW1

This stage computes the parameters w_1 , w_{1m} , and w_{D1} (defined in Part 1, Chapter 4) that are associated with material fluxes across surface H_1 . To compute these quantities we must first define several auxiliary parameters.

$\bar{w}'_{D1}(i,j,t_m)$ = vertical velocity at level z_1 during neutral and unstable conditions (input from P8)

$$\sigma_{w1}(i,j,t_m) = \begin{cases} 0.6w_*(i,j,t_m) & \text{if } L(i,j,t_m) < 0; \\ 0 & \text{if } L(i,j,t_m) \geq 0 \end{cases} \quad (12-24)$$

$$\dot{z}_1(i,j,t_m) = [z_1(i,j,t_m) - z_1(i,j,t_{m-1})](\Delta t)^{-1}$$

where

$$z_1(i,j,t_m) = h_1(i,j,t_m) + h_0(i,j,t_m)$$

(12-25)

where $\Delta t = 3600$ sec is the time interval at which h_1 and h_0 values are available.

Let w_m be the solution of the following transcendental equation:

$$\frac{\sigma_{w1}}{\sqrt{2\pi}} \exp \left[-\frac{(w_m - \bar{w}'_{D1})^2}{2\sigma_{w1}^2} \right] + \frac{\bar{w}'_{D1}}{2} [1 - \text{erf}(\frac{w_m - \bar{w}'_{D1}}{\sqrt{2}\sigma_{w1}})] = \frac{\psi_c \bar{w}_c}{1 - \sigma_{T1}} \quad (12-26)$$

where $\text{erf}(x)$ is defined by (12-16), ψ is from (12-23), etc. (Note that σ_{w1} , \bar{w}'_{D1} , ψ , σ_c , \bar{w}_c , σ_{T1} and hence w_m are all functions of (i,j) and t_m). Now let

$$\bar{w}_{R1}(i,j,t_m) = \bar{w}'_{D1}(i,j,t_m) - \dot{z}_1(i,j,t_m). \quad (12-27)$$

At each grid point (i,j) and each hour t_m compute

$$w_1(i,j,t_m) = \begin{cases} \frac{\psi \sigma_c \bar{w}_c}{1 - \sigma_{T1}} + \frac{\dot{z}_1}{2} [1 + \text{erf}(\frac{w_m - \bar{w}'_{D1}}{\sqrt{2} \sigma_{w1}})], & \text{if } L(i,j,t_m) \leq 0; \\ \dot{z}_1(i,j,t_m), & \text{if } L(i,j,t_m) > 0; \end{cases} \quad (12-28)$$

$$w_{1M}(i,j,t_m) = \begin{cases} \frac{\bar{w}_{R1}}{2} - \frac{\sigma_{w1}}{\sqrt{2\pi}} \exp[-\frac{\bar{w}_{R1}^2}{2\sigma_{w1}^2}] \\ - \frac{\bar{w}_{R1}}{2} \text{erf}(\frac{\bar{w}_{R1}}{\sqrt{2}\sigma_{w1}}), & \text{if } L(i,j,t_m) \leq 0 \\ -\eta_{vs}(i,j,t_m), & \text{if } L(i,j,t_m) > 0. \end{cases} \quad (12-29)$$

$$\bar{w}_{D1}(i,j,t_m) = \begin{cases} \bar{w}'_{D1}(i,j,t_m), & \text{if } L(i,j,t_m) \leq 0; \\ w_1(i,j,t_m) + w_{1M}(i,j,t_m), & \text{if } L(i,j,t_m) > 0. \end{cases} \quad (12-30)$$

To evaluate the function erf in (12-28 and 12-29) in the limit as $\sigma_{w1} \rightarrow 0$, the following procedure should be used.

$$\text{if } \sigma_{w1} = 0, \text{ erf } \left(\frac{A}{\sqrt{2}\sigma_{w1}} \right) = \text{SIGN}(A) \cdot 1 \quad (12-31)$$

This condition should be encountered only rarely since $\sigma_{w1} = 0$ when $L > 0$ (see Eq. 12-24) and in this case w_1 and w_{1M} have the forms given in (12-28) and (12-29) that do not involve the error function.

The input and output requirements of Stage WW1 are summarized in Table 12-2. The processor and its interfaces with the processor network are illustrated in Figure 12-2.

Table 12-2 Input and output variables of each stage of Processor P12.

Input Variable	Description	Source	Stage	Output Variable	Description
$h_1(i,j,t_m)$	thickness (m) of Layer 1 in cell (i,j) at hour t_m	P7	K	$K_1(i,j,t_m)$	horizontal eddy diffusivity (m^2/sec) in Layer 1, cell (i, hour t_m
$h_2(i,j,t_m)$	thickness (m) of Layer 2	P8		$K_2(i,j,t_m)$	same as K_1 except Layer 2
$h_3(i,j,t_m)$	thickness (m) of Layer 3	P8		$K_3(i,j,t_m)$	same as K_1 except Layer 3
$\sigma_c(i,j,t_m)$	fraction ($0 \leq \sigma_c \leq 1$) of sky covered by cumulus clouds in cell (i,j) at hour t_m	RAW		$w_*(i,j,t_m)$	convective velocity scale (m/sec) in cell (i,j), hour t_m
$\bar{w}_c(i,j,t_m)$	cumulus cloud updraft velocity (m/sec) in cell (i,j) at hour t_m	P8			
$Q(i,j,t_m)$	surface heat flux ($^{\circ}K$ m/sec) in cell (i,j) at hour t_m	P4			
$T_{vn}(t_m)$	surface virtual temperature ($^{\circ}C$) at surface weather station n hour t_m	P3			
$u_*(i,j,t_m)$	friction velocity (m/sec) in cell (i,j), hour t_m	P4	WWO	$\lambda_+(i,j,t_m)$	fraction ($0 \leq \lambda_+ \leq 1$) of surface H_0 covered by rising fluid

Table 12-2 (Continued)

Input Variable	Description	Source	Stage	Output Variable	Description
$L(i,j,t_m)$	Obukhov length (m) in cell (i,j) at hour t_m	P4	WW0 (cont.)	$w_+(i,j,t_m)$	average speed (m/s) of fluid moving up relative to surface
$h_o(i,j,t_m)$	thickness (m) of Layer 0 in cell (i,j) at hour t_m	P7		$w_-(i,j,t_m)$	same as w_+ except speed of downward moving fluid
				$v(i,j,t_m)$	entrainment velocity (m/sec) of plumes in Layer 0
$\sigma_{T0}(i,j,t_m)$	fraction ($0 \leq \sigma_{T0} \leq 1$) of surface H_0 in cell (i,j) penetrated by terrain at hour t_m	P7		$\psi(i,j,t_m)$	cumulus flux partition function (dimensionless)
$\sigma_c(i,j,t_m)$	see Stage K input list above	RAW			
$\bar{w}_2(i,j,t_m)$	mean vertical air speed (m/sec) on top surface of Layer 2 in cell (i,j) at hour t_m	P8			
$\bar{w}_c(i,j,t_m)$	see Stage K input list above	P8			
$f\theta/\Delta\theta(i,j,t_m)$	entrainment velocity (m/sec) at mixed layer top in cell (i,j) at hour t_m	P8			
$\psi'(i,j,t_m)$	interim estimate of cumulus partition parameter (dimensionless) in cell (i,j)	P8			

Table 12.2 (Concluded)

Input Variable	Description	Source	Stage	Output Variable	Description
$\bar{w}_{D1}^i(i,j,t_m)$	vertical velocity (m/sec) on surface H_1 in neutral and unstable conditions	P8	WW1	$w_1(i,j,t_m)$	vertical velocity parameter (m/sec) on surface H_1
				$w_{1M}(i,j,t_m)$	vertical velocity parameter (m/sec) on surface H_1
$w_*(i,j,t_m)$	convective velocity scale (m/sec)	Stage K		$\bar{w}_{D1}(i,j,t_m)$	vertical velocity (m/sec) on surface H_1 due to horizontal divergence in the flow field.
$h_1(i,j,t_m)$	thickness (m) of Layer 1 at (i,j,t_m)	P7			
$h_0(i,j,t_m)$	thickness (m) of Layer 0	P7			
$L(i,j,t_m)$	Obukhov length scale (m) in cell (i,j) , hour t_m	P4			
$\psi(i,j,t_m)$	cumulus flux partition function (dimensionless)	Stage WWO			
$\sigma_c(i,j,t_m)$	fraction ($0 \leq \sigma_c \leq 1$) of sky covered by cumulus clouds in cell (i,j) at hour t_m	RAW			
$\bar{w}_c(i,j,t_m)$	cumulus updraft velocity scale (m/sec)	P8			
$\sigma_{T1}(i,j,t_m)$	fraction ($0 \leq \sigma_{T1} \leq 1$) of surface H_1 penetrated by terrain	P7			
$\eta_{vs}(i,j,t_m)$	cold layer growth rate (m/sec)	P7			

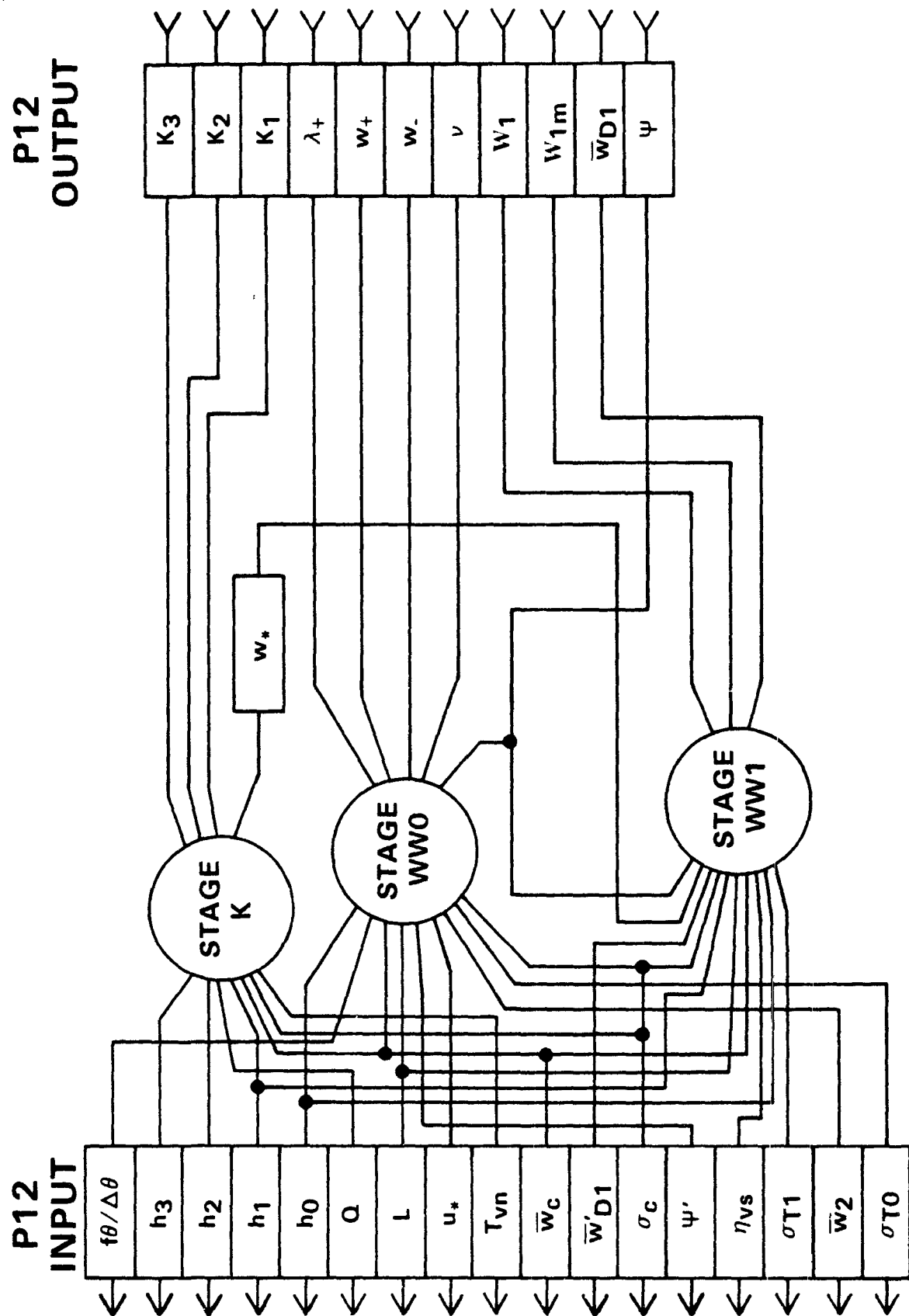


Figure 12-2. Illustration of Processor P12 and its input and output interfaces with the processor network.

SECTION 12

PROCESSOR P15

DEVELOPMENT

Processor P15 computes deposition resistances r and deposition velocities β for those pollutant species for which empirical data are available. These parameters are related through the friction velocity u_* , which is a function of local wind speed. To avoid coupling this processor to processor P11, which computes the flow fields, we will use friction velocity estimates based on the "raw" surface wind observations, namely those generated by P3, which are available in the PIF. These "raw" values constrain the magnitudes of the wind velocities generated by Processor P11; consequently, any inconsistencies between deposition velocity estimates based on the u_* values derived from the raw data and those implied by the output of P11 are most likely much smaller than the level of uncertainty in the empirical relationship between β and u_* that we employ here.

Step 1

Compute deposition resistances for each pollutant species. In this task we must adopt a numbering convention for the pollutants. In Part 1 of this report, we initiated the convention that species NO is pollutant "1"; NO₂ is pollutant "2"; and O₃ is pollutant "3". Beyond this the numbering is unspecified and one is free to select whatever system is convenient. In this

Processor description we will refer to all pollutants other than NO, NO₂, and O₃ by their names and leave the assignment of numbers to them as a task to be performed during the implementation phase of this work.

The deposition resistance $r(\underline{x}, t; \alpha)$ (sec/m) for species α averaged over the NEROS grid cell centered at \underline{x} at hour t is assumed to be

$$r(\underline{x}, t; \alpha) = \frac{\sum_{n=1}^{10} \tau(\underline{x}, n) r_n(\alpha, L)}{\sum_{n=1}^{10} \tau(\underline{x}, n)} \quad (15-1)$$

where $r_n(\alpha, L)$ is the deposition resistance of species α over land use type n during atmospheric conditions characterized by Obukhov length L at hour t . In Tables 15-1, 2, and 3 we list the r_n values currently available for several pollutants.

Table 15-1. Deposition resistances (sec/m) for SO₂ as a function of land use type n and stability L

(From Sheih, et al., 1979)

$n =$	$L < 0$	$L = \infty$	$L > 0$
1	900	900	10^3
2	100	300	10^3
3	100	300	10^3
4	100	300	10^3
5	100	300	10^3
6	100	300	10^3
7	0	0	0
8	0	0	0
9	70	250	800
10	100	300	10^3

use 0.0 if
 $L > 0$ and
 $RH(\underline{x}) \geq 0.9$

The surface relative humidity $RH(x,t)$ in each cell can be interpolated from the surface station values RH_n available from P3 using a weighting scheme like that employed in Eq. 12-8.

Table 15-2. Deposition resistances (sec/m) for ozone as a function of land use type n and stability L .
(From Wesely, 1981)

$n =$	$L < 0$	$L = \infty$	$L > 0$
1	300	400	400
2	70	200	400
3	150	200	300
4	60	300	$1.5 \cdot 10^3$
5	150	400	$1.5 \cdot 10^3$
6	70	300	$1.5 \cdot 10^3$
7 lake ocean	10^4 $2 \cdot 10^3$	10^4 $2 \cdot 10^3$	10^4 $2 \cdot 10^3$
8	0.0	0.0	0.0
9	100	250	300
10	100	200	350

Resistances for other pollutant species are not available in the current literature. Deposition velocities for several pollutants other than SO_2 and O_3 onto "vegetation" were reported by Hill and Chamberlain in 1975 (see Table 6 of McMahon and Denison (1979)), but these pertain to only one land use type and moreover, the associated atmospheric stability conditions were not specified. Lacking any other source of data, we propose to use the Hill and Chamberlain data to estimate the resistances of each species relative to O_3 ,

and subsequently to use that estimate and the values given in Table 12-2 to deduce crude estimates of resistances. From the Hill and Chamberlain data we estimate that the difference $\Delta r_2(\alpha)$ between the resistance of species α and that of ozone over agricultural land ($n=2$) (under unknown conditions of L) are as follows.

Table 15-3 Deposition resistances of several pollutants relative to that of ozone over agricultural land. (Deduced from data of Hill and Chamberlain, 1971)

Species (α)	$\Delta r_2 [=r_2(O_3)-r_2(\alpha)](\text{sec/m})$
O_3	0
SO_2	+25
CO	$<-10^5$
NO	-940
PAN	-100
NO_2	+ 7

If we assume that these values apply for $L<0$, then we can estimate $r_2(\text{PAN}, L<0)$, for example, to be

$$\begin{aligned}
 r_2(\text{PAN}, L<0) &= r_2(O_3, L<0) - \Delta r_2(\text{PAN}) \\
 &= 70 + 100 \\
 &= 170 \text{ sec/m.}
 \end{aligned}$$

One conflict that is readily apparent with this method is that the value of $r_2(SO_2, L<0)$ deduced from Table 12-3 does not agree with the value given in Table 12-1. This discrepancy is indicative of the wide scatter in the

reported deposition rates of the various species. In the interim, we propose that approximate values of $r_n(\alpha, L)$ be derived from the Δr_2 method above. That is, we assume

$$r_2(\alpha, L < 0) = r_2(3, L < 0) - \Delta r_2(\alpha) \quad (15-2)$$

for species $\alpha = \text{CO}, \text{NO}, \text{NO}_2$ and PAN. The values for the other land use categories $n=1, 3, 4 \dots 10$ and other L values can be taken as having the same ratio to the $n=2, L < 0$ values as those given above for ozone.

The output of Step 2 should be deposition resistances $r(\underline{x}, \alpha)$ (sec/m) for species $\alpha = \text{O}_3, \text{SO}_2, \text{CO}, \text{NO}, \text{NO}_2$ and PAN for each cell \underline{x} of the NEROS grid for each hour of the simulation period. These values are used in the next Step to compute deposition velocities.

Step 2

Compute the average deposition velocity $\beta(\underline{x}, t; \alpha)$ (m s^{-1}) of each species α in each NEROS grid cell at hour t using the following expression from Sheih et al. (1979):

$$\beta(\underline{x}, t; \alpha) = 0.4u_* \left[\ln\left(\frac{z}{z_0}\right) + 2.6 + 0.4u_* r(\underline{x}, t; \alpha) - \psi_c \right]^{-1} \quad (15-3)$$

where u_* is the friction velocity (m s^{-1}) in the cell centered at \underline{x} at hour t (from P4); z_0 is the effective surface roughness (m) for this cell (from P4); z is the elevation at which the concentration of species α is taken for the purpose of estimating the deposition flux from β (we will use

$$z = \frac{1}{2} \Delta z_0 \approx 10\text{m} \quad (15-4)$$

see Part I, Eq. 5-6b); and the function ψ_c is given by (Sheih et al., 1979)

$$\psi_c = \begin{cases} \exp \{0.598 + 0.390 \ln (-z/L) - 0.090 [\ln (-z/L)]^2\}, & \text{if } L < 0; \\ -5z/L, & \text{if } L > 0; \end{cases} \quad (15-5)$$

where L is the Obukhov length (m) for the cell centered at \underline{x} at hour t (from P4).

The inputs and outputs of each step of Processor P15 are summarized in Table 15-1; and the processor and its interfaces with the processor network are illustrated in Figure 15-1.

Table 15-1 Summary of the input and output parameters of each Step of Processor P15.

Input Parameter	Description	Source	Step	Output Parameter	Description
$r(\underline{x},n)$	fraction of NEROS cell centered at \underline{x} in land use type n , $n=1,2,\dots,10$. (dimensionless)	RAW	1	$r(\underline{x},t;\alpha)$	effective deposition resistance (sec/m) of cell centered at \underline{x} to deposition of species $\alpha=O_3, NO, NO_2$, etc. at hour t .
$RH_n(t)$	relative humidity (dimensionless) at surface weather station n at hour t .	P3			
$L(\underline{x},t)$	Obukhov length (m) in cell centered at \underline{x} at time t .	P4			
$z_0(\underline{x})$	surface roughness (m) of cell centered at \underline{x} .	P4	2	$\beta(\underline{x},t;\alpha)$	effective deposition velocity (m/sec) of species $\alpha=O_3, NO, NO_2$, etc., in cell centered at \underline{x} at hour t . Reference level $z=10m$)
$u_*(\underline{x},t)$	friction velocity (m/sec) in cell at \underline{x} at hour t .	P4			
$L(\underline{x},t)$	Obukhov length (m) in cell at \underline{x} at hour t .	P4			
$r(\underline{x},t;\alpha)$	deposition resistance (see Step 1 output).	Step 1			

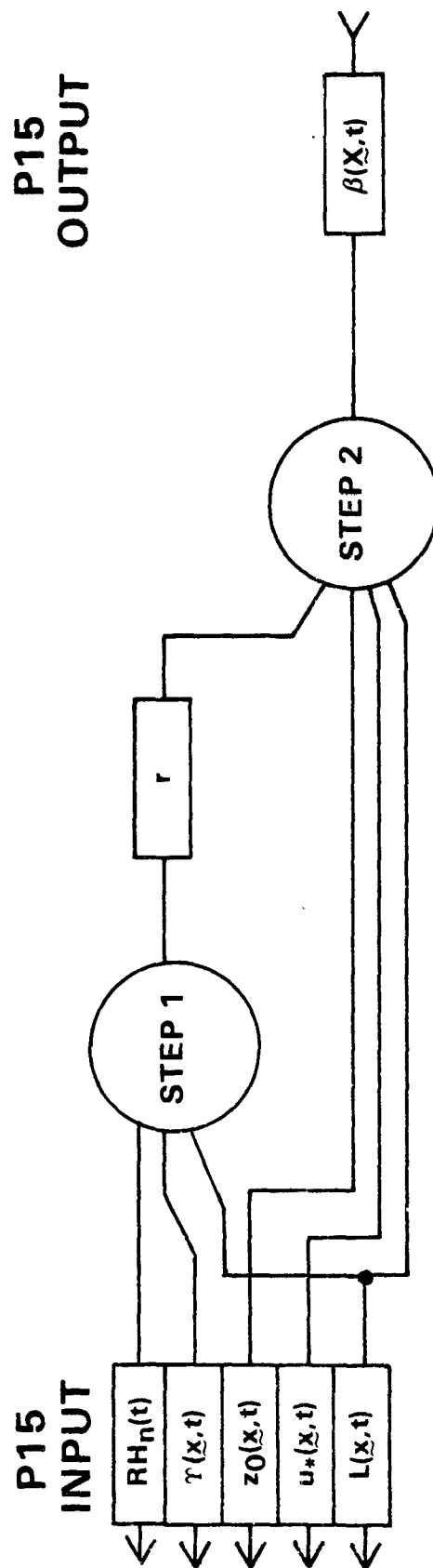


Figure 15-1. Illustration of Processor P15 and its input and output interfaces with the processor network.

SECTION 13

THE B-MATRIX COMPILER

INTRODUCTION

The b-matrix compiler (BMC) translates the variables generated by the network of processors into the elements of the "b-matrix" defined in Part 1, Section 9, and into the variables required in the transport and diffusion terms of the "Γ-equation," also defined in Part 1, Section 9. The interface between the BMC and the processor network is the model input file (MIF). This is illustrated schematically in Figure 1-1.

The mathematical relationships among the MIF variables and the b-matrix elements were summarized in Appendix C of Part 1. A complicating aspect of these relationships is that the values of a small group of the b-matrix elements are dependent on the local ozone concentration, which is not known until during execution of the model. Fortunately, all of the matrix elements in this group can have only one of two predeterminable values, depending upon the local value of the function U_0 which is defined as follows:

$$U_0 = \begin{cases} 1, & \text{if } \zeta_{NO} > \zeta Q_{O_3} < O_3 >_1; \\ 0, & \text{otherwise} \end{cases} \quad (16-1)$$

where ζ_{NO} is the local emission rate of NO in Layer 0 and

$$Q_x = \frac{w_- \lambda_-}{w_+ \lambda_+ + (1-\zeta) \beta_x}, \text{ all species } x. \quad (16-2)$$

Thus, the BMC must provide to the model both of the possible values of each b-matrix element that is concentration dependent. The appropriate value can then be selected during execution of the model based on the local value of U_0 . In the next section we present the expressions for each of the b-matrix elements in terms of the MIF variables. (Definitions of each variable can be found in Table 13-1 at the end of this section.)

THE B-MATRIX ELEMENTS

Let

$$e_w^x \equiv (\sigma_{T0} - \sigma_{T1})\beta_x - (1 - \sigma_{T1})(w_1 + w_{1m}) \quad (16-3)$$

$$e_0^x \equiv w_- \lambda_- - w_+ \lambda_+ (1 - \xi)(1 - \alpha)Q_x \quad (16-4)$$

Ozone (O_3)

$$b_{11} = \begin{cases} b_{11}^* = \frac{1}{h_1} [e_w^0 + h_1 + (1 - \sigma_{T0})e_0^0], & \text{if } U_0 = 1; \\ b_{11}^{**} = \frac{1}{h_1} [e_w^0 + h_1 + (1 - \sigma_{T0})(e_0^0 - \frac{(1 - \alpha)u^2 \xi Q_{O_3}}{(\beta_{O_3} + u)})], & \text{if } U_0 = 0. \end{cases} \quad (16-5)$$

$$b_{12} = \frac{1}{h_1} (1 - \sigma_{T1})w_{1m} \quad (16-6)$$

$$b_{13} = 0 \quad (16-7)$$

$$g_1 = \begin{cases} g_{10_3}^* = 0, & \text{if } U_0 = 1; \\ g_{10_3}^{**} = - \frac{(1 - \sigma_{T0})(1 - \alpha)u \tilde{S}_{NO}}{h_1(\beta_{O_3} + u)} \end{cases} \quad (16-8)$$

Nitric oxide (NO)

$$b_{11} = \frac{1}{h_1} [e_w^{NO} + \dot{h}_1 + (1-\sigma_{T0})(e_o^{NO} - \frac{1-\alpha}{\nu+\beta_{NO}} \nu^2 \zeta_{Q_{NO}})] \quad (16-9)$$

$$b_{12} = \frac{1}{h_1} (1-\sigma_{T1}) w_{1m} \quad (16-10)$$

$$b_{13} = 0 \quad (16-11)$$

$$g_1 = \begin{cases} g_{1NO}^* - \hat{g}_{NO} <0_3>_1, & \text{if } U_0 = 1; \\ g_{1NO}^{**}, & \text{if } U_0 = 0. \end{cases} \quad (16-12)$$

where

$$g_{1NO}^* \equiv s_1^{NO} + \frac{(1-\sigma_{T0})(1-\alpha)}{h_1(\beta_{NO}+\nu)} \nu \tilde{s}_{NO} \quad (16-13)$$

$$g_{1NO}^{**} \equiv s_1^{NO} \quad (16-14)$$

$$\hat{g}_{1NO} \equiv \frac{(1-\sigma_{T0})(1-\alpha)}{h_1(\beta_{NO}+\nu)} \nu^2 \zeta_{Q_{O_3}}. \quad (16-15)$$

Nitrogen dioxide (NO₂)

$$b_{11} = \frac{1}{h_1} [e_w^{NO_2} + \dot{h}_1 + (1-\sigma_{T0})(e_o^{NO_2} - \frac{(1-\alpha)}{\nu+\beta_{NO_2}} \nu^2 \zeta_{Q_{NO_2}})] \quad (16-14)$$

$$b_{12} = \frac{1}{h_1} (1-\sigma_{T1}) w_{1m} \quad (16-15)$$

$$b_{13} = 0 \quad (16-16)$$

$$g_1 = \begin{cases} g_{1NO_2}^* + \hat{g}_{NO_2} <0_3>_1, & \text{if } U_0 = 1; \\ g_{1NO_2}^{**}, & U_0 = 0. \end{cases} \quad (16-17)$$

where

$$g_{1\text{NO}_2}^* \equiv s_1^{\text{NO}_2} + \frac{(1-\sigma_{\text{T0}})(1-\alpha)}{h_1(\beta_{\text{NO}_2} + \nu)} \nu \tilde{s}_{\text{NO}} \quad (16-18)$$

$$g_{1\text{NO}_2}^{**} \equiv s_1^{\text{NO}_2} + \frac{(1-\sigma_{\text{T0}})(1-\alpha)\nu}{h_1(\beta_{\text{NO}_2} + \nu)} (\tilde{s}_{\text{NO}} + \tilde{s}_{\text{NO}_2}) \quad (16-19)$$

$$\hat{g}_{1\text{NO}_2} \equiv \frac{(1-\sigma_{\text{T0}})(1-\alpha)}{h_1(\beta_{\text{NO}_2} + \nu)} \nu^2 \xi Q_{03} \quad (16-20)$$

species χ (excluding O_3 , NO and NO_2)

$$b_{11} = \frac{1}{h_1} [e_w^\chi + \dot{h}_1 + (1-\sigma_{\text{T0}})(e_0^\chi - \frac{1-\alpha}{\nu+\beta_\chi} \nu^2 \xi Q_\chi)] \quad (16-21)$$

$$b_{12} = \frac{1}{h_1} (1-\sigma_{\text{T1}}) w_{1m} \quad (16-22)$$

$$b_{13} = 0 \quad (16-23)$$

$$g_{1\chi} = s_1^\chi + \frac{(1-\sigma_{\text{T0}})(1-\alpha)}{h_1(\nu+\beta_\chi)} \nu \tilde{s}_\chi \quad (16-24)$$

all species

$$b_{21} = \frac{1}{h_2} (1-\sigma_{\text{T1}})(w_1 + w_{1m} - \bar{w}_{\text{D1}}) \quad (16-25)$$

$$b_{22} = \frac{1}{h_2} [\dot{h}_2 + \sigma_{\text{T1}} \beta_\chi + (1-\sigma_{\text{T1}})(\bar{w}_{\text{D1}} - w_{1m}) - \dot{z}_2 + \frac{\psi \sigma_c (\bar{w}_2 - \bar{w}_c)}{1-\sigma_c} + \frac{f\theta}{\Delta\theta} (1-\sigma_c + \sigma_c \psi)] \quad (16-26)$$

$$b_{23} = - \frac{1}{h_2} (1-\sigma_c) \frac{f\theta}{\Delta\theta} \quad (16-27)$$

$$g_2 = s_2 \quad (16-28)$$

Ozone (O_3)

$$b_{31} = \begin{cases} b_{31}^* \equiv \frac{\psi M Q_{O_3}}{h_3} [1-\xi], & \text{if } U_o = 1; \\ b_{31}^{**} \equiv \frac{\psi M Q_{O_3}}{h_3} \left[\frac{\xi v}{\beta_{O_3} + v} + 1-\xi \right], & \text{if } U_o = 0. \end{cases} \quad (16-29)$$

$$b_{32} = \frac{1}{h_3} (1-\psi)M \quad (16-30)$$

$$b_{33} = \frac{1}{h_3} (-M + \dot{H}_3 U_3) \quad (16-31)$$

$$g_3 = \begin{cases} g_{303}^* \equiv \frac{1}{h_3} \dot{H}_3 U_3 C_{\infty}^{O_3}, & \text{if } U_o = 1; \\ g_{303}^{**} \equiv \frac{1}{h_3} \left[\frac{\psi M \xi \tilde{S}}{\xi(\beta_{O_3} + v)} + \dot{H}_3 U_3 C_{\infty}^{O_3} \right], & \text{if } U_o = 0. \end{cases} \quad (16-32)$$

Nitric oxide (NO)

$$b_{31} = \frac{\psi M Q_{NO}}{h_3} \left[\frac{\xi v}{v + \beta_{NO}} + 1-\xi \right] \quad (16-33)$$

$$b_{32} = \frac{1}{h_3} (1-\psi)M \quad (16-34)$$

$$b_{33} = \frac{1}{h_3} [-M + \dot{H}_3 U_3] \quad (16-35)$$

$$g_3 = \begin{cases} g_{3NO}^* + \hat{g}_{3NO} <O_3>_1, & \text{if } U_o = 1; \\ g_{3NO}^{**}, & \text{if } U_o = 0. \end{cases} \quad (16-36)$$

where

$$g_{3NO}^* = \frac{1}{h_3} [\dot{H}_3 U_3 C_{\infty}^{NO} - \frac{\psi M \xi \tilde{S}_{NO}}{\xi(\beta_{NO} + v)}] \quad (16-37)$$

$$g_{3NO}^{**} = \frac{1}{h_3} \dot{H}_3 U_3 c_{\infty}^{NO} \quad (16-38)$$

$$\hat{g}_{3NO} = \frac{\psi M \xi u Q_{O_3}}{h_3 (\beta_{NO} + u)} \quad (16-39)$$

Nitrogen dioxide (NO_2)

$$b_{31} = \frac{\psi M Q_{NO_2}}{h_3} \left[\frac{\xi u}{u + \beta_{NO_2}} + 1 - \xi \right] \quad (16-40)$$

$$b_{32} = \frac{1}{h_3} (1 - \psi) M \quad (16-41)$$

$$b_{33} = \frac{1}{h_3} (-M + \dot{H}_3 U_3) \quad (16-42)$$

$$g_3 = \begin{cases} g_{3NO_2}^* - \hat{g}_{3NO_2} < O_3 >_1, & \text{if } U_o = 1; \\ g_{3NO_2}^{**}, & \text{if } U_o = 0 \end{cases} \quad (16-43)$$

where

$$g_{3NO_2}^* = \frac{1}{h_3} [\dot{H}_3 U_3 c_{\infty}^{NO_2} - \frac{\psi M \xi \tilde{S}_{NO_2}}{\xi (\beta_{NO_2} + u)}] \quad (16-44)$$

$$g_{3NO_2}^{**} = \frac{1}{h_3} [\dot{H}_3 U_3 c_{\infty}^{NO_2} - \frac{\psi M \xi}{\xi (\beta_{NO_2} + u)} (\tilde{S}_{NO} + \tilde{S}_{NO_2})] \quad (16-45)$$

$$\hat{g}_{3NO_2} = \frac{\psi M \xi u Q_{O_3}}{h_3 (\beta_{NO_2} + u)} \quad (16-46)$$

species χ (excluding O_3 , NO and NO_2)

$$b_{31} = \frac{\psi M Q_\chi}{h_3} \left[\frac{\xi u}{u + \beta_\chi} + 1 - \xi \right] \quad (16-47)$$

$$b_{32} = \frac{1}{h_3} (1 - \psi) M \quad (16-48)$$

$$b_{33} = \frac{1}{h_3} [-M + \dot{H}_3 U_3] \quad (16-49)$$

$$g_{3\chi} = \frac{1}{h_3} \dot{H}_3 U_3 C_\infty^\chi - \frac{\psi M \xi \tilde{\zeta}_\chi}{h_3 \xi (u + \beta_\chi)} \quad (16-50)$$

where

$$U_3 = \begin{cases} 1, & \text{if } \dot{H}_3 > 0; \\ 0, & \text{if } \dot{H}_3 \leq 0. \end{cases} \quad (16-51)$$

$$M = \sigma_c \left[\frac{\bar{w}_2 - \bar{w}_c}{1 - \sigma_c} + f\theta/\Delta\theta \right] \quad (16-52)$$

$$\dot{H}_3 = d\bar{H}_3/dt \quad (16-53)$$

PREPARATION OF TERMS IN THE Γ -EQUATION

In designing the algorithm that treats the advection and diffusion processes, we assumed that these phenomena could be expressed in the form (see Eq. 9-5 of Part 1)

$$\frac{\partial \Gamma}{\partial t} + u \frac{\partial \Gamma}{\partial x} + v \frac{\partial \Gamma}{\partial y} - K_x \frac{\partial^2 \Gamma}{\partial x^2} - K_y \frac{\partial^2 \Gamma}{\partial y^2} = 0 \quad (16-54)$$

Consequently, the basic equation 2-29 of Part 1 must be cast in a form compatible with (16-54). The only terms in (2-29) that are involved in this transformation are

$$\begin{aligned}
& \frac{\partial}{\partial t} \langle c \rangle_j + \mu_\lambda \langle u \rangle_j \frac{\partial \langle c \rangle_j}{\partial \lambda} + \mu_\phi \langle v \rangle_j \frac{\partial \langle c \rangle_j}{\partial \phi} \\
& + \mu_\lambda \langle u'c' \rangle_j \frac{\partial \ln V_j}{\partial \lambda} + \mu_\phi \langle v'c' \rangle_j \frac{\partial \ln V_j}{\partial \phi} \\
& + \mu_\lambda \frac{\partial}{\partial \lambda} \langle u'c' \rangle_j + \mu_\phi \frac{\partial}{\partial \phi} \langle v'c' \rangle_j = 0
\end{aligned} \tag{16-55}$$

where $\mu_\lambda = (a \cos \phi)^{-1}$ and $\mu_\phi = a^{-1}$ are metric factors and a is the radius of the earth. The fluctuation quantities u' , v' and c' in (16-55) represent deviations of the value of the given parameter at any point in space from the local cell averaged value, denoted by $\langle \rangle_j$. In Section 7 of Part 1, we proposed to express the fluxes $\langle u'c' \rangle_j$, etc. associated with the subgrid scale fluctuations in the gradient transfer form (see Eq. 7-2, Part 1)

$$\langle u'c' \rangle_j = -K_j \mu_\lambda \frac{\partial \langle c \rangle_j}{\partial \lambda} \tag{16-56a}$$

$$\langle v'c' \rangle_j = -K_j \mu_\phi \frac{\partial \langle c \rangle_j}{\partial \phi} \tag{16-56b}$$

where the K_j are diffusivities specified in Stage K of processor P12. Making use of (16-56) in (16-55) we get

$$\begin{aligned}
& \frac{\partial \langle c \rangle_j}{\partial t} + [\mu_\lambda \langle u \rangle_j - \mu_\lambda^2 K_j \frac{\partial \ln V_j}{\partial \lambda} - \mu_\lambda^2 \frac{\partial K_j}{\partial \lambda}] \frac{\partial \langle c \rangle_j}{\partial \lambda} \\
& + [\mu_\phi \langle v \rangle_j - \mu_\phi^2 K_j \frac{\partial \ln V_j}{\partial \phi} - \mu_\phi^2 \frac{\partial K_j}{\partial \phi}] \frac{\partial \langle c \rangle_j}{\partial \phi}
\end{aligned}$$

$$- \mu_{\lambda}^2 K_j \frac{\partial^2 \langle c \rangle_j}{\partial \lambda^2} - \mu_{\phi}^2 K_j \frac{\partial^2 \langle c \rangle_j}{\partial \phi^2} = 0 \quad (16-57)$$

This equation is of the form (16-54) required by the algorithm in the model that handles the advection and diffusion processes (see Appendix A of P7). Two basic operations are now necessary to complete the preparation of the equation for numerical solution: (1) to convert the units of all parameters -- the model treats the equations in (λ, ϕ) space rather than physical space (x, y) ; (2) to convert the effective advection velocities, i.e., the terms in brackets in (16-57), into coordinates (λ^*, ϕ^*) of the upstream trajectories associated with each grid point in the model domain (see Figure 7-A1 of P7). Below we outline the details of specific operations that are required.

Step 1

Four parameter fields are involved in these operations: the two velocity components $\langle u \rangle_j$ and $\langle v \rangle_j$, the diffusivities K_j ; and the cell volumes V_j . Values of each of these are available in MIF for each layer $j=1,2,3$ and for each grid cell in the model domain. All data in the MIF are in mks units. This means that the units of $\langle u \rangle$ and $\langle v \rangle$ are $m \cdot s^{-1}$; K has units of $m^2 s^{-1}$; and V has units of m^3 . The first task is to convert all length units from meters to radians.

This is accomplished using the metric factors μ_{λ} and μ_{ϕ} which are measures of the arc angles in radians of longitude and latitude, respectively, per unit length on the earth's surface. Thus, for example, $\mu_{\lambda} \langle u \rangle_j$ is the east-west component of wind speed in radians (of longitude) per second.

Let (I,J) denote (column, row) of any cell in the model domain. The metric factor μ_λ varies with J , namely

$$\mu_\lambda(J) = (a \cos \phi_J)^{-1} \quad (16-58)$$

where ϕ_J is the latitude in radians of row J , but μ_ϕ is a constant, namely

$$\mu_\phi = a^{-1} \quad (16-59)$$

where a is the earth's radius:

$$a = 6,367,333. \text{ meters} \quad (16-60)$$

Now convert the velocity and diffusivity fields obtained from the MIF into their corresponding values in (λ, ϕ) space for each layer $j=1,2,3$ and grid point (I,J) as follows:

$$\langle u(I,J) \rangle_j^* = \mu_\lambda(J) \langle u(I,J) \rangle_j, \quad (16-61)$$

$$\langle v(I,J) \rangle_j^* = \mu_\phi \langle v(I,J) \rangle_j, \quad (16-62)$$

$$K_{xj}^*(I,J) = [\mu_\lambda(I,J)]^2 K_j(I,J), \quad (16-63)$$

$$K_{yj}^*(I,J) = \mu_\phi^2 K_j(I,J). \quad (16-64)$$

The K_{xj}^* and K_{yj}^* fields should be recorded directly in the output file of the BMC for input into the model.

Step 2

Take the natural log of each cell volume V_j in each layer at each grid

point to produce arrays of $(\ln V_j)$. For each layer j compute estimates of $\frac{\partial}{\partial \lambda} \ln V_j$ at every grid point (I, J) as follows

$$\begin{aligned} \frac{\partial}{\partial \lambda} \ln V_j(I, J) \approx DXLV(I, J, j) = [\ln(V_j(I+1, J)) \\ - \ln(V_j(I-1, J))]/(2\delta\lambda) \end{aligned} \quad (16-65)$$

where

$$\delta\lambda = \frac{1}{4} \left(\frac{2\pi}{360} \right) = \text{model grid interval in } \lambda.$$

On the western boundary where $I=1$, use

$$DXLV(I, J, j) = [\ln(V_j(2, J)) - \ln(V_j(1, J))]/\delta\lambda \quad (16-66)$$

and on the eastern boundary

$$DXLV(I_{MAX}, J, j) = [\ln(V_j(I_{MAX}, J)) - \ln(V_j(I_{MAX}-1, J))]/\delta\lambda \quad (16-67)$$

In the same manner define

$$\begin{aligned} \frac{\partial}{\partial \phi} \ln V_j(I, J) \approx DYLV(I, J, j) = [\ln(V_j(I, J+1)) \\ - \ln(V_j(I, J-1))]/(2\delta\phi) \end{aligned} \quad (16-68)$$

where

$$\delta\phi = 1/6 \left(\frac{2\pi}{360} \right) = \text{grid interval in } \phi. \quad (16-69)$$

On the south and north boundaries, where $J=1$ and J_{MAX} , respectively, use approximations similar to (16-66) and (16-67) for $DYLV(I, J, j)$.

Step3

Form approximations of the derivatives of K_{xj}^* and K_{yj}^* as follows:

$$\frac{\partial K_{xj}^*}{\partial \lambda} \approx DXKX(I, J, j) = [K_{xj}^*(I+1, J) - K_{xj}^*(I-1, J)]/(2\delta\lambda) \quad (16-70)$$

$$\frac{\partial K_{yj}^*}{\partial \phi} \approx DYKY(I,J,j) = [K_{yj}^*(I,J+1) - K_{yj}^*(I,J-1)] / (2\delta\phi)$$

Use approximations similar to (16-66) and (16-67) to treat grid points on the boundaries.

Step 4

Form the effective advection velocity components, i.e., the terms in brackets in (16-57) as follows.

$$u_{eff}(I,J,j) = \langle u(I,J) \rangle_j^* - K_{xj}^*(I,J) * DXLV(I,J,j) - DXKX(I,J,j) \quad (16-71)$$

$$v_{eff}(I,J,j) = \langle v(I,J) \rangle_j^* - K_{yj}^*(I,J) * DYLV(I,J,j) - DYKY(I,J,j) \quad (16-72)$$

Values of u_{eff} and v_{eff} must be computed for each layer $j=1,2,3$; each grid point in the model domain; and each time step Δt ($= 30$ min.).

Step 5

Compute the "back track" points associated with each grid point (I,J), each layer $j=1,2,3$, and each time step. This is done as follows:

Let $u_{eff}(I,J,j,N)$, $v_{eff}(I,J,j,N)$ denote the

effective velocity components, (16-71) and (16-72), at time step N, i.e., at time $t=t_0+N\Delta t$. Consider a given grid cell (I,J,j) at a given time step N. Compute

$$\Delta\lambda_1 = -u_{\text{eff}}(I,J,j,N)\Delta\tau \quad (16-73)$$

$$\Delta\phi_1 = -v_{\text{eff}}(I,J,j,N)\Delta\tau \quad (16-74)$$

where $\Delta\tau = \Delta t/n$, say $\Delta\tau = \Delta t/3 = 10$ minutes. These increments define a point (λ_1, ϕ_1) in (λ, ϕ) space, namely

$$\begin{aligned} \lambda_1 &= I(\delta\lambda) + \Delta\lambda_1 \\ \phi_1 &= J(\delta\phi) + \Delta\phi_1. \end{aligned} \quad (16-75)$$

Fit a biquintic polynomial to the $(u_{\text{eff}}, v_{\text{eff}})$ values at time step N on the 36-grid-point square centered at the cell nearest (λ_1, ϕ_1) . Note that the polynomial must be in terms of (λ, ϕ) rather than (x, y) . With this polynomial and a linear interpolation in time between $N\Delta t$ and $(N-1)\Delta t$, estimate the values of $(u_{\text{eff}}, v_{\text{eff}})$ at the point (λ_1, ϕ_1) at time $N\Delta t - \Delta\tau$, i.e.,

$$u_{\text{eff}}(\lambda_1, \phi_1, j, N\Delta t - \Delta\tau), v_{\text{eff}}(\lambda_1, \phi_1, j, N\Delta t - \Delta\tau).$$

Now compute the new point

$$\begin{aligned} \lambda_2 &= \lambda_1 + [-u_{\text{eff}}(\lambda_1, \phi_1, j, N\Delta t - \Delta\tau)\Delta\tau] \\ \phi_2 &= \phi_1 + [-v_{\text{eff}}(\lambda_1, \phi_1, j, N\Delta t - \Delta\tau)\Delta\tau]. \end{aligned} \quad (16-76)$$

Using the biquintic space approximation and the linear time interpolation again to estimate u_{eff} and v_{eff} at $(\lambda_2, \phi_2, N\Delta t - 2\Delta\tau)$, compute finally

$$\begin{aligned} (\lambda^*) \lambda_{\text{BT}j} &= \text{LAMBT}(I,J,j,N) = \lambda_2 + [-u_{\text{eff}}(\lambda_2, \phi_2, j, N\Delta t - 2\Delta\tau)\Delta\tau] \\ (\phi^*) \phi_{\text{BT}j} &= \text{PHIBT}(I,J,j,N) = \phi_2 + [-v_{\text{eff}}(\lambda_2, \phi_2, j, N\Delta t - 2\Delta\tau)\Delta\tau]. \end{aligned} \quad (16-77)$$

These are the coordinates of the "back track" point associated with cell (I,J,j) at time $N\Delta t$ when the subinterval $\Delta\tau = \Delta t/3$. This is the point indicated by (x^*, y^*) in Figure 7-A1 of P7. Values of LAMBT and PHIBT should be recorded on the b-matrix tape, i.e., the output file of the BMC, for all I,J,j and all time steps $N=1, \dots, N_{\text{MAX}}$.

The diffusivity fields K_{xj}^* and K_{yj}^* should also be recorded on the b-matrix tape for all I,J,j and all times steps $N=1,\dots,NMAX$.

The b-matrix compiler is illustrated in Figure BMC-1, and each of the variables in the MIF is defined in Table BMC-1.

Table BMC-1. Definitions of parameters in the Model Input File (MIF).

Parameter	Definition
h_n	Thickness of model layer n , $n=1,2,3$.
$\langle u \rangle_n$	Average east-west wind component in model layer $n=1,2,3$.
$\langle v \rangle_n$	Average north-south wind component in model layer $n=1,2,3$.
K_n	Horizontal eddy diffusivity in model layer $n=1,2,3$.
σ_{T0}	Fraction of the top surface of Layer 0 penetrated by terrain in a given grid cell.
σ_{T1}	Fraction of the top surface of Layer 1 penetrated by terrain in a given grid cell.
σ_c	Fraction of sky covered by cumulus clouds in a given cell.
v	Plume entrainment velocity in Layer 0.
ζ	Fraction of Layer 0 occupied by line and point source plumes.
β_x	Deposition velocity of pollutant species X .
λ_+	Fraction of the top surface of Layer 0 covered by ascending fluid.
w_+	Mean speed of upward moving fluid on top surface of Layer 0.
w_-	Mean speed of descending fluid on top surface of Layer 0.
ω_1	Composite vertical turbulence parameter on top surface of Layer 1.

Table BMC-1. (continued)

Parameter	Definition
w_{1m}	Composite vertical turbulence parameter on top surface of Layer 1.
\bar{w}_{D1}	Mean vertical air velocity on top surface of Layer 1 induced by flow divergence in Layer 1.
\bar{w}_2	Mean vertical air velocity on top surface of Layer 2.
\bar{w}_c	Cumulus updraft velocity scale.
$f\theta/\Delta\theta$	Turbulent entrainment velocity at mixed layer top.
ψ	Fraction of cumulus cloud volume flux drawn from Layer 0.
\dot{z}_2	Local time rate of change of the elevation of the top of Layer 2.
\dot{H}_3	Volume flux across top of Layer 3.
\tilde{S}_x	Emission rate of surface sources of pollutant x.
S_1^x	Emission rate of sources of pollutant x in Layer 1.
S_2^x	Emission rate of sources of pollutant x in Layer 2.
c_∞^x	Concentration of species x in air above the top of model Layer 3.

REFERENCES

- Artoz, M. A. and J. C. Andre, (1980): "Similarity Studies of Entrainment in Convective Mixed Layer", Boundary Layer Meteor., Vol. 19, pp 51-66.
- Brost, R. and J. C. Wyngaard, (1978): "A Model Study of the Stably Stratified Planetary Boundary Layer", J. Atmos. Sci., Vol. 35, pp 1427-1440.
- Bullock, O. R. (1983): "Spatial and Temporal Interpolation of NEROS Radiosonde Winds", M.S. Thesis, Dept. of Marine, Earth and Atmospheric Sciences, N.C. State University, 105 pages.
- Demerjian, K. L., (1983): personal communication.
- Demerjian, K. L. and K. L. Schere (1979): "Applications of a Photochemical Box Model for Ozone Air Quality in Houston, Texas". Proceedings, Ozone/Oxidants: Interactions with the Total Environment II, Houston, TX, 14-17 Oct. 1979, APCA, Pittsburgh, PA, pp 329-352.
- Godowitch, J. M. and J. K. S. Ching (1980): "Formation and Growth of the Nocturnal Inversion Layer at an Urban and Rural Location", Proc. Second AMS Joint Conference on Applications of Air Pollution Meteorology, New Orleans, LA, pp 165-172.
- Golder, D., (1972): "Relations Among Stability Parameters in the Surface Layer", Boundary Layer Meteor., Vol. 3, pp 47-58.
- Haltiner, G. J., (1971): Numerical Weather Prediction, John Wiley and Sons, New York, NY. 317 pages.
- Hill, A. C. and E. M. Chamberlain, (1976): "The Removal of Water Soluble Gases from the Atmosphere by Vegetation", Proc. Symp. on Atmosphere - Surface Exchange of Particles and Gases, ERDA Symp. Series, NTIS, pp 153-170.
- Holtslag, A. A. M. and A. P. Van Ulden, (1983): "A Simple Scheme for Daytime Estimates of the Surface Fluxes from Routine Weather Data", J. Climate and Applied Meteor., Vol. 22, pp 517-529.
- Jones, F. L., R. W. Moksad and A. R. Laird, (1981): "A Simple Method for Estimating the Influence of Cloud Cover on the NO₂ Photolysis Rate Constant", J. Air Poll. Cont. Assoc., Vol. 31, pp 42-45.
- Lamb, R. G., (1983a): "Air Pollution Models as Descriptors of Cause-Effect Relationships", Atmos. Envir., (in press).
- Lamb, R. G., (1983b): "Theoretical Issues in Long Range Transport Modeling", Preprint Volume, AMS Sixth Symposium on Turbulence and Diffusion, Boston, Mass., pp 241-244.
- Lamb, R. G. (1983c): "Causality and Atmospheric Phenomena" (in preparation).

- Lamb, R. G. (1983d): "A Regional Scale (1000 km) Model of Photochemical Air Pollution. Part 1: Theoretical Formulation", EPA report EPA-600/3-83-035. 226 + xi pages. NTIS-PB83-207688.
- McMahon, R. A. and P. J. Denison, (1979): "Empirical Atmospheric Deposition Parameters - A Survey", Atmos. Environ., Vol. 13, pp 571-585.
- Melgarejo, J. W. and J. W. Deardorff, (1974): "Stability Functions for the Boundary-Layer Resistance Laws Based Upon Observed Boundary-Layer Heights", J. Atmos. Sci., Vol. 31, pp 1324-1333.
- Nieuwstadt, F. T. M. and H. Tennekes, (1981): "A Rate Equation for the Nocturnal Boundary-Layer Height", J. Atmos. Sci., Vol. 38, pp 1418-1428.
- Sheih, C. M., M. L. Wesely and B. B. Hicks, (1979): "Estimated Dry Deposition Velocities of Sulfur Over the Eastern United States and Surrounding Regions", Atmos. Envir., Vol. 13, pp 1361-1368.
- Wesley, M. L., (1981): "Turbulent transport of ozone to surfaces common in the eastern half of the United States" submitted to Advances in Environ. Sci. and Tech., Vol. 12.
- Zeman, O., (1979): "Parameterization of the Dynamics of Stable Boundary Layers and Nocturnal Jets", J. Atmos. Sci., Vol. 36, pp 792-804.
- Zilitinkevich, S. S., (1972): "On the Determination of the Height of the Ekman Boundary-Layer", Boundary Layer Meteor., Vol. 3, pp 141-145.

TECHNICAL REPORT DATA <i>(Please read Instructions on the reverse before completing)</i>		
1. REPORT NO.	2.	3. RECIPIENT'S ACCESSION NO.
4. TITLE AND SUBTITLE A REGIONAL SCALE (1000 KM) MODEL OF PHOTOCHEMICAL AIR POLLUTION Part 2. Input Processor Network Design		5. REPORT DATE 6. PERFORMING ORGANIZATION CODE
7. AUTHOR(S) Robert G. Lamb		8. PERFORMING ORGANIZATION REPORT
9. PERFORMING ORGANIZATION NAME AND ADDRESS Same as Block 12		10. PROGRAM ELEMENT NO. CDWA1A/02-1335 (FY-84) 11. CONTRACT/GRANT NO.
12. SPONSORING AGENCY NAME AND ADDRESS Environmental Sciences Research Laboratory--RTP, NC Office of Research and Development Environmental Protection Agency Research Triangle Park, North Carolina 27711		13. TYPE OF REPORT AND PERIOD COVERED In-house 14. SPONSORING AGENCY CODE EPA/600/09
15. SUPPLEMENTARY NOTES		
16. ABSTRACT Detailed specifications are given for a network of data processors and submodels that can generate the parameter fields required by the regional oxidant model formulated in Part 1 of this report. Operations performed by the processor network include simulation of the motion and depth of the nighttime radiation inversion layer; simulation of the depth of the convective mixed and cloud layers; estimation of the synoptic-scale vertical motion fields; generation of ensembles of layer-averaged horizontal winds; calculation of vertical turbulence fluxes, pollutant deposition velocities, parameters for a subgrid-scale concentration fluctuation parameterization scheme; and many other functions. This network of processors and submodels, in combination with the core model developed in Part 1, represent the EPA's first-generation regional oxidant model.		
17. KEY WORDS AND DOCUMENT ANALYSIS		
a. DESCRIPTORS	b. IDENTIFIERS/OPEN ENDED TERMS	c. COSATI Field/Group
18. DISTRIBUTION STATEMENT RELEASE TO PUBLIC	19. SECURITY CLASS (This Report) UNCLASSIFIED 20. SECURITY CLASS (This page) UNCLASSIFIED	21. NO. OF PAGES 22. PRICE